Gas-Phase Nucleic Acid Ion-Electron Reactions: Implementation, Characterization, Fragmentation Pathways, and Mechanistic Aspects

by

Jiong Yang

A dissertation submitted in partial fulfillment
of the requirements for the degree of
Doctor of Philosophy
(Chemistry)
in The University of Michigan
2007

Doctoral Committee:

Assistant Professor Kristina I. Hakansson, Chair
Professor Philip C. Andrews
Professor Carol A. Fierke
Professor Robert T. Kennedy

To My Dear Family

Acknowledgements

The finishing of the thesis brings to an end to the exceptional journey of my Ph.D. studies. During these five memorable years, I have benefited tremendously from the guidance, help and friendship of many professors and colleagues. I would like to take this opportunity to express my gratitude to them all.

First of all, I would like thank my advisor Dr. Kristina Håkansson. Kristina's passion and knowledge of research inspired me a lot. I have learned to think critically, approach a problem systematically and pay more attention to details. I will carry what I learned from her into my future work. I sincerely thank Kristina for all the encouragement, guidance and research support throughout my Ph.D. research.

Second, I would like to thank my Ph.D. committee who guided my research work and provided valuable comments on my research proposal and this thesis: Prof. Philip C. Andrews, Prof. Carol A. Fierke and Prof. Robert T. Kennedy. This dissertation would not have been completed without your critique, guidance and help.

Third, I would like to thank my dear labmates: Julie, Natasa, Jason, Jingjie, Yibing, Hye Kyong, Chris, Hangtian, Bo, Hyun Ju, Wen, and our previous colleagues: Gabriella, Liping and Haichuan. You are the group that made my everyday research life more colorful. Thanks for all your friendship and help!

My research has been funded by a starter grant from the Petroleum Research Fund, a research award from the American Society for Mass Spectrometry (to Kristina), a CAREER award from the National Science Foundation (CHE-05-47699), and the University of Michigan. I would like to thank the Department of Chemistry at the University of Michigan for providing me with financial support through a teaching

assistantship. Last but not least, I would like to thank my wife and parents for their continuous support. My wife Liu Yao inspired me to conquer difficulties I have met in my studies and in life. This dissertation is dedicated to them.

Jiong Yang

Aug 15, 2007

Ann Arbor, MI

TABLE OF CONTENTS

LIST OF TABLES

Table

LIST OF FIGURES

Figure

LIST OF SCHEMES

Scheme

LIST OF APPENDICES

Appendix

LIST OF ABBREVIATIONS

Abbreviation	
A	Adenine
A	Adenosine
A	Ampere
B	Base
C	Cytidine
C	Cytosine
CHEF	Correlated harmonic excitation fields
CAD	Collision-activated dissociation
Da	Dalton
DNA	Deoxyribonucleic Acid
DR	Double resonance
e	Electron
EID	Electron induced dissociation
ESI	Electrospray ionization
ECD	Electron capture dissociation
EDD	Electron detachment dissociation
FA	Formic acid
FRET	Fluorescence resonance energy transfer

FT-ICR	Fourier transform ion cyclotron resonance
G	Guanine
G	Guanosine
HPLC	High performance liquid chromatography
ICR	Ion cyclotron resonance
IRMPD	Infrared multiphoton dissociation
k	Thousand
m	Messenger
M	Molarity
M	Precursor ion
m/z	Mass-to-charge ratio
MALDI	Matrix assisted laser desorption/ionization
MS	Mass spectrometry
MS/MS	Tandem mass spectrometry
OMe	Methoxy
Q	Quadrupole (mass filter)
PNA	Peptide nucleic acid
ppm	part per million
PSD	Post-source decay
PTMs	Posttranslational modifications
r	Ribosomal
RNA	Ribonucleic Acid
t	Transfer

T	Tesla, a unit of magnetic field
T	Thymidine
T	Thymine
U	Uracil
U	Uridine
UV	Ultraviolet
v	Volume
μ	Micro
ΔU	Potential difference

ABSTRACT

Gas-Phase Nucleic Acid Ion-Electron Reactions: Implementation, Characterization, Fragmentation Pathways, and Mechanistic Aspects

by

Jiong Yang

Chair: Kristina I. Håkansson

Traditional tandem mass spectrometry, including collision activated dissociation (CAD) and infrared multiphoton dissociation (IRMPD), is valuable for nucleic acid characterization, particularly for chemically modified oligonucleotides, which cannot be effectively characterized by enzymatic techniques. However, one disadvantage is secondary fragmentation, which complicates spectral interpretation and reduces sensitivity. In this dissertation, alternative gas-phase fragmentation strategies involving radical ion chemistry; electron capture dissociation (ECD) and electron detachment dissociation (EDD), are explored for nucleic acid characterization. EDD was implemented for the first time on a commercial Fourier transform ion cyclotron resonance (FT-ICR) mass spectrometer and shown to yield complementary fragmentation

pathways compared to CAD and IRMPD, and higher sensitivity than ECD due to the negative ion mode operation. Optimum fragmentation efficiency was obtained at 16-22 eV. Higher oligodeoxynucleotide charge states provided improved EDD data, presumably due to more extended gas-phase structures.

Oligoribonucleotide ECD fragmentation patterns were found to be nucleobase dependent, suggesting that cleavage proceeds following electron capture at the nucleobases. EDD provided complete sequence coverage of hexamer RNAs without nucleobase dependence, suggesting that EDD proceeds following direct electron detachment from the phosphate backbone. FT-IC double resonance (DR) was applied for the first time to characterize IRMPD and EDD fragmentation pathways of oligodeoxynucleotide anions. Results from these experiments suggest that IRMPD proceeds via a similar mechanism as proposed for CAD. Charge reduced radical precursor ions were found to constitute intermediates in EDD of thymidine-containing oligodeoxynucleotides. Furthermore, (*a*/*z* minus thymine) ions (*a* and *z* type ions correspond to backbone C-O bond cleavage) mainly originate from secondary fragmentation of *a*/*z* radical ions for the DNA dT_6.

ECD and EDD were extended to the characterization of three types of chemically modified oligonucleotides. 2'-methoxy and methylphosphonate modified oligonucleotides underwent limited fragmentation in ECD whereas complete sequence coverage was obtained in most cases from ECD of DNAs containing abasic sites (i. e., a hydrogen has replaced a nucleobase). EDD appeared to be more powerful than both ECD and IRMPD as it provided full sequence coverage and spectra are straightforward to interpret. Overall, EDD shows great promise for analysis of antisense compounds and modified nucleic acids.

CHAPTER 1

INTRODUCTION

1.1. NUCLEIC ACIDS

Nucleic acids, including deoxyribonucleic acid (DNA) and ribonucleic acid (RNA), have a variety of roles in cellular metabolism and carry genetic information. They are the energy medium in metabolic transactions; the essential chemical links in the response of cells to hormones and other extracellular impulses; and the structural components of enzyme cofactors and metabolic intermediates [1]. DNA carries the genetic information of a cell and contains thousands of genes, each of which determines the sequence of a protein molecule. Genetic DNA is situated in the nucleus and organized into chromosomes. When proteins are needed, the corresponding genes are transcribed into RNA. The RNA is first processed and transported out of the nucleus and proteins are synthesized based on the code carried by messenger (m)RNA. Nucleic acids and their complexes with other molecules are also important in areas as diverse as basic biology, virology, drug discovery, forensics, chemical diagnostics, and research on the origin of life. RNA molecules are unique biopolymers in that they can carry not

only genetic information but also catalytic function [2]. Several small catalytic RNAs, such as the hammerhead ribozyme [3], hepatitis delta virus ribozyme [4], and hairpin ribozyme [5], have been well studied but the mechanisms of catalysis are still not fully understood. Moreover, oligonucleotides may undergo natural covalent modifications that are most often present in transfer (t)-RNA and in ribosomal (r)-RNA, or unnatural ones that result from reactions with exogenous compounds [6-8].

Nucleic acids are long chain polymers of nucleotides, which are composed of a heterocyclic base, a sugar, and a phosphate group. Both DNA and RNA contain two purine bases, adenine (A) and guanine (G), and two pyrimidines: cytosine (C) occurs in both DNA and RNA, but the second pyrimidine is thymine (T) in DNA and uracil (U) in RNA. The difference between DNA and RNA is not only the base composition, but also the structure of the sugar ring: 2'-deoxy-D-ribose in DNA and D-ribose in RNA. In the nucleic acid polymer chain, the nucleosides/deoxynucleosides are linked together by phosphate groups attached to the 3'hydroxyl of one nucleoside and to the 5' hydroxyl of the adjacent nucleoside/deoxynucleoside.

Chemically modified oligonucleotides play an important role in biomedical/pharmaceutical research, especially for antisense applications. Many traditional drugs combat diseases by targeting faulty proteins, but antisense oligonucleotides intervene at an earlier stage, by preventing the production of these incorrect proteins. Antisense oligonucleotides are typically 13–25 nucleotides long and designed to hybridize to mRNA by Watson-Crick binding [9], as shown in Figure 1-1.

There are two common kinds of antisense oligonucleotides. The first type is small, gene-specific and targets specific strands of mRNA. Naturally occurring RNase H will destroy RNA strands hybridized to the antisense oligonucleotides, thus blocking the production of corresponding proteins. The second type of oligonucleotide is similar to the first type, but relies on a ribozyme to destroy the targeted mRNA, allowing a single

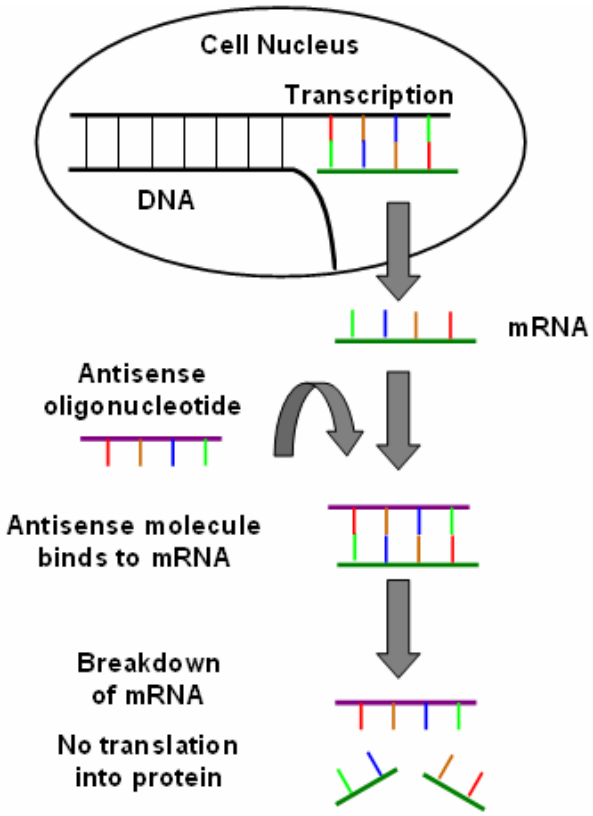

Figure 1-1. Antisense strategy: Antisense oligonucleotides are designed to turn off certain genes by binding to stretches of their messenger RNA. This figure is adopted from reference [11].

oligonucleotide to bind with several different strands of mRNA. Antisense oligonucleotides are widely used as therapeutics for malignant disease and there is a rapid increase in the number of antisense molecules progressing past Phase I, II and III clinical trials [10, 11]. Many antisense compounds are modified oligonucleotides, such as analogs with unnatural bases, modified sugars (especially at the 2' position of the ribose), or altered phosphate backbones [12].

Oligonucleotides have also been used to bind to the major groove of double helical DNA, thereby forming a local triple helix, a therapeutic strategy termed the "antigene" approach [13]. These triple-helix oligonucleotides are designed to bind with a specific section of the DNA, preventing its transcription into RNA. For example, peptide nucleic acids (a DNA/RNA mimic with a pseudopeptide backbone) have been found to cause more than 50% site-specific inhibition when binding to the nontranscribed strand [14].

Helicase-catalyzed disruption of double-stranded nucleic acids is vital to DNA replication, recombination, and repair in all forms of life. Chemically modified oligonucleotides have been used as substrates to study the relative influence of specific chemical interactions between helicases and their substrates over a series of multistep catalytic events [15]. Three types of modified oligonucleotides have been studied: 5'-DNA-PNA-DNA-3' chimera, and oligonucleotides with methylphosphonate-modified backbones or abasic sites.

In addition to traditional enzymatic sequencing methods, several techniques

have been developed to characterize nucleic acids. NMR spectroscopy is widely used for RNA structural analysis [16, 17] but suffers from limited sensitivity. Another powerful approach is chemical labeling followed by fluorescence resonance energy transfer (FRET) measurements [18], which can provide *single molecule* sensitivity [19]. However, structural information from FRET is limited to distance constraints for the added fluorophores and does not provide a detailed picture. Tandem mass spectrometry (MS/MS) has been widely applied to characterize the structure of nucleic acids [20-22]. Chemically modified oligonucleotides cannot be characterized by classical enzymatic techniques whereas mass spectrometry is more versatile and highly accurate. In particular, MS/MS has the advantage in characterizing the modification, such as altered sugar ring, phosphate backbone and unnatural base. MS/MS can also be used to probe gas-phase structure and folding of nucleic acids.

1.2. IONIZATION METHODS FOR NUCLEIC ACID MASS SPECTROMETRIC ANALYSIS

1.2.1. Electrospray Ionization

Electrospray ionization (ESI) is a powerful technique for producing intact biomolecular ions *in vacuo* from large and complex species in solution and has been proven to be a very "soft" ionization method [23]. In ESI, solution containing analyte is pushed through a narrow inner diameter (~50 μm) capillary held at an electric potential of 3-6 kV with respect to the entrance of the mass spectrometer (located ~3-20 mm

away), corresponding to an electric field of ~10^6 V/m. Analytes can exist as ions in solution, either in protonated/metal adducted cationic forms or as anions. Depending on the polarity of the electric field, either cations or anions will accumulate at the tip of the capillary, resulting in increased coulombic repulsion and electrostatic nebulization (electrospray) of the liquid. In order to assist nebulization, organic solvent is usually added to the solution to decrease the surface tension compared to that of pure water. Furthermore, nebulizing gas (i.e., nitrogen) can also be added (so called ion spray or pneumatically assisted electrospray [24]). The resulting mist contains multiply charged droplets from which solvent is rapidly evaporating. Heating of the mass spectrometer inlet or addition of hot drying gas is often used to assist solvent evaporation, which results in an increase in droplet charge density, causing disruption of droplets into smaller offspring droplets from Coulomb repulsion overcoming surface tension. According to the charge residue mechanism [25], this process occurs in multiple steps until the analyte is free of solvent, thereby forming free gas-phase ions. In the ion evaporation mechanism [26], the surface electric field at a certain droplet size is high enough to cause field desorption (i.e., ejection) of analyte ions from the droplets. Figure 1-2 shows a diagram of a typical ESI source. ESI has been shown to successfully ionize oligonucleotides as large as 8000 base pairs, corresponding to a molecular mass of 5 M Da [27]. ESI has a major advantage in that it forms multiply charged ions from large molecules, thereby facilitating tandem mass spectrometric analysis (see sections 1.4 and 1.5. below).

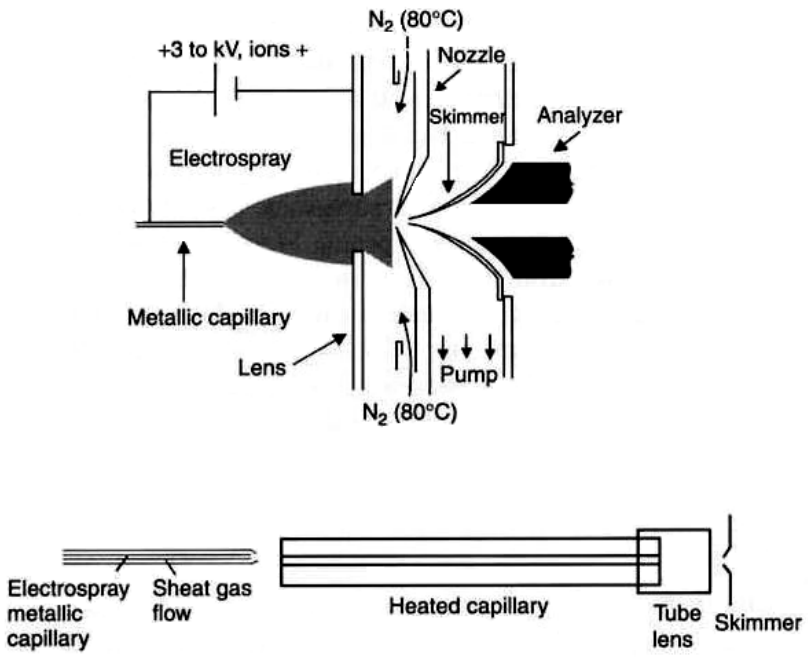

Figure 1-2. Diagram of ESI source with a curtain of heated nitrogen to assist desolvation (top), or with a heated capillary for desolvation (bottom). This figure is reproduced from reference [28] with permission.

1.2.2. Matrix Assisted Laser Desorption/Ionization

Matrix assisted laser desorption/ionization (MALDI) [29, 30] is a laser-based soft ionization method that has proven to be one of the most successful ionization methods for mass spectrometric analysis and investigation of large molecules. Analyte molecules are mixed with an excess of matrix-solution, which usually consists of organic acids (e.g., 3,5-dimethoxy-4-hydroxycinnamic acid, α-cyano-4-hydroxycinnamic acid, or 2,5-dihydroxybenzoic acid) in organic solvent (normally acetonitrile or ethanol) often containing some trifluoroacetic acid. This solution is spotted onto a MALDI plate and

the solvent evaporates, leaving analyte/matrix crystals. The MALDI spot is irradiated by an intense (1-10μJ) pulse from either an ultraviolet (UV) or infrared laser. In UV-MALDI, the matrix absorbs most of the laser energy, resulting in ejection of both matrix and analyte species into the gas-phase. The precise ionization mechanism is not well understood but is thought to involve gas-phase proton transfer reactions [31]. Figure 1-3 shows a diagram of the principle of MALDI. In contrast to ESI, MALDI generally produces singly-charged ions, but multiply charged ions ($[M + nH]^{n+}$) can also be observed for large species. The first MALDI mass spectra of small oligonucleotides were reported in 1990 [32, 33]. The detection limit of MALDI coupled with time-of-flight mass spectrometry can be as low as 250 attomol [34]. ESI and MALDI are complementary ionization techniques that both are highly sensitive.

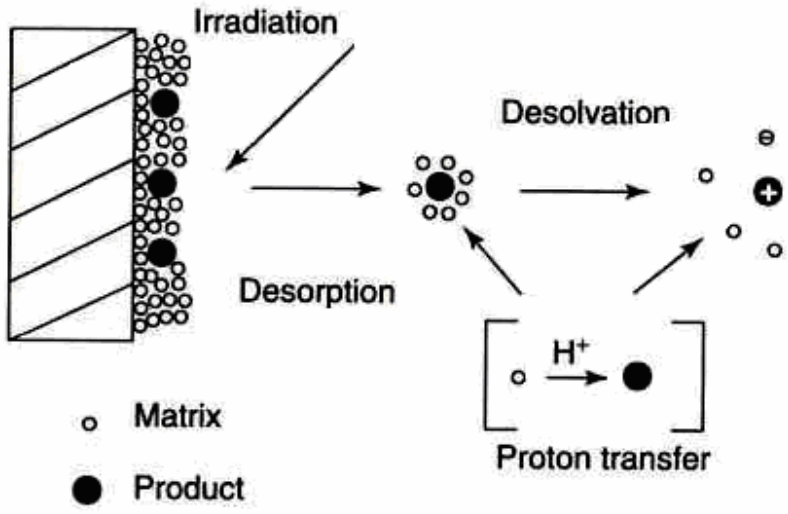

Figure 1-3. Diagram of the principle of MALDI. This figure is reproduced from reference [28] with permission.

1.3. FOURIER TRANSFORM ION CYCLOTRON RESONANCE MASS SPECROMETRY

Fourier transform ion cyclotron resonance mass spectrometry (FT-ICR MS) was introduced by Comisarow and Marshall in 1974 [35, 36]. Today it is widely practiced for peptide and protein [37, 38], oligonucleotide and nucleic acid [39, 40], and polymer [41, 42] characterization due to its high mass accuracy and high resolution.

There are four major components of an FT-ICR instrument: a superconducting magnet, an ICR cell located in the center of the magnetic field and consisting of two pairs of opposing plate electrodes (see Figure 1-4, top left), and ultra-high-vacuum and data acquisition systems. The basic operating principle of FT-ICR MS is to obtain ion m/z values by detecting their "cyclotron" frequency in a static magnetic field. The cyclotron frequency, ω, is determined by the magnetic field strength and m/z ratio as shown in equation (1) in which ω is the ion cyclotron frequency, B is the magnetic field strength, m is the ion mass, z is the number of elementary charges, and e is the elementary charge. Ions are transferred along the magnet field lines from the ESI source and trapped in the ICR cell radially by the Lorenz force (shown in equation (2) in which $\mathbf{v}$ is the ion velocity) and axially by trapping electrodes. Following trapping, ions are excited into coherent motion by an rf voltage, usually a frequency sweep covering the entire m/z range of interest, applied differentially between two opposite cell plates. Another pair of plates will detect the image current induced by ion clouds orbiting at increased cyclotron radius. The resulting time domain signal is converted to the frequency domain by Fourier

transformation, and ion cyclotron frequency is further converted to *m*/*z* values by applying equation (1). Figure 1-4 shows detection in the ICR cell, as well as time-domain, frequency domain, and m/z-domain FT-ICR signal from bovine ubiquitin, a 9 kDa protein.

$$\omega = zeB/m \qquad (1)$$

$$\mathbf{F} = ez\mathbf{v} \times \mathbf{B} \qquad (2)$$

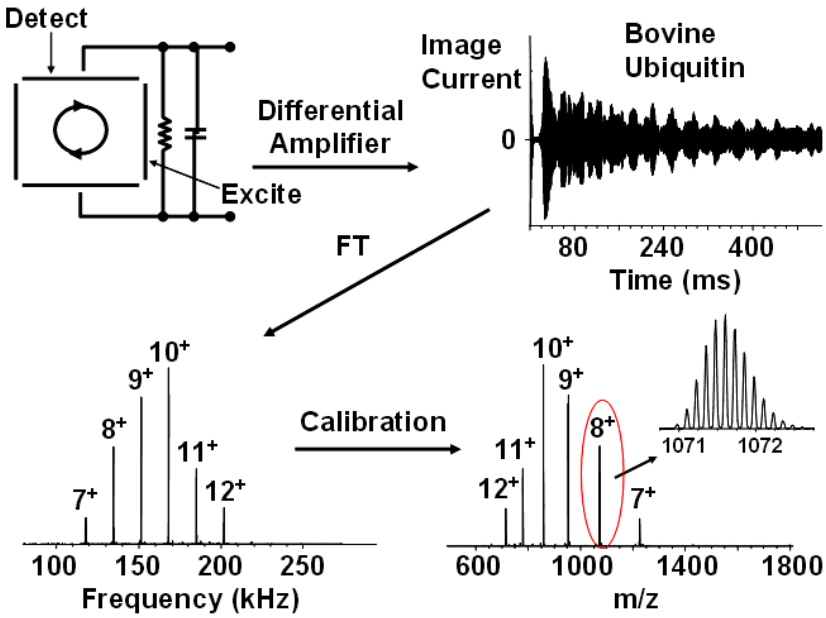

Figure 1-4. Time domain signal from bovine ubiquitin, a 9 kDa protein (upper right) obtained by excitation and detection of ions in an ICR cell (upper left). Frequency domain (lower left) FT-ICR signal is obtained through Fourier transformation and the corresponding mass spectrum (lower right for multiply charged bovine ubiquitin) is obtained by applying the equation $\omega = zeB/m$. The inset shows the baseline isotopic resolution that is routinely attained by FT-ICR.

Because FT-ICR MS measures frequency, which can be measured very accurately, unprecedented mass accuracy can be achieved. Mass measurements as accurate as 1 ppm can be obtained on a routine basis for large biomolecular ions [43, 44], and sub-ppm accuracy is obtained for low-m/z (<300) ions [45].

In addition to providing high mass accuracy, FT-ICR MS also offers superior mass resolving power compared to other mass analyzers. In the low-pressure limit, the resolving power is directly proportional to the duration of the time domain signal [46]. In the ultra-high-vacuum environment of the analyzer, the detection signal often lasts for several seconds and resolving power exceeding 10^6 can be obtained for large proteins. For example, Kelleher et al. have detected a 112 kDa protein with unit mass resolution [47]. One advantage of isotopic resolution is that it allows a direct determination of the charge state, q, of an ion from the isotopic distribution [48]. In addition to the long lasting transients, FT-ICR MS has higher resolving power than other mass analyzers that rely on differences in kinetic energy for separating the ions, such as time-of-flight or sector instruments, because ion cyclotron frequency is independent of ion velocity [49].

Both ESI and MALDI are used for biomolecular FT-ICR MS. The low charge states of MALDI-generated ions (see section 1.2 above) allow more ions to be accumulated in the ICR trap for a given charge capacity, providing better utilization of the limited dynamic range of FT-ICR MS. However, a shortcoming of this approach is that the velocity distribution of ions formed by MALDI is broad with high velocities [50], which makes it more difficult to trap the ions efficiently in the ICR cell. Also, singly

charged ions cannot be fragmented as efficiently in MS/MS studies. The multiple charging resulting from ESI increases the mass range of FT-ICR MS and improves MS/MS capability. Furthermore, *m*/*z* values of ESI-generated ions are generally below 2,000, which is highly compatible with FT-ICR MS because its resolving power is higher for low-*m*/*z* ions [51].

1.4. TRADITIONAL TANDEM MASS SPECTROMETRY FOR NUCLEIC ACID ANALYSIS

Tandem mass spectrometry, also termed MS/MS, refers to any mass spectrometric method that involves as least two stages of mass analysis [52]. Its principle is shown in scheme 1-1 and can be achieved in two ways: in time by performing a series of mass analyses in a fixed spectrometer, or in space by utilizing two consecutive mass analyzers. MS/MS is a well-established technique for characterizing oligonucleotides and PCR products [20, 40, 53-57], including characterization of genetic markers, such as short tandem repeats and single nucleotide polymorphisms [58]. Traditional MS/MS strategies include collision-activated dissociation (CAD) [59], infrared multiphoton dissociation (IRMPD) [60], nozzle-skimmer dissociation [61], surface-induced dissociation [62], and post-source decay (PSD) [63]. CAD and IRMPD are the two most widely used fragmentation methods for oligonucleotide characterization and they both involve dissociation of even-electron ions from slow heating.

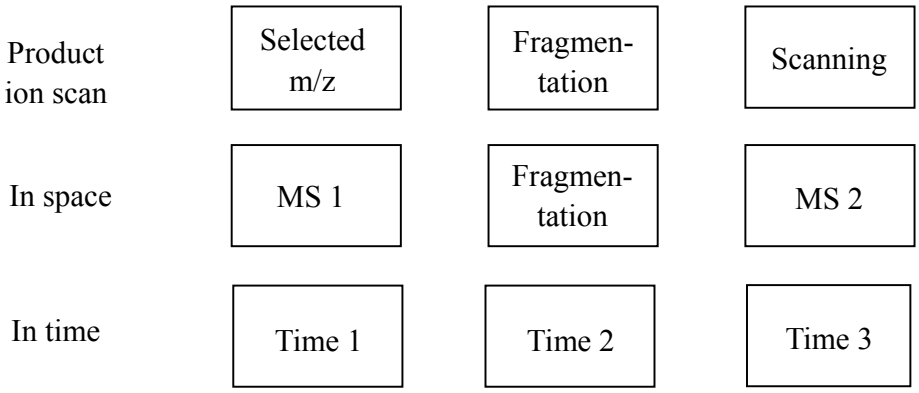

Scheme 1-1. Comparison of a product ion scan by space-based and time-based tandem mass spectrometers. The scheme is adopted from reference [28].

In this dissertation, McLuckey nomenclature [21] (shown in Figure 1-5) is used to discuss oligonucleotide product ions. Eight types of fragments can be achieved by cleaving the four possible sites of a phosphodiester bond: a_n, b_n, c_n and d_n are the symbols for fragments containing the 5' end of the oligonucleotide and w_n, x_n, y_n and z_n are the symbols for fragments containing the 3' end. The subscript, n, denotes the number of nucleotide residues in that particular product ion.

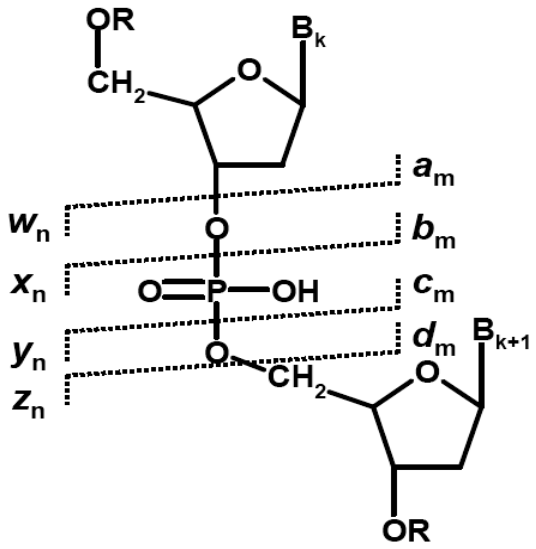

Figure 1-5. Nomenclature for oligonucleotide product ions. Figure is adopted from reference [21].

1.4.1. Collision-Activated Dissociation

Collision-activated dissociation is the most widely used tandem mass spectrometric technique. There are two regimes of collision-activated dissociation: high-energy collisions and low energy collisions. The high-energy collision regime generally involves electronic excitation [64]. Helium is the most commonly used target gas and precursor ions are accelerated by several kV. Low-energy collisions (accelerating voltage of <100 V) mostly involve vibrational excitation [65]. Heavier gases such as argon and xenon are typically used as they can transfer more energy to the target ions. In this dissertation, all CAD experiments involve low-energy collisions with argon.

McLuckey and co-workers first applied CAD to characterize negatively charged oligonucleotide ions in a quadrupole ion trap instrument [21]. In such experiments, neutral base (B) loss is a major fragmentation pathway but sequence-specific backbone cleavage, mainly in terms of (*a* - B) and *w* ions, is also observed [21, 66]. The mechanism of CAD of oligonucleotides has been studied for over ten years. Gross and coworkers proposed that there is intramolecular proton transfer from backbone phosphates to adjoining nucleobases, thereby creating a zwitterionic intermediate that dissociates via loss of a neutral base [66]. A major disadvantage of CAD is secondary fragmentation, such as water and additional base loss, which complicates spectral interpretation and reduces sensitivity. Enhanced sensitivity has been reported through incorporation of a 7-deaza purine analog, eliminating extensive depurination [67]. Additional and complementary information can be obtained through fragmentation of radical anions, as demonstrated by McLuckey et al. through ion-ion reactions [68] and by Hvelplund and co-workers through high-energy collisions with noble gas atoms [69]. Particularly, reduced nucleobase loss is seen.

1.4.2. Infrared Multiphoton Dissociation

Infrared multiphoton dissociation [60, 70] is another valuable vibrational excitation fragmentation method. IRMPD fragmentation patterns of oligonucleotides are similar to those of CAD. In FT-ICR MS, IRMPD minimizes the pumping down time compared to in-cell CAD, which requires introduction of gas into the ICR cell.

McLafferty and coworkers have demonstrated IRMPD for characterization of large biomolecules, including oligonucleotides [60]. Sannes-Lowery and Hofstadler implemented IRMPD in the external ion reservoir of an FT-ICR instrument to characterize modified oligonucleotides and found that sequence-specific (*a* - B) and *w*-type ions can provide a rapid and accurate readout of the sequence of modified oligonucleotides [70]. Brodbelt and co-workers have compared CAD and IRMPD of deprotonated and protonated oligonucleotides in a quadrupole ion trap and found that IRMPD can minimize uninformative [M - B] ions, which dominate in CAD spectra, and free phosphate and nucleobase ions can be observed, which can help to identify modified bases [71]. However, nucleobase loss is still observed as a major fragmentation pathway in IRMPD and such ions are not desired because they do not provide sequence-specific information.

1.5. GAS-PHASE ION-ELECTRON REACTIONS

1.5.1. Electron Capture Dissociation

Electron capture dissociation (ECD) involves radical ion chemistry and provides unique fragmentation patterns for peptides and proteins [37], peptide nucleic acids [72], polymers [41] and lantibiotics [73]. Scheme 1-2 shows the ECD fragmentation pathway. In all cases, complementary structural information is obtained compared to traditional MS/MS of even-electron ions. In particular, extremely "soft" fragmentation is achieved for peptides and proteins: backbone bonds can be cleaved

without losing labile posttranslational modifications, allowing their localization. Also, backbone covalent bonds can be ruptured without breaking noncovalent interactions of a protein's higher order structure [74]. The latter feature has been exploited in the investigation of protein gas-phase folding and unfolding [75, 76]. It has been found that ECD dissociation channels differ from other MS/MS techniques for oligonucleotides as well [39]. However, in those experiments, the fragmentation was nucleobase specific and rather limited. More recent results with an improved electron injection system [77] and the possibility to mass-selectively accumulate precursor ions (improving sensitivity) demonstrate more extensive fragmentation, resulting in complete sequencing of small (5- to 7-mer) oligonucleotides [78].

$$[M + nH]^{n+} + e^{-}_{(<1\ eV)} \rightarrow [M + nH]^{(n-1)+\bullet} \rightarrow \text{backbone cleavage}$$

Scheme 1-2. Electron capture dissociation fragmentation route.

The main caveat for analyzing oligonucleotides by ECD is the requirement for positively charged precursor ions. Negative ion mode results in higher sensitivity due to the sugar-phosphate backbone, which undergoes facile deprotonation.

1.5.2. Electron detachment dissociation

Electron detachment dissociation (EDD), introduced by Zubarev and co-workers in 2001, involves higher energy (≥ 10 eV) electrons than ECD and has been

shown to provide fragmentation similar to ECD for negatively charged peptide ions [79]. Scheme 1-3 shows the EDD fragmentation pathway. For peptide dianions, electron detachment is followed mainly by N-C_α and C_α-C bond cleavage [79-81]. As for ECD, more extensive backbone fragmentation can be obtained with EDD compared to techniques based on vibrational excitation, resulting in enhanced peptide sequence coverage [80]. Further similarity between these two ion-electron reaction techniques is evident from the retention of a labile sulfate group, rendering EDD a potential tool for localizing posttranslational modifications in acidic peptides [79].

$$[M - nH]^{n-} + e^-_{fast\ (>10\ eV)} \rightarrow [M - nH]^{(n-1)-\bullet} + 2e^- \rightarrow \text{further fragmentation}$$

Scheme 1-3. Electron detachment dissociation fragmentation route.

1.6. DISSERTATION OVERVIEW

The research work in this dissertation focuses on the implementation of electron detachment dissociation in FT-ICR MS and its application for characterizing nucleic acids and their analogs. Fragmentation pathways and mechanistic aspects are discussed as well.

Chapter 2 describes the first demonstration of EDD experiments performed with a heated filament electron source in a 7 T commercial Fourier transform ion cyclotron resonance mass spectrometer, and an improved implementation with a hollow dispenser cathode electron source, providing increased fragmentation efficiency and

sensitivity. EDD is shown to provide rich fragmentation patterns, complementary to CAD and IRMPD, for small oligonucleotides and complete oligonucleotide sequencing is easily achieved. In comparison to ECD, enhanced sensitivity is achieved through negative ion mode operation (on average a 10-fold improvement so far in terms of concentration sensitivity). The work in this chapter has been published in *Analytical Chemistry* (2005, volume 77, pages 1876-1882).

Chapter 3 presents a detailed characterization of the influence of electron current, electron energy distribution, cathode bias voltage, and electron extraction lens voltage in EDD. The potential difference, ΔU, between the cathode and the extraction lens is a crucial parameter for successful EDD. We found that the lens voltage serves to regulate the number of electrons passing through the ICR cell and that the electron energy distribution is narrow (< 0.5 V) at different cathode bias voltages. Optimum EDD efficiency at fixed electron current (around 4 μA) was obtained at electron energies of 16-22 eV for the oligodeoxynucleotide dT_6 and for the peptide substance P.

Chapter 4 extends the ECD and EDD application to hexamer oligoribonucleotides. The ECD results show a strong nucleobase dependence, supporting an ECD cleavage mechanism involving electron capture at the nucleobases, consistent with recent theoretical work for neutral DNA [82]. However, only limited backbone cleavage was observed in ECD, precluding complete sequencing. EDD appears more promising for RNA structural characterization because more extensive backbone cleavage was observed at higher sensitivity. Here, *w* and *d* ion series

constitute the most abundant fragmentation channels, similar to EDD of DNA. The EDD cleavage process is proposed to be initiated via direct electron detachment from the deprotonated phosphate backbone. EDD provided full sequence coverage for all oligomer RNAs. The work in this chapter has been published in the *Journal of the American Society for Mass Spectrometry* (2006, volume 17, pages 1369-1375).

Chapter 5 explores the fragmentation pathways in EDD of oligomer DNAs by Fourier transform ion cyclotron double resonance (DR) experiments. First, DR experiments were utilized to characterize fragmentation pathways in IRMPD of oligodeoxynucleotides, confirming that fragmentation 3' to adenine, cytosine, and guanine bases proceeds via a neutral base loss intermediate whereas alternative pathways are involved in backbone cleavage 3' to thymine. DR-EDD verified that EDD fragmentation of dT_6 may proceed via a radical intermediate and suggested that (*a* - T) ions in EDD of dT_6 may originate from secondary fragmentation of radical *a*-type ions.

Chapter 6 investigates ECD and EDD of chemically modified oligonucleotides and shows that EDD appears to be a more effective tool for structural characterization of such oligonucleotides. We also aimed at gaining mechanistic insights although no conclusive information was obtained from these experiments.

Chapter 7 summarizes all results discussed in this dissertation, and presents a future outlook. There are two appendices: one discusses extension of ECD and EDD to metal-adducted oligonucleotides and the other discusses the application of electron induced dissociation (EID) of singly charged oligomer DNA.

1.7. BIBLIOGRAPHY

1. Nelson, D. L.; Cox, M. M. *Lehninger Principles of Biochemistry*, Third ed.; Worth Publishers: New York, 2000.
2. Walter, N. G.; Harris, D. A.; Pereira, M. J. B.; Rueda, D. In the Fluorescent Spotlight: Global and Local Conformational Changes of Small Catalytic RNAs. *Biopolymers* **2001,** *61*, 224-242.
3. Rueda, D.; Wick, K.; McDowell, S. E.; Walter, N. G. Diffusely Bound Mg^{2+} Ions Slightly Reorient Stems I and II of the Hammerhead Ribozyme to Increase the Probability of Formation of the Catalytic Core. *Biochemistry* **2003,** *42*, 9924-9936.
4. Jeong, S.; Sefcikova, J.; Tinsley, R. A.; Rueda, D.; Walter, N. G. Trans-Acting Hepatitis Delta Virus Ribozyme: Catalytic Core and Global Structure are Dependent on the 5' Substrate Sequence. *Biochemistry* **2003,** *42*, 7727-7740.
5. Zhuang, X. W.; Kim, H.; Pereira, M. J. B.; Babcock, H. P.; Walter, N. G.; Chu, S. Correlating Structural Dynamics and Function in Single Ribozyme Molecules. *Science* **2002,** *296*, 1473-1476.
6. Guymon, R.; Pomerantz, S. C.; Crain, P. F.; McCloskey, J. A. Influence of phylogeny on posttranscriptional modification of rRNA in thermophilic prokaryotes: the complete modification map of 16S rRNA of *Thermus thermophilus*. *Biochemistry* **2006,** *45*, 4888-4899.
7. Björk, G. R.; Ericson, J. U.; Gustafsson, C. E. D.; Hagervall, T. G.; Jönsson, Y. H.; Wikström, P. M. Transfer RNA modification. *Annu. Rev. Biochem.* **1987,** *56*,

263-287.

8. Sprinzl, M.; Horn, C.; Brown, M.; Ioudovitch, A.; Steinberg, S. Compilation of tRNA sequences and sequences of tRNA genes. *Nucleic Acids Res.* **1998,** *26*, 148-153.
9. Dias, N.; Stein, C. A. Antisense Oligonucleotides: Basic Concepts and Mechanisms. *Mol. Cancer Ther.* **2002,** *1*, 347-355.
10. Tamm, I. Antisense Therapy in Malignant Diseases: Status Quo and Quo Vadis? *Clin. Sci.* **2006,** *110*, 427-442.
11. Aboul-Fadl, T. Antisense Oligonucleotides: The State of the Art. *Curr. Med. Chem.* **200**5**,** *12*, 2193-2214.
12. Cook, P. D. *Antisense Drug Technology: Principles, Strategies and Applications*, Marcel Dekker, Inc.: New York, 2001.
13. Hélène, C. Rational Design of Sequence-specific Oncogene Inhibitors Based on Antisense and Antigene Oligonucleotides. *Eur. J. Cancer* **1991,** *27*, 1466-1471.
14. Hanvey, J. C.; Peffer, N. J.; Bisi, J. E.; Thomson, S. A.; Cadilla, R.; Josey, J. A.; Ricca, D. J.; Hassman, C. F.; Bonham, M. A.; Au, K. G.; Carter, S. G.; Bruckenstein, D. A.; Boyd, A. L.; Noble, S. A.; Babiss, L. E. Antisense and Antigene Properties of Peptide Nucleic Acids. *Science* **1992,** *258*, 1481-1485.
15. Eoff, R. L.; Spurling, T. L.; Raney, K. D. Chemically Modified DNA Substrates Implicate the Importance of Electrostatic Interactions for DNA Unwinding by Dda Helicase. *Biochemistry* **2005,** *44*, 666-674.

16. Fürtig, B.; Richter, C.; Wöhnert, J.; Schwalbe, H. NMR Spectroscopy of RNA. *ChemBioChem* **2003,** *4*, 936-962.

17. Al-Hashimi, H. M. Dynamics-Based Amplification of RNA Function and Its Characterization by Using NMR Spectroscopy. *ChemBioChem* **2005,** *6*, 1506-1519.

18. Selvin, P. R. Fluorescence resonance energy transfer. *Methods Enzymol.* **1995,** *246*, 6264-6268.

19. Zhuang, X. Single-molecule RNA Science. *Annu. Rev. Biophys. Biomol. Struct.* **2005,** *34*, 399-414.

20. Hofstadler, S. A.; Sannes-Lowery, K. A.; Hannis, J. C. Analysis of Nucleic Acids by FTICR MS. *Mass Spectrom. Rev.* **2005,** *24*, 265-285.

21. McLuckey, S. A.; Van Berkel, G. J.; Glish, G. L. Tandem Mass Spectrometry of Small, Multiply-charged Oligonucleotides. *J. Am. Soc. Mass Spectrom.* **1992,** *3*, 60-70.

22. Juhasz, P.; Roskey, M. T.; Smirnov, I. P.; Haff, L. A.; Vestal, M. L.; Martin, S. A. Applications of Delayed Extraction Matrix-Assisted Laser Desorption Ionization Time-of-Flight Mass Spectrometry to Oligonucleotide Analysis. *Anal. Chem.* **1996,** *68*, 941-946.

23. Fenn, J. B.; Mann, M.; Meng, C. K.; Wong, S. F.; Whitehouse, C. M. Electrospray Ionization for Mass Spectrometry of Large Biomolecules. *Science* **1989,** *246*, 64-71.

24. Bruins, A. P.; Covey, T. R.; Henion, J. D. Ion Spray Interface for Combined Liquid Chromatography/Atmospheric Pressure Ionization Mass Spectrometry. *Anal. Chem.*

1987, *59*, 2642-2646.

25. Dole, M.; Mack, L. L.; Hines, R. L.; Mobley, R. C.; Ferguson, L. D.; Alice, M. B. Molecular Beams of Macroions. *J. Chem. Phys.* **1968,** *49*, 2240-2249.
26. Iribarne, J. V.; Thomson, B. A. On the Evaporation of Small Ions from Charged Droplets. *J. Chem. Phys.* **1976,** *64*, 2287-2294
27. Schultz, J. C.; Hack, A. C.; Benner, W. H. Mass Determination of Megadalton-DNA Electrospray Ions Using Charge Detection Mass Spectrometry. *J. Am. Soc. Mass Spectrom.* **1998,** *9*, 305-313.
28. de Hoffmann, E.; Stroobant, V. *Mass Spectrometry Principles and Applications*, Second ed.; John Wiley & Sons, LTD: Chichester, 2002.
29. Tanaka, K.; Waki, H.; Ido, Y.; Akita, S.; Yoshida, Y.; Yoshida, T. Protein and Polymer Analyses up to *m/z* 100 000 by Laser Ionization Time-of-flight Mass Spectrometry. *Rapid Commun. Mass Spectrom.* **1988,** *2*, 151-153.
30. Karas, M.; Hillenkamp, F. Laser Desorption Ionization of Proteins with Molecular Masses Exceeding 10000 Daltons. *Anal. Chem.* **1988,** *60*, 2299-2301.
31. Karas, M.; Kruger, R. Ion Formation in MALDI: The Cluster Ionization Mechanism *Chem. Rev.* **2003,** *103*, 427-439.
32. Börnsen, K. O.; Schär, M.; Widmer, H. M. Matrix-Assisted Laser Desorption and Ionization Mass Spectrometry and Its Applications in Chemistry. *Chimia* **1990,** *44*, 412-416.
33. Spengler, B.; Pan, Y.; Cotter, R. J.; Kan, L. S. Molecular Weight Determination of

Underivatized Oligodeoxyribonucleotides by Positive-ion Matrix-assisted Ultraviolet Laser-Desorption Mass Spectrometry. *Rapid Commun. Mass Spectrom.* **1990,** *4*, 99-102.

34. Zhang, Z. Y.; Zhou, L. H.; Zhao, S. K.; Deng, H. M.; Deng, Q. Y. 3-hydroxycoumarin as a New Matrix for Matrix-assisted Laser Desorption/ionization Time-of-flight Mass Spectrometry of DNA. *J. Am. Soc. Mass Spectrom.* **2006,** *17*, 1665-1668.
35. Comisarow, M. B.; Marshall, A. G. Fourier Transform Ion Cyclotron Resonance Spectroscopy. *Chem. Phys. Lett.* **1974,** *25*, 282-283.
36. Comisarow, M. B.; Marshall, A. G.. Frequency-Sweep Fourier Transform Ion Cyclotron Resonance Spectroscopy. *Chem. Phys. Lett.* **1974,** *26*, 489-490.
37. Zubarev, R. A.; Kelleher, N. L.; McLafferty, F. W. Electron Capture Dissociation of Multiply Charged Protein Cations. A Nonergodic Process. *J. Am. Chem. Soc.* **1998,** *120*, 3265-3266.
38. Ge, Y.; Lawhorn, B. G.; ElNaggar, M.; Strauss, E.; Park, J. H.; Begley, T. P.; McLafferty, F. W. Top Down Characterization of Larger Proteins (45 kDa) by Electron Capture Dissociation Mass Spectrometry. *J. Am. Chem. Soc.* **2002,** *124*, 672-678.
39. Håkansson, K.; Hudgins, R. R.; Marshall, A. G.; O'Hair, R. A. J. Electron Capture Dissociation and Infrared Multiphoton Dissociation of Oligodeoxynucleotide Dications. *J. Am. Soc. Mass Spectrom.* **2003,** *14*, 23-41.

40. Muddiman, D. C.; Smith, R. D. Sequencing and Characterization of Larger Oligonucleotides by Electrospray Ionization Fourier Transform Ion Cyclotron Resonance Mass Spectrometry. *Rev. Anal. Chem.* **1998,** *17*, 1-68.

41. Cerda, B. A.; Horn, D. M.; Breuker, K.; McLafferty, F. W. Sequencing of Specific Copolymer Oligomers by Electron-Capture-Dissociation Mass Spectrometry. *J. Am. Chem. Soc.* **2002,** *124*, 9287-9291.

42. Koster, S.; Duursma, M. C.; Boon, J. J.; Heeren, R. M. A.; Ingemann, S.; van Benthem, R. A. T. M.; de Koster, C. G. Electron Capture and Collisionally Activated Dissociation Mass Spectrometry of Doubly Charged Hyperbranched Polyesteramides. *J. Am. Soc. Mass Spectrom.* **2003,** *14*, 332-341.

43. Green, M. K.; Vestling, M. M.; Johnston, M. V.; Larsen, B. S. Distinguishing Small Molecular Mass Differences of Proteins by Mass Spectrometry. *Anal. Biochem.* **1998,** *260*, 204-211.

44. Bruce, J. E.; Anderson, G. A.; Wen, J.; Harkewicz, R.; Smith, R. D. High Mass-measurement Accuracy and 100% Sequence Coverage of Enzymatically Digested Bovine Serum Albumin from an ESI-FTICR Mass Spectrum. *Anal. Chem.* **1999,** *71*, 2595-2599.

45. Rodgers, R. P.; Blumer, E. N.; Freitas, M. A.; Marshall, A. G. Complete Compositional Monitoring of the Weathering of Transportation Fuels based on Elemental Compositions from Fourier Transform Ion Cyclotron Resonance Mass Spectrometry. *Environ. Sci. Technol.* **2000,** *34*, 1671-1678.

46. Marshall, A. G.; Comisarow, M. B.; Parisod, G. Relaxation and Spectral Line Shape in Fourier Transform Ion Cyclotron Resonance Spectroscopy. *J. Chem. Phys.* **1979,** *71*, 4434-4444.

47. Kelleher, N. L.; Senko, M. W.; Siegel, M. M.; McLafferty, F. W. Unit Resolution Mass Spectra of 112 kDa Molecules with 3 Da Accuracy. *J. Am. Soc. Mass Spectrom.* **1997,** *8*, 380-383.

48. Henry, K. D.; McLafferty, F. W. Electrospray Ionization with Fourier-Transform Mass Spectrometry. Charge State Assignment from Resolved Isotopic Peaks. *Org. Mass Spectrom.* **1990,** *25*, 490-492.

49. Håkansson, K.; Quenzer, T. L.; Marshall, A. G.; Emmett, M. R. *Mass Spectrometry and Hyphenated Techniques in Neuropeptide Research*, First ed.; John Wiley & Sons, LTD.: Chichester, 2002.

50. Gluckmann, M.; Karas, M. The Initial Ion Velocity and its Dependence on Matrix, Analyte and Preparation Method in Ultraviolet Matrix-Assisted Laser Desorption/Ionization. *J. Mass Spectrom.* **1999,** *34*, 367-477.

51. Marshall, A. G.; Hendrickson, C. L.; Jackson, G. S. Fourier Transform Ion Cyclotron Resonance Mass Spectrometry: A Primer. *Mass Spectrom. Rev.* **1998,** *17*, 1-35.

52. McLafferty, F. W. *Tandem Mass Spectrometry*, Wiley-Interscience: New York, 1983.

53. Murray, K. K. DNA Sequencing by Mass Spectrometry. *J. Mass Spectrom.* **1996,** *31*, 1203-1215.

54. Ni, J.; Pomerantz, S. C.; Rozenski, J.; Zhang, Y.; McCloskey, J. A. Interpretation of

Oligonucleotide Mass Spectra for Determination of Sequence Using Electrospray Ionization and Tandem Mass Spectrometry. *Anal. Chem.* **1996,** *68*, 1989-1999.

55. Benson, L. M.; Null, A. P.; Muddiman, D. C. Advantages of *Thermococcus kodakaraenis* (KOD) DNA Polymerase for PCR-mass Spectrometry Based Analyses. *J. Am. Soc. Mass Spectrom.* **2003,** *14*, 601-604.
56. Banoub, J. H.; Newton, R. P.; Esmans, E.; Ewing, D. F.; Mackenzie, G. Recent Developments in Mass Spectrometry for the Characterization of Nucleosides, Nucleotides, Oligonucleotides, and Nucleic Acids. *Chem. Rev.* **2005,** *105*, 1869-1916.
57. Wu, J.; McLuckey, S. A. Gas-phase Fragmentation of Oligonucleotide Ions. *Int. J. Mass Spectrom.* **2004,** *237*, 197-241.
58. Null, A. P.; Muddiman, D. C. Perspectives on the Use of Electrospray Ionization Fourier Transform Ion Cyclotron Resonance Mass Spectrometry for Short Tandem Repeat Genotyping in the Post-Genome Era. *J. Mass Spectrom.* **2001,** *36*, 589-606.
59. McLuckey, S. A. Principles of Collisional Activation in Analytical Mass Spectrometry. *J. Am. Soc. Mass Spectrom.* **1992,** *3*, 599-614.
60. Little, D. P.; Speir, J. P.; Senko, M. W.; O'Connor, P. B.; McLafferty, F. W. Infrared Multiphoton Dissociation of Large Multiply-charged Ions for Biomolecule Sequencing. *Anal. Chem.* **1994,** *66*, 2809-2815.
61. Little, D. P.; Chorush, R. A.; Speir, J. P.; Senko, M. W.; Kelleher, N. L.; McLafferty, F. W. Rapid Sequencing of Oligonucleotides by High-resolution Mass-spectrometry.

J. Am. Chem. Soc. **1994,** *116*, 4893-4897.

62. Mabud, M. D. A.; Dekrey, M. J.; Cooks, R. G. Surface-induced Dissociation of Molecular-ions. *Int. J. Mass Spectrom.* **1985,** *67*, 285-294.
63. Berhane, B. T.; Limbach, P. A. Stable Isotope Labeling for Matrix-assisted Laser Desorption/ionization Mass Spectrometry and Post-source Decay Analysis of Ribonucleic Acids. *J. Mass Spectrom.* **2003,** *38*, 872-878
64. Yamaoka, H.; Dong, P.; Durup, J. Energetics of the Collision-Induced Dissociations $C_2H_2^+ \rightarrow C_2H^+ + H$ and $C_2H_2^+ \rightarrow H^+ + C_2H$. *J. Chem. Phys.* **1969,** *51*, 3465-3476.
65. Schwartz, R. N.; Slawsky, Z. I.; Herzfeld, K. F. Calculation of Vibrational Relaxation Times in Gases. *J. Chem. Phys.* **1952,** *20*, 1591-1599
66. Wang, Z.; Wan, K. X.; Ramanathan, R.; Taylor, J. S.; Gross, M. L. Structure and Fragmentation Mechanisms of Isomeric T-rich Oligodeoxynucleotides: A Comparison of Four Tandem Mass Spectrometric Methods. *J. Am. Soc. Mass Spectrom.* **1998,** *9*, 683-691.
67. Hannis, J. C.; Muddiman, D. C. Tailoring the Gas-phase Dissociation and Determining the Relative Energy of Activation for Dissociation of 7-deaza Purine Modified Oligonucleotides Containing a Repeating Motif. *Int. J. Mass Spectrom.* **2002,** *219*, 139-150.
68. McLuckey, S. A.; Stephenson, J. L.; O'Hair, R. A. J. Decompositions of Odd- and Even-electron Anions Derived from Deoxypolyadenylates. *J. Am. Soc. Mass Spectrom.* **1997,** *8*, 148-154.

69. Liu, B.; Hvelplund, P.; Brondsted Nielsen, S.; Tomita, S. Electron Loss and Dissociation in High Energy Collisions between Multiply Charged Oligonucleotide Anions and Noble Gases. *Int. J. Mass Spectrom.* **2003,** *230*, 19-24.

70. Sannes-Lowery, K. A.; Hofstadler, S. A. Sequence Confirmation of Modified Oligonucleotides using IRMPD in the External Reservoir of an Electrospray Ionization Fourier Transform Ion Cyclotron Mass Spectrometer. *J. Am. Soc. Mass Spectrom.* **2003,** *14*, 825-833.

71. Keller, K. M.; Brodbelt, J. S. Collisionally Activated Dissociation and Infrared Multiphoton Dissociation of Oligonucleotides in a Quadrupole Ion Trap. *Anal. Biochem.* **2004,** *326*, 200-210.

72. Olsen, J. V.; Haselmann, K. F.; Nielsen, M. L.; Budnik, B. A.; Nielsen, P. E.; Zubarev, R. A. Comparison of Electron Capture Dissociation and Collisionally Activated Dissociation of Polycations of Peptide Nucleic Acids. *Rapid Commun. Mass Spectrom.* **2001,** *15*, 969-974.

73. Kleinnijenhuis, A. J.; Duursma, M. C.; Breukink, E.; Heeren, R. M. A.; Heck, A. J. R. Localization of Intramolecular Monosulfide Bridges in Lantibiotics Determined with Electron Capture Dissociation. *Anal. Chem.* **2003,** *75*, 3219-3225.

74. Horn, D. M.; Ge, Y.; McLafferty, F. W. Activated Ion Electron Capture Dissociation for Mass Spectral Sequencing of Larger (42 kDa) Proteins. *Anal. Chem.* **2000,** *72*, 4778-4784.

75. Horn, D. M.; Breuker, K.; Frank, A. J.; McLafferty, F. W. Kinetic Intermediates in

the Folding of Gaseous Protein Ions Characterized by Electron Capture Dissociation Mass Spectrometry. *J. Am. Chem. Soc.* **2001,** *123*, 9792-9799.

76. Breuker, K.; Oh, H.; Horn, D. M.; Cerda, B. A.; McLafferty, F. W. Detailed Unfolding and Folding of Gaseous Ubiquitin Ions Characterized by Electron Capture Dissociation. *J. Am. Chem. Soc.* **2002,** *124*, 6407-6420.
77. Håkansson, K.; Chalmers, M. J.; Quinn, J. P.; McFarland, M. A.; Hendrickson, C. L.; Marshall, A. G. Combined Electron Capture and Infrared Multiphoton Dissociation for Multistage MS/MS in an FT-ICR Mass Spectrometer. *Anal. Chem.* **2003,** *75*, 3256-3262.
78. Schultz, K. N.; Håkansson, K. Rapid Electron Capture Dissociation of Mass-Selectively Accumulated Oligodeoxynucleotide Dications. *Int. J. Mass Spectrom.* **2004,** *234*, 123-130.
79. Budnik, B. A.; Haselmann, K. F.; Zubarev, R. A. Electron Detachment Dissociation of Peptide Di-anions: an Electron-hole Recombination Phenomenon. *Chem. Phys. Lett.* **2001,** *342*, 299-302.
80. Haselmann, K. F.; Budnik, B. A.; Kjeldsen, F.; Nielsen, M. L.; Olsen, J. V.; Zubarev, R. A. Electronic Excitation gives Informative Fragmentation of Polypeptide Cations and Anions. *Eur. Mass Spectrom.* **2002,** *8*, 117-121.
81. Kjeldsen, F.; Silivra, O. A.; Ivonin, I. A.; Haselmann, K. F.; Gorshkov, M.; Zubarev, R. A. C-alpha-C Backbone Fragmentation Dominates in Electron Detachment Dissociation of Gas-phase Polypeptide Polyanions. *Chem. Eur. J.* **2005,** *11*,

1803-1812.

82. Berdys, J.; Anusiewicz, I.; Skurski, P.; Simons, J. Damage to Model DNA Fragments from Very Low-Energy (<1 eV) Electrons. *J. Am. Chem. Soc.* **2004,** *126*, 6441-6447.

CHAPTER 2

IMPLEMENTATION OF ELECTRON DETACHMENT DISSOCIATION IN FOURIER TRANSFORM ION CYCLOTRON RESONANCE MASS SPECTROMETRY AND ITS APPLICATION FOR OLIGODEOXYNUCLEOTIDE CHARACTERIZATION

In this chapter we show the implementation of EDD on a commercial Fourier transform ion cyclotron resonance mass spectrometer utilizing two different configurations: a heated filament electron source and an indirectly heated hollow dispenser cathode electron source. Filament EDD is demonstrated, to our knowledge, for the first time although the dispenser cathode configuration provides higher EDD efficiency and richer fragmentation patterns for hexamer oligodeoxynucleotides. EDD of oligodeoxynucleotides allows complete sequencing at enhanced sensitivity.

2.1. INTRODUCTION

Tandem mass spectrometry is a well-established technique for oligonucleotide sequencing, including characterization of genetic markers, such as short tandem repeats and single nucleotide polymorphisms [1]. Most MS/MS strategies, such as CAD and IRMPD, involve the dissociation of even-electron anions. In those cases, neutral base (B) loss is a major fragmentation pathway. However, sequence-specific backbone cleavage, mainly in terms of (*a* - B) and *w* ions is also observed, in which *a* ions contain

the 5’ end of the oligonucleotide and *w* ions contain the 3’ end [2, 3]. Similar behavior has been reported for modified oligonucleotides [4]. A major disadvantage of CAD and IRMPD, i.e. vibrational excitation, is secondary fragmentation, such as water and additional base loss, which complicates spectral interpretation and reduces sensitivity.

ECD has been shown to provide extensive fragmentation, resulting in complete sequencing of small (5- to 7-mer) oligonucleotides [5]. However, the main problem with analyzing oligonucleotides by ECD is the requirement for positively charged precursor ions. Negative ion mode results in higher sensitivity due to the sugar-phosphate backbone, which undergoes facile deprotonation. EDD involves electron-ion reactions in negative mode and has been shown to provide fragmentation similar to ECD but for negatively charged peptide ions [6]. More extensive backbone fragmentation can be obtained with EDD compared to techniques based on vibrational excitation, resulting in enhanced peptide sequence coverage [7]. Here, we show that two different EDD configurations result in similar fragmentation patterns as ECD for hexamer oligonucleotides, allowing complete sequencing at enhanced sensitivity.

2.2. EXPERIMENTAL SECTION

2.2.1. Sample Preparation

Reversed-phase high performance liquid chromatography (HPLC) purified oligodeoxynucleotides (dA_6, dC_6, dG_6 and dT_6) were purchased from TriLink BioTechnologies, Inc. (San Diego, CA) as their crude sodium salts. Stock solutions of 0.1 mM in 0.1% formic acid (FA) (Acros Organics/Fisher, Fair Lawn, NJ) were prepared for desalting by C_{18} ZipTips (Millipore, Billerica, MA). Oligonucleotides were washed

with water containing 0.1 % FA 5 times and eluted in 2 x 5 µL 1:1 (v/v) acetonitrile:water (Fisher, Fair Lawn, NJ) with 0.1% FA and diluted 5-10 fold prior to electrospray ionization. The final electrospray solvent consisted of 1:1 (v/v) isopropanol:water (Fisher) with 10 mM ammonium acetate (Fisher). Reversed-phase HPLC purified 5'-phosphorylated dT_6 (pdT_6) and d(GCATAC) from TriLink BioTechnologies in ammonium salt were used without further purification at a concentration of 5-10 µM.

2.2.2. Fourier Transform Ion Cyclotron Resonance Mass Spectrometry

All experiments were performed with an actively shielded 7.0 T FT-ICR mass spectrometer with a quadrupole front-end (APEX-Q, Bruker Daltonics, Billerica, MA). Figure 2-1 shows a schematic diagram of this instrument. Oligonucleotide solutions were infused via an external Apollo electrospray ion source at a flow rate of 70 - 80 µL/h with the assistance of N_2 nebulizing gas. The off-axis sprayer was grounded and the inlet capillary was set to 4 kV for generation of oligonucleotide anions. N_2 drying gas (212 °C) was applied to assist desolvation of ESI droplets. Ions were accumulated in the first hexapole for 0.1 s, transferred through the mass-selective quadrupole (6-10 m/z isolation window), and mass-selectively accumulated in the second hexapole for 1-4 s. Ions were transferred through high-voltage ion optics and captured by gas-assisted dynamic (hollow cathode experiments) or static (filament experiments) trapping with argon as the collision gas in an Infinity ICR cell [8]. The experimental sequence up to the ICR cell fill was looped 2-4 times to achieve a precursor ion signal-to-noise ratio of 200-400. For static trapping, the potential was - 1.2 V and for dynamic trapping, the

initial potential was - 2.5 V followed by a 4 s pumping delay. Prior to excitation and detection (for dynamic trapping), the trapping voltages were lowered to - 0.8 V. Thus, the observed mass accuracies were higher for the hollow cathode experiments. All mass spectra were acquired with XMASS (version 6.1, Bruker Daltonics) in broadband mode from m/z 200 to 2,000 with 256 or 512k data points and summed over 20-32 scans. Data processing was performed with the MIDAS analysis software [9, 10]. A Hanning window function was applied and the data set was zero filled once prior to fast Fourier transformation followed by magnitude calculation. A peak list was generated and exported to Microsoft Excel for internal frequency-to-mass calibration with a two-term calibration equation [11] (the calibration could not be performed with MIDAS due to compatibility issues with the Bruker data files). The calculated masses of the $[M - 2H]^{2-}$ precursor ions and the charge-reduced $[M - 2H]^{-\bullet}$ species were used for calibration. Only assignments better than 20 ppm were included. The reason behind that relatively high tolerance is the deterioration of the mass accuracy as a result of the simultaneous storage of anions and electrons, which drastically deviates from ideal space charge conditions. Above m/z 700, product ions were only assigned if a clear ^{13}C isotopic peak was present. For lower mass ions, a combination of mass accuracy and ion abundance was used.

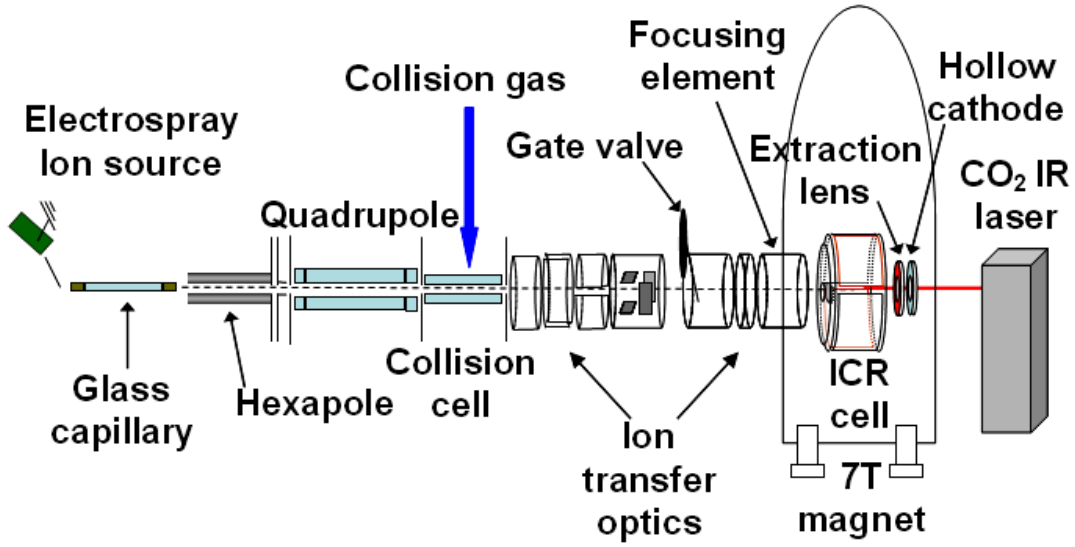

Figure 2-1. Schematic diagram of our 7 T ESI-Q-FT-ICR mass spectrometer.

2.2.3. Electron Detachment Dissociation

Our first EDD configuration consisted of a directly heated rhenium filament (3.3 A heating current), placed ~100 mm behind the ICR cell. The filament was positively biased (11 V), except for during the EDD event when the bias voltage was pulsed to - 21 to - 23 V for 0.2-1 s. Figure 2-2 shows a schematic diagram of the directly heated filament EDD configuration. An improved EDD configuration, installed at a later stage, utilizes an indirectly heated hollow dispenser cathode [12], which replaced the directly heated filament. A schematic diagram of the latter configuration is shown in Figure 2-3. The inner and outer diameters of the cathode are 3.5 and 7.6 mm, respectively, and the distance from the cathode to the cell is 88 mm. A heating current of 1.8 A was applied to a heater element located behind the cathode. During EDD, the cathode voltage was pulsed from 11 V to - (16 to 18) V for 1-2 s. A lens electrode (6

mm inner diameter) located immediately in front of the cathode was used to focus the electron beam.

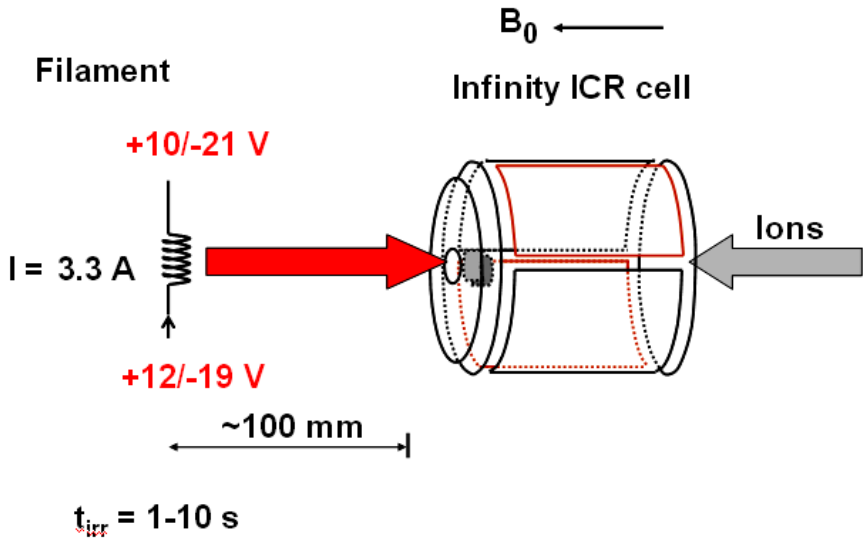

Figure 2-2. Schematic diagram of a directly heated filament EDD configuration.

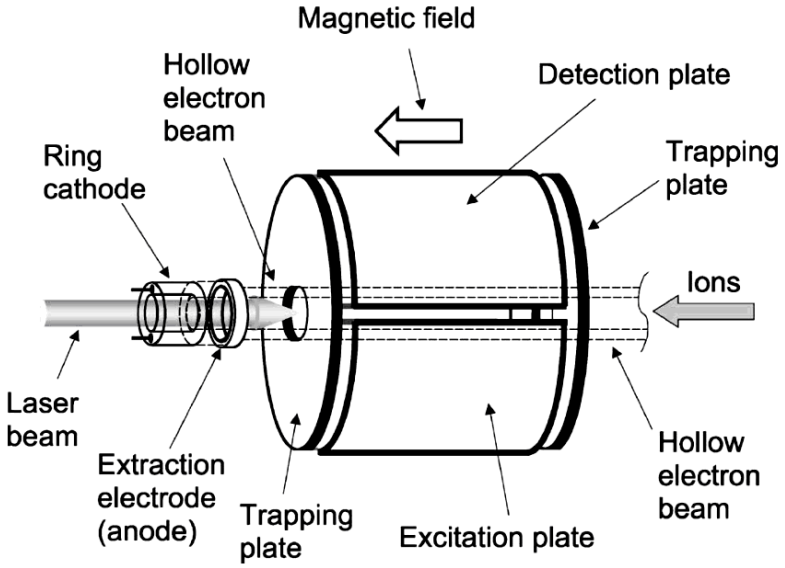

Figure 2-3. Schematic diagram of an indirectly heated hollow dispenser cathode EDD configuration. This figure is reproduced from reference [12] with permission.

2.3. RESULTS AND DISCUSSION

2.3.1. Filament Electron Detachment Dissociation of dA_6 Anions

An example of oligonucleotide EDD from our first directly-heated filament configuration is shown in Figure 2-4 and product ion assignments are given in Table 2-1. Doubly deprotonated dA_6 was dissociated at a filament bias voltage of - 21 V with an optimum irradiation time of 200 ms. Mainly even-electron *d*/*w*-type ions are observed (these ions cannot be distinguished based on mass alone due to the symmetry of dA_6). In fact, the entire series is present in the spectrum, allowing complete sequencing. In addition, one *a*/*z*-type radical ion (labeled $a_5^{-\bullet}$) and one (*c*/*x* - B) ion are seen. The presented spectrum is much more information-rich than our previous filament ECD data for dA_6, which only resulted in charge reduction to the $[M + 2H]^{+\bullet}$ radical species and very minor adenine base loss [13]. However, no base loss from charge-reduced dA_6 is observed in EDD. Thus, for dA_6, EDD has the added advantage (besides negative mode operation) of providing significantly more sequence information than ECD under similar conditions. In addition to the expected singly charged product ions discussed above, two doubly charged products are observed: d_5^{2-}/w_5^{2-} and $[M - B - 2H]^{2-}$. Such ions were also detected in recent ECD experiments and were suggested to be formed from a zwitterionic precursor ion structure [5]. In EDD, an alternative explanation could be direct dissociative electronic or vibrational excitation (electron-induced dissociation, EID [14]) as an accompanying pathway. However, further experiments are needed to fully elucidate the origin of these ions. The two rather abundant doubly charged peaks observed at m/z 964 and 989, respectively, are not present in rf-only mode and are hypothesized to result from ion-molecule reactions in the quadrupole.

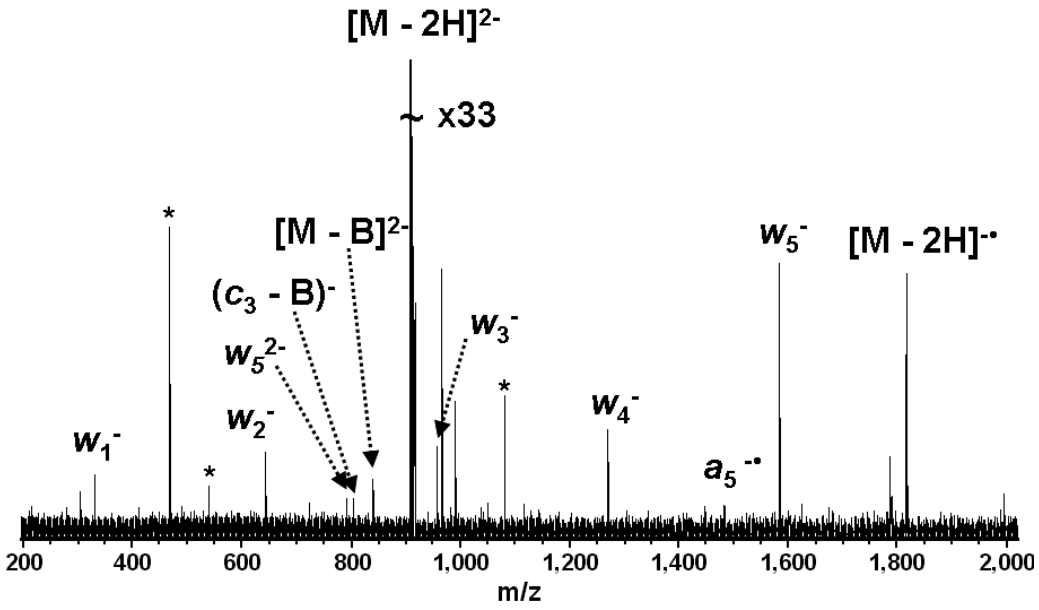

Figure 2-4. EDD (21 eV electrons, 200 ms irradiation, 30 scans) of dA_6 with a heated filament electron source. A complete *d*/*w* (only one label is given) ion series is observed, allowing full sequencing of the oligonucleotide. Electronic noise spikes are labeled with asterisks.

Table 2-1 Product ions observed following directly heated filament EDD (200 ms irradiation, - 21 V bias, 30 scans) of dA_6. Ions labeled *w* can also be *d* ions, ions labeled *a* can also be *z* ions, and ions labeled *c* can also be *x* ions.

Observed m/z	Calculated m/z	Assignment	Error (ppm)
330.0669	330.0609	w_1^-	18
643.1287	643.1185	w_2^-	16
723.1625	723.1446	$(a_3 - A)^-$?	25
790.6536	790.6420	w_5^{2-}	15
803.1137	803.1110	$(c_3 - A)^-$	3.4

839.6727	839.6604	$[M - A - 2H]^{2-}$	- 15
907.1876	907.1876	$[M - 2H]^{2-}$	Calibrant
914.2065		Unknown^{2-}	
956.1894	956.1761	w_3^-	14
964.1996		Unknown^{2-}	
989.1968		Unknown^{2-}	
1269.249	1269.234	w_4^-	12
1483.323	1483.307	$a_5^{-\bullet}$	11
1582.309	1582.291	w_5^-	11
1786.378	1786.380	$[M - CO - 2H]^{-\bullet}$?	- 1.1
1814.375	1814.375	$[M - 2H]^{-\bullet}$	Calibrant

Comparison of our EDD data to previous radical oligonucleotide anion dissociation experiments reveals similarities as well as differences. Electron transfer from CCl_3^+ followed by CAD of $[dA_3 - 2H]^{-\bullet}$ in an ion trap resulted mainly in *d*/*w* ions, as in EDD [15]. In addition, one *a*/*z* ion was observed although as an even-electron species rather than the radical *a*/*z* ion observed in EDD. Transfer of a hydrogen atom should be facilitated at the longer activation period during ion trap CAD compared to EDD. In stark contrast to EDD, the ion trap experiments resulted in sugar cross-ring cleavage, which may again be explained by the longer activation period, allowing for secondary fragmentation processes. Similar cross-ring cleavage products were also observed in 100 keV collisions of $[dA_5 - 2H]^{2-}$ with He gas, which results in abundant charge-reduced radical species from electron loss [16]. In the latter experiments, similar to EDD and ion trap CAD of odd-electron ions, *d*/*w* ions dominate and *a*/*z* ions are observed, in contrast to low-energy CAD of even-electron ions. In addition, high-energy CAD experiments yield (*a*/*z* - B) ions, similar to EDD. However, in contrast to EDD and ion trap CAD of odd-electron ions but similar to ECD, base loss from the charge-reduced species is observed. High energy collisions also result in a doubly charged $[M - B - 2H]^{2-}$ ion that can be formed as explained above for EDD.

2.3.2. Hollow Cathode Electron Detachment Dissociation of dA_6 Anions

An improved EDD configuration, consisting of an indirectly heated hollow dispenser cathode [12], has replaced the directly heated filament used above. The major advantage of a dispenser cathode over a filament is the high electron generation efficiency and narrow energy distribution [17]. Figure 2-5 shows an EDD spectrum of dA_6, obtained by applying a - 17 V bias voltage to the hollow dispenser cathode for 1 second. Product ion assignments are listed in Table 2-2. The spectrum shows much more extensive fragmentation compared to the filament EDD above, and the relative product ion abundances are higher. As for the filament, the complete *d*/*w* ion series dominates the spectrum. One additional radical *a*/*z* ion and two additional (*c*/*x* - B) ions are observed. In addition to those species, four (*a*/*z* - B) ions are detected. With the filament, one possible (*a*/*z* - B) ion was seen but with a rather high (25 ppm) mass error, rendering the assignment uncertain. Other ions not present in the filament spectrum include four *c*/*x* products and three (*d*/*w* - B) products. Doubly charged d_5^{2-}/w_5^{2-} and $[M - B - 2H]^{2-}$ ions are detected at higher relative abundance than in filament EDD. Thus, it is more likely those species result from an EID-type or electronic excitation process rather than being formed from a zwitterion precursor because the electrospray and ion transfer conditions were identical in the two cases.

The hollow cathode EDD spectrum is very similar to our previous ECD data obtained with a solid dispenser cathode electron source [5]. EDD results in three more *c*/*x*-type ions and one more (*d*/*w* - B) ion compared to ECD. In addition, the detected *a*/*z* ions are radicals in EDD and even-electron species in ECD. However, because the ECD experiments were performed on a different instrument with different cell pressure

and ion number, it is difficult to make a direct comparison. Neither ion-ion reactions in an ion trap [15], nor high energy collisions with helium [16] resulted in *c*/*x*, (*c*/*x* - B), or (*d*/*w* - B) ions, illustrating unique behavior in EDD. Thus, use of a dispenser cathode provides additional fragmentation pathways and higher efficiency EDD.

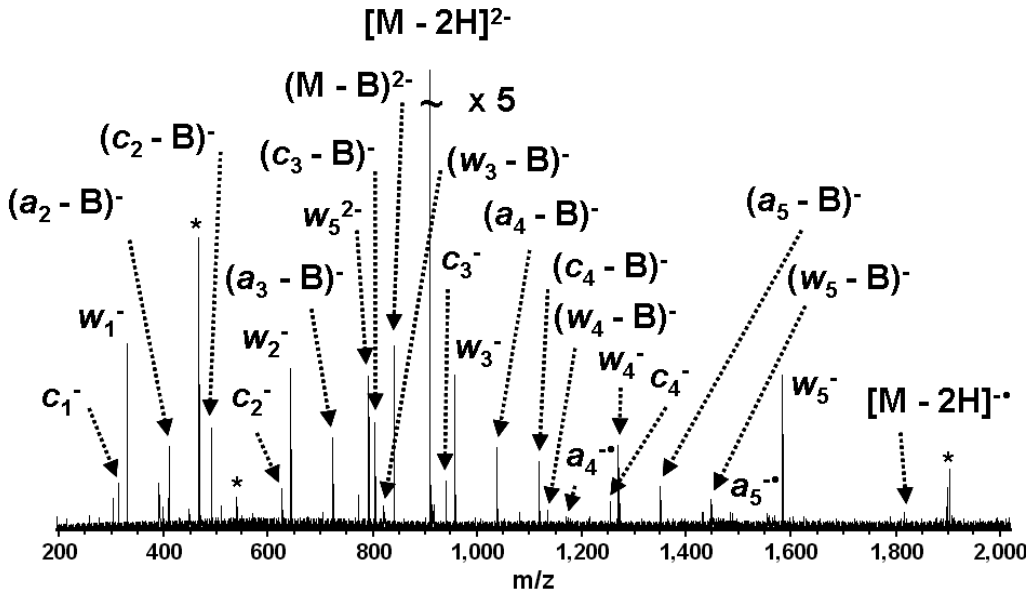

Figure 2-5. EDD (17 eV electrons, 1 s irradiation, 30 scans) of dA_6 with an indirectly heated hollow dispenser cathode electron source. Much more extensive fragmentation is observed compared to the filament EDD shown in Figure 2-4. Only one label is given for *d*/*w*, *c*/*x* and *a*/*z* ion series. Increases in fragmentation efficiency and sensitivity are also evident. Electronic noise spikes are labeled with asterisks.

Table 2-2. Product ions observed following indirectly heated dispenser cathode EDD (1 s irradiation, - 17 V bias, 30 scans) of dA_6. Ions labeled *w* can also be *d* ions, ions labeled *a* can also be *z* ions, and ions labeled *c* can also be *x* ions.

Observed m/z	Calculated m/z	Assignment	Error (ppm)
312.0510	312.0503	c_1^-	2.2
330.0617	330.0609	w_1^-	2.4
410.0879	410.0870	$(a_2 - A)^-$	2.2
490.0541	490.0534	$(c_2 - A)^-$	1.4
625.1082	625.1079	c_2^-	0.5
643.1193	643.1185	w_2^-	1.2
723.1451	723.1446	$(a_3 - A)^-$	0.7
790.6420	790.6420	w_5^{2-}	< 0.1
803.1114	803.1110	$(c_3 - A)^-$	0.5
821.1216	821.1216	$(w_3 - A)^-$	< 0.1
839.6606	839.6604	$(M - A - 2H)^{2-}$	0.2
907.1876	907.1876	$[M - 2H]^{2-}$	Calibrant
938.1633	938.1655	c_3^-	- 2.4
956.1764	956.1761	w_3^-	0.3
1036.202	1036.202	$(a_4 - A)^-$	< 0.1
1116.168	1116.169	$(c_4 - A)^-$	- 0.9
1134.179	1134.179	$(w_4 - A)^-$	< 0.1
1170.251	1170.249	$a_4^{-\bullet}$	1.7
1251.222	1251.223	c_4^-	- 0.8
1269.234	1269.234	w_4^-	< 0.1
1349.245	1349.260	$(a_5 - A)^-$	- 11
1447.233	1447.237	$(w_5 - A)^-$	- 2.8
1483.308	1483.307	$a_5^{-\bullet}$	0.7
1582.293	1582.291	w_5^-	1.3
1814.375	1814.375	$[M - 2H]^{-\bullet}$	Calibrant

2.3.3. Hollow Cathode Electron Detachment Dissociation of dC_6 Anions

Inspired by the improved EDD of dA_6 obtained with the hollow dispenser cathode, we performed similar experiments for the remaining set of hexamer homodeoxyoligonucleotides. Figure 2-6 shows the EDD spectrum from dC_6 and the product ion assignments are given in Table 2-3. The overall appearance of the dC_6 EDD

spectrum is similar to the one obtained for dA_6 with the dispenser cathode. Again, the entire *d*/*w* ion series is present as well as one complementary radical *a*/*z* ion and several (*a*/*z* - B), (*c*/*x* - B), and (*d*/*w* - B) ions. The most abundant product ion corresponds to doubly deprotonated d_5/w_5 and a high magnitude $[M - B - 2H]^{2-}$ ion is also observed. Because cytosine has a higher proton affinity than adenine [18], polydC is more likely to have a zwitterion structure than polydA, correlating with our observations. However, the discussion for dA_6 above suggested more probable direct dissociative vibrational/electronic excitation as the source of doubly charged products. We believe electronic excitation is more probable than vibrational excitation because IRMPD (i.e. vibrational excitation) of cytidine-containing oligonucleotides display facile cytosine loss, which does not occur in EDD. The dC_6 EDD spectrum also contains one (*d*/*w* + H_2O) ion. Similar species have been observed in ECD of polydC and were suggested to be formed via a rearrangement involving the terminal hydroxyl groups [13].

Liu et al. investigated a cytidine-rich oligonucleotide, d(GCCCC), with high energy CAD [16]. As for dA_5, *d*/*w* ions dominate the spectrum, in correlation with our EDD data. They also detected three even-electron *a*/*z* ions and two (*a*/z - B) ions. However, in contrast to EDD, they observed sugar cross-ring cleavage and neutral cytosine loss from the charge-reduced species, which can be explained by accompanying vibrational excitation.

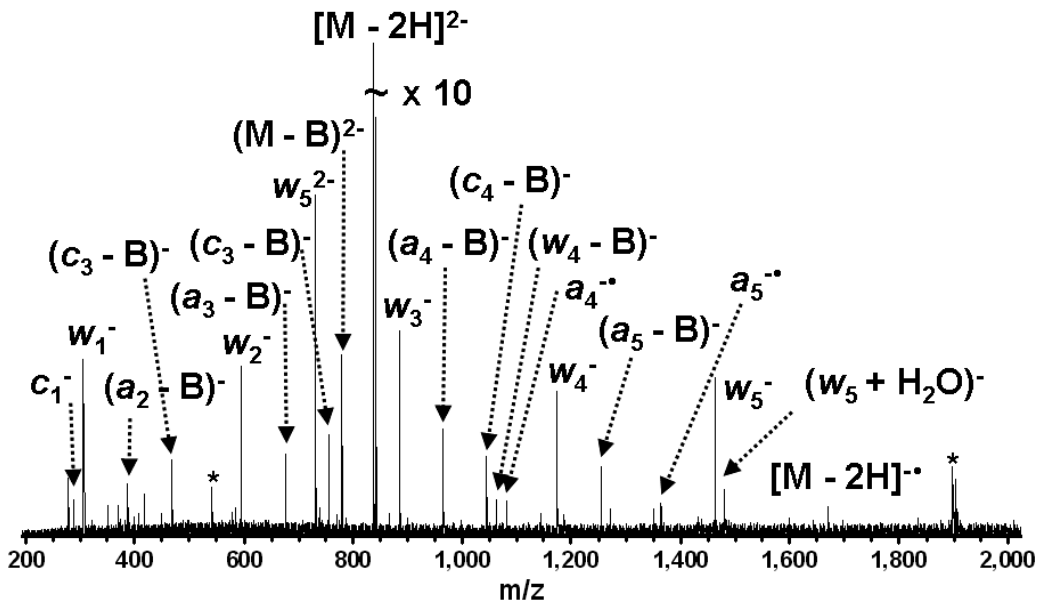

Figure 2-6. EDD (17 eV electrons, 1 s irradiation, 30 scans) of dC_6 with an indirectly heated hollow dispenser cathode electron source. Only one label is given for *d*/*w*, *c*/*x* and *a*/*z* ion series. The spectrum is similar to EDD of dA_6, see Figure 2-5. However, more abundant doubly charged products are detected, possibly due to the higher proton affinity of cytosine compared to adenine, promoting a zwitterionic gas-phase structure. Electronic noise spikes are labeled with asterisks.

Table 2-3. Product ions observed following indirectly heated dispenser cathode EDD (1 s irradiation, - 17 V bias, 30 scans) of dC_6. Ions labeled *w* can also be *d* ions, ions labeled *a* can also be *z* ions, and ions labeled *c* can also be *x* ions.

Observed m/z	Calculated m/z	Assignment	Error (ppm)
288.0394	288.0390	c_1^-	1.4
306.0499	306.0495	w_1^-	1.3
386.0763	386.0759	$(a_2 - C)^-$	1.0

466.0422	466.0422	$(c_2 - C)^-$	< 0.1
595.0961	595.0959	w_2^-	0.3
675.1224	675.1223	$(a_3 - C)^-$	0.2
730.6138	730.6139	w_5^{2-}	- 0.1
755.0882	755.0886	$(c_3 - C)^-$	- 0.5
779.6323	779.6323	$[M - C - 2H]^{2-}$	< 0.1
835.1539	835.1539	$[M - 2H]^{2-}$	Calibrant
884.1427	884.1423	w_3^-	0.5
964.1686	964.1687	$(a_4 - C)^-$	- 0.1
1044.135	1044.135	$(c_4 - C)^-$	< 0.1
1062.147	1062.146	$(w_4 - C)^-$	0.9
1173.189	1173.189	w_4^-	< 0.1
1253.214	1253.215	$(a_5 - C)^-$	- 0.8
1363.253	1363.251	$a_5^{-\bullet}$	1.5
1462.238	1462.235	w_5^-	2.1
1480.247	1480.246	$(w_5 + H_2O)^-$	0.7
1670.307	1670.307	$[M - 2H]^{-\bullet}$	Calibrant

2.3.4. Hollow Cathode Electron Detachment Dissociation of dG_6 Anions

Figure 2-7 shows the spectrum obtained from hollow cathode EDD of dG_6 and Table 2-4 lists the corresponding assigned product ions. The mass spectrum resulting from EDD of dG_6 is very similar to EDD of dA_6 and dC_6 in that all *d*/*w* ions are observed. In addition, four (*a*/*z* - B) and one (*c*/*x* - B) ion are detected. However, no *a*/*z* or *c*/*x* ions are seen, correlating with the labile nature of guanine. Depurination is a dominant fragmentation pathway in vibrational excitation of nucleic acids [19]. Also, facile guanine loss is observed in ECD of both DNAs [5, 13] and PNAs [20]. Base loss from charge-reduced dG_6 is seen in EDD, in contrast to dA_6 and dC_6. Finally, one product ion is observed, corresponding to (*d*/*w* - B) with an additional loss of water. A combination of water and base loss was previously observed from the precursor ions in ECD of dG_5 [5, 13].

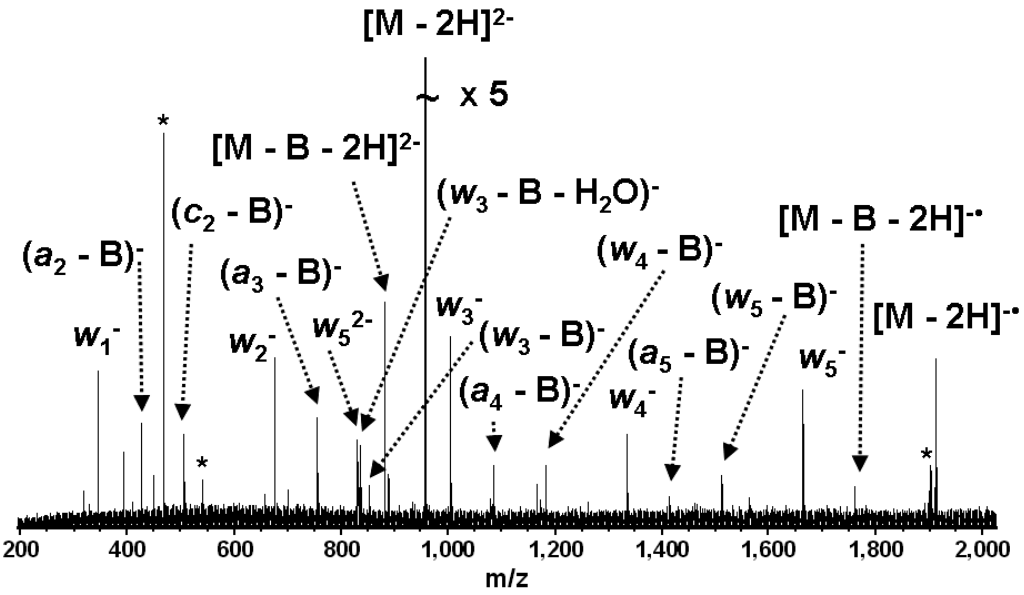

Figure 2-7. EDD (17 eV electrons, 1 s irradiation, 30 scans) of dG_6 with an indirectly heated hollow dispenser cathode electron source. The spectrum is similar to EDD of dA_6 and dC_6, see Figures 2-5 and 2-6. However, no *a*/*z*, or *c*/*x* ions are observed, correlating with the labile nature of guanine. Only one label is given for *d*/*w*, *c*/*x* and *a*/*z* ion series. Electronic noise spikes are labeled with asterisks.

Table 2-4. Product ions observed following indirectly heated dispenser cathode EDD (1 s irradiation, - 17 V bias, 30 scans) of dG_6. Ions labeled *w* can also be *d* ions, ions labeled *a* can also be *z* ions, and ions labeled *c* can also be *x* ions.

Observed m/z	Calculated m/z	Assignment	Error (ppm)
346.0563	346.0558	w_1^-	1.4
426.0824	426.0820	$(a_2 - G)^-$	0.9
506.0484	506.0483	$(c_2 - G)^-$	0.2
675.1090	675.1083	w_2^-	1.0

755.1356	755.1345	$(a_3 - G)^-$	1.5
830.6286	830.6293	w_5^{2-}	- 0.8
835.1014	835.1008	$(w_3 - G - H_2O)^-$	0.7
853.1105	853.1114	$(w_3 - G)^-$	-1.1
879.6476	879.6477	$(M - G - 2H)^{2-}$	- 0.1
955.1724	955.1724	$[M - 2H]^{2-}$	Calibrant
1004.161	1004.161	w_3^-	< 0.1
1084.188	1084.187	$(a_4 - G)^-$	0.9
1182.165	1182.164	$(w_4 - G)^-$	0.9
1333.217	1333.213	w_4^-	3.0
1413.245	1413.240	$(a_5 - G)^-$	3.5
1511.220	1511.216	$(w_5 - G)^-$	2.7
1662.267	1662.266	w_5^-	0.6
1759.292	1759.295	$[M - G - 2H]^{-\bullet}$	- 1.7
1910.344	1910.344	$[M - 2H]^{-\bullet}$	Calibrant

2.3.5. Hollow Cathode Electron Detachment Dissociation of dT_6 Anions

Our current EDD approach allows analysis of thymidine-rich oligonucleotides, which was not possible with ECD due to the low proton affinity of thymine nucleobases. Although promotor and coding regions in DNA have been shown to have a high GC content, we believe it is important to establish the effect of each nucleotide individually before ECD/EDD can be widely applied to nucleic acid characterization. The hollow cathode EDD spectrum from dT_6 is shown in Figure 2-8 and the assigned product ions are listed in Table 2-5. As for the other homooligodeoxynucleotides, the entire *d*/*w* ion series is present, easily allowing complete sequencing. Three complementary *a*/*z* ions are also detected. For a_3, a mixture of even- and odd-electron ions is observed, see the inset in Figure 2-8. Other detected ions include four *c*/*x* ions, four (*a*/*z* - B), and two doubly charged *d*/*w* ions. As polydT is unlikely to exist as a zwitterion species due to its low proton affinity, the latter ions are most likely formed through direct dissociative electronic or vibrational excitation. Finally, for dT_6, a minor species corresponding to sugar cross-ring cleavage, resulting in a so-called Σ ion [16], is observed.

Gross, Hillenkamp and co-workers have undertaken extensive characterization of T-rich oligonucleotides to elucidate their fragmentation mechanism in CAD [2, 21-24]. In MALIDI PSD spectra of singly deprotonated d(TGTT), d(TTGT), d(GTTT), d(TTTG), d(TGCT), and d(TGTTCT) they observed several *c*, *x*, *a*, and *z*-type ions [21], in analogy with EDD. As PSD is induced by high-energy collisions [25], electronic excitation is plausible.

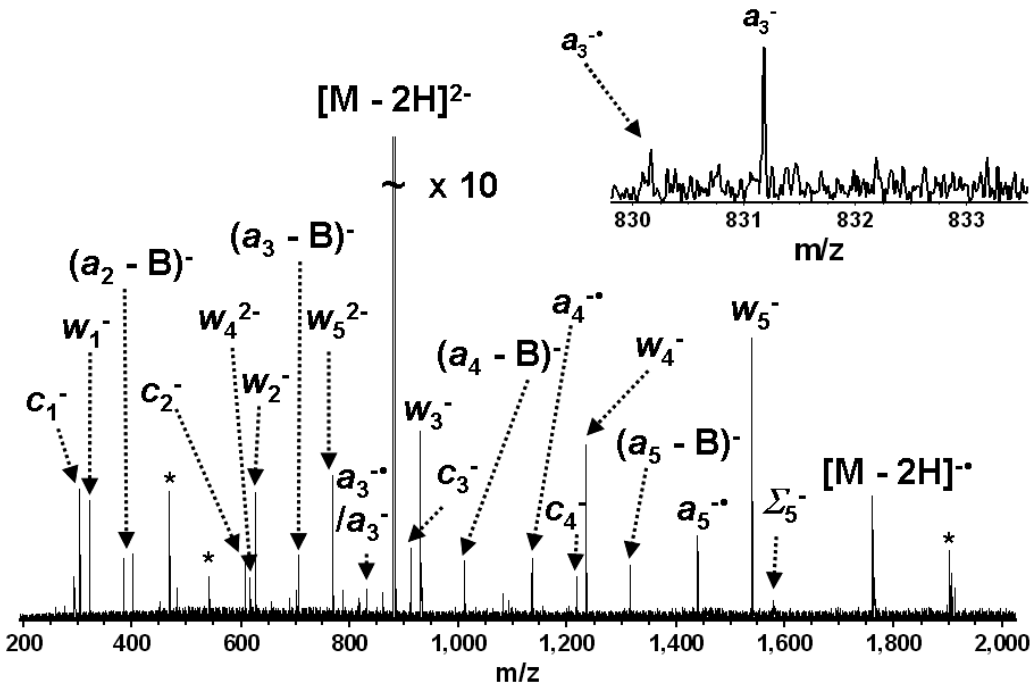

Figure 2-8. EDD (17 eV electrons, 1 s irradiation, 20 scans) of dT_6 with an indirectly heated hollow dispenser cathode electron source. The data is similar to EDD of dA_6, dC_6, and dG_6. The inset illustrates the mixture of radical and even-electron species for the a_3/z_3 ion. Only one label is given for *d*/*w*, *c*/*x* and *a*/*z* ion series. Electronic noise spikes are labeled with asterisks.

Table 2-5. Product ions observed following indirectly heated dispenser cathode EDD (1 s irradiation, - 17 V bias, 20 scans) of dT_6. Ions labeled *w* can also be *d* ions, ions labeled *a* can also be *z* ions, and ions labeled *c* can also be *x* ions.

Observed m/z	Calculated m/z	Assignment	Error (ppm)
303.0393	303.0387	c_1^-	2.0
321.0498	321.0493	w_1^-	1.6
401.0765	401.0755	$(a_2 - T)^-$	2.5
607.0857	607.0847	c_2^-	1.6
616.0902	616.0901	w_4^{2-}	0.2
625.0962	625.0953	w_2^-	1.4
705.1222	705.1215	$(a_3 - T)$-	1.0
768.1132	768.1136	w_5^{2-}	- 0.5
785.0895	785.0879	$(c_3 - T)^-$	2.0
830.1534	830.1566	$a_3^{-\bullet}$	- 3.9
831.1655	831.1644	a_3^-	1.3
880.1529	880.1529	$[M - 2H]^{2-}$	Calibrant
911.1306	911.1308	c_3^-	- 0.2
929.1417	929.1414	w_3^-	0.3
1009.112	1009.168	$(a_4 - T)^-$	- 55
1089.134	1089.134	$(c_4 - T)^-$	< 0.1
1134.202	1134.202	$a_4^{-\bullet}$	< 0.1
1215.179	1215.177	c_4^-	1.7
1233.188	1233.187	w_4^-	0.8
1313.209	1313.214	$(a_5 - T)^-$	- 3.8
1438.248	1438.249	$a_5^{-\bullet}$	- 0.7
1537.232	1537.233	w_5^-	- 0.7
1760.305	1760.305	$[M - 2H]^{-\bullet}$	Calibrant

2.3.6. Hollow Cathode Electron Detachment Dissociation of 5'-phosphorylated dT_6

In order to clarify whether the most prevalent EDD products, *d*/*w* ions, are *w* or *d* ions, or a mixture of both species, we investigated the EDD fragmentation pathways of non-symmetric 5'-phosphorylated dT_6. The hollow cathode EDD spectrum of pdT_6 is shown in Figure 2-9 and product ion assignments are listed in Table 2-6. EDD of pdT_6 results in complete *d* and *w* ion series, three $a^{\bullet}$, four (*a* - B), and one *c* ion.

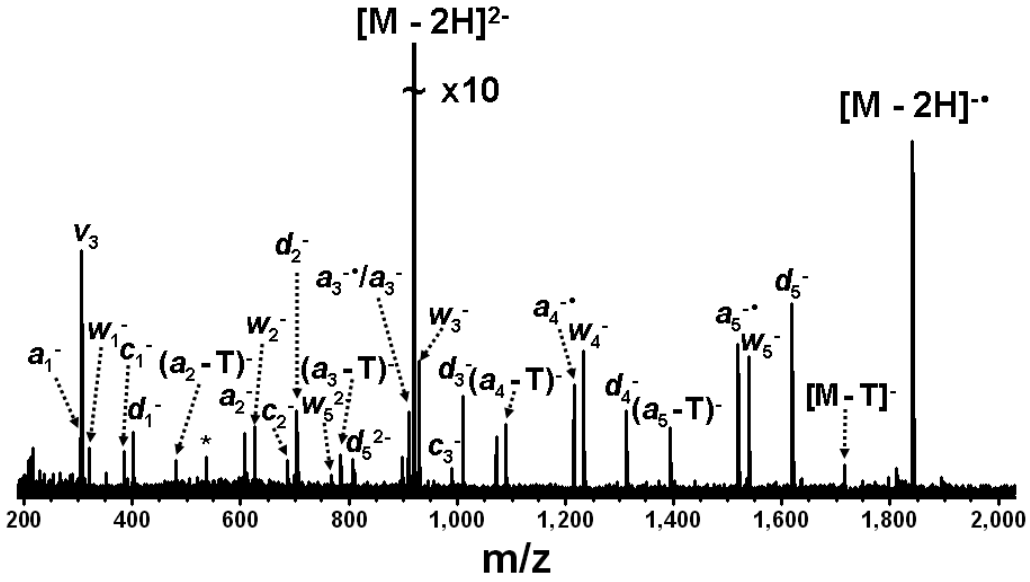

Figure 2-9. EDD of pdT_6 (2 s irradiation, - 18.1 V bias, 32 scans) results in complete *d* and *w* ion series. For $a^{\bullet}$ ions, complementary to the *w* ions, radical-mediated nucleobase loss is observed. Electronic noise spikes are labeled with asterisks.

$a^{\bullet}$ ions, complementary to even-electron *w* ions, are observed. However, we did not detect $z^{\bullet}$ ions, complementary to the *d* ions. The latter finding may be rationalized by the proposed structures of $a^{\bullet}$ and $z^{\bullet}$ ions [13] with different radical environments. For $a^{\bullet}$ ions, the proximity of the nucleobase can result in radical-mediated nucleobase loss, which is observed. However, other pathways are available for $z^{\bullet}$ ions that may render them less stable.

Table 2-6. Product ions observed following indirectly heated dispenser cathode EDD (2 s irradiation, - 18.1 V bias, 32 scans) of pdT_6. Ions labeled a_4 and a_5 can also be x_4 and x_5 ions, and w_5 can also be b_5 as they have identical mass.

Observed m/z	Calculated m/z	Assignment	Error (ppm)
303.0381	303.0387	a_1^-	-2.0
321.0489	321.0493	w_1^-	-1.3
401.0151	401.0156	d_1^-	1.3
481.0407	481.0418	$(a_2 - T)^-$	-2.3
607.0847	607.0847	a_2^-	< 0.1
625.0944	625.0953	w_2^-	-1.4
687.0513	687.0510	c_2^-	0.4
705.0614	705.0616	d_2^-	-0.3
768.1115	768.1131	w_5^{2-}	-2.1
785.0864	785.0880	$(a_3 - T)^-$	-2.0
808.0974	808.0962	d_5^{2-}	1.5
910.1261	910.1230	$a_3^{-\bullet}$	3.4
911.1294	911.1308	a_3^-	-1.5
920.1361	920.1361	$[M - 2H]^{2-}$	Calibrant
929.1407	929.1413	w_3^-	0.4
991.0937	991.0971	c_3^-	-3.4
1009.108	1009.108	d_3^-	< 0.1
1089.132	1089.134	$(a_4 - T)^-$	-1.8
1214.169	1214.169	$a_4^{-\bullet}$	< 0.1
1233.187	1233.187	w_4^-	< 0.1
1313.157	1313.154	d_4^-	2.3
1393.191	1393.180	$(a_5 - T)^-$	7.9
1518.217	1518.215	$a_5^{-\bullet}$	1.3
1537.236	1537.233	w_5^-	2.0
1617.202	1617.200	d_5^-	1.2
1773.336	1773.336	$[M - 2H]^{-\bullet}$	Calibrant

2.3.7. Hollow Cathode Electron Detachment Dissociation of d(GCATAC)

We also performed hollow cathode EDD of d(GCATAC), which contains all four deoxynucleotides. Figure 2-10 shows the hollow cathode EDD spectrum and product ion assignments are listed in Table 2-7. This oligonucleotide is also asymmetric,

thereby allowing us to distinguish between *d*/*w*, *a*/*z*, etc. ions. For example, both d_5 and w_5 ions are present. In addition, a radical z_5 ion but no a_5 ion is detected. Thus, it is likely that the assigned *d*/*w*, *a*/*z*, etc. ions for the homooligonucleotides discussed above are mixtures of two different species. Two *d*-type ions were observed by Liu et al. in high energy CAD of d(GCCCC) [16]. However, those *d* ions were of lower abundance than the detected *w*-type ions in the same mass range. Assuming an analogy with EDD, both the d_2/w_2 and d_4/w_4 species should contain contributions from the *w* ion series and complete sequencing is again possible. For d(GCATAC), a doubly charged w_5 ion as well as doubly charged species corresponding to both adenine and cytosine base loss are observed.

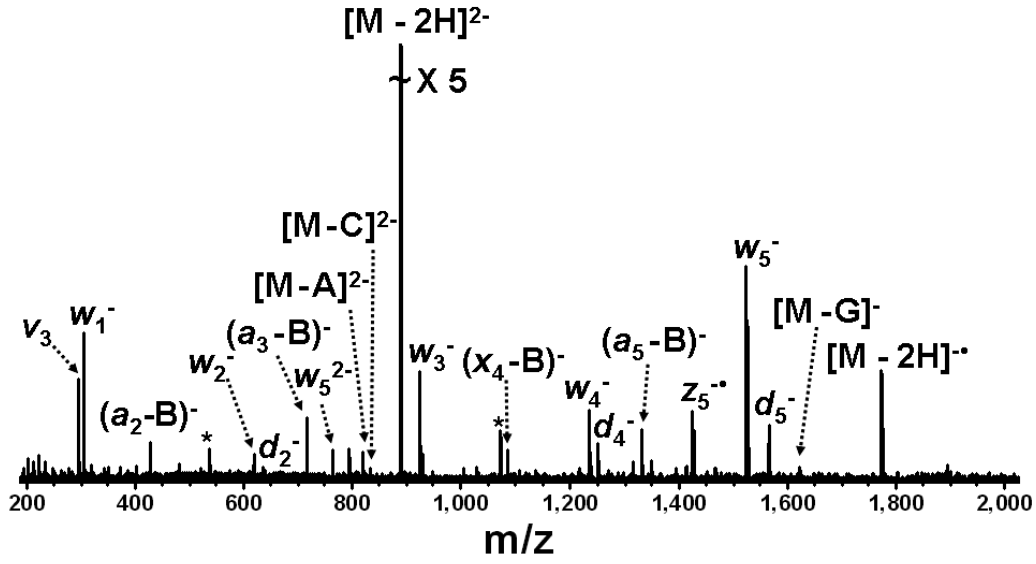

Figure 2-10. EDD of d(GCATAC) (2 s irradiation, - 18.1 V bias, 32 scans) results in a complete *w* ion series, and three *d* ions. The latter ions are generally not observed in tandem mass spectrometry, such as CAD and IRMPD. Electronic noise spikes are labeled with asterisks.

Table 2-7. Product ions observed following indirectly heated dispenser cathode EDD (2 s irradiation, - 18.1 V bias, 32 scans) of d(GCATAC).

Observed m/z	Calculated m/z	Assignment	Error (ppm)
306.0472	306.0495	w_1^-	-7.5
426.0803	426.0820	$(a_2 - B)^-$	-4.0
619.1053	619.1071	w_2^-	-2.9
635.0982	635.1021	d_2^-	-6.1
715.1281	715.1283	$(a_3 - B)^-$	-0.3
762.1230	762.1249	w_5^{2-}	-2.5
819.1414	819.1408	$(M - A - 2H)^{2-}$	0.7
831.1485	831.1464	$(M - C - 2H)^{2-}$	2.5
886.6680	886.6680	$[M - 2H]^{2-}$	Calibrant
923.1536	923.1532	w_3^-	0.4
1083.158	1083.146	$(x_4 - B)^-$	11.1
1236.216	1236.211	w_4^-	4.0
1252.213	1252.206	d_4^-	5.6
1332.233	1332.232	$(a_5 - T)^-$	0.8
1426.284	1426.272	$z_5^{-\bullet}$	8.4
1525.269	1525.257	w_5^-	7.9
1565.265	1565.263	d_5^-	1.3
1623.312	1623.294	$(M - G - H)^-$	11.1
1773.336	1773.336	$[M - 2H]^{-\bullet}$	Calibrant

2.4. CONCLUSION

To our knowledge, this chapter demonstrates for the first time EDD experiments performed with a standard heated filament electron source. The achieved oligonucleotide data shows more extensive fragmentation than previous ECD experiments under similar conditions. Implementation of a hollow dispenser cathode electron source increases EDD fragmentation efficiency and sensitivity. In particular, we demonstrate that EDD provides information-rich fragmentation patterns complementary to vibrational excitation for small oligonucleotides. For example, *d*-type ions and radical *a* and *z*-type ions, absent from CAD and IRMPD spectra, are

commonly observed as well as *c*/*x* and (*c*/*x* - B) ions. Complete oligonucleotide sequencing is easily achieved. The observed fragmentation is very similar to dispenser cathode ECD of the same species and, to some extent, to spectra obtained from other techniques involving dissociation of oligonucleotide radical ions. In contrast to previous high energy CAD and ion trap CAD of oligonucleotide radicals, we only observe minor sugar cross ring cleavage, possibly due to the shorter time-scale of EDD, minimizing secondary fragmentation. In comparison to ECD, enhanced sensitivity is achieved through negative ion mode operation (on average a 10-fold improvement so far in terms of concentration sensitivity). The detection of doubly charged product ions from doubly charged precursors indicates that EDD conditions promote direct dissociative electronic excitation although other explanations for the formation of those ions are also discussed.

2.5. BIBLIOGRAPHY

1. Null, A. P.; Muddiman, D. C. Perspectives on the Use of Electrospray Ionization Fourier Transform Ion Cyclotron Resonance Mass Spectrometry for Short Tandem Repeat Genotyping in the Post-Genome Era. *J. Mass Spectrom.* **2001,** *36*, 589-606.
2. Wang, Z.; Wan, K. X.; Ramanathan, R.; Taylor, J. S.; Gross, M. L. Structure and Fragmentation Mechanisms of Isomeric T-rich Oligodeoxynucleotides: A Comparison of Four Tandem Mass Spectrometric Methods. *J. Am. Soc. Mass Spectrom.* **1998,** *9*, 683-691.
3. Wu, J.; McLuckey, S. A. Gas-phase Fragmentation of Oligonucleotide Ions. *Int. J. Mass Spectrom.* **2004,** *237*, 197-241.

4. Sannes-Lowery, K. A.; Hofstadler, S. A. Sequence Confirmation of Modified Oligonucleotides using IRMPD in the External Reservoir of an Electrospray Ionization Fourier Transform Ion Cyclotron Mass Spectrometer. *J. Am. Soc. Mass Spectrom.* **2003,** *14*, 825-833.
5. Schultz, K. N.; Håkansson, K. Rapid Electron Capture Dissociation of Mass-Selectively Accumulated Oligodeoxynucleotide Dications. *Int. J. Mass Spectrom.* **2004,** *234*, 123-130.
6. Budnik, B. A.; Haselmann, K. F.; Zubarev, R. A. Electron Detachment Dissociation of Peptide Di-anions: an Electron-hole Recombination Phenomenon. *Chem. Phys. Lett.* **2001,** *342*, 299-302.
7. Haselmann, K. F.; Budnik, B. A.; Kjeldsen, F.; Nielsen, M. L.; Olsen, J. V.; Zubarev, R. A. Electronic Excitation gives Informative Fragmentation of Polypeptide Cations and Anions. *Eur. Mass Spectrom.* **2002,** *8*, 117-121.
8. Caravatti, P.; Allemann, M. The Infinity Cell: A New Trapped-ion Cell with Radiofrequency Covered Trapping Electrodes for Fourier Transform Ion Cyclotron Resonance Mass Spectrometry. *Org. Mass Spectrom.* **1991,** *26*, 514-518.
9. Senko, M. W.; Canterbury, J. D.; Guan, S.; Marshall, A. G. A High-Performance Modular Data System for FT-ICR Mass Spectrometry. *Rapid Commun. Mass Spectrom.* **1996,** *10*, 1839-1844.
10. Blakney, G. T.; Hendrickson, C. L.; Emmett, M. R.; Marshall, A. G., Improved MIDAS Data Station for FT-ICR Mass Spectrometry. In *Proceedings of 50th ASMS Conference on Mass Spectrometry and Allied Topics*, Orlando, FL, 2002.

11. Ledford, E. B., Jr.; Rempel, D. L.; Gross, M. L. Space Charge Effects in Fourier Transform Mass Spectrometry Mass Calibration. *Anal. Chem.* **1984,** *56*, 2744-2748.
12. Tsybin, Y. O.; Witt, M.; Baykut, G.; Kjeldsen, F.; Hakansson, P. Combined Infrared Multiphoton Dissociation and Electron Capture Dissociation with a Hollow Electron Beam in Fourier Transform Ion Cyclotron Resonance Mass Spectrometry. *Rapid Commun. Mass Spectrom.* **2003,** *17*, 1759-1768.
13. Håkansson, K.; Hudgins, R. R.; Marshall, A. G.; O'Hair, R. A. J. Electron Capture Dissociation and Infrared Multiphoton Dissociation of Oligodeoxynucleotide Dications. *J. Am. Soc. Mass Spectrom.* **2003,** *14*, 23-41.
14. Cody, R. B.; Freiser, B. S. Electron Impact Excitation of Ions from Organics: an Alternative to Collision Induced Dissociation. *Anal. Chem.* **1979,** *51*, 547 - 551.
15. McLuckey, S. A.; Stephenson, J. L.; O'Hair, R. A. J. Decompositions of Odd- and Even-electron Anions Derived from Deoxypolyadenylates. *J. Am. Soc. Mass Spectrom.* **1997,** *8*, 148-154.
16. Liu, B.; Hvelplund, P.; Brondsted Nielsen, S.; Tomita, S. Electron Loss and Dissociation in High Energy Collisions between Multiply Charged Oligonucleotide Anions and Noble Gases. *Int. J. Mass Spectrom.* **2003,** *230*, 19-24.
17. Tsybin, Y. O.; Hakansson, P.; Budnik, B. A.; Haselmann, K. F.; Kjeldsen, F.; Gorshkov, M.; Zubarev, R. A. Improved Low-energy Electron Injection Systems for High Rate Electron Capture Dissociation in Fourier Transform Ion Cyclotron Resonance Mass Spectrometry. *Rapid Commun. Mass Spectrom.* **2001,** *15*, 1849-1854.

18. Vrkic, A. K.; O'Hair, R. A. J.; Foote, S.; Reid, G. E. Fragmentation Reactions of all 64 Protonated Trimer Oligodeoxynucleotides and 16 Mixed Base Tetramer Oligodeoxynucleotides via Tandem Mass Spectrometry. *Int. J. Mass Spectrom.* **2000,** *194*, 145-164.
19. Hannis, J. C.; Muddiman, D. C. Tailoring the Gas-phase Dissociation and Determining the Relative Energy of Activation for Dissociation of 7-deaza Purine Modified Oligonucleotides Containing a Repeating Motif. *Int. J. Mass Spectrom.* **2002,** *219*, 139-150.
20. Olsen, J. V.; Haselmann, K. F.; Nielsen, M. L.; Budnik, B. A.; Nielsen, P. E.; Zubarev, R. A. Comparison of Electron Capture Dissociation and Collisionally Activated Dissociation of Polycations of Peptide Nucleic Acids. *Rapid Commun. Mass Spectrom.* **2001,** *15*, 969-974.
21. Gross, J.; Hillenkamp, F.; Wan, K. X.; Gross, M. L. Metastable Decay of Negatively Charged Oligodeoxynucleotides Analyzed with Ultraviolet Matrix-assisted Laser Desorption/ionization Post-source Decay and Deuterium Exchange. *J. Am. Soc. Mass Spectrom.* **2001,** *12*, 180-192.
22. Wan, K. X.; Gross, J.; Hillenkamp, F.; Gross, M. L. Fragmentation Mechanisms of Oligodeoxynucleotides Studied by H/D Exchange and Electrospray Ionization Tandem Mass Spectrometry. *J. Am. Soc. Mass Spectrom.* **2001,** *12*, 193-205.
23. Wan, K. X.; Gross, M. L. Fragmentation Mechanisms of Oligodeoxynucleotides: Effects of Replacing Phosphates with Methylphosphonates and Thymines with Other Bases in T-rich Sequences. *J. Am. Soc. Mass Spectrom.* **2001,** *12*, 580-589.

24. Wang, Y.; Taylor, J. S.; Gross, M. L. Fragmentation of Electrospray-produced Oligodeoxynucleotide Ions Adducted to Metal Ions. *J. Am. Soc. Mass Spectrom.* **2001,** *12*, 550-556.

25. Spengler, B. Post-source Decay Analysis in Matrix-assisted Laser Desorption/ionization Mass Spectrometry of Biomolecules *J. Mass Spectrom.* **1997,** *32*, 1019-1036.

CHAPTER 3

CHARACTERIZATION OF ELECTRON CURRENT, ELECTRON ENERGY, AND CHARGE STATE EFFECTS IN ELECTRON DETACHMENT DISSOCIATION

In chapter 2, we demonstrated that EDD can provide extensive oligonucleotide backbone fragmentation, complementary to that of other MS/MS techniques. In our EDD implementation, the potential difference between a hollow cathode electron source and an extraction lens located in between the cathode and the ICR cell was crucial for successful fragmentation with changes as small as 0.2 V drastically altering fragmentation efficiency, a behavior that was not fully understood. In this chapter, we present a detailed characterization of the electron current passing through the ICR cell, and electron energy distributions, as functions of this potential difference, the cathode bias voltage, extraction lens voltage, and the cathode heating current under EDD conditions. Our results show that the extraction lens voltage serves to regulate the number of electrons passing through the ICR cell. Electron energy distributions remain narrow (< 0.5 eV) at increased cathode bias voltage and the electron current decreases dramatically with decreased cathode heating current. However, similar electron numbers passing through the ICR cell can be obtained at low (1.2 A) and high (1.8 A) heating current by adjusting the extraction lens voltage. This characteristic allowed us to investigate the influence of electron energy *at fixed electron number* and we found that

optimum EDD efficiency was obtained with 16-22 eV electrons. We also investigated the influence of charge state on oligonucleotide EDD efficiency and sequence coverage and found that higher charge states provided improved data for a DNA 10-mer, presumably due to a more extended gas-phase structure.

3.1. INTRODUCTION

Chapter 2 demonstrated the utility of EDD for oligonucleotide characterization and showed extensive backbone fragmentation of oligodeoxynucleotides, complementary to that of other MS/MS techniques, such as CAD and IRMPD [1]. An extension of EDD to oligoribonucleotide characterization [2] is presented in Chapter 4. Our group also showed that EDD can preferentially cleave C-S and S-S bonds in multiply charged disulfide-bonded peptide anions [3], and retain higher order structure of DNA hairpins [4]. Recently Fabris and co-workers have applied EDD to oligonucleotide characterization and observed more extensive fragmentation compared to ECD [5]. Furthermore, Amster and coworkers found that EDD produces information-rich tandem mass spectra for glycosaminoglycans, including both cross ring and glycosidic cleavage product ions [6]. The same group used EDD to distinguish the epimers glucuronic acid and iduronic acid in heparan sulfate tetrasaccharides based on diagnostic product ions, which are not observed in CAD or IRMPD [7].

In our previous EDD implementation [3] (described in Chapter 2) on a 7 T Bruker Q-FT-ICR mass spectrometer equipped with an indirectly heated hollow cathode electron source [8], optimum fragmentation efficiency was observed at ~ - 18 V cathode bias voltage, an extraction lens voltage of ~ - 19 V, an irradiation time of 2 seconds, and a cathode heating current of 1.8 A (see Figure 3-1 for a schematic drawing of this set-up).

We found that precise tuning of the potential difference (ΔU) between the cathode and the extraction lens was crucial for successful EDD with an optimum around 1 V at 1.8 A heating current, which is the standard heating current used for ECD with the same instrument. Changes of ΔU as small as 0.2 V drastically altered the EDD fragmentation efficiency, a behavior that we did not fully understand at that time. In this chapter, we present a detailed characterization of the electron current passing through the ICR cell and the electron energy distribution as functions of the cathode bias voltage, extraction lens voltage, and cathode heating current in EDD. We also show characterization of EDD efficiency and sequence coverage as functions of precursor ion charge state and electron energy (the latter experiment being greatly facilitated by the insights gained from electron current measurements).

3.2. EXPERIMENTAL SECTION

3.2.1. Sample Preparation

Reverse phase high performance liquid chromatography purified dA_6, dC_6, dT_6, and d(CTATCAGTGA) oligonucleotide sodium salts were purchased from TriLink BioTechnologies (San Diego, CA) and the peptide substance P (H-RPKPQQFFGLM-NH_2) was from Sigma (St. Louis, MO). Negative ion mode electrospray solvent consisted of 1:1 (v/v) isopropanol:water (Fisher, Fair Lawn, New Jersey) with 10 mM ammonium acetate (Fisher). The final concentration of samples was 2-20 μM.

3.2.2. Fourier Transform Ion Cyclotron Resonance Mass Spectrometry

All experiments were performed with a 7 Tesla Q-FT-ICR mass spectrometer (Bruker Daltonics, Billerica, MA), shown in Figure 2-1. The electrospray source was recently upgraded to include dual ion funnels (Apollo II ESI source, Bruker Daltonics). For EDD fragmentation efficiency characterization, experiments investigating the role of precursor ion charge state were performed with the old ESI source (Apollo I, Bruker Daltonics) whereas all other experiments were performed with the new dual ion funnel source. The ESI flow rate was 70 μL/h in both cases. EDD was performed with an indirectly heated hollow dispenser cathode electron source (Heat Wave, Watsonville, CA). The heater was set to approximately 8.5 V, generating a heating current of 1.8 A, unless specified otherwise. All mass spectra were acquired with XMASS (version 7.0.6, Bruker Daltonics) in broadband mode with 256 or 512k data points and summed over 20-30 scans. Data processing was performed as described in section 2.2.2. EDD efficiency calculations were performed by dividing the total product ion abundance with the abundance of precursor ions prior to fragmentation. All abundances were normalized to their associated charge.

3.2.3. Electron Current and Energy Measurements

Electron current and energy measurements were performed by measuring the electron current impinging on a floating focusing element on the opposite side of the ICR cell (see Figure 3-1) with a digital multimeter (John Fluke, Everett, MA). The floating voltage necessary for measuring energy distributions was generated by a DC power

supply (Goodwill Instrument, Taibei, Taiwan). Electron energy distributions were obtained by derivatizing the electron current with respect to the floating voltage.

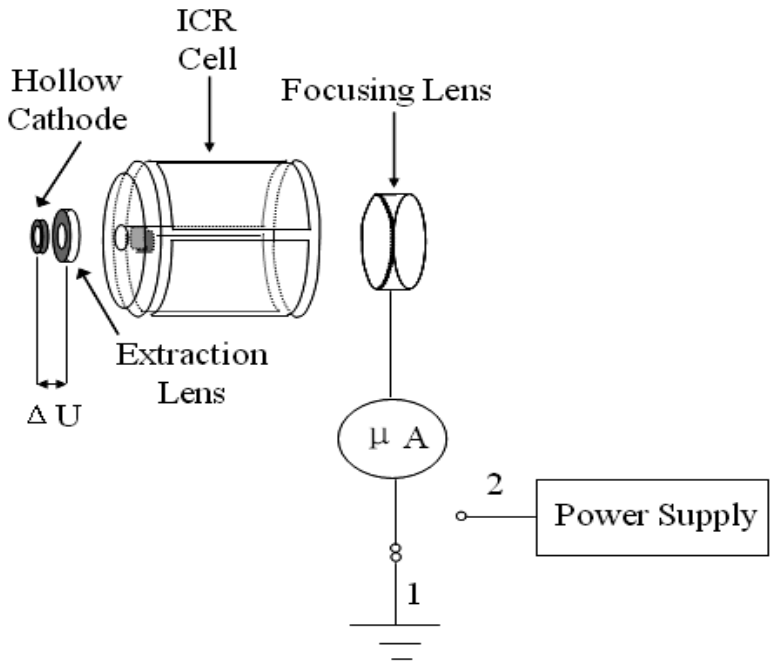

Figure 3-1. Experimental configuration for electron current and energy measurements. The microammeter was connected to ground (1) when measuring electron current through the ICR cell, and connected to a floating power supply (2) when measuring the electron energy distribution.

3.3. RESULTS AND DISCUSSION

3.3.1. Electron Current as a Function of Cathode Bias Voltage and Extraction Lens Voltage

Our first series of experiments involved measurements of electron current passing through the ICR cell as a function of cathode bias voltage at fixed ΔU (equal to 1

V). These experiments were motivated by our observation that EDD fragmentation efficiency and fragmentation pattern changed dramatically if the cathode bias voltage was increased from - 18 V (the experimentally determined optimum) to - 30 V at fixed irradiation time and ΔU. At higher cathode bias voltage, precursor ions were almost completely depleted but no product ions were observed. One possible explanation for this behavior is that product ions are too energetic (due to more energetic electrons) and are either ejected from the cell, or further fragmenting. However, an alternative explanation may be that there is a change in electron number as well as electron energy. Injection of too many electrons could cause space charge-related ejection of anions. Figure 3-2 shows that the electron current through the ICR cell increases linearly in the cathode bias voltage range from - 20 to - 80 V. Thus, both the electron energy and electron number increase with increasing cathode bias voltage. By comparing the electron current at - 18 V and - 30 V, it is evident that ~50% more electrons are passing through the cell at the higher current, which is consistent with the second hypothesis above, i.e., too many electrons are generated, thereby causing space charge-driven anion ejection.

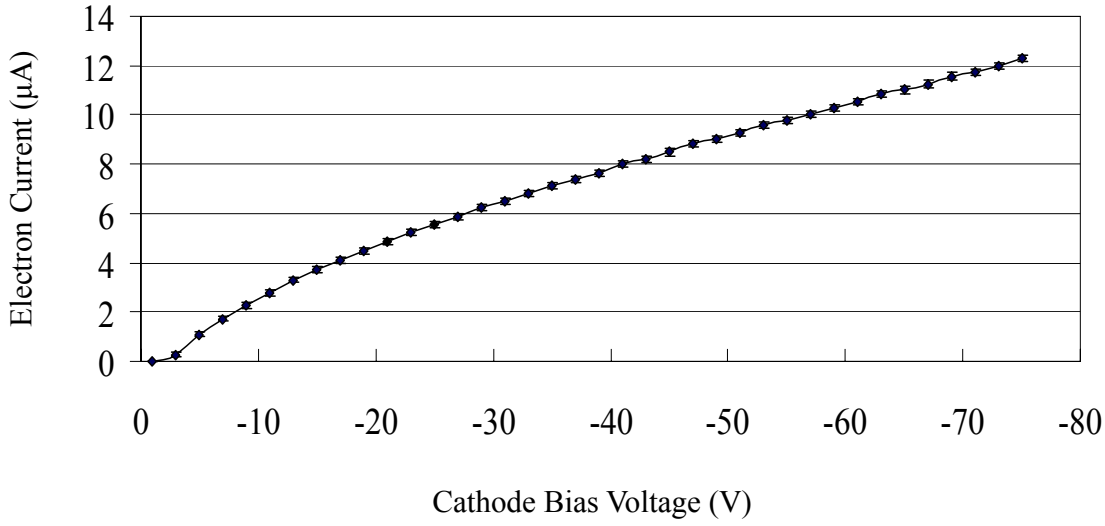

Figure 3-2. Electron current through the ICR cell as a function of cathode bias voltage when the potential difference, ΔU, between the cathode and the extraction lens was kept constant (equal to 1 V). The cathode heating current was 1.8 A.

A second series of experiments involved measuring the electron current passing through the ICR cell as a function of the extraction lens voltage at fixed cathode bias voltage (- 18.0 V), as shown in Figure 3-3. From this graph, it is seen that the electron current almost doubled when the extraction lens voltage was changed from - 19.0 V (found to be optimum in our previous experiments [3]) to - 18.8 V. A change from - 19.0 V to - 18.0 V, i.e., only one volt, resulted in an eight-fold current increase. Thus, the previously observed crucial influence of the extraction lens voltage in EDD can be clearly understood as this parameter serves to regulate the number of electrons passing through the ICR cell.

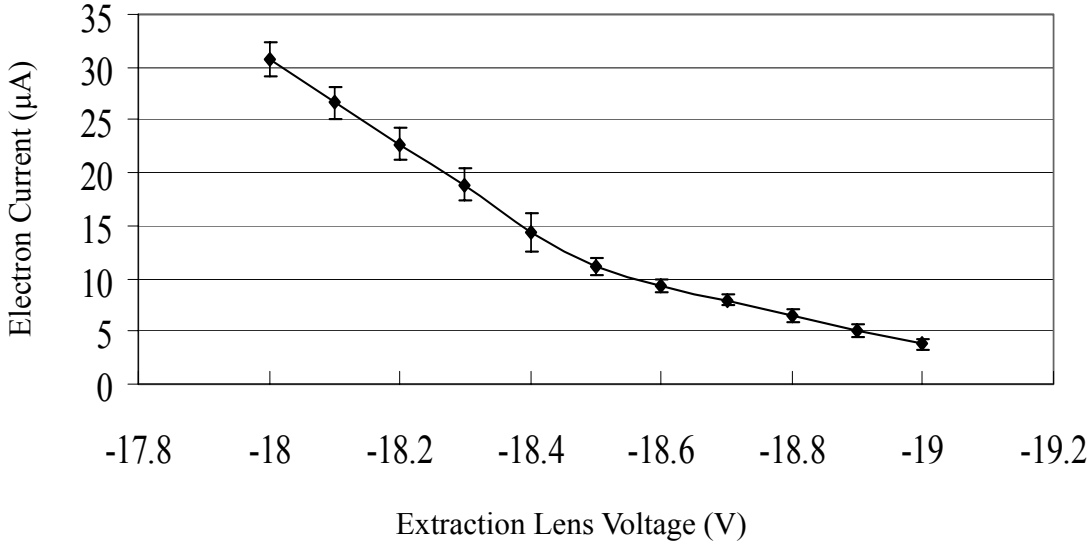

Figure 3-3. Electron current through the ICR cell as a function of extraction lens voltage at fixed cathode bias voltage (- 18.0 V).

3.3.2. Electron Energy Distributions at EDD Conditions

In order to better understand the EDD fragmentation process, it is desirable to determine the electron energy distribution in addition to the electron number and mean energy. Electrons emitted from an indirectly heated dispenser cathode are expected to have narrow energy distributions, which was also found experimentally (about 1 eV full width at half maximum) [9]. Figure 3-4 shows the electron energy distribution measured in our instrument at a cathode bias voltage of - 18.0 V and extraction lens voltage of - 19.0 V (i.e., our previously determined experimental optimum). The distribution is narrow (< 0.5 eV) and the measured maximum was 0.7 eV lower than the applied cathode bias voltage. Similar measurements at cathode bias voltages of - 8, - 10, - 12, - 14, and - 16 V performed at a ΔU of 1 V showed that there is, on average, a 0.7 eV

difference between the observed maximum of the energy distribution and the voltage applied to the cathode. Such reduction of the electron energy has been observed previously and was explained by the space potential of the electron beam [10].

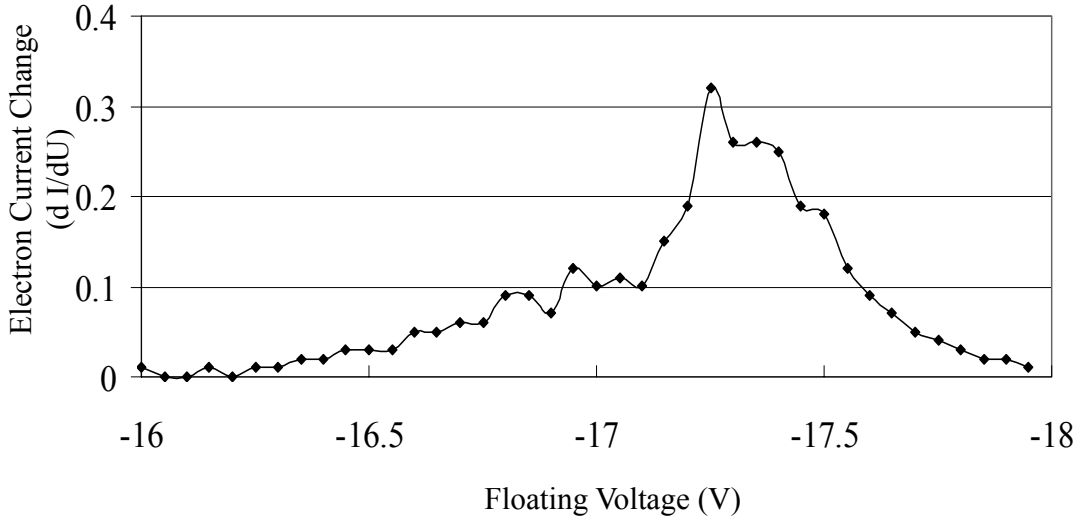

Figure 3-4. Electron energy distribution at an applied cathode bias voltage of - 18.0 V and extraction lens voltage of - 19.0 V. The heating current was 1.8 A.

3.3.3. EDD Fragmentation Efficiency as a Function of Cathode Bias Voltage at Fixed Electron Current

From the experiments reported above, we found that two parameters change when the cathode bias voltage is changed; the electron energy and the electron current passing through the ICR cell. Thus in order to measure EDD fragmentation efficiency as a function of electron energy alone, it is necessary to utilize parameters that provide a fixed electron number. Such experiments can be designed based on the data presented in Figures 3-2 and 3-3: fixed electron current through the ICR cell is obtained by

adjusting the difference between the cathode bias voltage and the extraction lens voltage, i.e., ΔU. Figure 3-5 displays the experimentally obtained EDD fragmentation efficiency for the oligonucleotide dT_6 and the peptide substance P as function of cathode bias voltage at fixed electron current. These graphs show that the optimum EDD efficiency at fixed electron current (around 4 μA) is obtained at electron energies of 16-22 eV, i.e., significantly higher energy than, e.g., the ionization energy of phosphate anions (1.16-4.57 eV [11]; we proposed that deprotonated phosphate groups constitute the initial site of electron detachment in oligonucleotide anions [2]). However, it is well known from electron ionization of neutral molecules that the optimal energy is significantly higher (70 eV) than their ionization energy due to the inefficient energy transfer by electrons. In EDD, the targets are deprotonated biomolecules in which longer bond lengths likely exist in the vicinity of deprotonated sites such that the de Broglie wavelength of electrons (~2.7 Å at 20 eV) matches more closely.

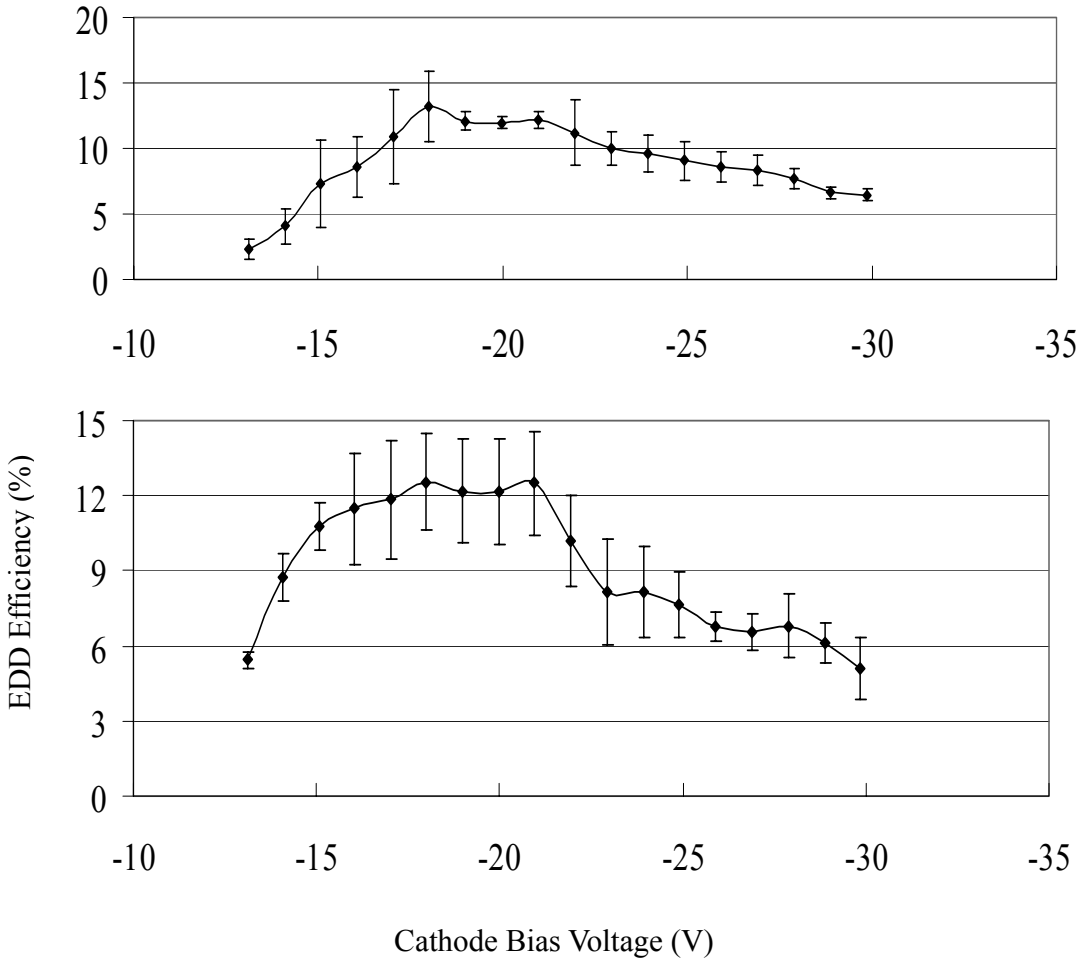

Figure 3-5. EDD efficiency of the oligonucleotide dT_6 (top) and the peptide substance P (bottom) at different cathode bias voltages at fixed electron current (~ 4 μA). The optimum EDD efficiency was obtained at an electron energy of 16-22 eV.

3.3.4. Can We Perform EDD at Lower Cathode Temperature?

As mentioned above, the recommended cathode heating current for ECD is 1.8 A (a temperature of around 900 ^{o}C [9]). This high temperature may cause undesired heating of precursor ions that can result in thermally induced dissociation. In order to minimize this problem, it would be desirable to perform EDD at lower cathode heating

current. The data presented above in Figures 3-2 and 3-3 suggest that it should be possible to compensate for the resulting lower electron number by adjusting ΔU. In order to investigate this hypothesis, we measured the electron current passing through the ICR cell at different cathode heating currents at fixed cathode bias voltage (- 18.0 V) and extraction lens voltage (- 19.0 V). The results of these experiments are shown in Figure 3-6. As expected, the electron current decreases dramatically with decreasing cathode temperature. At lower cathode temperature, insufficient numbers of electrons are generated from the cathode to allow efficient EDD. However, at a heating current of, e.g., 1.2 A, the same electron current (4 μA) passing through the ICR cell can be obtained by changing the cathode bias voltage to - 19 V and maintaining the extraction lens voltage at - 19 V. At these conditions, the maximum of the energy distribution remains virtually unchanged (as shown in Figure 3-7) compared to that observed at 1.8 A (Figure 3-4) and the total electron number is approximately the same. At the lower cathode temperature (heating current of 1.2 A), we found a 1.6 V difference between the observed maximum of the energy distribution and the voltage applied to the cathode. Figure 3-8 shows EDD spectra from the oligonucleotide dT_6 at cathode heating currents of 1.2 and 1.8 A, respectively, at fixed electron current. Nearly identical EDD spectra were observed at these two settings, clearly demonstrating that control of the electron number passing through the ICR cell is crucial for successful EDD.

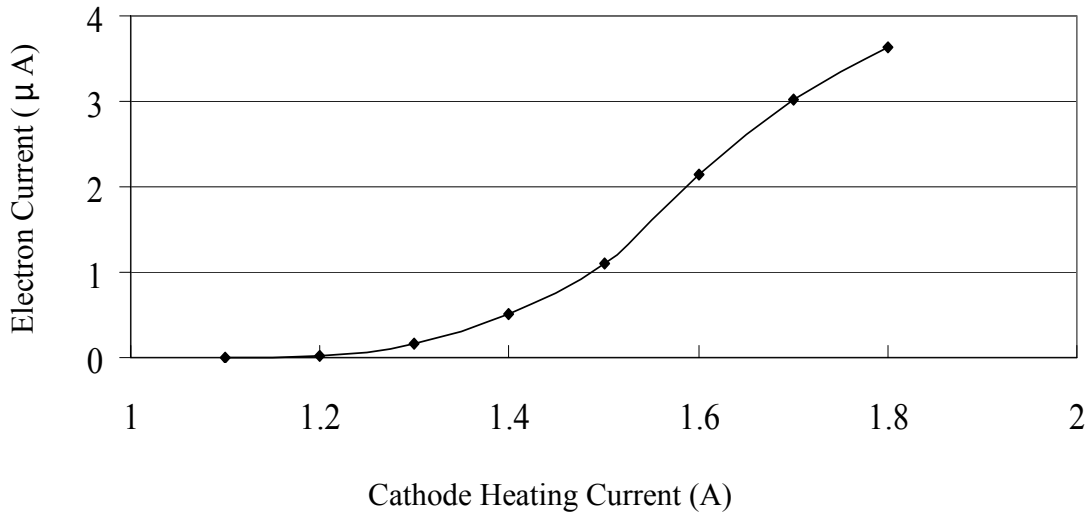

Figure 3-6. Electron current passing through the ICR cell as a function of cathode heating current at fixed cathode bias voltage (- 18.0 V) and extraction lens voltage (- 19.0 V).

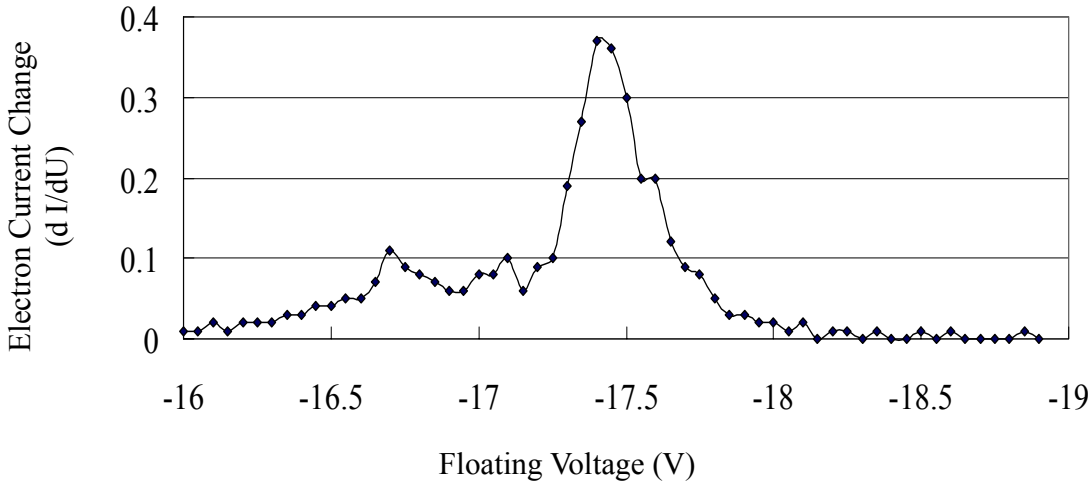

Figure 3-7. Electron energy distribution at -19.0 V cathode bias voltage, -19.0 V extraction lens voltage, and 1.2 A heating current.

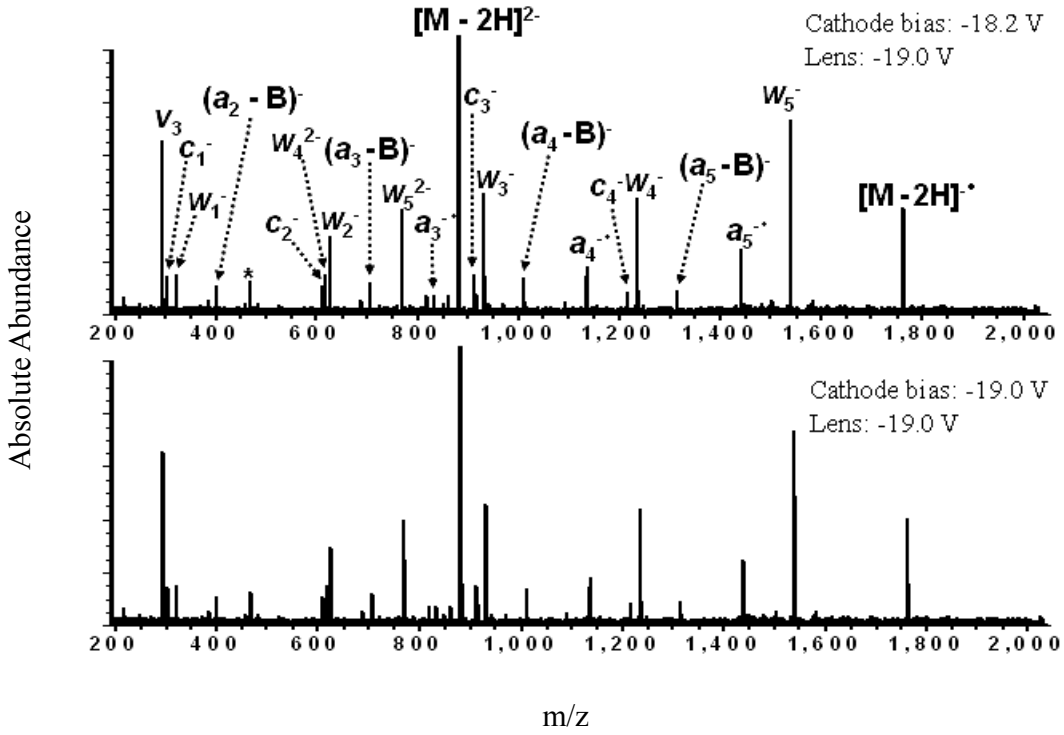

Figure 3-8. EDD spectra (same scale) of the oligonucleotide dT_6 at different cathode heating current: 1.8 A (top) and 1.2 A (bottom) but at fixed electron current passing through the ICR cell. (* = electronic noise).

3.3.5. The Role of Precursor Ion Charge State in EDD

Following ESI, we usually observe several charge states of macromolecular precursor ions of interest and have to decide what charge state to use for MS/MS experiments. Charge state plays a crucial role in both CAD/IRMPD and ECD [12-14] due to its influence on several factors such as ion stability, gas-phase structure, accessible kinetic energy, and electron capture cross section. However, the role of charge state in EDD has, to our knowledge, not been previously investigated. Table 3-1 shows the EDD fragmentation efficiency of the oligonucleotide hexamers dA_6, dC_6 and dT_6 in their doubly and triply deprotonated states. These results show that higher EDD efficiency

was obtained at the higher charge state although similar fragmentation patterns were obtained at both charge states.

Table 3-1. EDD fragmentation efficiency of hexamer oligonucleotides at different charge states.

	dA_6		dC_6		dT_6	
Charge State	-2	-3	-2	-3	-2	-3
EDD Fragmentation Efficiency	27%	48%	21%	40%	22%	27%

Additional data were collected for a longer oligonucleotide; the 10-mer d(CTATCAGTGA), which was observed in three different charge states. Figure 3-9 shows the EDD spectra obtained for the doubly, triply, and quadruply deprotonated forms of this oligonucleotide at the same experimental conditions. EDD of the 4^- charge state (Figure 3-9a) resulted in extensive *d* and *w*-type product ions from backbone C-O bond cleavage [15] as well as several complementary radical *a* and *z*-type ions. The overall EDD efficiency was 35% and cleavage at all backbone interresidue bonds was observed. For the triply deprotonated 10-mer, fewer backbone cleavages were seen (Figure 3-9b) compared to the 4^- charge state and the EDD efficiency was lower: 16%. However, two (*a* - B)-type product ions (not observed for the 4^- charge state) were detected. In EDD of the doubly deprotonated 10-mer (Figure 3-9c), we found the most dominant product ions to correspond to (*a* - B)-type ions and only two *w*-type ions were observed. The EDD efficiency was further reduced to 5%. Thus, for this 10-mer, the amount of

sequence information decreased drastically with decreasing charge state. An increase in negative charge could potentially decrease EDD efficiency due to Coulomb repulsion between anions and electrons. However, for the relatively fast electrons involved, this effect seems minor. By contrast, the more unfolded conformations of higher charge states appear to result in the opposite effect, especially for longer chain oligonucleotides. This result is consistent with our previous data, which showed that EDD retains intramolecular interactions [1, 4].

Figure 3-9. EDD spectra from the quadruply (a), triply (b), and doubly (c) deprotonated 10-mer oligonucleotide d(CTATCAGTGA) at a cathode bias voltage of - 18.1 V, an extraction lens voltage of - 19.0 V, and a cathode heating current of 1.8 A. (* = electronic noise).

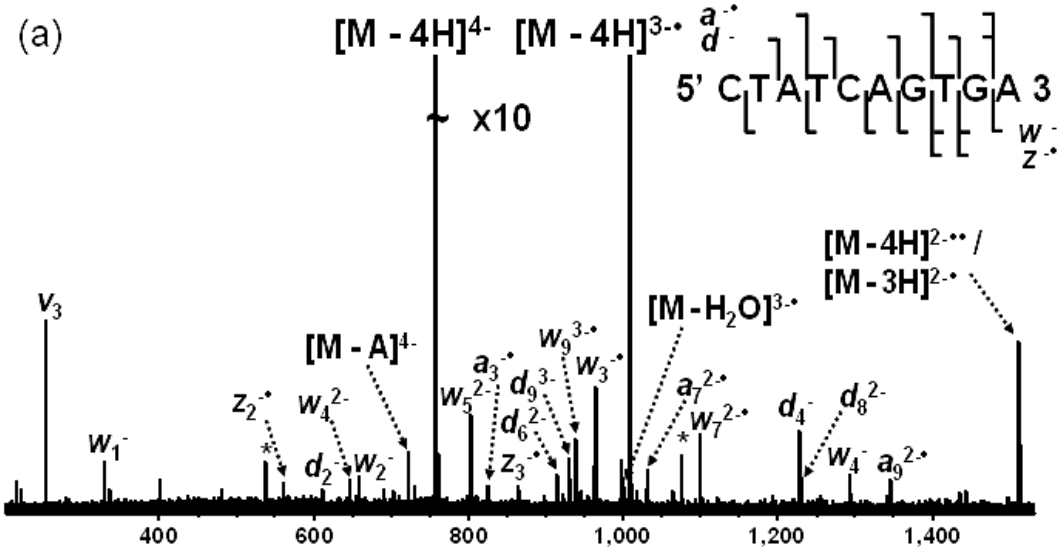

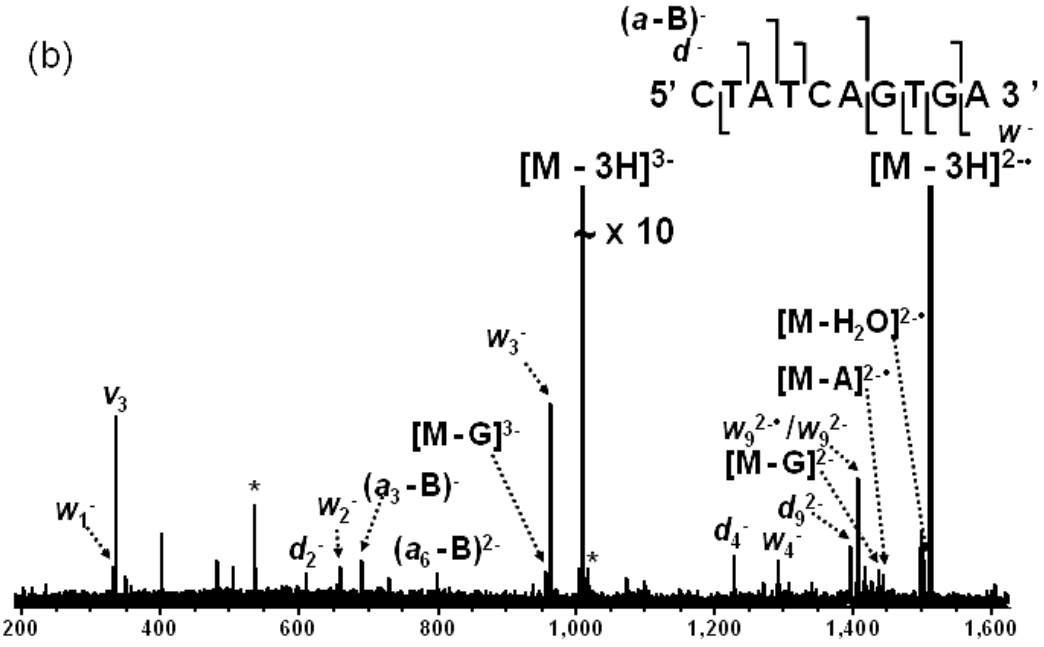
(b)
(a-B)-
d-
5' CTATCAGTGA 3'
w-
[M - 3H]3-
[M - 3H]2-•
x 10
[M-H2O]2-•
w3-
[M-A]2-•
v3
[M-G]3-
w92-•/w92-
[M-G]2-
w1-
*
w2-
(a3-B)-
d92-
d2-
(a6-B)2-
d4-
w4-
*
200
400
600
800
1,000
1,200
1,400
1,600
m/z

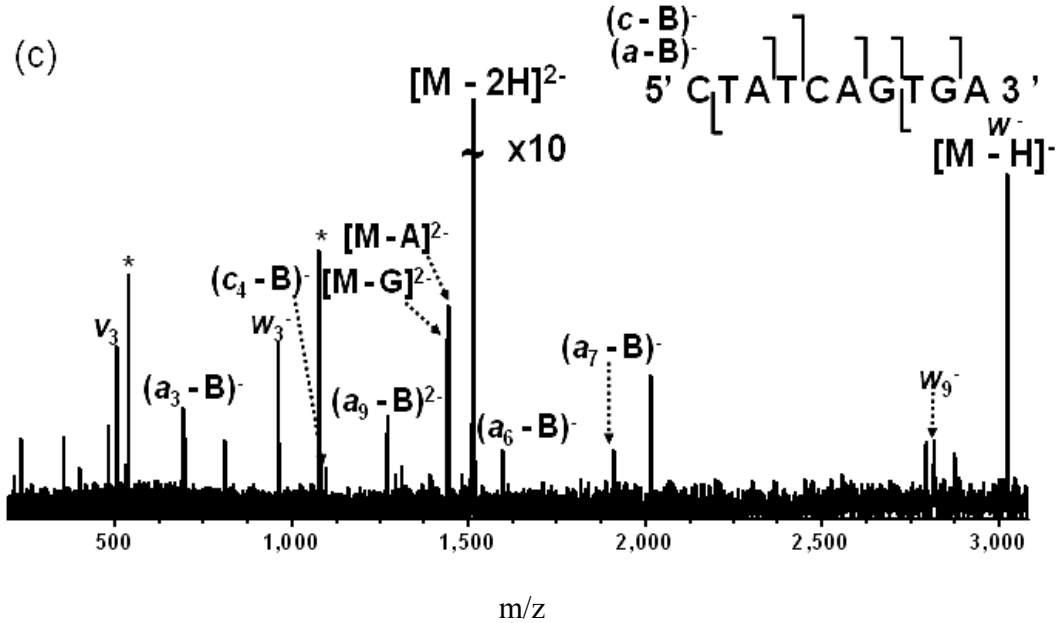
(c)
(c-B)-
(a-B)-
[M - 2H]2-
5' CTATCAGTGA 3'
x10
w-
[M - H]-
*
[M-A]2-
*
(c4-B)-
[M-G]2-
v3
w3-
(a7-B)-
(a3-B)-
(a9-B)2-
w9-
(a6-B)-
500
1,000
1,500
2,000
2,500
3,000
m/z

3.4. CONCLUSION

This chapter demonstrates that the potential difference between the cathode and the extraction lens (ΔU) is a crucial parameter for successful EDD. The extraction lens voltage serves to regulate the number of electrons passing through the ICR cell. Energy distributions of generated electrons are narrow (< 0.5 V) over a range (- 8 to - 18 V) of cathode bias voltages and measured maxima of the energy distributions are around 0.7 eV lower than the applied cathode bias voltage. Optimum EDD efficiency at fixed electron current (around 4 μA) was obtained at electron energies of 16-22 eV for the oligodeoxynucleotide dT_6 and for the peptide substance P. The electron current decreases dramatically with decreased cathode heating current. However, similar quality EDD can be achieved at lower heating current (1.2 A) by decreasing ΔU. For oligodeoxynucleotides, the EDD efficiency and sequence coverage seems to increase with increasing precursor ion charge state.

3.5. BIBLIOGRAPHY

1. Yang, J.; Mo, J.; Adamson, J. T.; Håkansson, K. Characterization of Oligodeoxynucleotides by Electron Detachment Dissociation Fourier Transform Ion Cyclotron Resonance Mass Spectrometry. *Anal. Chem.* **2005,** *77*, 1876-1882.
2. Yang, J.; Håkansson, K. Fragmentation of Oligoribonucleotides from Gas-phase Ion-electron Reactions. *J. Am. Soc. Mass Spectrom.* **2006,** *17*, 1369-1375.
3. Kalli, K.; Håkansson, K. Preferential Cleavage of S-S and C-S Bonds in Electron Detachment Dissociation and Infrared Multiphoton Dissociation of Disulfide-linked Peptide Anions. *Int. J. Mass Spectrom.* **2007,** *263*, 71-81.

4. Mo, J.; Håkansson, K. Characterization of Nucleic Acid Higher Order Structure by Tandem High Resolution Mass Spectrometry. *Anal. Bioanal. Chem.* **2006,** *386*, 675-681.
5. Kellersberger, K. A.; Fabris, D., Electron Capture Dissociation (ECD) of Structured Nucleic Acids. *Proceedings of the 53rd ASMS Conference on Mass Spectrometry and Applied Topics* San Antonio, TX, 2005.
6. Wolff, J. J.; Amster, I. J.; Chi, L. L.; Linhardt, R. J. Electron Detachment Dissociation of Glycosaminoglycan Tetrasaccharides. *J. Am. Soc. Mass Spectrom.* **2007,** *18*, 234-244.
7. Wolff, J. J.; Chi, L. L.; Linhardt, R. J.; Amster, I. J. Distinguishing Glucuronic from Iduronic Acid in Glycosaminoglycan Tetrasaccharides by Using Electron Detachment Dissociation. *Anal. Chem.* **2007,** *79*, 2015-2022.
8. Tsybin, Y. O.; Witt, M.; Baykut, G.; Kjeldsen, F.; Hakansson, P. Combined Infrared Multiphoton Dissociation and Electron Capture Dissociation with a Hollow Electron Beam in Fourier Transform Ion Cyclotron Resonance Mass Spectrometry. *Rapid Commun. Mass Spectrom.* **2003,** *17*, 1759-1768.
9. Tsybin, Y. O.; Witt, M.; Baykut, G.; Håkansson, P. Electron Capture Dissociation Fourier Transform Ion Cyclotron Resonance Mass Spectrometry in the Electron Energy Range 0-50 eV. *Rapid Commun. Mass Spectrom.* **2004,** *18*, 1607-1613.
10. Freiser, B. S.; Beauchamp, J. L. Electron impact dissociation of cyanobenzene radical cations by ion cyclotron resonance spectroscopy. *Chem. Phys. Lett.* **1976,** *42*, 380-382.

11. Wang, X. B.; Vorpagel, E. R.; Yang, X.; Wang, L. Experimental and Theoretical Investigations of the Stability, Energetics, and Structures of H_2PO^{4-}, $H_2P_2O_7^{2-}$, and $H_3P_3O_{10}^{2-}$ in the Gas Phase. *J. Phys. Chem. A* **2001,** *105*, 10468-10474.
12. Keller, K. M.; Zhang, J. M.; Oehlers, L.; Brodbelt, J. S. Influence of Initial Charge State on Fragmentation Patterns for Noncovalent Drug/DNA Duplex Complexes. *J. Am. Soc. Mass Spectrom.* **2005,** *40*, 1362-1371
13. Fukui, K.; Naito, Y.; Akiyama, Y.; Takahashi, K. Charge-state Selective Fragmentation Analysis for Protonated Peptides in Infrared Multiphoton Dissociation. *Int. J. Mass Spectrom.* **2004,** *235*, 25-32.
14. Iavarone, A. T.; Paech, K.; Williams, E. R. Effects of Charge State and Cationizing Agent on the Electron Capture Dissociation of a Peptide. *Anal. Chem.* **2004,** *76*, 2231-2238.
15. Wu, J.; McLuckey, S. A. Gas-phase Fragmentation of Oligonucleotide Ions. *Int. J. Mass Spectrom.* **2004,** *237*, 197-241.

CHAPTER 4

ELECTRON CAPTURE AND ELECTRON DETACHMENT DISSOCIATION OF OLIGORIBONUCLEOTIDES

Chapter 2 demonstrated that EDD can provide complementary sequence-specific cleavage of DNA compared to CAD and IRMPD. Similar results have been reported for ECD. However, EDD is preferred over ECD due to more extensive fragmentation at higher sensitivity (due to its negative ion mode operation). In this Chapter, we extend the radical ion chemistry of both ECD and EDD to the characterization of RNA. Compared to DNA, rather limited information is currently available on the gas-phase fragmentation of RNA. We found that the ECD fragmentation patterns of the oligoribonucleotides A_6, C_6, and CGGGGC are nucleobase dependent, suggesting that cleavage proceeds following electron capture at the nucleobases. Only limited backbone cleavage was observed in ECD. EDD, on the other hand, provided complete sequence coverage for the RNAs A_6, C_6, G_6, U_6, CGGGGC, and GCAUAC. The EDD fragmentation patterns were different from those observed with CAD and IRMPD in that the dominant product ions correspond to *d*- and *w*-type ions rather than *c*- and *y*-type ions. The minimum differences between oligoribonucleotides suggest that EDD proceeds following direct electron detachment from the phosphate backbone.

4.1. INTRODUCTION

McCloskey and co-workers pioneered mass spectrometric analysis of nucleic acids [1, 2] and have applied LC-MS to the interrogation of RNA reaction mechanisms and to the characterization of RNA modifications [3-5]. RNA oligonucleotides (oligoribo-nucleotides) have been much less characterized with MS/MS than DNA oligonucleotides and their fragmentation pathways are not as well understood. A couple of investigations have shown that low energy CAD results primarily in abundant *c*-type ions and their complementary *y*-type ions as the major sequence ions [6, 7] and a similar pattern was observed with IRMPD [8]. We have shown that irradiation of gas-phase oligodeoxynucleotide dications with low energy (<0.2 eV) electrons (ECD [9-12]) provides complementary sequence-specific backbone cleavage with the major product ions being *w* and *d* ion series (corresponding to cleavage of carbon-oxygen bonds at different sides of an interresidue phosphate group [13]). In addition, radical *a*/z as well as (*a*/*z* - B) and (*c*/*x* - B) ions are produced but nucleobase loss constitutes a minor fragmentation pathway [14, 15]. ECD has also been shown to be 'soft' enough to retain gas-phase hydrogen bonding in dA_6 (similar to protein ECD [16]), thereby allowing characterization of higher order structure [15]. However, because ECD requires cationic precursor ions, its sensitivity for nucleic acid characterization is limited. EDD, involving irradiation with ≥10 eV electrons, was introduced by Zubarev and co-workers in 2001 as a means to invoke radical ion mediated fragmentation pathways for biomolecular anions [17]. We have demonstrated that EDD can provide extensive backbone fragmentation of oligodeoxynucleotides at higher sensitivity than ECD [18] (described in Chapter 2). In addition, EDD can cleave backbone covalent bonds without rupturing non-covalent

interactions, thereby having potential for characterizing higher order structure. In this Chapter, we present the fragmentation pathways in ECD and EDD of hexamer oligoribonucleotides and discuss the utility of these two gas-phase ion-electron reaction techniques for structural characterization of RNA.

4.2. EXPERIMENTAL SECTION

4.2.1. Sample Preparation

Anion-exchange and high performance liquid chromatography purified A_6, C_6, G_6, CGGGGC and GCAUAC and polyacrylamide gel electrophoresis purified U_6 ammonium salts from TriLink BioTechnologies (San Diego, CA) were used without further purification. Negative mode electrospray solvent consisted of 1:1 (v/v) isopropanol:water (Fisher, Fair Lawn, New Jersey) with 10 mM ammonium acetate (Fisher). Positive mode electrospray solvent consisted of 1:1 (v/v) acetonitrile:water (Fisher) with 0.5% formic acid (ACROS Organics, Fair Lawn, NJ). The final oligoribonucleotide concentration was 5 to 20 μM with the exception of G_6, which was electrosprayed at 100 μM.

4.2.2. Fourier Transform Ion Cyclotron Resonance Mass Spectrometry

All experiments were performed with a 7 T Q-FT-ICR mass spectrometer, shown in Figure 2-1. Samples were infused via an external Apollo electrospray ion source at a flow rate of 70 μL/h, mass selectively externally accumulated for 1-10 s (except for the oligonucleotide G_6, which was accumulated for 60 s) and captured in the ICR cell by dynamic trapping. The accumulation, ion transfer and capture events were

looped twice for improved precursor ion abundance. For ECD experiments, further isolation was accomplished by correlated harmonic excitation fields (CHEF) [19] inside the ICR cell. ECD and EDD were performed before the trapping plate voltages were ramped down. The initial trapping voltage was - 2 V and the voltage during excitation and detection was - 1 V. The indirectly heated hollow dispenser cathode was used to generate electrons for ECD and EDD. During the EDD event, the cathode voltage was pulsed to -18 V for 2 s. A lens located in front of the cathode was kept at - 19 V throughout the experiment. For ECD, the cathode voltage was pulsed to - 1 V for 35-80 ms. The lens electrode was kept at + 1 V. All mass spectra were acquired with the XMASS software (Bruker) in broadband mode from m/z 200 to 2,000 with 256k data points and summed over 32-50 scans. The calculated masses of the doubly charged precursor ions and the charge-reduced species were used for internal calibration of all spectra, except for EDD of A_6 and U_6, which did not produce the latter species. In those two cases, the w_5/d_5 product ion was used instead. Product ions were assigned based on a 15 ppm error criterion.

4.3. RESULTS AND DISCUSSION

4.3.1. Electron Capture Dissociation of A_6 Dications

Figure 4-1 shows an ECD spectrum of the doubly protonated RNA A_6 and product ion assignments are given in Table 4-1. The most abundant product ion in the spectrum corresponds to the charge-reduced species, which has captured an electron but not dissociated. The isotopic distribution of this singly charged ion indicates that it is mainly a radical ion, $[M + 2H]^{+\bullet}$, i.e. no significant hydrogen loss (or gain) to produce an

even-electron species is seen [20]. The $[M + 2H]^{+\bullet}$ species was also dominant in ECD of dA_6 [15] in contrast to other oligodeoxynucleotides, which dissociated more readily. The greater stability of A_6 and dA_6 charge-reduced species is attributed to the presence of intramolecular hydrogen bonds between the adenine bases and the phosphate backbone, preventing product ions from separating and thereby from being detected. Such intramolecular gas-phase hydrogen bonding was previously proposed from both molecular modeling and gas-phase hydrogen exchange experiments [21, 22].

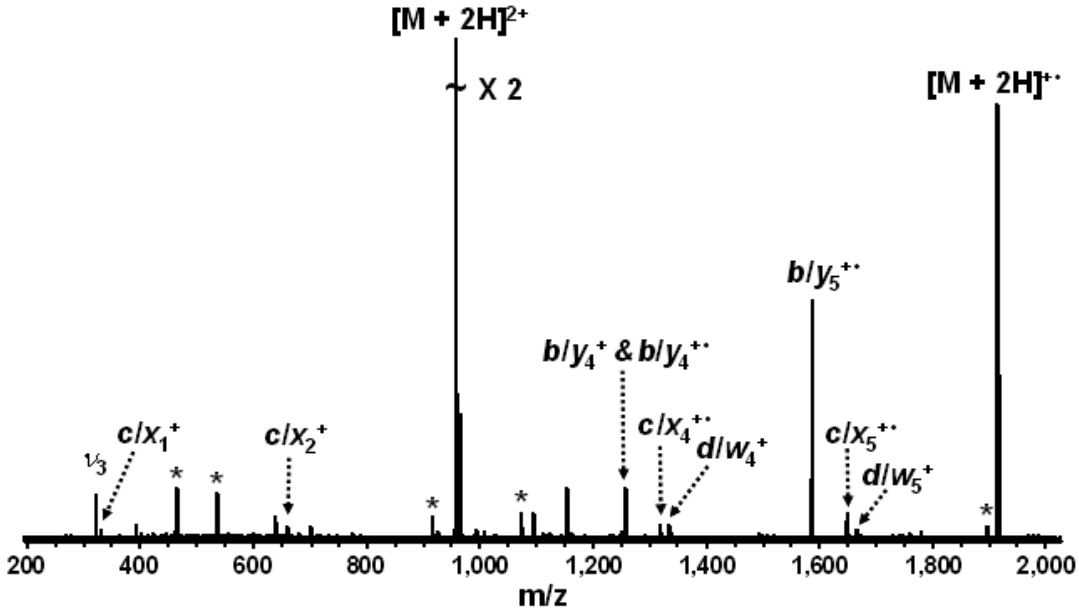

Figure 4-1. ECD (- 1 V bias voltage, 80 ms irradiation, 32 scans) of the RNA A_6. *b*/*y*, *c*/*x* and *d*/*w* ions are observed in addition to an abundant charged reduced radical species, $[M + 2H]^{+\bullet}$. Electronic noise spikes are labeled with asterisks.

In addition to the abundant charge-reduced radical species, several *b*/*y*, *c*/*x* and *d*/*w* product ions are observed in ECD of A_6 (these ion pairs cannot be distinguished due

to identical mass). The most abundant of these are radical ions, i.e. they contain one additional hydrogen atom compared to their even-electron counterparts. However, a complete ion series is not observed for either ion type. In low energy CAD and IRMPD of oligomer RNA, *y* and *c*-type ions are the most abundant products in addition to relatively minor *w* and (*a* - B) ions [7, 8]. It has been proposed that complementary *c* and *y* ion pairs result from direct cleavage of the 5' P-O bond [23]. Thus, neutral nucleobase loss is not expected for RNA, in contrast to CAD and IRMPD of DNA, which proceeds through a base loss intermediate [24]. Similarly, no base loss, [M - B], ions are observed in ECD of A_6.

Table 4-1. Product ions observed from ECD (80 ms irradiation, - 1 V bias, 32 scans) of A_6. Ions labeled *w* can also be *d* ions, ions labeled *b* can also be *y* ions, and ions labeled *c* can also be *x* ions.

Observed m/z	Calculated m/z	Assignment	Error (ppm)
330.0568	330.0598	c_1^+	-9.1
659.1139	659.1123	c_2^+	2.4
957.1869	957.1869	$[M + 2H]^{2+}$	Calibrant
1255.260	1255.262	b_4^+	-1.6
1256.263	1256.269	$b_4^{+\bullet}$	-4.8
1318.212	1318.225	$c_4^{+\bullet}$	-9.9
1335.218	1335.228	w_4^+	-7.5
1584.307	1584.314	b_5^+	-4.4
1585.311	1585.322	$b_5^{+\bullet}$	-6.9
1647.271	1647.278	$c_5^{+\bullet}$	-4.2
1664.280	1664.280	w_5^+	< 0.1
1914.374	1914.374	$[M + 2H]^{+\bullet}$	Calibrant

The observed product ions are quite different from ECD of the DNA dA_6, which mainly resulted in *d*/*w*-type ions but no *b*/*y* or *c*/*x* ions [15]. This drastically different fragmentation behavior is presumably due to different preferred fragmentation pathways as a result of the hydroxyl group of the 2' sugar position.

4.3.2. Electron Capture Dissociation of C_6 Dications

The mass spectrum resulting from ECD of C_6 is shown in Figure 4-2. Product ion assignments are listed in Table 4-2. The result is markedly different from that of A_6 (Figure 4-1) in that only two *d*/*w* and (*d*/*w* + H_2O) ions are observed and no *b*/*y* or *c*/*x* ions are present. Very limited backbone cleavage is seen and full sequence coverage cannot be obtained from the detected product ions. The abundance of the charge reduced non-dissociated species is much lower than for A_6. The different dissociation behavior of C_6 compared to A_6 suggests that the ECD cleavage mechanism for RNA involves the nucleobases. Because the nucleobases are the most likely sites of protonation, one can envision electron capture being preferred at those locations, creating a radical site that can progress to ultimately result in cleavage of the phosphodiester backbone. Electron capture at DNA nucleobases has been shown to be energetically favored over direct capture by P=O bonds for near zero eV electrons interacting with *neutral* DNA [25]. We argue that this preference should be even stronger in the presence of nucleobase protonation. The same authors showed that electron attachment to nucleobases can cause backbone C-O bond cleavage, i.e. the analog of *a*/*w* or *d*/*z*-type cleavage, as previously proposed by Sanche and coworkers as an important route to DNA damage [26]. The different behavior for A_6, i.e. the dominance of *b*/*y* and *c*/*x* ions, may be related to its

propensity for intramolecular hydrogen bonding between the nucleobases and the phosphate backbone, which could promote alternate radical migration as compared to C_6. It is possible that alternate cleavage would also be observed for the same oligonucleotide by varying the electron energy, similar to theoretical results obtained for neutral DNA [25, 26]. However, because we are operating in the "multi-pass" ECD regime, i.e. electrons are reflected through the ICR cell and can therefore cool to the optimum energy for capture [27], such experiments are difficult to perform in our current configuration.

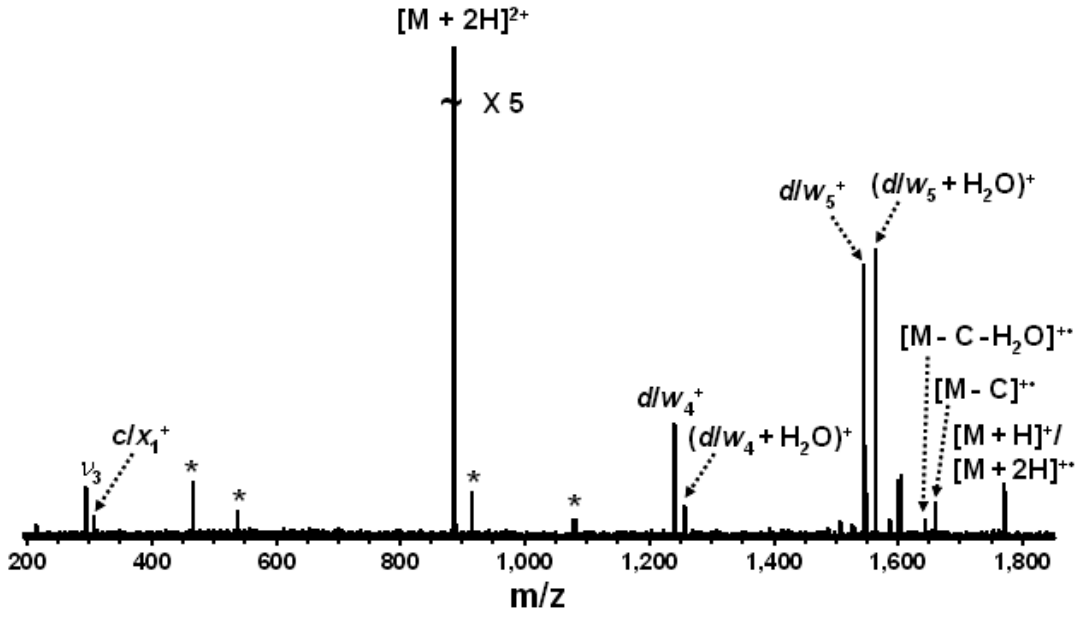

Figure 4-2. ECD (- 1 V bias voltage, 80 ms irradiation, 32 scans) of the RNA C_6. The most abundant products correspond to *w*/*d* and (*w*/*d* + H_2O) ions. Electronic noise spikes are labeled with asterisks.

Table 4-2. Product ions observed from ECD (50 ms irradiation, - 1 V bias, 32 scans) of C_6. Ions labeled *w* can also be *d* ions and ions labeled *c* can also be *x* ions.

Observed m/z	Calculated m/z	Assignment	Error (ppm)
306.0496	306.0485	c_1^+	3.6
885.1532	885.1532	$[M + 2H]^{2+}$	Calibrant
1239.181	1239.183	w_4^+	-1.6
1257.194	1257.194	$(w_4 + H_2O)^+$	< 0.1
1544.227	1544.224	w_5^+	1.9
1562.234	1562.235	$(w_5 + H_2O)^+$	-0.6
1641.243	1641.253	$[M - C - H_2O + H]^{+\bullet}$	-6.1
1659.263	1659.264	$[M - C + H]^{+\bullet}$	-0.6
1769.294	1769.299	$[M + H]^+$	-2.8
1770.307	1770.307	$[M + 2H]^{2+\bullet}$	Calibrant

Abundant (*d*/*w* + H_2O) ions were also found in ECD of the oligodeoxynucleotide dC_6 and were proposed to be formed from a pentavalent phosphorane intermediate involving the 5' hydroxyl group [14]. Such a rearrangement does not involve the 2' position of the sugar and can therefore also be envisioned for RNA.

4.3.3. Electron Capture Dissociation of CGGGGC Dications

Doubly protonated precursor ions were not detected for G_6 or U_6. U_6 has a very low proton affinity [21] and guanosine oligomers can easily form quadruplexes, which can be difficult to solublize. The G_6 hexamer may represent the worst possible scenario because it is long enough to allow quadruplex formation but short enough to not have a sufficient number of phosphate groups to aid solubility. Thus, in order to

investigate the influence of guanine on the ECD fragmentation of RNA, we analyzed the G-rich oligonucleotide CGGGGC.

Figure 4-3 shows an ECD spectrum of GGGGC, obtained by applying a – 1 V bias voltage to the hollow dispenser cathode for 70 ms and Table 4-3 lists the corresponding ECD product assignments. Here, both *w*/*d*, *c*/*x*, and *b*/*y* fragments as well as one (*w*/*d* - G) ion were observed, although the former ions dominated. The charge reduced radical species was more dominant than for C_6. As for the other oligoribonucleotides, backbone cleavage was limited. The appearance of the CGGGGC ECD spectrum was more similar to the one for C_6 (Figure 4-2) than the one for A_6 (Figure 4-1) although no (*d*/*w* + H_2O) ions were observed. Guanine, being a purine, has also been shown to be involved in extensive gas-phase intramolecular hydrogen bonding [28], which may explain the presence of *b*/*y* and *c*/*x* ions, as observed for A_6. However, the hybrid nature of CGGGGC may result in *d*/*w* ion formation as the preferred fragmentation pathway, similar to C_6.

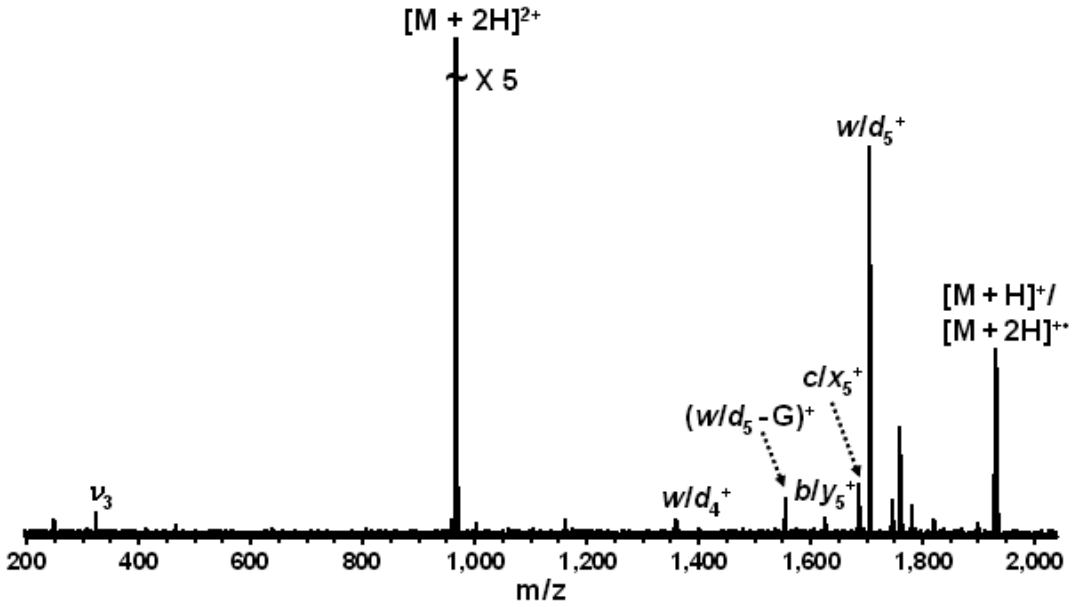

Figure 4-3. ECD (- 1 V bias voltage, 70 ms irradiation, 50 scans) of the RNA CGGGGC. Incomplete *w*/*d*, *c*/*x*, *b*/*y*, and (*w*/*d* - G) ion series are present.

Table 4-3. Product ions observed from ECD (40 ms irradiation, - 1 V bias, 50 scans) of the RNA CGGGGC. Ions labeled *w* can also be *d* ions, ions labeled *b* can also be *y* ions, and ions labeled *c* can also be *x* ions.

Observed m/z	Calculated m/z	Assignment	Error (ppm)
965.1655	965.1655	$[M + 2H]^{2+}$	Calibrant
1359.202	1359.201	w_4^+	0.7
1553.199	1553.199	$(w_5 - G)^+$	< 0.1
1625.289	1625.290	$b_4^{+\bullet}$	- 0.6
1686.238	1686.238	c_5^+	< 0.1
1704.249	1704.249	w_5^+	< 0.1
1929.317	1929.324	$[M + H]^+$	- 3.6
1930.331	1930.331	$[M + 2H]^{+\bullet}$	Calibrant

4.3.4. Electron Capture Dissociation of GCAUAC Cations

In order to further investigate the ECD behavior of a hybrid oligoribonucleotide and also discriminate between *a* and *z*, *b* and *y*, *c* and *x* as well as *w* and *d* ions, the asymmetric oligoribonucleotide GCAUAC was analyzed. Figure 4-4 shows the corresponding ECD spectrum and product ions are listed in Table 4-4. Similar to the results for symmetric oligoribonucleotides, only limited backbone cleavage is observed with *d* and *w*-type ions being dominant. No *b*/*y* ions were detected in this spectrum. Thus, the precise identity of the *b*/*y* ions observed above remains unclear. However, for GCAUAC, one *c*-type ion was observed, rendering its complementary *y* ions the most probable assignment for *b*/*y* ion pairs, similar to the dissociation observed in CAD and IRMPD.

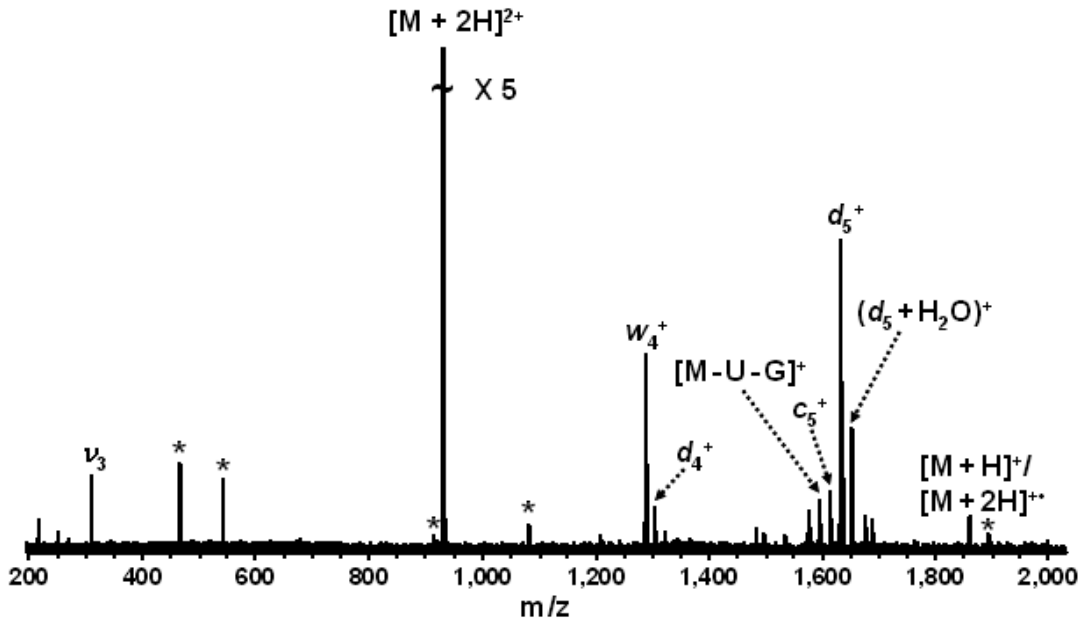

Figure 4-4. ECD (- 1 V bias voltage, 35 ms irradiation, 32 scans) of the RNA GCAUAC. Electronic noise spikes are labeled with asterisks.

Table 4-4. Product ions observed from ECD (35 ms irradiation, - 1 V bias, 32 scans) of the RNA GCAUAC.

Observed m/z	Calculated m/z	Assignment	Error (ppm)
929.6595	929.6595	$[M + 2H]^{2+}$	Calibrant
1288.193	1288.189	w_4^+	3.1
1304.185	1304.184	d_4^+	0.8
1595.253	1595.235	$[M - G - U]^+$	11.3
1615.230	1615.226	c_5^+	2.5
1633.242	1633.237	d_5^+	3.1
1651.252	1651.247	$(w_5 + H_2O)^+$	3.0
1858.297	1858.312	$[M + H]^+$	-8.1
1859.319	1859.319	$[M + 2H]^{+\bullet}$	Calibrant

4.3.5. Electron Detachment Dissociation of A_6 Dianions

The ECD data discussed above show that only limited backbone cleavage is observed for oligoribonucleotides, contrary to the rather extensive cleavage observed for DNA [15] Thus, the 2' hydroxyl group is likely involved in the dissociation process, consistent with a mechanism depicting initial electron capture at the nucleobases. However, for both DNA and RNA oligonucleotides, ionization in positive mode, which is required for ECD, is not very efficient and dT_6 and U_6 could not be characterized. We have shown in Chapter 2 that negative mode ionization results in a ten-fold improvement in sensitivity and that EDD can provide extensive cleavage of hexamer DNAs [18]. Thus, the oligoribonucleotides discussed above were also subjected to EDD.

An EDD spectrum of the RNA A_6 is shown in Figure 4-5 and Table 4-5 lists the corresponding EDD products. Doubly deprotonated A_6 anions were dissociated at a cathode bias voltage of - 18.1 V with 2 s irradiation time. The entire *d*/*w* and *c*/*x* ion series, three *b*/*y*, one *a*/*z*, one (*c*/*x* - B), and one (*d*/*w* + H_2O) ion were observed. The

presence of a plentitude of sequence-specific product ions is similar to the EDD behavior of the DNA dA_6 [18]. However, some differences are noted: First, we do not observe a charge reduced radical ion in EDD of A_6 and only one radical product ion, $[M - A]^{-\bullet}$, is present. Second, we did not observe *b*/*y* or (*d*/*w* + H_2O) ions in EDD of dA_6, and, third, *c*/*x* ions are more abundant in EDD of the RNA A_6. We believe these differences may be rationalized by the presence of the 2' hydroxyl group. A proposed mechanism for EDD of peptides involves electron detachment from deprotonated sites, e.g., backbone amide nitrogens [29]. The preferred deprotonation sites in oligonucleotides are the backbone phosphate groups. Thus, direct electron detachment from the backbone is likely although a detailed cleavage mechanism has not yet been proposed. Such a process, occurring remote from the nucleobases, rationalizes the small differences observed in EDD of various DNA sequences [18] and it is also consistent with the lower ionization energy of phosphate anions (in the range of 1.16 to 4.57 eV [30]) as compared to the most readily ionized nucleobase (guanine, 8.24 eV [31]). However, regardless of mechanism, the data in Figure 4-5 demonstrate much more extensive fragmentation in EDD compared to ECD of A_6. In addition, the cleavage pattern in EDD is complementary to that of CAD, IRMPD and ECD in that *w*/*d*-type ions are the most abundant products rather than *c* and *y*-type ions. Finally, the EDD data allows complete sequencing.

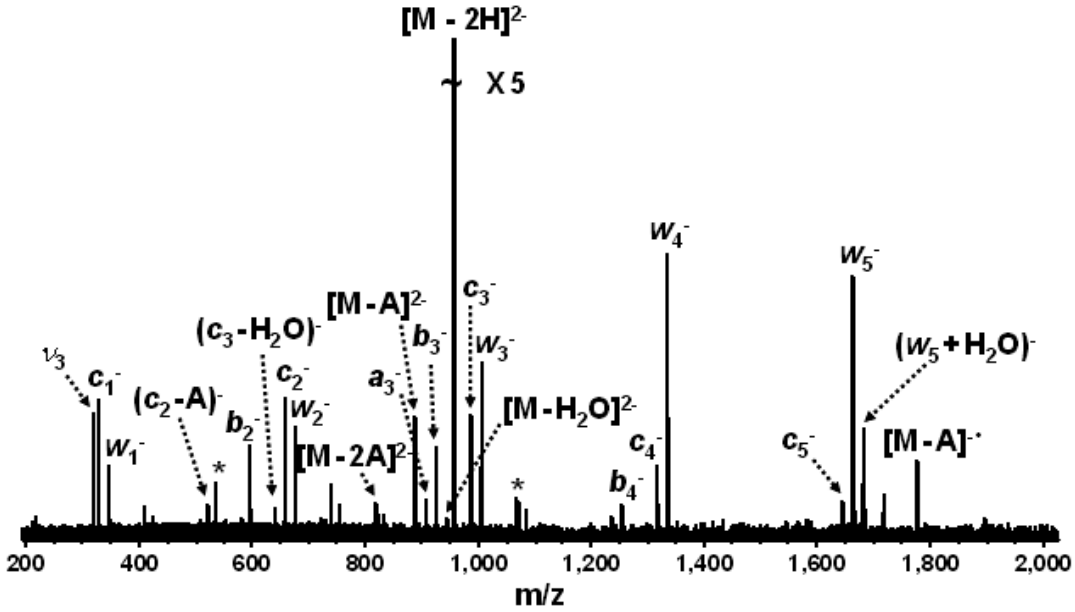

Figure 4-5. EDD (- 18.1 V bias voltage, 2 s irradiation, 32 scans) of the RNA A_6. Complete *d*/*w* and *c*/*x* ion series are observed (only one of the labels is given), allowing full sequencing of the oligonucleotide. Electronic noise spikes are labeled with asterisks.

Table 4-5. Product ions observed from EDD (2 s irradiation, - 18.1 V bias, 32 scans) of A_6. Ions labeled *w* can also be *d* ions, ions labeled *a* can also be *z* ions, ions labeled *c* can also be *x* ions and ions labeled *b* can also be *y* ions.

Observed m/z	Calculated m/z	Assignment	Error (ppm)
328.0416	328.0453	c_1^-	-11.3
346.0524	346.0558	w_1^-	-9.8
522.0414	522.0433	$(c_2 - A)^-$	-3.6
595.1362	595.1421	b_2^-	-9.9
639.0892	639.0872	$(c_2 - H_2O)^-$	3.1
657.0940	657.0978	c_2^-	-5.8
675.1045	675.1084	w_2^-	-5.8
820.1220	820.1179	$[M - 2A]^{2-}$	5.0
887.6446	887.6452	$[M - A]^{2-}$	-0.7

906.1810	906.1840	a_3^-	-3.3
924.1929	924.1946	b_3^-	-1.8
955.1724	955.1724	$[M - 2H]^{2-}$	Calibrant
986.1512	986.1503	c_3^-	0.9
1004.158	1004.161	w_3^-	-3.0
1253.245	1253.247	b_4^-	-1.6
1315.204	1315.203	c_4^-	0.8
1333.213	1333.213	w_4^-	< 0.1
1644.211	1644.255	c_5^- ?	-26.8
1662.266	1662.266	w_5^-	Calibrant
1680.265	1680.276	$(w_5 + H_2O)^-$	-6.5
1775.283	1775.290	$[M - A]^{-\bullet}$	-3.9

4.3.6. Electron Detachment Dissociation of C_6 Dianions

Figure 4-6 shows an EDD spectrum from C_6 and the products are presented in Table 4-6. As for A_6 (Figure 4-5), the entire *d*/*w* and *c*/*x* ion series are present as well as two complementary *a*/*z* ions, three *b*/*y*, and two (*d*/*w* + H_2O) ions. Base loss is a minor fragmentation pathway and, again, the *d*/*w* ion series constitutes the dominant fragmentation channel. These data support a cleavage mechanism involving direct electron detachment from the phosphate backbone because there is no apparent nucleobase effect.

In addition to the singly charged product ions listed above, several doubly charged fragments are observed, including c/x_5^{2-}, b/y_5^{2-}, and w/d_5^{2-}. Doubly charged ions are not expected in EDD of doubly charged precursor ions because the fragmentation proceeds via charge reduction [17]. However, such ions have been previously observed and were suggested to either be formed from zwitterionic precursor ions, or to be a result of direct vibrational or electronic excitation (electron-induced dissociation (EID) [32, 33]). As for A_6, more extensive backbone cleavage is observed in EDD compared to ECD and full sequence coverage is obtained.

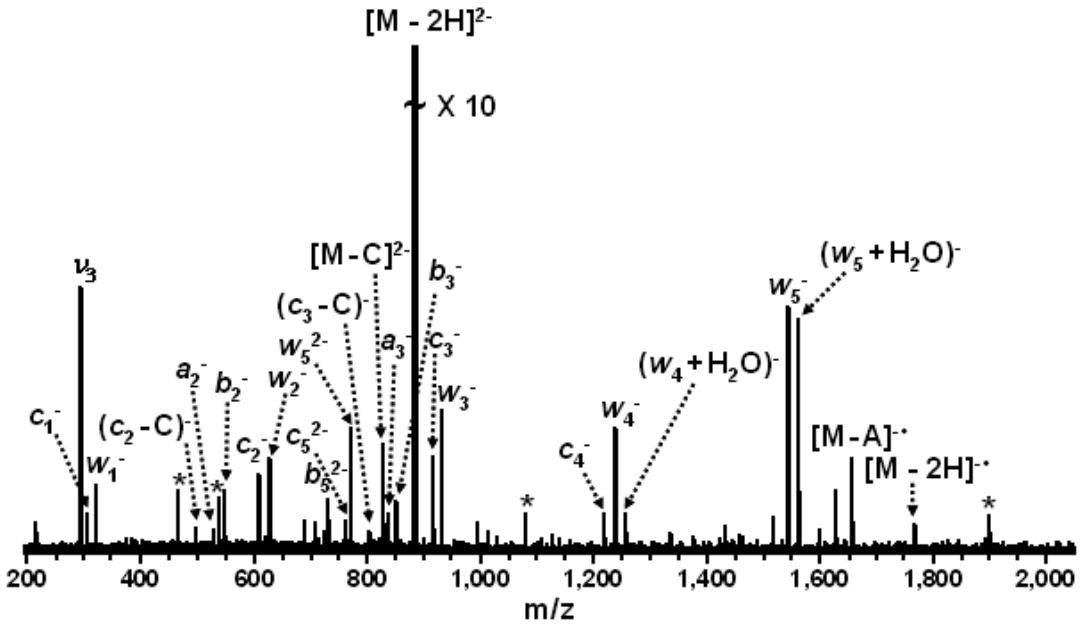

Figure 4-6. EDD (- 18.1 V bias voltage, 2 s irradiation, 32 scans) of the RNA C_6. A complete *d*/*w* ion series is observed, allowing full sequencing of the oligonucleotide. Electronic noise spikes are labeled with asterisks.

Table 4-6. Product ions observed from EDD (2 s irradiation, - 18.3 V bias, 32 scans) of C_6. Ions labeled *w* can also be *d* ions, ions labeled *a* can also be *z* ions, ions labeled *c* can also be *x* ions and ions labeled *b* can also be *y* ions.

Observed m/z	Calculated m/z	Assignment	Error (ppm)
304.0344	304.0339	c_1^-	1.6
322.0445	322.0445	w_1^-	< 0.1
498.0340	498.0320	$(c_2 - C)^-$	4.0
529.1090	529.1089	a_2^-	0.2
547.1204	547.1195	b_2^-	1.6
609.0759	609.0752	c_2^-	1.1
627.0869	627.0858	w_2^-	1.8
715.0751	715.0796	$(w_5 - C)^{2-}$	-6.3

723.1074	723.1070	$(a_3 - C)^-$	0.6
730.6191	730.6181	b_5^{2-}	1.4
761.5938	761.5959	c_5^{2-}	-2.8
770.6016	770.6012	w_5^{2-}	0.5
803.0792	803.0733	$(c_3 - C)^-$	7.3
827.6162	827.6171	$[M - C]^{2-}$	-1.1
834.1515	834.1502	a_3^-	1.6
852.1635	852.1608	b_3^-	3.2
883.1387	883.1387	$[M - 2H]^{2-}$	Calibrant
914.1176	914.1165	c_3^-	1.2
932.1260	932.1271	w_3^-	-1.2
1219.145	1219.158	c_4^-	-10.7
1237.164	1237.168	w_4^-	-3.2
1255.179	1255.179	$(w_4 + H_2O)^-$	< 0.1
1542.207	1542.210	w_5^-	-1.9
1560.216	1560.220	$(w_5 + H_2O)^-$	-2.6
1655.226	1655.234	$[M - C]^{-\bullet}$	-4.8
1766.277	1766.277	$[M - 2H]^{2-}$	Calibrant

4.3.7. Electron Detachment Dissociation of G_6 and CGGGGC Dianions

As mentioned above, the oligoribonucleotide G_6 can be difficult to solublize. Thus, a higher concentration (100 μM) and longer accumulation time (60 s) were needed to build up sufficient signal for EDD. Figure 4-7 shows the EDD spectrum from G_6 and Table 4-7 lists the corresponding products. As for A_6 and C_6 (Figure 4-5 and 4-6), the entire *d*/*w* and *c*/*x* ion series are present as well as some *b*/*y*, (*d*/*w* + H_2O) and nucleobase loss fragment ions.

Base loss is more abundant for G_6 than for the other oligomer RNAs, consistent with previous EDD and ECD experiments of DNA and PNA, which also showed facile guanine loss [15, 18, 34]. However, guanine loss is still a minor fragmentation pathway and the *d*/*w* ion series constitutes the dominant fragmentation channel.

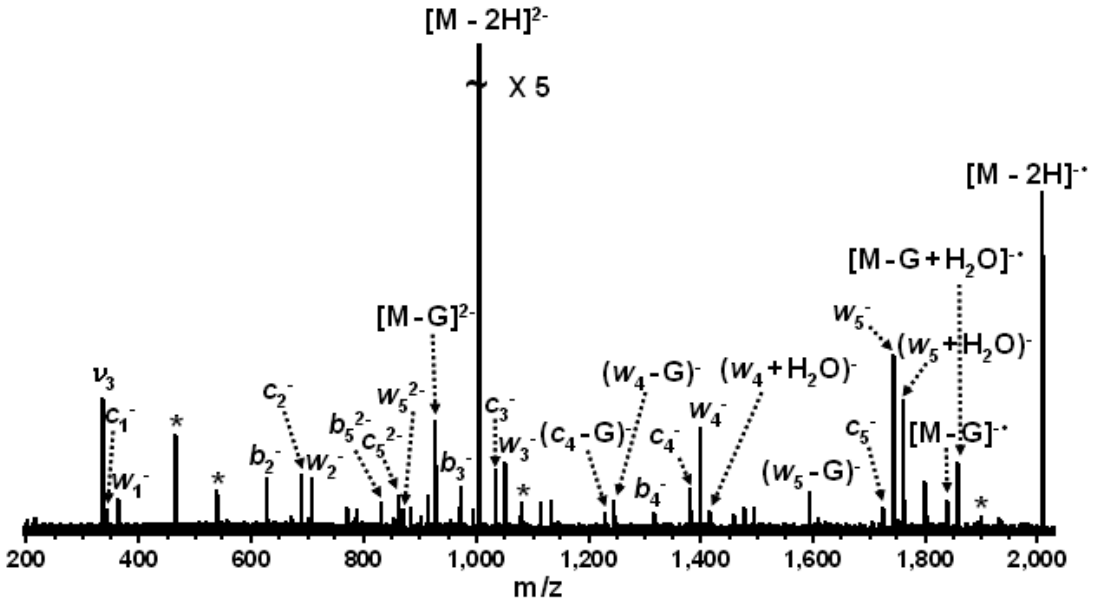

Figure 4-7. EDD (- 18.3 V bias voltage, 2 s irradiation, 32 scans) of the RNA G_6. Complete *d*/*w* and *c*/*x* ion series are observed, allowing full sequencing of the oligonucleotide. Electronic noise spikes are labeled with asterisks.

Table 4-7. Product ions observed from EDD (2 s irradiation, - 18.3 V bias, 32 scans) of G_6. Ions labeled *w* can also be *d* ions, ions labeled *a* can also be *z* ions, ions labeled *c* can also be *x* ions and ions labeled *b* can also be *y* ions.

Observed m/z	Calculated m/z	Assignment	Error (ppm)
344.0394	344.0401	c_1^-	-2.0
362.0500	362.0507	w_1^-	-1.9
627.1298	627.1318	b_2^-	-3.2
689.0879	689.0875	c_2^-	0.6
707.0992	707.0981	w_2^-	1.6
830.6301	830.6334	b_5^{2-}	-4.0
861.6118	861.6112	c_5^{2-}	0.7
870.6100	870.6165	w_5^{2-}	-7.5
927.6326	927.6324	$[M - G]^{2-}$	0.2
972.1780	972.1792	b_3^-	-1.2

1003.157	1003.157	$[M - 2H]^{2-}$	Calibrant
1034.135	1034.135	c_3^-	0.0
1052.145	1052.146	w_3^-	-1.0
1228.131	1228.133	$(c_4 - G)^-$	-1.6
1246.143	1246.144	$(w_4 - G)^-$	-0.8
1317.230	1317.227	b_4^-	2.3
1379.181	1379.182	c_4^-	-0.7
1397.187	1397.193	w_4^-	-4.3
1415.209	1415.204	$(w_4 + H_2O)^-$	3.5
1591.181	1591.191	$(w_5 - G)^-$	-6.3
1724.239	1724.230	c_5^-	5.2
1742.247	1742.240	w_5^-	4.0
1760.247	1760.251	$(w_5 + H_2O)^-$	-2.3
1837.228	1837.254	$[M - G]^{-\bullet}$	-14.2
1855.245	1855.265	$[M - G + H_2O]^{-\bullet}$	-10.8
2006.314	2006.314	$[M - 2H]^{2-}$	Calibrant

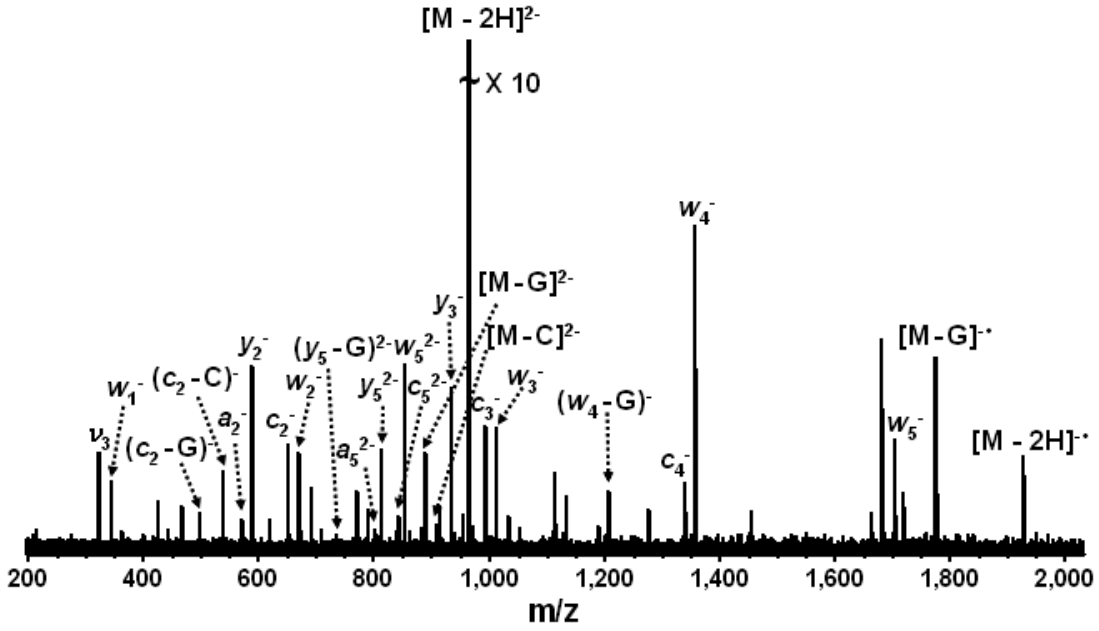

Figure 4-8. EDD (- 18.2 V bias voltage, 2 s irradiation, 32 scans) of the RNA CGGGGC. Again, complete *d*/*w* and *c*/*x* ion series are observed, allowing full sequencing of the oligonucleotide. Electronic noise spikes are labeled with asterisks.

The EDD behavior of G_6 was observed to be rather sensitive to the experimental conditions, similar to ECD of dA_6 [15], possibly due to variations in the gas-phase structure with more or less intramolecular hydrogen bonding. The precursor ions of CGGGGC were easier to generate than those of G_6. However, their fragmentation patterns were very similar, except that no (w/d + H_2O) ions were detected for CGGGGC and more abundant doubly charged product ions were observed for that oligonucleotide, consistent with the presence of cytosine.

Table 4-8. Product ions observed from EDD (2 s irradiation, - 18.2 V bias, 32 scans) of CGGGGC. Ions labeled *w* can also be *d* ions, ions labeled *a* can also be *z* ions, ions labeled *c* can also be *x* ions and ions labeled *b* can also be *y* ions.

Observed m/z	Calculated m/z	Assignment	Error (ppm)
322.0470	322.0444	w_1^-	7.9
498.0355	498.032	$(c_2 - G)^-$	6.9
538.0406	538.0382	$(c_2 - C)^-$	4.4
569.1184	569.1151	a_2^-	5.7
587.1281	587.1256	y_2^-	4.2
649.0837	649.0814	c_2^-	3.5
667.0948	667.0919	w_2^-	4.3
735.1089	735.1056	$(y_5 - G)^{2-}$	4.4
801.6238	801.6251	a_5^{2-}	-1.6
810.6328	810.6303	y_5^{2-}	3.0
841.6117	841.6082	c_5^{2-}	4.1
850.6150	850.6135	w_5^{2-}	1.8
887.6265	887.6262	$[M - G]^{2-}$	0.3
907.6339	907.6293	$[M - C]^{2-}$	5.0
914.1633	914.1625	a_3^-	0.8
932.1738	932.1730	y_3^-	0.8
963.1509	963.1509	$[M - 2H]^{2-}$	Calibrant
994.1282	994.1288	c_3^-	-0.7
1012.140	1012.139	w_3^-	0.6
1206.133	1206.137	$(w_4 - G)^-$	-3.6

1339.176	1339.176	c_4^-	-0.2
1357.183	1357.187	w_4^-	-2.8
1702.227	1702.234	w_5^-	-4.3
1776.247	1776.262	$[M - G]^-$	-7.2
1926.301	1926.301	$[M - 2H]^{2-}$	Calibrant

4.3.8. Electron Detachment Dissociation of U_6 Dianions

Figure 4-9 shows the EDD spectrum from U_6 and Table 4-9 lists the EDD product ions. As for the other RNAs (Figures 4-5 to 4-8), the entire *d*/*w* ion series is present as well as some *c*/*x* and *b*/*y* ions. No base loss product ions are observed. One difference compared to EDD of A_6, C_6, and G_6 is that the abundances of *b*/*y* and *c*/*x* ions are comparable to those of *d*/*w* ions. However, U_6 is unique in that it is highly unlikely to be zwitterionic due to its low proton affinity (similar to dT_6 [18]). The effect of salt bridges on the EDD mechanism is unknown but may influence the fragmentation behavior.

Because U_6 is not likely to be zwitterionic, the doubly charged products c_5^{2-}, b_5^{2-} and w_5^{2-} are likely a result of direct vibrational or electronic excitation. As for the other RNAs, full sequencing can be accomplished from the *d*/*w* ion series.

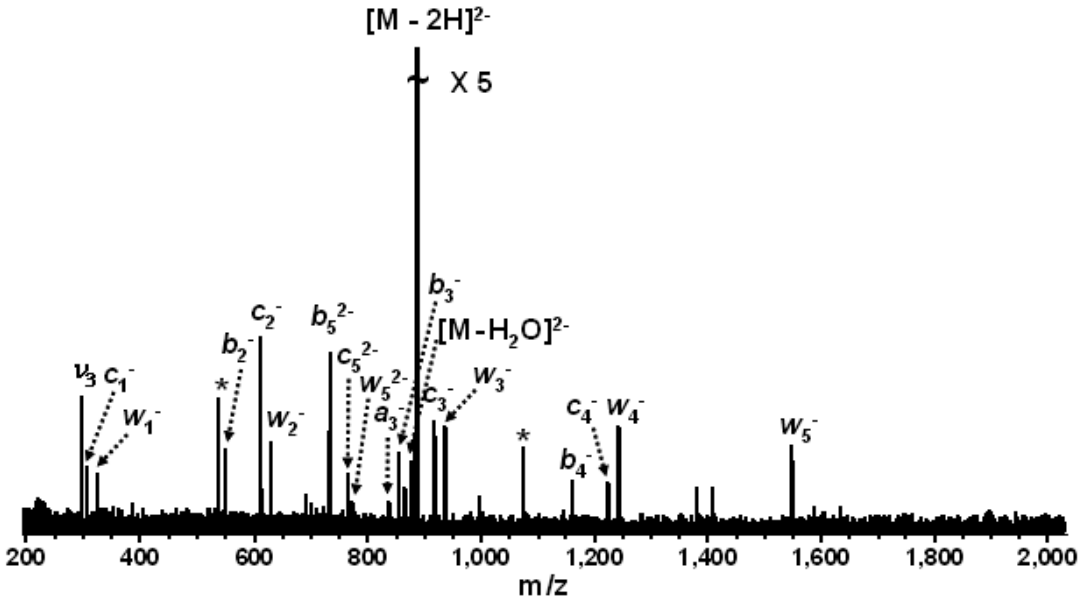

Figure 4-9. EDD (- 18.1 V bias voltage, 2 s irradiation, 32 scans) of the RNA U_6. A complete *d*/*w* ion series is observed, allowing full sequencing of the oligonucleotide. Electronic noise spikes are labeled with asterisks.

Table 4-9. Product ions observed from EDD (2 s irradiation, - 18.1 V bias, 32 scans) of U_6. Ions labeled *w* can also be *d* ions, ions labeled *a* can also be *z* ions, ions labeled *c* can also be *x* ions and ions labeled *b* can also be *y* ions.

Observed m/z	Calculated m/z	Assignment	Error (ppm)
305.0136	305.0180	c_1^-	-14.4
323.0251	323.0285	w_1^-	-10.5
549.0833	549.0876	b_2^-	-7.8
611.0408	611.0433	c_2^-	-4.1
629.0490	629.0538	w_2^-	-7.6
733.0791	733.0781	b_5^{2-}	1.4
764.0532	764.0560	c_5^{2-}	-3.7
773.0631	773.0612	w_5^{2-}	2.5
855.1135	855.1128	b_3^-	0.8

877.0861	877.0854	$[M - H_2O]^{2-}$	0.8
886.0907	886.0907	$[M - 2H]^{2-}$	Calibrant
917.0707	917.0686	c_3^-	2.3
935.0829	935.0791	w_3^-	4.1
1161.141	1161.138	b_4^-	2.6
1223.093	1223.094	c_4^-	-0.8
1241.111	1241.104	w_4^-	5.6
1547.130	1547.130	w_5^-	Calibrant

4.3.9. Electron Detachment Dissociation of GCAUAC Dianions

As for the ECD experiments, we characterized the hybrid oligoribonucleotide GCAUAC to determine the precise identity of ambiguous ion pairs. Table 4-10 lists the product ions observed in the corresponding EDD spectrum (Figure 4-10). Extensive backbone cleavage, including the entire *w* ion series, three *d*-type, four *c*-type, one *x*-type, and three *y*-type ions were detected along with a couple of doubly charged products and products involving nucleobase and/or water loss. This range of fragments reveals that the most probable assignment of *b*/*y* and *c*/*x* ion pairs are as *y* and *c* ions, similar to the dissociation observed in CAD and IRMPD. By contrast, the observed *w*/*d* ion pairs are likely a mixture of both *w* and *d*-type ions, as observed in EDD of DNA.

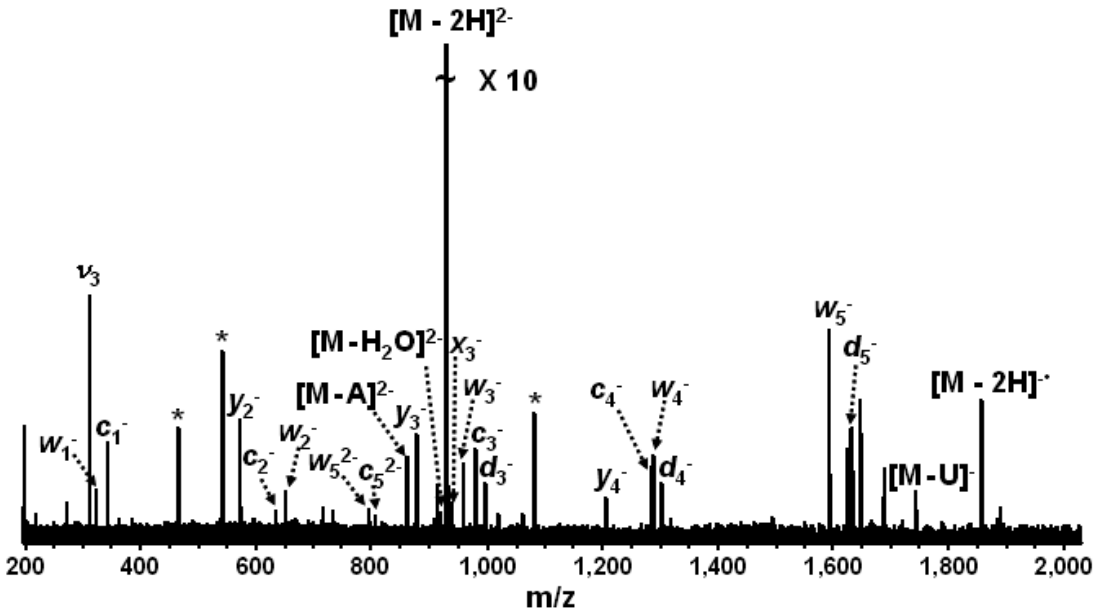

Figure 4-10. EDD (- 18.2 V bias voltage, 2 s irradiation, 32 scans) of the RNA GCAUAC. A complete *w* ion series is observed, allowing full sequencing of the oligonucleotide. Electronic noise spikes are labeled with asterisks.

Table 4-10. Product ions observed from EDD (2 s irradiation, - 18.2 V bias, 32 scans) of the RNA GCAUAC.

Observed m/z	Calculated m/z	Assignment	Error (ppm)
322.0433	322.0444	w_1^-	- 3.4
344.0390	344.0401	c_1^-	- 3.2
571.1315	571.1306	y_2^-	1.6
649.0808	649.0814	c_2^-	- 0.9
651.0997	651.0969	w_2^-	4.3
795.1051	795.1044	w_5^{2-}	0.9
806.1061	806.1022	c_5^{2-}	4.8
860.1172	860.1177	$[M - A]^{2-}$	- 0.6
877.1580	877.1559	y_3^-	2.4
918.6394	918.6396	$[M - H_2O]^{2-}$	- 0.2
927.6449	927.6449	$[M - 2H]^{2-}$	Calibrant
939.1186	939.1117	x_3^-	7.3

957.1233	957.1222	w_3^-	1.1
978.1355	978.1339	c_3^-	1.6
996.1460	996.1445	d_3^-	1.5
1206.206	1206.208	y_4^-	- 1.7
1284.162	1284.159	c_4^-	2.3
1286.169	1286.175	w_4^-	- 4.7
1302.183	1302.170	d_4^-	10
1591.211	1591.216	w_5^-	- 3.1
1631.231	1631.222	d_5^-	5.5
1744.240	1744.270	$[M - U]^-$ (?)	- 17.2
1855.289	1855.289	$[M - 2H]^{2-}$	Calibrant

4.4. CONCLUSIONS

We demonstrate ECD and EDD of hexamer oligoribonucleic acids. The ECD results show a strong nucleobase dependence: A_6 generated mostly *c*/*x* and *b*/*y*-type ions, similar to the fragmentation patterns observed in CAD and IRMPD, whereas C_6 only yielded *d* and *w*-type ions (similar to ECD of DNA). Other RNAs showed a mixture of those ion types. This behavior supports an ECD cleavage mechanism involving electron capture at the nucleobases, consistent with recent theoretical work for neutral DNA. Such a mechanism can be influenced by the presence of a 2' hydroxyl group. However, only limited backbone cleavage was observed in ECD, precluding complete sequencing. EDD appears more promising for RNA structural characterization because more extensive backbone cleavage was observed at higher sensitivity. Here, *w* and *d* ion series constitute the most abundant fragmentation channels, similar to EDD of DNA. The only exception is U_6 for which *w*/*d*-type cleavage competes with *b*/*y* and *c*/x -type cleavage. We propose that the EDD cleavage process is initiated via direct electron detachment from the deprotonated phosphate backbone. EDD provided full sequence coverage for all RNAs.

4.5. BIBLIOGRAPHY

1. Limbach, P. A.; Crain, P. F.; McCloskey, J. A. Molecular Mass Measurement of Intact Ribonucleic Acids via Electrospray Ionization Quadrupole Mass Spectrometry. *J. Am. Soc. Mass Spectrom.* **1995,** *6*, 27-39.
2. Crain, P. F.; McCloskey, J. A. Applications of Mass Spectrometry to the Characterization of Oligonucleotides and Nucleic Acids. *Curr. Opin. Biotechnol.* **1998,** *9*, 25-34.
3. Polson, A. G.; Crain, P. F.; Pomerantz, S. C.; McCloskey, J. A.; Bass, B. L. The Mechanism of Adenosine to Inosine Conversion by the Double-stranded RNA Unwinding/modifying Activity: a High-performance Liquid Chromatography-mass Spectrometry Analysis. *Biochemistry* **1991,** *30*, 11507-11514.
4. Limbach, P. A.; Crain, P. F.; McCloskey, J. A. Summary: The Modified Nucleosides of RNA. *Nucleic Acids Res.* **1994,** *22*, 2183-2196.
5. Pomerantz, S. C.; McCloskey, J. A. Detection of the Common RNA Nucleoside Pseudouridine in Mixtures of Oligonucleotides by Mass Spectrometry. *Anal. Chem.* **2005,** *77*, 4687-4697.
6. Schürch, S.; Bernal-Méndez, E.; Leumann, C. J. Electrospary Tandem Mass Spectrometry of Mixed-Sequence RNA/DNA Oligonucleotides. *J. Am. Soc. Mass Spectrom.* **2002,** *13*, 936-945.
7. Tromp, J. M.; Schürch, S. Gas-Phase Dissociation of Oligoribonucleotides and their Analogs Studied by Electrospray Ionization Tandem Mass Spectrometry. *J. Am. Soc. Mass Spectrom.* **2005,** *16*, 1262-1268.

8. Sannes-Lowery, K. A.; Hofstadler, S. A. Sequence Confirmation of Modified Oligonucleotides using IRMPD in the External Reservoir of an Electrospray Ionization Fourier Transform Ion Cyclotron Mass Spectrometer. *J. Am. Soc. Mass Spectrom.* **2003,** *14*, 825-833.
9. McLafferty, F. W.; Horn, D. M.; Breuker, K.; Ge, Y.; Lewis, M. A.; Cerda, B.; Zubarev, R. A.; Carpenter, B. K. Electron Capture Dissociation of Gaseous Multiply Charged Ions by Fourier Transform Ion Cyclotron Resonance. *J. Am. Soc. Mass Spectrom.* **2001,** *12*, 245-249.
10. Zubarev, R. A. Reactions of Polypeptide Ions with Electrons in the Gas Phase. *Mass Spectrom. Rev.* **2003,** *22*, 57-77.
11. Zubarev, R. A. Electron-capture Dissociation Tandem Mass Spectrometry. *Curr. Opin. Biotechnol.* **2004,** *15*, 12-16.
12. Cooper, H. J.; Håkansson, K.; Marshall, A. G. The Role of Electron Capture Dissociation in Biomolecular Analysis. *Mass Spectrom. Rev.* **2005,** *24*, 201-222.
13. McLuckey, S. A.; Van Berkel, G. J.; Glish, G. L. Tandem Mass Spectrometry of Small, Multiply-charged Oligonucleotides. *J. Am. Soc. Mass Spectrom.* **1992,** *3*, 60-70.
14. Håkansson, K.; Hudgins, R. R.; Marshall, A. G.; O'Hair, R. A. J. Electron Capture Dissociation and Infrared Multiphoton Dissociation of Oligodeoxynucleotide Dications. *J. Am. Soc. Mass Spectrom.* **2003,** *14*, 23-41.
15. Schultz, K. N.; Håkansson, K. Rapid Electron Capture Dissociation of Mass-Selectively Accumulated Oligodeoxynucleotide Dications. *Int. J. Mass Spectrom.* **2004,** *234*, 123-130.

16. Horn, D. M.; Breuker, K.; Frank, A. J.; McLafferty, F. W. Kinetic Intermediates in the Folding of Gaseous Protein Ions Characterized by Electron Capture Dissociation Mass Spectrometry. *J. Am. Chem. Soc.* **2001,** *123*, 9792-9799.
17. Budnik, B. A.; Haselmann, K. F.; Zubarev, R. A. Electron Detachment Dissociation of Peptide Di-anions: an Electron-hole Recombination Phenomenon. *Chem. Phys. Lett.* **2001,** *342*, 299-302.
18. Yang, J.; Mo, J.; Adamson, J. T.; Håkansson, K. Characterization of Oligodeoxynucleotides by Electron Detachment Dissociation Fourier Transform Ion Cyclotron Resonance Mass Spectrometry. *Anal. Chem.* **2005,** *77*, 1876-1882.
19. de Koning, L. J.; Nibbering, N. M. M.; van Orden, S. L.; Laukien, F. H. Mass Selection of Ions in a Fourier Transform Ion Cyclotron Resonance Trap Using Correlated Harmonic Excitation Fields (CHEF). *Int. J. Mass Spectrom. Ion Processes* **1997,** *165*, 209-219.
20. Breuker, K.; Oh, H.; Cerda, B. A.; Horn, D. M.; McLafferty, F. W. Hydrogen Atom Loss in Electron Capture Dissociation: a Fourier Transform Ion Cyclotron Resonance Study with Single Isotopomeric Ubiquitin Ions. *Eur. J. Mass Spectrom.* **2002,** *8*, 177-180.
21. Green-Church, K. B.; Limbach, P. A. Mononucleotide Gas-Phase Proton Affinities as Determined by the Kinetic Method. *J. Am. Soc. Mass Spectrom.* **2000,** *11*, 24-32.
22. Green-Church, K. B.; Limbach, P. A.; Freitas, M. A.; Marshall, A. G. Gas-phase Hydrogen/deuterium Exchange of Positively Charged Mononucleotides by use of Fourier-transform Ion Cyclotron Resonance Mass Spectrometry. *J. Am. Soc. Mass Spectrom.* **2001,** *12*, 268-277.

23. Cerny, R. L.; Tomer, K. B.; Gross, M. L.; Grotjahn, L. Fast atom bombardment combined with tandem mass spectrometry for determining structures of small oligonucleotides. *Anal. Biochem.* **1987,** *165*, 175-182.
24. Wan, K. X.; Gross, J.; Hillenkamp, F.; Gross, M. L. Fragmentation Mechanisms of Oligodeoxynucleotides Studied by H/D Exchange and Electrospray Ionization Tandem Mass Spectrometry. *J. Am. Soc. Mass Spectrom.* **2001,** *12*, 193-205.
25. Berdys, J.; Anusiewicz, I.; Skurski, P.; Simons, J. Damage to Model DNA Fragments from Very Low-Energy (<1 eV) Electrons. *J. Am. Chem. Soc.* **2004,** *126*, 6441-6447.
26. Li, X.; Sevilla, M. D.; Sanche, L. Density Functional Theory Studies of Electron Interaction with DNA: Can Zero eV Electrons Induce Strand Breaks? *J. Am. Chem. Soc.* **2003,** *125*, 13668-13669.
27. McFarland, M. A.; Chalmers, M. J.; Quinn, J. P.; Hendrickson, C. L.; Marshall, A. G. Evaluation and Optimization of Electron Capture Dissociation Efficiency in Fourier Transform Ion Cyclotron Resonance Mass Spectrometry. *J. Am. Soc. Mass Spectrom.* **2005,** *16*, 1060-1066.
28. Griffey, R. H.; Greig, M. J.; Robinson, J. M.; Laude, D. A. Gas-phase Hydrogen-deuterium Exchange in Phosphorothioate d(GTCAG) and d(TCGAT). *Rapid Commun. Mass Spectrom.* **1999,** *13*, 113-117.
29. Kjeldsen, F.; Silivra, O. A.; Ivonin, I. A.; Haselmann, K. F.; Gorshkov, M.; Zubarev, R. A. C-alpha-C Backbone Fragmentation Dominates in Electron Detachment Dissociation of Gas-phase Polypeptide Polyanions. *Chem. Eur. J.* **2005,** *11*, 1803-1812.

30. Wang, X. B.; Vorpagel, E. R.; Yang, X.; Wang, L. Experimental and Theoretical Investigations of the Stability, Energetics, and Structures of H_2PO^{4-}, $H_2P_2O_7^{2-}$, and $H_3P_3O_{10}^{2-}$ in the Gas Phase. *J. Phys. Chem. A* **2001,** *105*, 10468-10474.
31. Hush, N. S.; Cheung, A. S. Ionization Potentials and Donor Properties of Nucleic Acid Bases and Related Compounds. *Chem. Phys. Lett.* **1975,** *34*, 11-13.
32. Budnik, B. A.; Haselmann, K. F.; Elkin, Y. N.; Gorbach, V. I.; Zubarev, R. A. Applications of Electron-Ion Dissociation Reactions for Analysis of Polycationic Chitooligosaccharides in Fourier Transform Mass Spectrometry. *Anal. Chem.* **2003,** *75*, 5994-6001.
33. Cody, R. B.; Freiser, B. S. Electron Impact Excitation of Ions from Organics: an Alternative to Collision Induced Dissociation. *Anal. Chem.* **1979,** *51*, 547 - 551.
34. Olsen, J. V.; Haselmann, K. F.; Nielsen, M. L.; Budnik, B. A.; Nielsen, P. E.; Zubarev, R. A. Comparison of Electron Capture Dissociation and Collisionally Activated Dissociation of Polycations of Peptide Nucleic Acids. *Rapid Commun. Mass Spectrom.* **2001,** *15*, 969-974.

CHAPTER 5

CHARACTERIZATION OF OLIGODEOXYNUCLEOTIDE FRAGMENTATION PATHWAYS IN INFRARED MULTIPHOTON DISSOCIATION AND ELECTRON DETACHMENT DISSOCIATION BY FOURIER TRANSFORM ION CYCLOTRON DOUBLE RESONANCE

Infrared multiphoton dissociation (IRMPD) is a vibrational excitation tandem mass spectrometric fragmentation method valuable for sequencing of oligonucleotides. For oligodeoxynucleotides, typical product ions correspond to sequence-specific 5' (*a* - base) and their complementary 3' *w*-type ions from carbon-oxygen bond cleavage at the 3' position of the deoxyribose from which a nucleobase is lost. Such fragmentation patterns are also observed in collision activated dissociation (CAD). The CAD oligodeoxynucleotide fragmentation mechanism has been characterized in detail. By contrast, fragmentation schemes in IRMPD have not been rigorously established. In this chapter, we apply for the first time Fourier transform ion cyclotron double resonance (DR) experiments to characterize IRMPD fragmentation pathways of oligodeoxynucleotide anions. Our results suggest that neutral base loss precedes backbone fragmentation but that T-rich oligodeoxynucleotides fragment via a different mechanism, similar to the mechanisms proposed for CAD. We also extend the DR approach to characterize intermediates in electron detachment dissociation of hexamer oligodeoxynucleotides.

Here, we found that charge reduced radical precursor ions constitute major intermediates for dT_6, d(GCATAC), and d(GCATGC). Furthermore, (*a*/*z* - T) ions (*z* ions correspond to C-O bond cleavage on the other side of a backbone phosphate group as compared to the formation of *a* ions) mainly originate from secondary fragmentation of *a*/*z* radical ions for the oligodeoxynucleotide dT_6.

5.1. INTRODUCTION

Tandem mass spectrometry is widely used for structural characterization and sequencing of oligonucleotides [1-4]. Compared with conventional enzymatic techniques, mass spectrometry provides rapid sequencing and is advantageous for characterizing modified oligonucleotides [5, 6]. Collision activated dissociation [7, 8], involving dissociation of even-electron anions, is a well established MS/MS technique for sequencing oligonucleotides. CAD is classified as a 'slow heating' technique, which, for oligodeoxynucleotides, results mainly in nucleobase (B) loss and sequence-specific (*a* - B) and *w*-type ions (McLuckey nomenclature [9]) from carbon-oxygen bond cleavage at the 3' position of the sugar from which a base is lost. Infrared multiphoton dissociation [6, 10] is an alternative vibrational excitation fragmentation method, providing similar oligonucleotide fragmentation patterns as CAD. For Fourier transform ion cyclotron resonance mass analysis, IRMPD eliminates the pumping down time required following in-cell CAD. McLafferty and co-workers have demonstrated the utility of IRMPD for characterization of large biomolecules, including oligonucleotides with up to 108 residues [8, 10]. Sannes-Lowery and Hofstadler implemented IRMPD in the external ion reservoir of an FT-ICR mass spectrometer to characterize modified oligonucleotides, resulting in increased sequence coverage and product ion yields compared to in-cell

IRMPD because ions are exposed to a range of laser irradiation times, and metastable ions are stabilized by the high gas pressure in this region [6]. With this approach, these authors found that sequence-specific (*a* - B) and *w*-type ions can provide rapid and accurate sequencing of modified oligonucleotides [6]. Brodbelt and co-workers have compared CAD and IRMPD of both deprotonated and protonated oligonucleotides in a quadrupole ion trap and found that IRMPD can minimize the uninformative [M - B] ions (in which M denotes the precursor ions), which dominate CAD spectra. Furthermore, free phosphate and nucleobase ions can be observed, which can aid the identification of modified bases [11].

Electron capture dissociation, which was introduced in 1998 by McLafferty and co-workers [12], has been shown to provide unique fragmentation patterns for peptides and proteins due to the associated gas-phase radical ion chemistry [12-14]. Håkansson et al. have shown that irradiation of gas-phase oligodeoxynucleotide dications with low energy electrons provides complementary sequence-specific backbone cleavage with the major product ions being *w* and *d* ion series [15]. In addition, radical *a*/z as well as (*a*/*z* - B) and (*c*/*x* - B) ions are produced but nucleobase loss constitutes a minor fragmentation pathway [15, 16]. ECD has also been shown to be 'soft' enough to retain gas-phase hydrogen bonding in dA_6 (similar to protein ECD [17]), thereby allowing characterization of higher order structure [16]. However, because ECD requires cationic precursor ions, its sensitivity for nucleic acid characterization is limited. Electron detachment dissociation, involving irradiation with ≥10 eV electrons, was introduced by Zubarev and co-workers as a means to induce radical ion mediated fragmentation pathways for biomolecular anions [18]. We have extended EDD to oligonucleotide characterization and demonstrated extensive backbone fragmentation of oligodeoxy- [19]

and oligoribo-nucleotides [20] (described in Chapters 2 and 4), complementary to that of other MS/MS techniques, such as CAD and IRMPD. Our group also showed that EDD can preferentially cleave C-S and S-S bonds in multiply charged disulfide-bonded peptide anions [21], and retain higher order structure of DNA hairpins [22].

Several groups have performed extensive research to explore oligonucleotide fragmentation pathways in CAD and several fragmentation mechanisms have been proposed. McLuckey and Habibi-Goudarzi proposed a two step fragmentation scheme (nucleobase loss followed by backbone cleavage) via 1,2-elimination involving hydrogens from the sugar [23]. These authors suggested that a nucleobase can be lost either as a neutral or as an anion and found the following order of preference for loss of anionic base: $A^- > T^- > G^- > C^-$ [23]. Similar conclusions were reached by Rodgers and co-workers [24]. Barry et al. proposed a base-catalyzed 2 step internal elimination scheme in which the 2' proton of the sugar is attacked by a negatively charged 3' phosphate oxygen and a base anion is lost [25]. Gross and co-workers proposed that intramolecular proton transfer occurs from an adjoining 5' phosphate to a nucleobase, thereby forming a zwitterionic intermediate which dissociates via loss of a neutral base followed by backbone cleavage [26]. The major proton source was verified by CAD of DNA with a methylphosphonate backbone [26]. Because IRMPD is also a 'slow heating' fragmentation technique, oligonucleotide fragmentation likely proceeds through the same mechanism as in CAD although, to our knowledge, experiments to explicitly address IRMPD fragmentation pathways have not been performed.

The EDD fragmentation mechanism has been the subject of only a few studies. Budnik and Zubarev proposed that high energy electrons (> 10 eV) can ionize peptide anions to create a positive radical charge (hole) [18]. The exothermicity of

intramolecular electron-hole recombination is about 5 eV, which can contribute to peptide backbone cleavage, including N-C_α bond breakage. Preferential cleavage of backbone bonds over side-chain loss in EDD of peptides has been confirmed by ab initio calculations [27]. Kjeldsen et al. found that EDD can result in preferential formation of $a^\bullet$ and *x* product ions (C_α-C peptide backbone bond cleavage) via dissociation of oxidized radical anions $[M - nH]^{(n-1)-\bullet}$ by a directionally restricted mechanism (unidirectional fragmentation) [28]. Amster and co-workers found that EDD produces information-rich tandem mass spectra for glycosaminoglycans, including both cross ring and glycosidic cleavage product ions [29]. The same group used EDD to distinguish the epimers glucuronic acid and iduronic acid in heparan sulfate tetrasaccharides based on diagnostic product ions, which are not observed in CAD or IRMPD [30]. These authors proposed a radical-initiated mechanism involving hydrogen rearrangement and simple alpha-cleavage [30]. However, the EDD fragmentation mechanism for oligonucleotides is still unknown. In EDD, we observe the *w* and (*a* - B) type ions typically seen in CAD and IRMPD. However *d*-type ions from cleavage between sugar 5' carbons and their neighboring oxygens (i.e., on the other side of the phosphate group compared to *w* ion formation), radical *a* and *z* type ions (where the latter is complementary to the *d* ions) without base loss, and *c* and *x* ions from cleavage of backbone P-O bonds, are also present as well as base loss from *c*, *x*, *d*, and *w* ions [19]. The co-existence of *a* and (*a* - B) ions may suggest that *a* ions (not observed in CAD/IRMPD) are precursors of (*a* - B) ions, which would then form through secondary fragmentation. Based on the absence of a nucleobase dependence, we have proposed that the EDD cleavage process is initiated via direct electron detachment from the deprotonated phosphate backbone, thereby generating charge reduced radical precursor ions as intermediates [20].

FT-IC double resonance (DR) experiments, first reported by Comisarow and co-workers [31], can provide information on intermediates in dissociation pathways. Such experiments involve selective excitation at particular cyclotron frequencies. If ions with corresponding m/z values exist in the ICR cell, they will be ejected and, consequently, if such ions serve as intermediates in fragmentation reactions, corresponding product ions will disappear from MS/MS spectra as long as the lifetime of the intermediate is sufficiently long to be affected by the excitation waveform. DR experiments have been used by Williams and co-workers to study gas-phase dissociation pathways of peptide clusters [32]. Cooper utilized DR to demonstrate that *b* ions observed in ECD of peptides are unlikely to be a result of secondary fragmentation of *c*-type ions [33]. O'Connor and co-workers recently applied DR to examine the lifetime of radical intermediates in ECD and deduce information about the gas-phase conformation of peptide ions [34]. Here, we apply DR to study both IRMPD and EDD fragmentation pathways of oligodeoxynucleotides.

5.2. EXPERIMENTAL SECTION

5.2.1. Sample Preparation

Reversed phase high performance liquid chromatography purified dA_6, dC_6, dT_6, d(GCATGC) and d(CTATCAGTGA) sodium salts, and d(GCATAC) ammonium salt were purchased from TriLink BioTechnologies, Inc. (San Diego, CA) and used without further purification. Negative mode electrospray solvent consisted of 1:1 (v/v) isopropanol:water (Fisher, Fair Lawn, New Jersey) with 10 mM ammonium acetate (Fisher). The final oligonucleotide concentration was 5 to 20 μM.

5.2.2. Fourier Transform Ion Cyclotron Resonance Mass Spectrometry

All experiments were performed with a 7 Tesla quadrupole-Fourier transform ion cyclotron resonance (Q-FT-ICR) mass spectrometer，shown in Figure 2-1. Samples were infused via an external Apollo electrospray ion source at a flow rate of 70 μL/h, mass selectively externally accumulated (6 m/z isolation window) for 0.5-4 s and captured in the ICR cell by dynamic trapping. The accumulation, ion transfer and capture events were looped 2-4 times for improved precursor ion abundance. IRMPD was performed with a vertically mounted 25 W, 10.6 μm, CO_2 laser (Synrad, Mukilteo, WA). The laser beam is deflected by two mirrors for alignment through the hollow dispenser cathode to the center of the ICR cell. The beam enters the vacuum system through a BaF_2 window. Photon irradiation was performed for 0.7-1.2 s at 3.0-4.5% laser power. The main purpose of employing low laser power was to increase the time scale of the dissociation event, thereby allowing for more well-defined frequency-domain DR. EDD was performed with an indirectly heated hollow dispenser cathode electron source (Heat Wave, Watsonville, CA). During the EDD event, the cathode voltage was pulsed to - 18.2 V for 2 s. A lens located in front of the cathode was kept at - 19 V throughout the experiment. The heater was set to approximately 8.5 V, generating a heating current of 1.8 A. Data processing was performed with the MIDAS analysis software [35]: a Hanning window function was applied and data sets were zero filled once prior to fast Fourier transformation followed by magnitude calculation. Peak lists were generated and exported to Microsoft Excel for internal frequency-to-mass calibration with a two-term calibration equation. The calculated masses of the $[M - 2H]^{2-}$ / $[M - 3H]^{3-}$ precursor ions and the typical IRMPD fragment w_1^- (for IRMPD experiments), or charge reduced precursor ions (for EDD experiments) were used for internal calibration. All mass

spectra were acquired with XMASS software (Bruker) in broadband mode from m/z 200 to 2,000 with 256k data points and summed over 20 scans.

5.2.3. Double Resonance

A modified experimental pulse program was used to perform DR-IRMPD or DR-EDD experiments. The pulse sequence for DR was the following: 1) turn on rf voltage with target ion's ICR frequency, 2) turn on the laser or electron source, 3) perform DR-IRMPD or DR-EDD for desired time period (typically 0.6-2.0 s), 4) turn off the laser or electron source, and 5) turn off the rf voltage. The amplitude of the DR rf waveform was tuned not to influence other ions in the spectra but still eject target ions as effectively as possible.

5.3. RESULTS AND DISCUSSION

5.3.1. DR-IRMPD of dA_6 and dC_6 Anions

IRMPD spectra of doubly deprotonated dA_6 with and without DR ejection at the frequency of $[M - A]^{2-}$ (corresponding to neutral loss of an adenine base) are shown in Figure 5-1 (only the m/z range from 200 to 1475 is included because there were no product ion peaks above 1475). In order to determine the abundance change of product ions upon DR, the y axes of all figures are shown at the same scale in units of absolute abundance. Figure 5-1a shows a typical IRMPD spectrum of dA_6 (without DR), resulting in abundant *w*, (*a* - A), (*c*/*x* - A) (both *c* and *x*-type product ion types have been reported in IRMPD of oligodeoxynucleotides [6] and they cannot be distinguished here due to the symmetric nature of dA_6), doubly charged *w* and [M - A] ions (A = adenine). The latter ion type corresponds to one of the dominant fragmentation pathways. When applying

DR at the frequency of the $[M - A]^{2-}$ ions (Figure 5-1b), a significant decrease in abundance was observed for all product ions: only very low abundance *w*, (*a* - A), doubly charged *w*, and [M - A] ions were detected. Incomplete ejection of $[M - A]^{2-}$ ions is likely due to the relatively small amplitude of the DR rf waveform, which was tuned not to interfere with other ions in the spectrum. This result clearly suggests that $[M - A]^{2-}$ is the major intermediate of the fragmentation process. The decrease of (*c*/*x* - A) ions indicates that they are also formed via an $[M - A]^{2-}$ intermediate although the detailed formation mechanism is not clear. DR ejection at the ICR frequency of $[M - A]^{-}$ (corresponding to loss of a base anion, which was not observed in the spectrum but could still constitute an intermediate in the fragmentation process) was also performed, not showing any influence on the product ion abundance. These data provide further evidence that IRMPD of oligonucleotides proceeds via a mechanism similar to that proposed by Gross and co-workers for CAD of oligodeoxynucleotide anions [26, 36]. This conclusion is further justified by the previous observation that adenine should be the nucleobase most easily lost as an anion [23], which does not appear to occur here. Similar results were observed in DR-IRMPD of dC_6 (see Figure 5-2). However, it is interesting to note that the w_5^{2-} ion abundance did not change upon DR at $[M - C]^{2-}$, suggesting that w_5^{2-} may not form via a neutral base loss intermediate for that oligonucleotide.

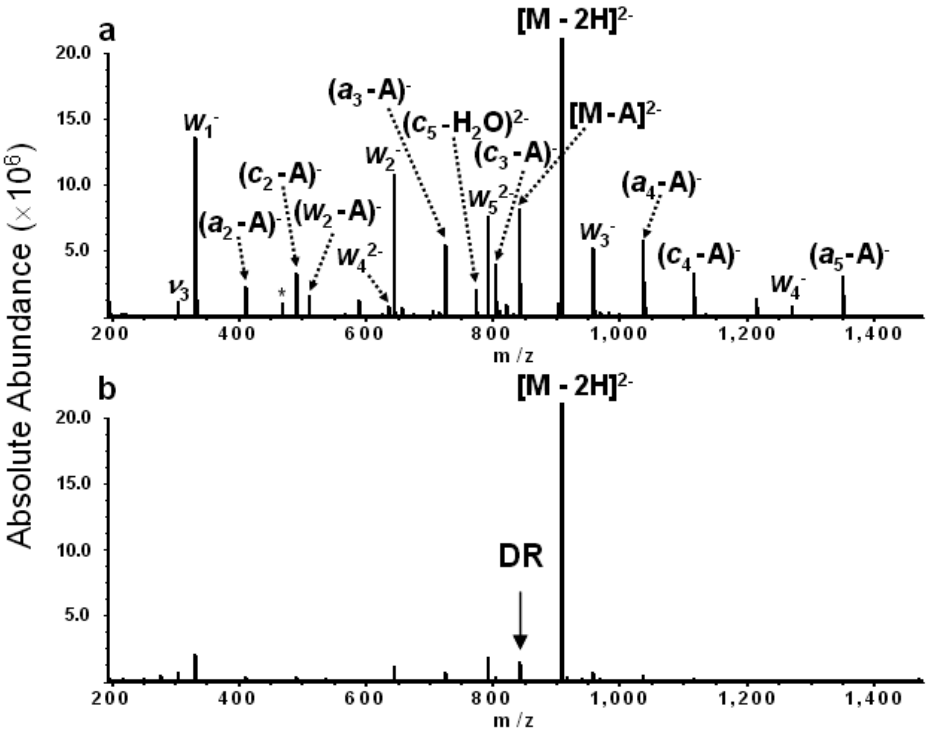

Figure 5-1. IRMPD spectra of doubly deprotonated dA_6 without (a) and with (b) double resonance ejection at the ICR frequency of $[M - A]^{2-}$. (The solid arrow indicates the m/z corresponding to the frequency of the DR rf waveform, * = electronic noise spike).

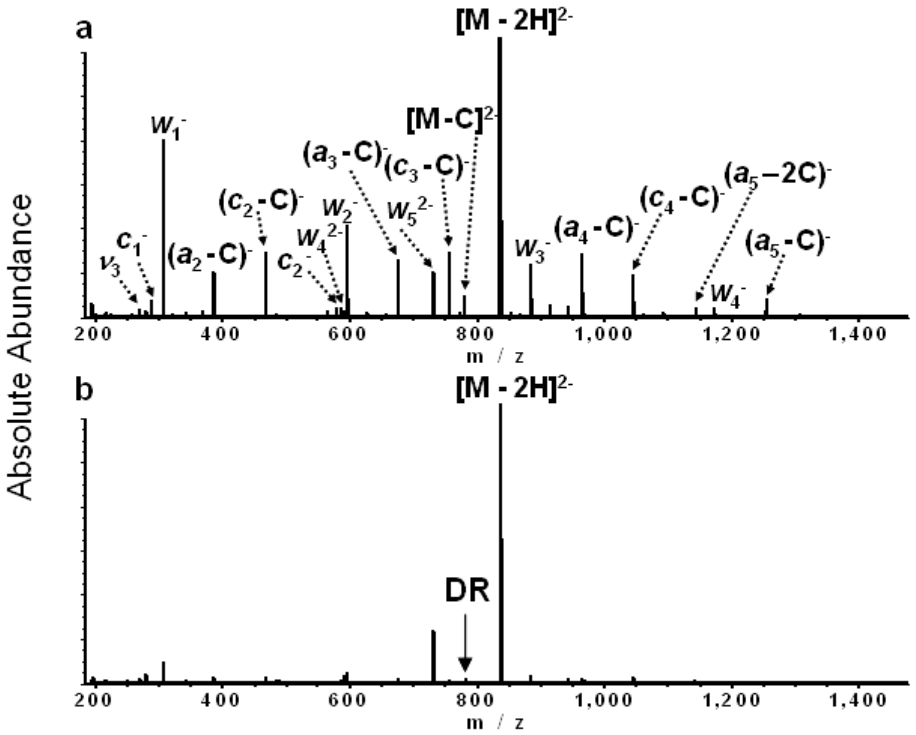

Figure 5-2. IRMPD spectra of doubly deprotonated dC_6 without (a) and with (b) DR ejection at the ICR frequency of $[M - C]^{2-}$. (The solid arrow indicates the m/z corresponding to the frequency of the DR rf waveform).

5.3.2. DR-IRMPD of dT_6 Anions

Figure 5-3 shows IRMPD of doubly deprotonated dT_6 without (a) and with (b) DR ejection at the frequency of $[M - T]^{2-}$ (corresponding to neutral loss of a thymine base). IRMPD of dT_6 results in extensive *w*, *a*, (*a* - T), (*c*/*x* - T) and doubly charged *w*/*d* ions. In CAD of oligonucleotide anions, cleavage on the 3' side of a thymidine residue is generally reduced and (*a* - T) ions are not typically observed unless there are multiple thymidines in a row [6]. This phenomenon has been ascribed to the low proton affinity of thymine, providing further support for the proton transfer mechanism proposed by Gross and co-workers [26, 36]. For dT_6, the observation of abundant (*a*/*z* - T) ions is

likely due to the absence of other nucleobases. Additionally, relatively abundant *a*/*z* ions are observed, which were not observed in IRMPD of dA_6 and dC_6, suggesting that such ions originate from a different fragmentation mechanism. As seen in Figure 5-3, ejection of $[M - T]^{2-}$ did not significantly affect the abundance of other product ions, suggesting that IRMPD fragmentation of dT_6 does not proceed via neutral base loss. Alternatively, the lifetime of a $[M - T]^{2-}$ intermediate may be shorter than the time it takes to eject such ions from the ICR cell by the DR rf waveform. Additional DR experiments with ejection at $[M - T]^{-}$ yielded the same result as for dA_6 and dC_6, i.e., there was no influence on other product ions.

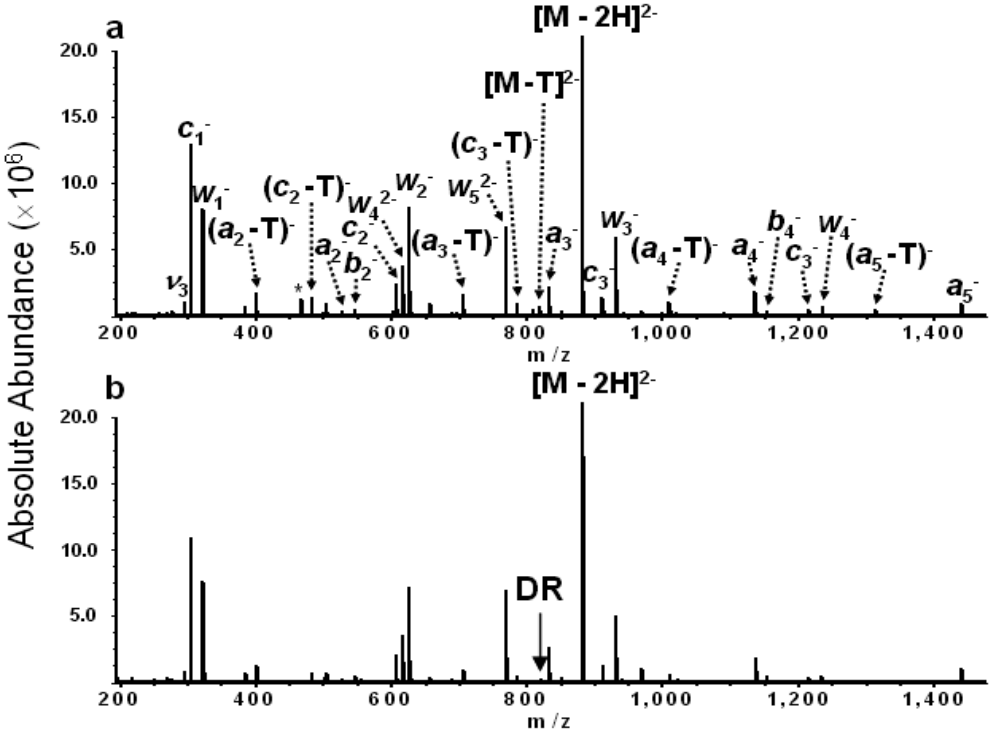

Figure 5-3. IRMPD spectra of doubly deprotonated dT_6 without (a) and with (b) DR ejection at the ICR frequency of $[M - T]^{2-}$. (The solid arrow indicates the m/z corresponding to the frequency of the DR rf waveform, * = electronic noise spike).

5.3.3. DR-IRMPD of d(GCATAC) and d(GCATGC) Anions

In order to gain further support for an IRMPD fragmentation mechanism involving neutral base loss as the first step, we extended our DR experiments to an oligonucleotide containing all four nucleobases with an asymmetric sequence, d(GCATAC). The asymmetry of this oligonucleotide ensures that most product ions can be unambiguously assigned (e.g., *d* and *w*-type ions, which have the same mass for the symmetric oligonucleotides studied above, can be assigned based on their different nucleotide composition). Figure 5-4a shows an IRMPD spectrum of doubly deprotonated d(GCATAC). Mainly the complementary $w_1/(a_5$ - A), $w_3/(a_3$ - A), and $w_4/(a_2$ - C) product ion pairs are observed. The formation of these fragment pairs involves neutral loss of adenine and cytosine. Neutral loss of both A, C, and G is seen from the precursor ions. Furthermore, a doubly charged w_5 anion is present but w_2, (a_4 - T), and $[M - T]^{2-}$ product ions were not detected. When we ejected $[M - A]^{2-}$ during the IRMPD process, drastic (~83±8% drop) influence on the abundance of product ions corresponding to backbone cleavage on the 3' side of the adenosine residues ($w_1/(a_5$ - A) and $w_3/(a_3$ - A)) was observed (Figure 5-4b). The abundance of other product ions was also decreased although to a much lower extent (~4% drop). We believe this phenomenon is due to the small ICR frequency difference between $[M - A]^{2-}$, $[M - C]^{2-}$, and $[M - G]^{2-}$ product ions. The limited duration of the DR rf waveform results in a frequency uncertainty that affects ions with close frequencies. Figure 5-4c shows the product ion pattern in DR-IRMPD with ejection at the frequency of $[M - C]^{2-}$. Here, only the w_4 and (a_2 - C) ions are drastically affected (~85±8% drop).

Gross and co-workers suggested that protons from an adjoining 5'-phosphate constitute the principal source for proton transfer to nucleobases during collisional

activation [26]. H/D exchange experiments showed that w_3 ions are formed in an alternative manner without losing guanosine in CAD of deuterated d(GTTT). This oligonucleotide does not contain a phosphate group on the 5' side of G and deuteron transfer from the phosphate located on the 3' side of G must overcome a sterochemical barrier [36]. For d(GCATAC) studied here the guanosine is also located at the 5' end and formation of w_5 ions would be subject to similar conditions as for d(GTTT) described above. The fragmentation pattern in DR-IRMPD with ejection at the frequency of $[M - G]^{2-}$ (Figure 5-4d) shows an average of 40% decrease for w_5^{2-}, which is lower than the corresponding product ion decrease observed when ejecting $[M - A]^{2-}$ and $[M - C]^{2-}$ ions (83 and 85%, respectively). This result is in agreement with the mechanism described by Gross and co-workers [36]. To further explore the influence of $[M - G]^{2-}$ ejection, we also performed DR-IRMPD of a different hexamer, d(GCATGC) (see Figure 5-5), which contains guanosine in the middle of the sequence. DR ejection of $[M - G]^{2-}$ resulted in 76±3% decreases of the w_1 and (a_5 - G) ions, corresponding to backbone cleavage on the 3' side of the guanosine in the fifth position, but only an average of 36% decrease of w_5^{2-} ions. Again the lower abundance decrease of w_5^{2-} ions suggests that a portion of them are formed via a different mechanism.

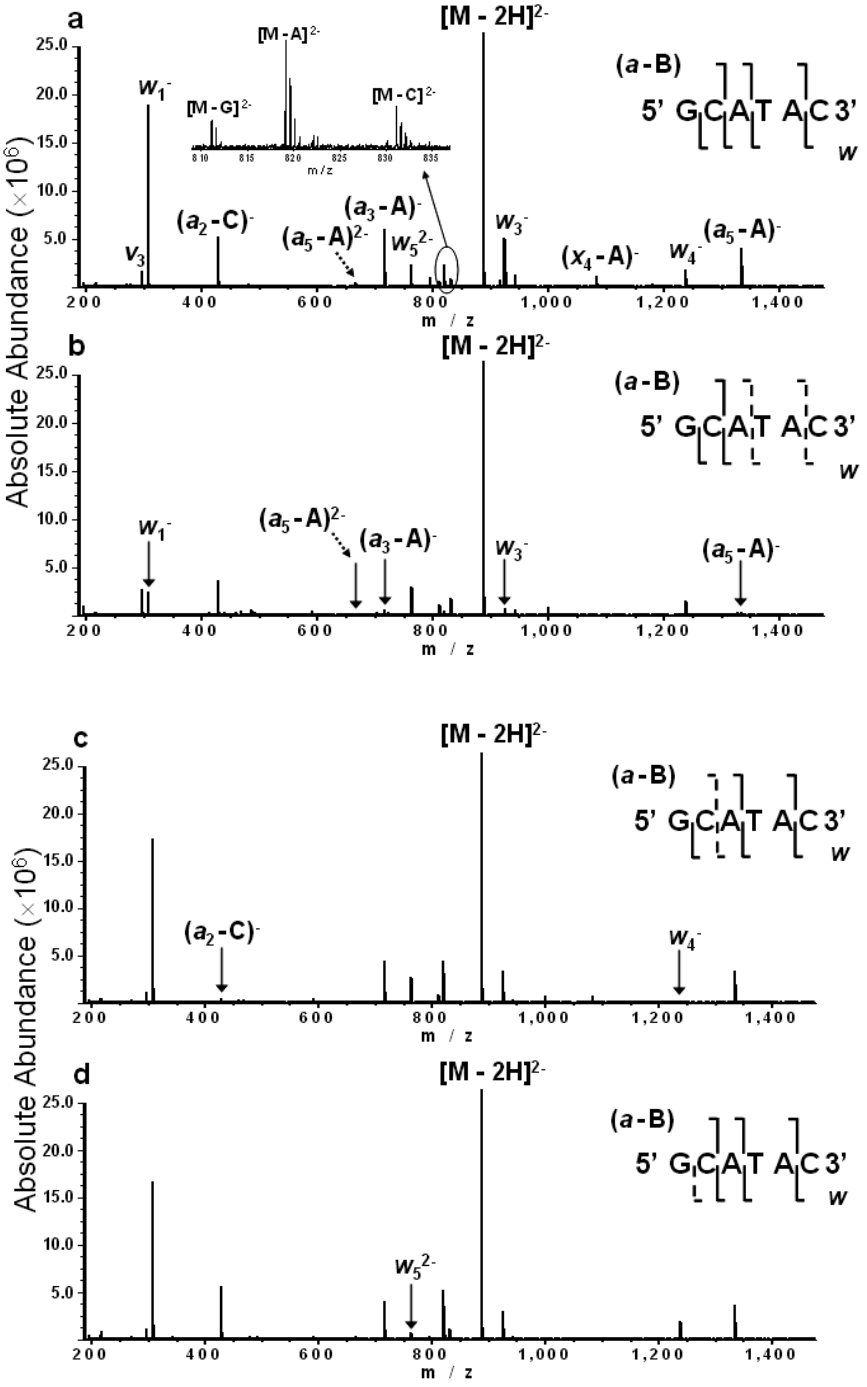

Figure 5-4. IRMPD spectra of doubly deprotonated d(GCATAC) without DR (a) and with DR ejection at the ICR frequencies of $[M - A]^{2-}$ (b), $[M - C]^{2-}$ (c), and $[M- G]^{2-}$ (d). (solid arrows indicate product ions that were significantly decreased in abundance).

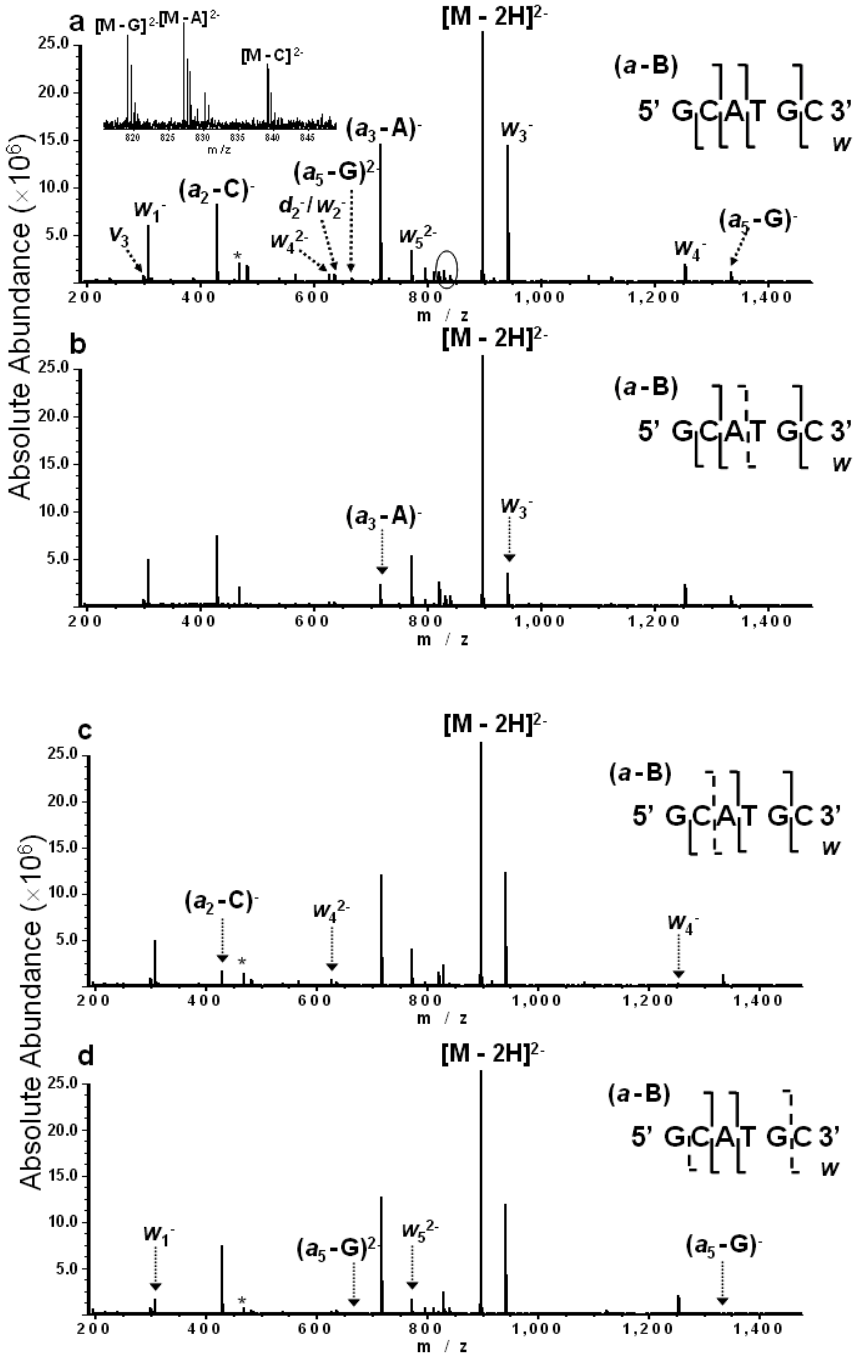

Figure 5-5. IRMPD spectra of doubly deprotonated d(GCATGC) without DR (a) and with DR ejection at the ICR frequencies of $[M - A]^{2-}$ (b), $[M - C]^{2-}$ (c), and $[M- G]^{2-}$ (d). (solid arrows indicate product ions that were significantly decreased in abundance, * = electronic noise spikes).

5.3.4. DR-IRMPD of d(CTATCAGTGA) Anions

We further extended our DR-IRMPD experiments to a 10mer oligonucleotide, d(CTATCAGTGA), as shown in Figure 5-6. In IRMPD without DR ejection (Figure 5-6a), backbone cleavage is observed at all interresidue positions, except after the first cytidine and after all thymidine residues, consistent with the data and fragmentation mechanism discussed above. The most abundant charge state of this 10mer, was a triply deprotonated species, rendering the frequency difference between the different [M - B] ions even smaller than for the doubly charged precursor ions discussed in the previous section. Compared to the experiments above, lower rf amplitude was used for DR ejection to minimize the influence on neighboring ions. Again, DR ejection at the frequencies of $[M - A]^{3-}$,$[M - C]^{3-}$, and $[M - G]^{3-}$ (Figures 5-6b-d, respectively) suggests that backbone fragmentation at a specific position proceeds via neutral loss of the base on the 5' side of the cleavage site (the abundance drop of the w_5^{2-} ion in Figure 5-6c is clarified in the inset of that figure). In summary, from IRMPD data of two 6mers and one 10mer oligodeoxynucleotide, we found that (*a* - A) ions are most easily formed, similar to observations by Sannes-Lowery and Hofstadler [6]. These results correlate with work by Green-Church and Limbach who showed that (deoxy)adenosine monophosphates have the highest proton affinities of all (deoxy)nucleoside 5'- and 3'-monophosphates [37].

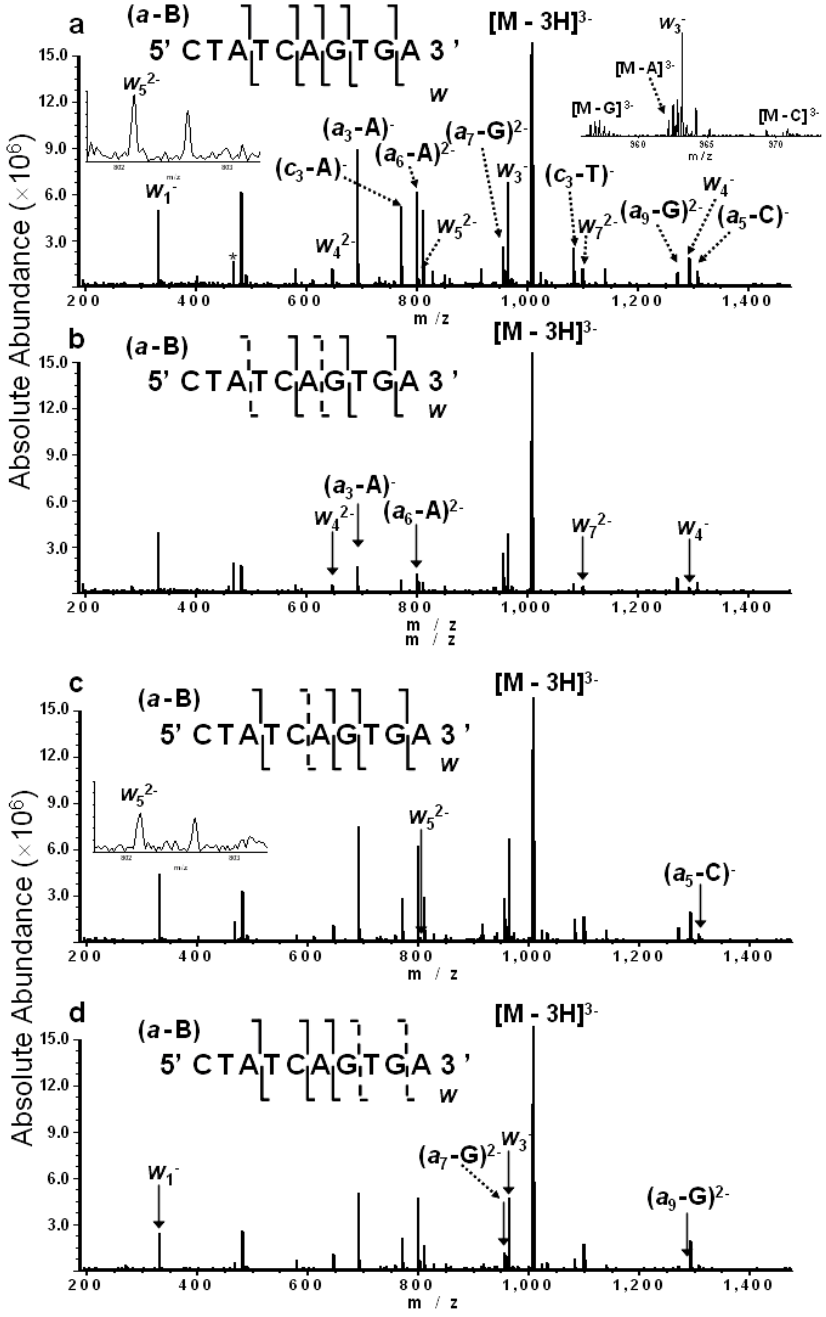

Figure 5-6. IRMPD spectra of triply deprotonated d(CTATCAGTGA) without DR (a) and with DR ejection at the ICR frequencies of $[M - A]^{3-}$ (b), $[M - C]^{3-}$ (c), and $[M - G]^{3-}$ (d). (solid arrows indicate product ions that were significantly decreased, * = electronic noise spikes).

5.3.5. DR-EDD of Hexamer Oligodeoxynucleotide Anions

The DR-IRMPD experiments described above strongly suggest that oligodeoxynucleotide fragmentation proceeds via the same mechanism in IRMPD as proposed by Gross and co-workers for CAD of the same type of molecule. This result was not unexpected because both IRMPD and CAD are 'slow heating' fragmentation techniques. Another important conclusion from these results, is that DR experiments, as implemented in our instrument, appear to be a good strategy for interrogating fragmentation intermediates. Thus, we proceeded to utilize DR ejection to characterize the EDD fragmentation process. Figure 5-7a shows a typical EDD spectrum of dT_6. The entire *d*/*w* ion series is present, easily allowing complete oligonucleotide sequencing. Three complementary *a*/*z* ions are also detected as well as four *c*/*x* ions, four (*a*/*z* - B) ions, and two doubly charged *d*/*w* ions. In DR-EDD with ejection at the frequency of the charge reduced radical precursor ion $[M - 2H]^{-\bullet}$ (Figure 5-7b), we observed a 69±4% abundance drop of the other product ions, except for the d_5^{2-}/w_5^{2-} and d_4^{2-}/w_4^{2-} ions. This behavior supports the notion that charge reduced radical precursor ions constitute a major intermediate in the fragmentation process. We previously proposed that the presence of doubly charged ions in EDD is due to direct electronic and/or vibrational excitation without electron detachment [19] (EIEIO-type process [38]), consistent with the lack of influence of the DR waveform. Similar results were observed in DR-EDD of d(GCATAC) and d(GCATGC) (see Figures 5-8 and 5-9). However, similar experiments with the oligonucleotides dA_6 and dC_6 did not result in significant changes in product ion abundance although charge reduced precursor ions were successfully ejected. As discussed above, two explanations may be envisioned: First, such radical intermediates are not involved in the fragmentation process for those oligonucleotides, or, second, the

life time of such intermediates is shorter than the time it takes to eject them from the ICR cell.

(*a*/*z* - B)-type ions are observed in both EDD and CAD/IRMPD. However, they may originate from different fragmentation pathways. The data presented above strongly suggest that the first event in IRMPD is neutral base loss followed by backbone cleavage. We have previously proposed that backbone cleavage in EDD is triggered by direct electron detachment from the phosphate backbone [20] because we did not find evidence for nucleobase-dependent fragmentation behavior. The resulting product ion pairs would be complementary *w* and radical *a*• ions, or *d* and radical *z*• ions. Radical *a* and *z* ions are observed in some spectra at rather low abundance [19]. If this hypothesis is true, ejection of *a*/*z* radical ions during the EDD process may result in reduction of the abundance of (*a*/*z* - B) ions. When performing DR-EDD of dT_6 with ejection at the frequency of a_5/z_5, a 70±21% drop of the abundance of (a/z_5 - T) was observed (Figure 5-7c). Similarly, DR ejection at the frequency of a_4/z_4 resulted in a 35±9% decrease of the abundance of (a/z_4 - B) ions (Figure 5-7d). DR ejection at the frequency of a_3/z_3 radical ions resulted in a 54±5% decrease of the (a/z_3 - B) ions (Figure 5-7e). A control experiment involving DR ejection at the frequency of $[M - T]^{2-}$ during the EDD process did not show any influence on product ion abundances. For the other oligodeoxynucleotides studied here (dA_6, dC_6, d(GCATAC) and d(GCATGC)), ejection of *a*/*z* ions did not affect the abundance of (*a*/*z* - B) ions, suggesting that the latter ions do not originate from *a*/*z* ions for these oligonucleotides, or that the lifetime of radical *a*/*z* ions is shorter than the time it takes to eject them from the ICR cell. The second explanation may be supported by the low abundance, or absence, of *a*•/*z*• ions in the corresponding spectra.

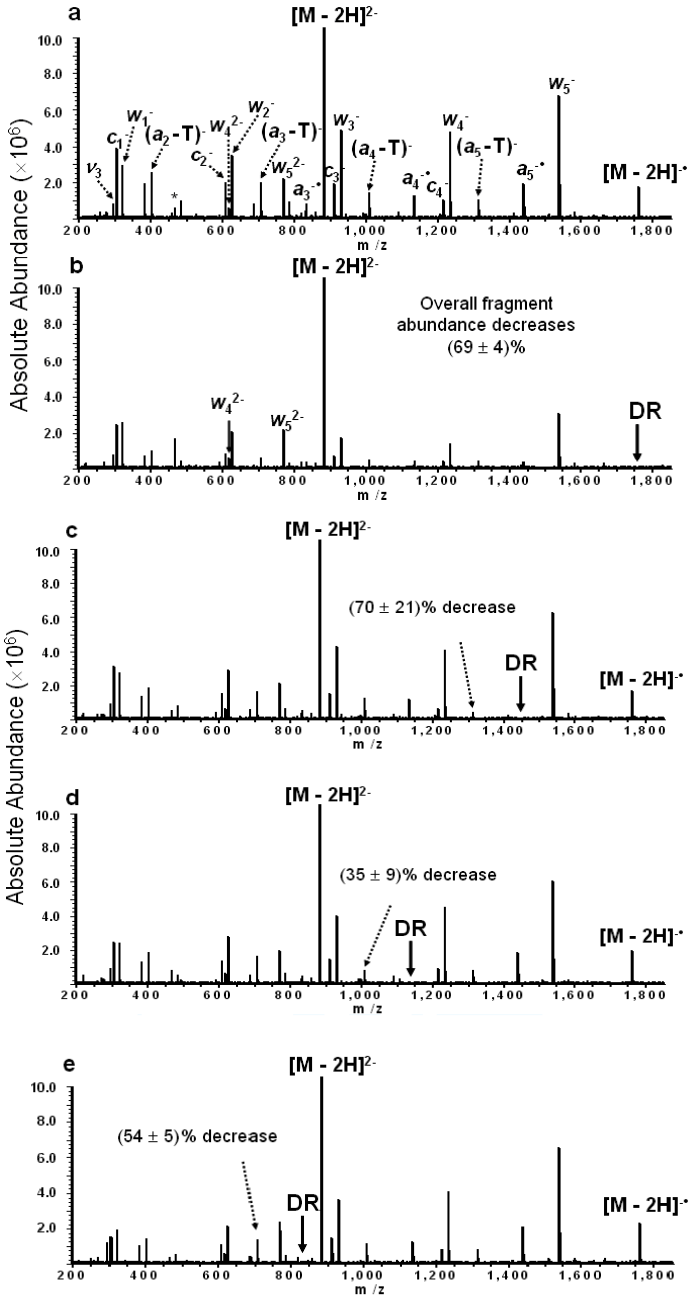

Figure 5-7. EDD spectra of doubly deprotonated dT_6 without DR (a) and with DR ejection at the frequencies of $[M - 2H]^{-\bullet}$ (b), $a_5^{-\bullet}$ (c), $a_4^{-\bullet}$ (d), and $a_3^{-\bullet}$ (e). (solid arrows indicate m/z values corresponding to the frequencies of the DR rf waveforms, * = electronic noise spikes). Ions labeled *w* can also be *d* ions, ions labeled *a* can also be *z* ions, and ions labeled *c* can also be *x* ions.

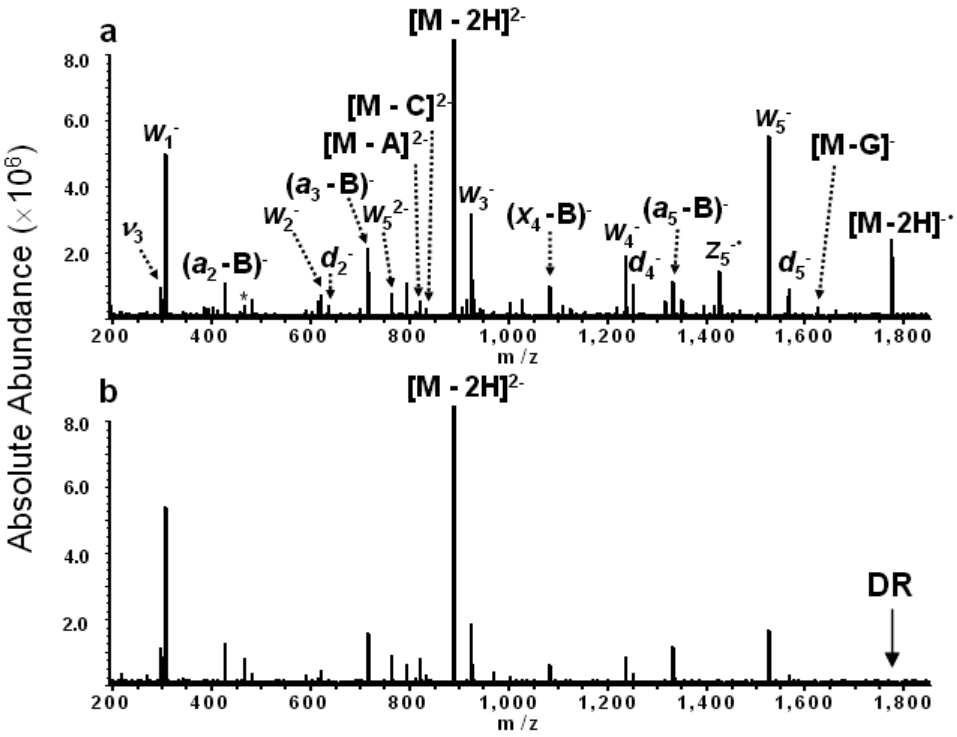

Figure 5-8. EDD spectra of doubly deprotonated d(GCATAC) without DR (a) and with DR ejection at the frequency of $[M - 2H]^{-\bullet}$ (b). (the solid arrow indicates the m/z value corresponding to the frequency of the DR rf waveform, * = electronic noise spike).

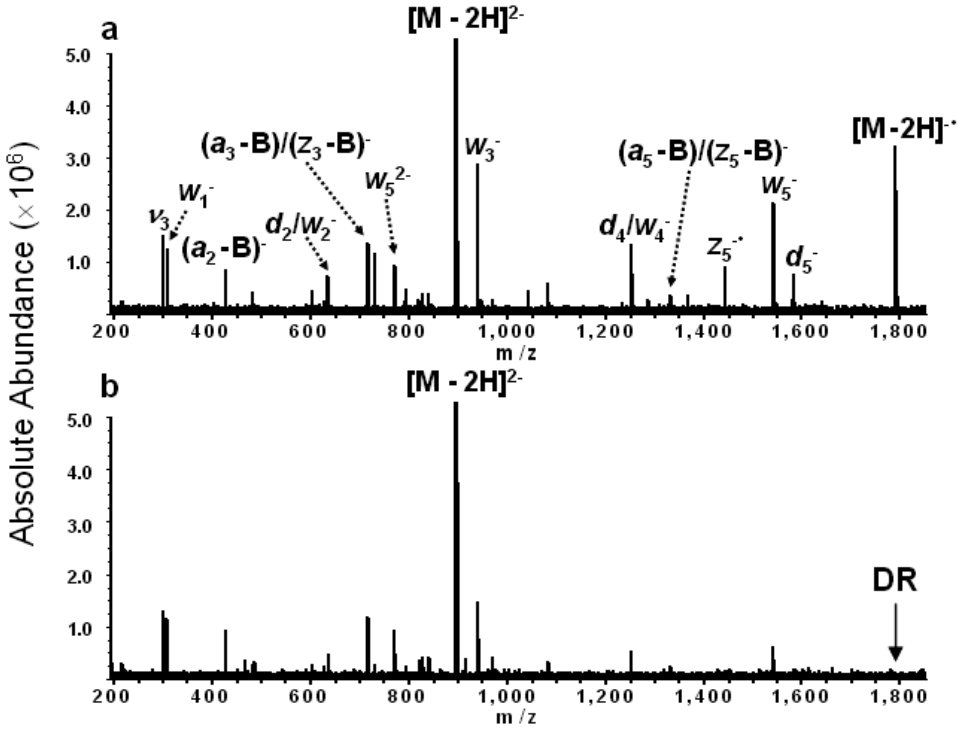

Figure 5-9. EDD spectra of doubly deprotonated d(GCATGC) without DR (a) and with DR ejection at the frequency of $[M - 2H]^{-\bullet}$ (b). (the solid arrow indicates the m/z value corresponding to the frequency of the DR rf waveform).

5.4. CONCLUSION

IRMPD of oligodeoxynucleotides mainly results in (*a* - B) and *w* ions, similar to CAD. We demonstrate for the first time FT-IC DR experiments to interrogate the IRMPD fragmentation mechanism of oligodeoxynucleotides. DR data strongly support the CAD mechanism proposed by Gross and co-workers involving neutral base loss as the first step preceded by proton transfer to the nucleobase to form a zwitterionic intermediate. T-rich oligodeoxynucleotides fragment via a different mechanism, not involving neutral base loss from precursor ions. DR-EDD experiments showed that ejection of charge reduced radical precursor ions drastically affects the abundance of

other product ions for thymine-containing oligonucleotides, thereby supporting the notion that such radical species constitute intermediates in the fragmentation process. However, DR ejection of charge reduced precursor ions did not affect EDD spectra of dA_6 and dC_6. Furthermore, DR ejection of *a*/*z* radical ions suggested that (*a*/*z* - T) ions observed in EDD are most likely formed via secondary fragmentation of *a*/*z* radical ions.

5.5. BIBLIOGRAPHY

1. Ni, J.; Pomerantz, S. C.; Rozenski, J.; Zhang, Y.; McCloskey, J. A. Interpretation of Oligonucleotide Mass Spectra for Determination of Sequence Using Electrospray Ionization and Tandem Mass Spectrometry. *Anal. Chem.* **1996,** *68*, 1989-1999.
2. Hofstadler, S. A.; Sannes-Lowery, K. A.; Hannis, J. C. Analysis of Nucleic Acids by FTICR MS. *Mass. Spectrom. Rev.* **2005,** *24*, 265-285.
3. Wu, J.; McLuckey, S. A. Gas-phase Fragmentation of Oligonucleotide Ions. *Int. J. Mass Spectrom.* **2004,** *237*, 197-241.
4. Frahm, J. L.; Muddiman, D. C. Nucleic Acid Analysis by Fourier Fransform Ion Cyclotron Resonance Mass Spectrometry at the Beginning of the Twenty-first Century. *Curr. Pharm. Design* **2005,** *11*, 2593-2613.
5. Murray, K. K. DNA Sequencing by Mass Spectrometry. *J. Mass Spectrom.* **1996,** *31*, 1203-1215.
6. Sannes-Lowery, K. A.; Hofstadler, S. A. Sequence Confirmation of Modified Oligonucleotides using IRMPD in the External Reservoir of an Electrospray Ionization Fourier Transform Ion Cyclotron Mass Spectrometer. *J. Am. Soc. Mass Spectrom.* **2003,** *14*, 825-833.

7. McLuckey, S. A. Principles of Collisional Activation in Analytical Mass Spectrometry. *J. Am. Soc. Mass Spectrom.* **1992,** *3*, 599-614.
8. Little, D. P.; Aaserud, D. J.; Valaskovic, G. A.; McLafferty, F. W. Sequence Information from 42-108-mer DNAs (Complete for a 50 mer) by Tandem Mass Spectrometry. *J. Am. Chem. Soc.* **1996,** *118*, 9352-9359.
9. McLuckey, S. A.; Van Berkel, G. J.; Glish, G. L. Tandem Mass Spectrometry of Small, Multiply-charged Oligonucleotides. *J. Am. Soc. Mass Spectrom.* **1992,** *3*, 60-70.
10. Little, D. P.; Speir, J. P.; Senko, M. W.; O'Connor, P. B.; McLafferty, F. W. Infrared Multiphoton Dissociation of Large Multiply-charged Ions for Biomolecule Sequencing. *Anal. Chem.* **1994,** *66*, 2809-2815.
11. Keller, K. M.; Brodbelt, J. S. Collisionally Activated Dissociation and Infrared Multiphoton Dissociation of Oligonucleotides in a Quadrupole Ion Trap. *Anal. Biochem.* **2004,** *326*, 200-210.
12. Zubarev, R. A.; Kelleher, N. L.; McLafferty, F. W. Electron Capture Dissociation of Multiply Charged Protein Cations. A Nonergodic Process. *J. Am. Chem. Soc.* **1998,** *120*, 3265-3266.
13. Zubarev, R. A. Reactions of Polypeptide Ions with Electrons in the Gas Phase. *Mass Spectrom. Rev.* **2003,** *22*, 57-77.
14. Cooper, H. J.; Håkansson, K.; Marshall, A. G. The Role of Electron Capture Dissociation in Biomolecular Analysis. *Mass Spectrom. Rev.* **2005,** *24*, 201-222.
15. Håkansson, K.; Hudgins, R. R.; Marshall, A. G.; O'Hair, R. A. J. Electron Capture Dissociation and Infrared Multiphoton Dissociation of Oligodeoxynucleotide Dications. *J. Am. Soc. Mass Spectrom.* **2003,** *14*, 23-41.

16. Schultz, K. N.; Håkansson, K. Rapid Electron Capture Dissociation of Mass-Selectively Accumulated Oligodeoxynucleotide Dications. *Int. J. Mass Spectrom.* **2004,** *234*, 123-130.
17. Horn, D. M.; Breuker, K.; Frank, A. J.; McLafferty, F. W. Kinetic Intermediates in the Folding of Gaseous Protein Ions Characterized by Electron Capture Dissociation Mass Spectrometry. *J. Am. Chem. Soc.* **2001,** *123*, 9792-9799.
18. Budnik, B. A.; Haselmann, K. F.; Zubarev, R. A. Electron Detachment Dissociation of Peptide Di-anions: an Electron-hole Recombination Phenomenon. *Chem. Phys. Lett.* **2001,** *342*, 299-302.
19. Yang, J.; Mo, J.; Adamson, J. T.; Håkansson, K. Characterization of Oligodeoxynucleotides by Electron Detachment Dissociation Fourier Transform Ion Cyclotron Resonance Mass Spectrometry. *Anal. Chem.* **2005,** *77*, 1876-1882.
20. Yang, J.; Håkansson, K. Fragmentation of Oligoribonucleotides from Gas-phase Ion-electron Reactions. *J. Am. Soc. Mass Spectrom.* **2006,** *17*, 1369-1375.
21. Kalli, K.; Håkansson, K. Preferential Cleavage of S-S and C-S Bonds in Electron Detachment Dissociation and Infrared Multiphoton Dissociation of Disulfide-linked Peptide Anions. *Int. J. Mass Spectrom.* **2007,** *263*, 71-81.
22. Mo, J.; Håkansson, K. Characterization of Nucleic Acid Higher Order Structure by Tandem High Resolution Mass Spectrometry. *Anal. Bioanal. Chem.* **2006,** *386*, 675-681.
23. McLuckey, S. A.; Habibi-Goudarzi, S. Decompositions of Multiply-Charged Oligonucleotide Anions. *J. Am. Chem. Soc.* **1993,** *115*, 12085-12095.
24. Rodgers, M. T.; Campbell, S.; Marzluff, E. M.; Beauchamp, J. L. Low-energy Collision-induced Dissociation of Deprotonated Dinucleotides: Determination of the

Energetically Favored Dissociation Pathways and the Relative Acidities of the Nucleic Acid Bases. *Int. J. Mass Spectrom. Ion Processes* **1994,** *137*, 121-149.

25. Barry, J. P.; Vouros, P.; Vanschepdael, A.; Law, S. J. Mass and Sequence Verification of Modified Oligonucleotides using Electrospray Tandem Mass-Spectrometry *J. Mass. Spectrom.* **1995,** *30*, 993-1006.
26. Wan, K. X.; Gross, M. L. Fragmentation Mechanisms of Oligodeoxynucleotides: Effects of Replacing Phosphates with Methylphosphonates and Thymines with Other Bases in T-rich Sequences. *J. Am. Soc. Mass Spectrom.* **2001,** *12*, 580-589.
27. Anusiewicz, I.; Jasionowski, M.; Skurski, P.; Simons, J. Backbone and Side-chain Cleavages in Electron Detachment Dissociation (EDD). *J. Phys. Chem. A* **2005,** *109*, 11332-11337
28. Kjeldsen, F.; Silivra, O. A.; Ivonin, I. A.; Haselmann, K. F.; Gorshkov, M.; Zubarev, R. A. C-alpha-C Backbone Fragmentation Dominates in Electron Detachment Dissociation of Gas-phase Polypeptide Polyanions. *Chem. Eur. J.* **2005,** *11*, 1803-1812.
29. Wolff, J. J.; Amster, I. J.; Chi, L. L.; Linhardt, R. J. Electron Detachment Dissociation of Glycosaminoglycan Tetrasaccharides. *J. Am. Soc. Mass Spectrom.* **2007,** *18*, 234-244.
30. Wolff, J. J.; Chi, L. L.; Linhardt, R. J.; Amster, I. J. Distinguishing Glucuronic from Iduronic Acid in Glycosaminoglycan Tetrasaccharides by Using Electron Detachment Dissociation. *Anal. Chem.* **2007,** *79*, 2015-2022.
31. Comisarow, M. B.; Grassi, V.; Parisod, G. Fourier Transform Ion Cyclotron Double Resonance. *Chem. Phys. Lett.* **1978,** *57*, 413-416.

32. Jurchen, J. C.; Garcia, D. E.; Williams, E. R. Gas-phase Dissociation Pathways of Multiply Charged Peptide Clusters. *J. Am. Soc. Mass Spectrom.* **2003,** *14*, 1373-1386.
33. Cooper, H. J. Investigation of the Presence of *b* Ions in Electron Capture Dissociation Mass Spectra. *J. Am. Soc. Mass Spectrom.* **2005,** *16*, 1932-1940.
34. Lin, C.; Cournoyer, J. J.; O'Connor, P. B. Use of a Double Resonance Electron Capture Dissociation Experiment to Probe Fragment Intermediate Lifetimes. *J. Am. Soc. Mass Spectrom.* **2006,** *17*, 1605-1615.
35. Senko, M. W.; Canterbury, J. D.; Guan, S.; Marshall, A. G. A High-Performance Modular Data System for FT-ICR Mass Spectrometry. *Rapid Commun. Mass Spectrom.* **1996,** *10*, 1839-1844.
36. Wan, K. X.; Gross, J.; Hillenkamp, F.; Gross, M. L. Fragmentation Mechanisms of Oligodeoxynucleotides Studied by H/D Exchange and Electrospray Ionization Tandem Mass Spectrometry. *J. Am. Soc. Mass Spectrom.* **2001,** *12*, 193-205.
37. Green-Church, K. B.; Limbach, P. A. Mononucleotide Gas-Phase Proton Affinities as Determined by the Kinetic Method. *J. Am. Soc. Mass Spectrom.* **2000,** *11*, 24-32.
38. Budnik, B. A.; Haselmann, K. F.; Elkin, Y. N.; Gorbach, V. I.; Zubarev, R. A. Applications of Electron-Ion Dissociation Reactions for Analysis of Polycationic Chitooligosaccharides in Fourier Transform Mass Spectrometry. *Anal. Chem.* **2003,** *75*, 5994-6001.

CHAPTER 6

GAS-PHASE ION-ELECTRON REACTIONS OF CHEMICALLY MODIFIED OLIGONUCLEOTIDES

Antisense compounds play an important role in cancer therapeutics. Such molecules often correspond to chemically modified oligonucleotides, which cannot be effectively characterized by traditional enzymatic techniques. Tandem mass spectrometry involving CAD or IRMPD is an alternative approach, shown to be valuable for characterization of antisense oligonucleotides. However the major fragmentation channels in CAD and IRMPD involve neutral nucleobase loss, thereby reducing their utility for analysis of modified bases. Furthermore, backbone cleavage on the 3' side of thymidine residues is often greatly reduced, which may prevent complete sequencing. We demonstrated in Chapters 2 and 4 that ECD and EDD can provide complementary sequence-specific information for oligomer DNA and RNA compared with CAD and IRMPD. In this Chapter, we extend these two gas-phase ion-electron reaction techniques to the characterization of three different types of chemically modified oligonucleotides: 2'-methoxy oligomer RNAs, oligomer DNAs with a methylphosphonate backbone, and oligomer DNAs containing abasic sites. We found that only limited backbone cleavage is observed for 2'-methoxy and methylphosphonate modified oligonucleotides in ECD, thereby rendering this technique less effective than IRMPD. By contrast, complete

sequence coverage was obtained in most cases from ECD of oligomer DNAs containing abasic sites. For such compounds, cleavages on the 3' side of abasic sites are missing in IRMPD in addition to the absence of cleavage 3' to thymidine. For all three types of modified oligonucleotides, EDD appeared to be the most powerful method as it provided full sequence coverage in all cases and spectra are straightforward to interpret.

6.1. INTRODUCTION

Chemically modified oligonucleotides play an important role in biomedical/pharmaceutical research, particularly for antisense applications. Many traditional drugs combat disease by targeting faulty proteins but antisense oligonucleotides intervene at an earlier stage by preventing the production of these incorrect proteins. Antisense oligonucleotides are typically 13–25 nucleotides long and designed to hybridize to messenger RNA by Watson-Crick base pairing [1]. Antisense compounds are widely used as therapeutics for malignant disease and there is a rapid increase in the number of antisense molecules progressing past Phase I, II and III clinical trials [2, 3]. Many antisense compounds are modified oligonucleotides, such as analogs with unnatural nucleobases, modified sugars (particularly at the 2' position of ribose), or altered phosphate backbones [4]. Traditional enzymatic sequencing techniques are not suitable for characterizing antisense compounds due to their altered chemical nature and alternative analytical approaches are therefore desired.

Tandem mass spectrometry is widely used to characterize a variety of biological molecules, including sequencing of oligonucleotides [5, 6]. MS/MS involving CAD or IRMPD of oligonucleotide anions has been shown to allow characterization of

chemically modified oligomer DNA and RNA [7-11]. However the major fragmentation channels in CAD and IRMPD often involve neutral nucleobase (B) loss [8, 9], which may reduce their utility for characterization of oligonucleotides with modified bases. Following base loss, oligodeoxynucleotides may undergo secondary fragmentation involving cleavage of backbone C-O bonds at the 3' position of the deoxyribose from which the base is lost [7, 8] to form 5' (*a* - B) and their complementary 3' *w*-type ions (McLuckey nomenclature [12]). Such cleavage is reduced for thymidine residues, which has been explained by a mechanism involving proton transfer to the nucleobase prior to base loss: the reduced cleavage at thymidine is due to its low proton affinity [13, 14]. Such reduction of backbone cleavage on the 3' side of thymidine residues was observed in IRMPD of modified oligonucleotides with phosphorothioate backbones, or 2' sugar substituents [9], thereby reducing sequence coverage.

Since the introduction of ECD in 1998 [15], several research groups have shown that this alternative MS/MS technique can provide unique fragmentation patterns for molecules as diverse as peptides and proteins [16], polymers [17], lantibiotics [18], and siderophores [19]. Our group has shown that ECD can be an alternative method for sequencing oligonucleotides from complementary product ions compared to CAD and IRMPD [20, 21]. However, the main disadvantage of analyzing oligonucleotides by ECD is the requirement for multiply positively charged precursor ions. Higher sensitivity can be obtained in negative ion mode due to the sugar-phosphate backbone of oligonucleotides, which is easily deprotonated. In 2001, Zubarev and co-workers introduced a new ion-electron reaction-based fragmentation method, operating in negative ion mode: EDD [22]. This technique provides unique fragmentation pathways

for peptide dianions, including predominant C_α-C backbone bond cleavage. We recently extended EDD to oligonucleotide characterization and demonstrated extensive backbone fragmentation for oligodeoxy- [23] (described in Chapter 2) and oligoribo-nucleotides [24] (described in Chapter 4), complementary to that of other MS/MS techniques, such as CAD and IRMPD. Fabris and co-workers have also applied EDD to oligonucleotide characterization and observed more extensive fragmentation compared to ECD [25]. Here, we extend both ECD and EDD to the characterization of three different types of chemically modified oligonucleotides: 2'-methoxy oligomer RNAs, oligomer DNAs with a methylphosphonate backbone, and oligomer DNAs containing abasic sites.

6.2. EXPERIMENTAL SECTION

6.2.1. Sample Preparation

Gel purified 2'-methoxy A_6, C_6, G_6, U_6 and GCAUAC, dA_6, dC_6, dG_6, dT_6 and d(GCATAC) with methylphosphonate backbones, d(GCXCGTAC), d(GCAXGTAC), d(GCACXTAC) and d(GCACGTAC) (in which X denotes an abasic site, i. e., a hydrogen has replaced a nucleobase) oligonucleotide ammonium salts were purchased from W. M. Keck Foundation Biotechnology Resource Lab (New Haven, CT) and used without further purification. Negative ion mode electrospray solvent consisted of 1:1 (v/v) isopropanol:water (Fisher, Fair Lawn, New Jersey) with 10 mM ammonium acetate (Fisher). Positive ion mode electrospray solvent consisted of 1:1 (v/v) acetonitrile:water (Fisher) with 0.5-1% formic acid (ACROS Organics, Fair Lawn, NJ). The final concentration of samples was 1-50 μM.

6.2.2. Fourier Transform Ion Cyclotron Resonance Mass Spectrometry

All experiments were performed with the 7 Tesla quadrupole-Fourier transform ion cyclotron resonance mass spectrometer shown in Figure 2-1. The ESI source was recently upgraded to include dual ion funnels (Apollo II ESI source, Bruker Daltonics). Most experiments were performed with the new source but some experiments with methylphosphonate oligonucleotides were performed with the older version of the source (Apollo I, Bruker Daltonics). Samples were infused at a flow rate of 70 μL/h and mass selectively externally accumulated (4 to 6 m/z isolation window). For ECD experiments, further isolation was accomplished by correlated harmonic excitation fields (CHEF) [26] inside the ICR cell. ECD and EDD were performed with an indirectly heated hollow dispenser cathode electron source (Heat Wave, Watsonville, CA). For ECD, the cathode voltage was pulsed to - 1 V for 20-80 ms. A lens located in front of the cathode was kept at + 1 V. During the EDD event, the cathode voltage was pulsed to -18.2 to -18.5 V for 2 s. The lens electrode was kept at - 19 V throughout the experiment. IRMPD was performed with a vertically mounted 25 W, 10.6 μm, CO_2 laser (Synrad, Mukilteo, WA). Photon irradiation was performed for 15-60 ms at 30% laser power. All mass spectra were acquired with XMASS (version 7.0.?6 Bruker Daltonics) in broadband mode with 256 or 512k data points and summed over 30-100 scans. Data processing was performed as described in Chapter 2. Briefly, a Hanning window function was applied and the data set was zero filled once prior to fast Fourier transformation followed by magnitude calculation. Peak lists were generated and exported to Microsoft Excel for internal frequency-to-mass calibration with a two-term

calibration equation. Only product ion assignments with an error less than 20 ppm were included.

6.3. RESULTS AND DISCUSSION

6.3.1. 2'-Methoxy Oligonucleotides

Figure 6-1 shows an ECD spectrum of doubly protonated 2'-methoxy (OMe) C_6. Very limited backbone cleavage is seen; only one radical *a*/*z* ion, $a_5/z_5^{\bullet}$, and two *w*/*d*-type ions, w_4/d_4 and w_5/d_5, were observed as well as (w_5/d_5 + H_2O) (*d* and *z*-type ion formation corresponds to cleavage of C-O bonds on the other side of the phosphate group as compared to the *w*/*a* product ion formation typically observed in CAD/IRMPD [12]; *w* and *d*, and *a* and *z* ions, respectively, cannot be distinguished based on mass alone due to the symmetry of 2'-OMe C_6). Unlabeled peaks are product ions which could not be assigned based on known fragmentation pathways. (w_5 + H_2O) product ions have also been observed in ECD of the DNA dC_6 and the RNA C_6 [20, 24]. Håkansson et al. proposed that formation of such product ions may proceed through a pentavalent phosphorane intermediate involving terminal hydroxyl groups [20]. In ECD of 2'-OMe C_6, charge reduced precursor ions, $[M + 2H]^{+\bullet}$, are also observed along with the corresponding product following hydrogen loss. The incomplete *d*/*w* ion series precludes complete sequencing of the oligonucleotide. The limited backbone cleavage does not appear to be due to a preference for base loss in the fragmentation process because such ions are of low abundance. The overall result is very similar to that observed from ECD of the RNA C_6 [24] (see Chapter 4). For 2'-OMe A_6 (see Figure 6-2), a very similar ECD fragmentation pattern was observed, except that the radical a_5/z_5 ion was absent. Another

difference was that abundant charge reduced precursor ions were present, a behavior that was also noted in ECD of both the DNA dA_6 [20] and the RNA A_6 [24]. This behavior has been explained from a high propensity of adenine to form intramolecular hydrogen bonds to the phosphate backbone, preventing product ions from separating and thereby from being detected.

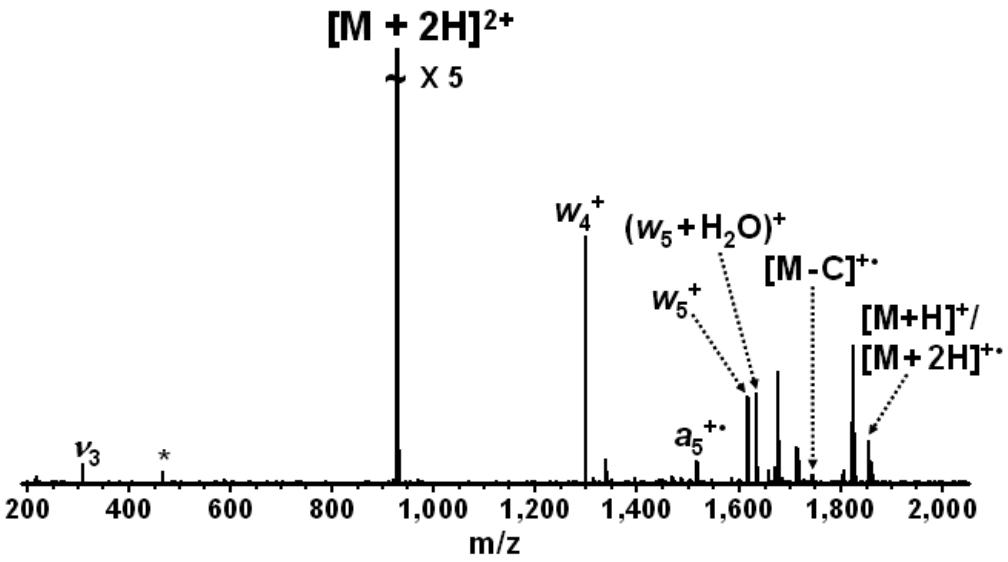

Figure 6-1. ECD (-1 V bias voltage, 40 ms, 50 scans) of doubly protonated 2'-methoxy C_6. Product ions labeled *w* can also be *d* ions, and the ion labeled *a* can also be a *z* ion. Electronic noise spike is labeled with an asterisk.

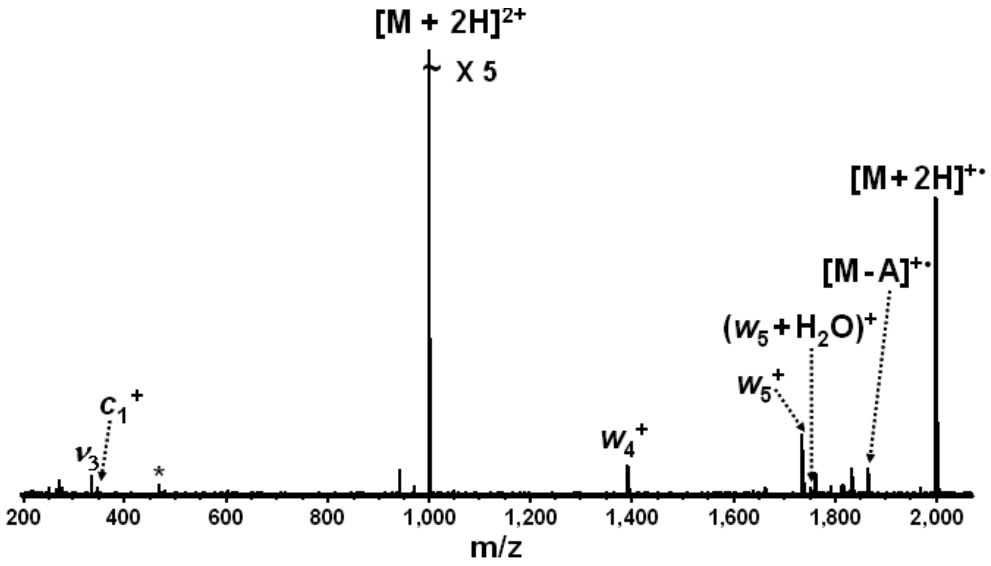

Figure 6-2. ECD (-1 V bias voltage, 45 ms, 50 scans) of doubly protonated 2'-methoxy A_6. Product ions labeled *w* can also be *d* ions, and the ion labeled *c* can also be an *x* ion. Abundant charge reduced precursor ions are observed. Electronic noise spike is labeled with an asterisk.

ECD of 2'-OMe G_6 (see Figure 6-3) yielded even fewer fragments: only w_5, (w_5 - G), $[M - G]^{2+}$, $[M - G]^{+\bullet}$, and abundant charge reduced precursor ions were detected. Facile guanine base loss was also seen in ECD of DNA [20], RNA [24] (see Chapter 4), and PNA [27]. Table 6-1 lists the product ions from ECD of doubly protonated 2'-OMe U_6. In ECD of this oligonucleotide, incomplete *d*/*w* ion series, base loss, and charge reduced precursor ions were present but the fragmentation efficiency was even lower than that of the other 2'-methoxy oligonucleotides.

In order to clarify the identity of *d*/*w* ions in ECD of 2'-methoxy modified oligonucleotides, the asymmetric modified oligonucleotide 2'-OMe GCAUAC was analyzed. The corresponding ECD spectrum (see Figure 6-4) contained z_4 and x_4 radical

ions, w_4, d_5, (w_5 + H_2O), (w_5 - C), and (d_5 + H_2O) even-electron backbone product ions, $[M - G]^{2+}$, and charge reduced precursor ions (*x* ions are formed from cleavage of the P-O bond adjacent to the C-O bond cleaved to form *w* ions [12]). The formation of (w_5 + H_2O) and (d_5 + H_2O) ions involve cleavage of a terminal nucleotide, consistent with the previously proposed involvement of terminal hydroxyl groups [20]. However, because such ions are relatively abundant for C-rich oligodeoxynucleotides [20, 21] and because formation of (w_5 + H_2O) and (d_5 + H_2O) both involve backbone cleavage on the 5' side of cytidine, the nucleobase could also be involved, either directly or sterically. The results from ECD of 2'-OMe GCAUAC imply that *d*/*w* ion series observed for symmetric 2'-methoxy oligonucleotides are mixtures of *d* and *w* ions. Overall, base composition did not appear to have a significant influence on the ECD fragmentation patterns of 2'-methoxy oligonucleotides, contrary to ECD of oligomer DNA and RNA [20, 24].

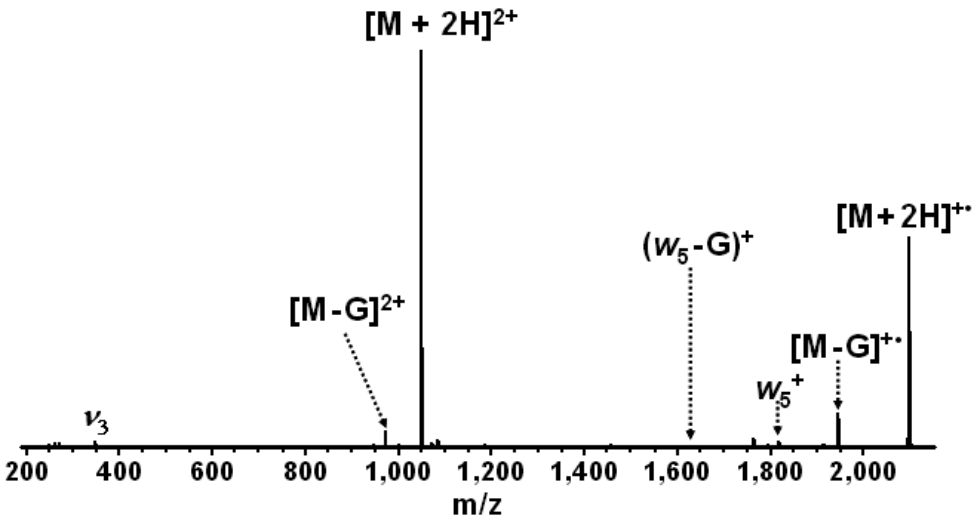

Figure 6-3. ECD (-1 V bias voltage, 40 ms, 50 scans) of doubly protonated 2'-methoxy G_6. Product ions labeled *w* can also be *d* ions. Abundant charge reduced precursor ions are detected.

Table 6-1. Product ions observed from ECD of doubly protonated 2'-methoxy U_6 (15 ms irradiation, -1 V bias, 50 scans). Ions labeled *w* can be also be *d* ions.

Observed m/z	Calculated m/z	Assignment	Error (ppm)
874.1410	874.1386	$[M - U]^{2+}$	2.7
930.1522	930.1522	$[M + 2H]^{+\bullet}$	Calibrant
979.1429	979.1408	w_3^+	2.1
1299.179	1299.182	w_4^+	- 2.3
1619.221	1619.223	w_5^+	- 1.2
1859.305	1859.297	$[M + H]^+$	4.3
1860.305	1860.305	$[M + 2H]^{+\bullet}$	Calibrant

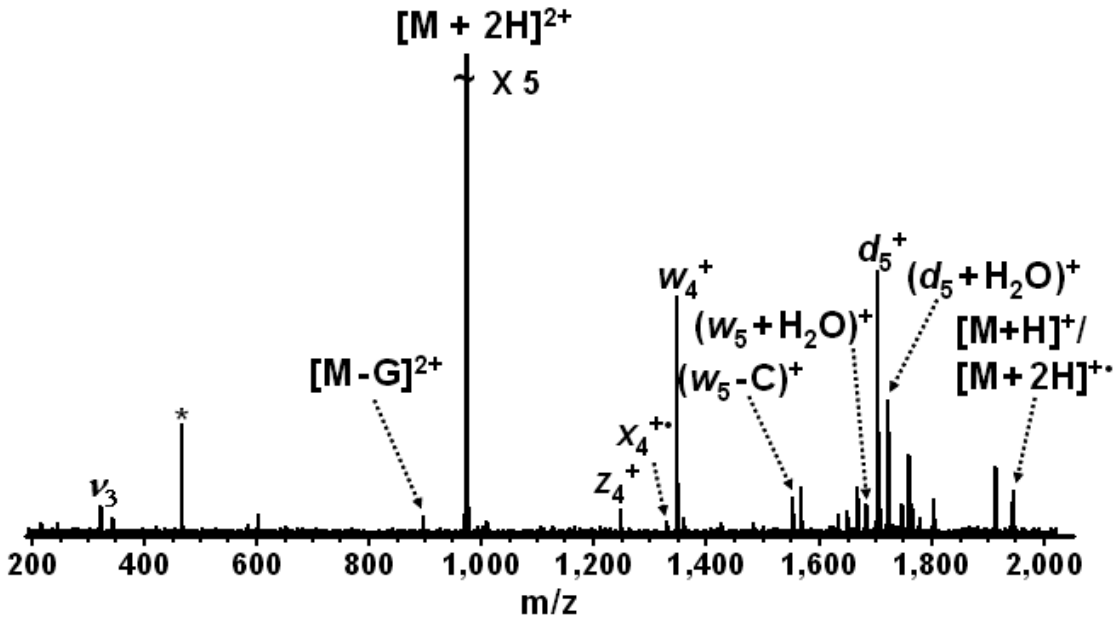

Figure 6-4. ECD (-1 V bias voltage, 35 ms, 50 scans) of doubly protonated 2'-methoxy GCAUAC. Electronic noise spike is labeled with an asterisk.

The ECD data discussed above show that only limited backbone cleavage is observed for 2'methoxy modified oligonucleotides, similar to ECD of RNA [24]. This behavior may be due to a high propensity for zwitterion formation in positive ion mode (with protonation of nucleobases and deprotonation of the phosphate backbone), thereby resulting in strong intramolecular salt bridges that prevent product ions from separating. Because we have shown that EDD can provide extensive backbone cleavage of both DNAs and RNAs, we also performed EDD of 2'-methoxy modified oligonucleotides. Figure 6-5 shows the mass spectrum resulting from EDD of 2'-OMe C_6 Doubly deprotonated precursor ions were dissociated at an electron energy of ~17.5 eV (cathode bias voltage of - 18.2 V) [28]) with 2 s irradiation time. Complete *d*/*w* and *c*/*x* ion series were observed (*c* ions are formed from cleavage of the P-O bond adjacent to the C-O bond cleaved to form *d* ions [12]), and two *b*/*y*-type ions (*b* and *y* ions are formed through cleavage of the P-O bond on the other side of the phosphorus atom as compared to formation of *c* and *x* ions [12]) were also present. This result is similar to EDD of the RNA C_6 [24] (Chapter 4). Compared with ECD, more sequence information is obtained with EDD for 2'-OMe C_6. For comparison, Figure 6-6 shows an IRMPD spectrum of the same modified oligonucleotide. Here, incomplete *d*/*w* ion series, complete *c*/*x* ion series, two *b*/*y*-type ions, and three *a*/*z*-type ions are observed together with extensive base loss from *a*/*z*, *c*/*x* and *d*/*w* ions. High m/z product ions are of low abundance. Compared with ECD and IRMPD data of same modified oligonucleotide, the EDD spectrum is more straightforward to interpret, although full sequence coverage was also obtained from IRMPD. Table 6-2 lists the product ions observed from EDD of 2'-OMe U_6. Again, complete *d*/*w* and *c*/*x* ion series dominate the spectrum and there are also three *b*/*y*-type,

and three *a*/*z*-type ions. The presence of doubly charged d_5^{2-}/w_5^{2-}, which were also observed in EDD of 2'-OMe A_6 and G_6 (Figures 6-7 and 6-8), suggests that electronic and/or vibrational excitation without electron detachment (EIEIO-type process [29]) occurs as a result of electron irradiation (doubly charged ions are highly unlikely to originate from the singly charged radical intermediate formed following electron detachment from the doubly charged precursor ions). Full sequence coverage was also achieved from EDD of 2'-OMe A_6 and G_6 from similar fragmentation patterns as observed for 2'-OMe C_6 and U_6. EDD of 2'-OMe GCAUAC (Figures 6-9) revealed that *d*/*w* ion series are mixtures of *d* and *w* ions, and that *c*/*x* ion series are also mixtures. Nevertheless, EDD appears to be a promising tool for characterizing 2'-methoxy modified oligonucleotides due to the less complex product ion patterns, which facilitate data interpretation.

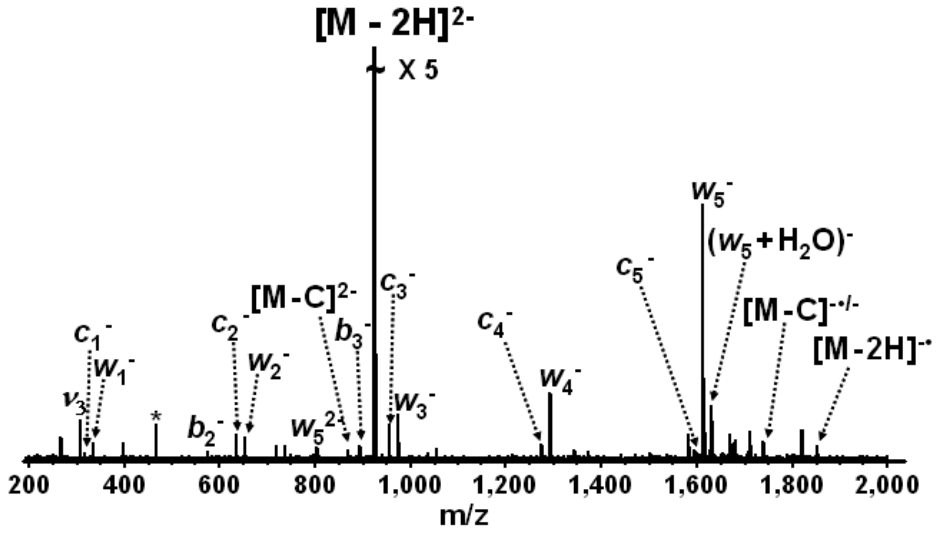

Figure 6-5. EDD (-18.2 V, 2 s, 50 scans) of doubly deprotonated 2'-methoxy C_6. Product ions labeled *w* can also be *d* ions, ions labeled *b* can also be *y* ions, and ions labeled *c* can also be *x* ions. Full series of *c*/*x* and *d*/*w* ions are observed, allowing full sequencing of the oligonucleotide. Electronic noise spike is labeled with an asterisk.

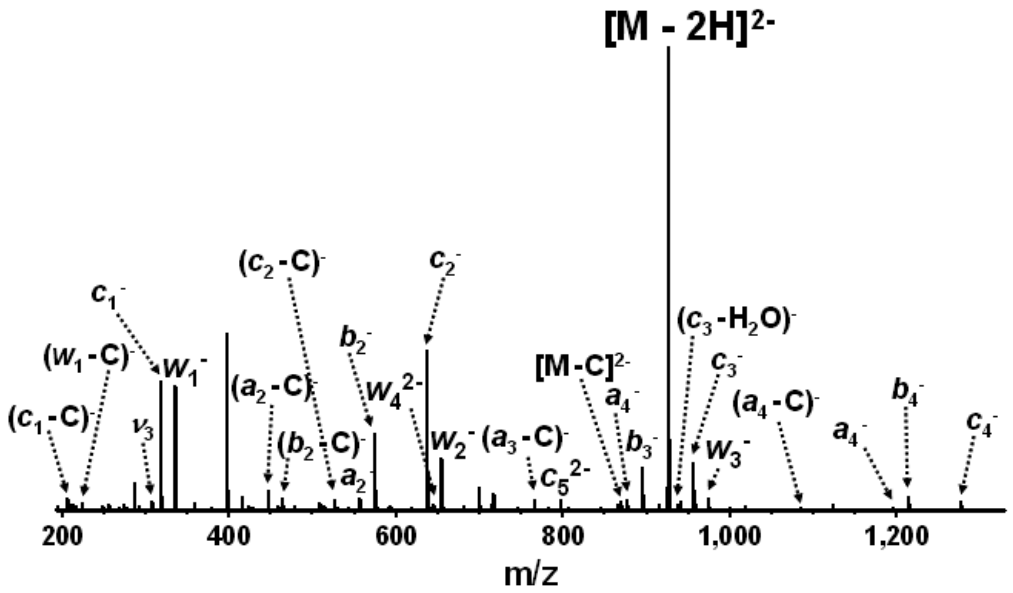

Figure 6-6. IRMPD (10.6 μm, 45 ms irradiation at 7.5 W laser power, 50 scans) of doubly deprotonated 2'-methoxy C_6. Ions labeled *b* can also be *y* ions, and ions labeled *c* can also be *x* ions. A complete *c*/*x* ion series allowed full sequencing of the oligonucleotide.

Table 6-2. Product ions observed from EDD (2 s, -18.2 V bias, 50 scans) of 2'-methoxy U_6. Product ions labeled *w* can be also be *d* ions, ions labeled *a* can be also be *z* ions, ions labeled *b* can be also be *y* ions, and ions labeled *c* can be also be *x* ions.

Observed m/z	Calculated m/z	Assignment	Error (ppm)
319.0309	319.0336	c_1^-	- 8.5
337.0466	337.0444	w_1^-	6.5
577.1224	577.1188	b_2^-	6.2

639.0756	639.0747	c_2^-	1.4
657.0851	657.0853	w_2^-	- 0.3
808.0939	808.1004	w_5^{2-}	- 8.0
879.1567	879.1491	a_3^-	8.6
897.1589	897.1597	b_3^-	- 0.9
928.1377	928.1377	$[M - 2H]^{2-}$	Calibrant
959.1137	959.1156	c_3^-	- 2.0
977.1231	977.1262	w_3^-	- 3.2
1198.178	1198.182	$a_4^{-\bullet}$	- 3.3
1279.1515	1279.157	c_4^-	- 4.3
1297.1615	1297.167	w_4^-	- 4.2
1518.212	1518.223	$a_5^{-\bullet}$	-7.2
1599.207	1599.197	c_5^-	6.3
1617.199	1617.208	w_5^-	-5.6
1633.231	1633.228	$[M - 2U]^-$	1.8
1635.219	1635.219	$(w_5 + H_2O)^-$	0.04
1744.247	1744.248	$[M - U]^{-\bullet}$	-0.6
1745.237	1745.255	$[M - U]^-$	-10.3
1838.229	1838.264	$[M - H_2O]^{-\bullet}$	-19.1
1856.275	1856.275	$[M - 2H]^{-\bullet}$	Calibrant

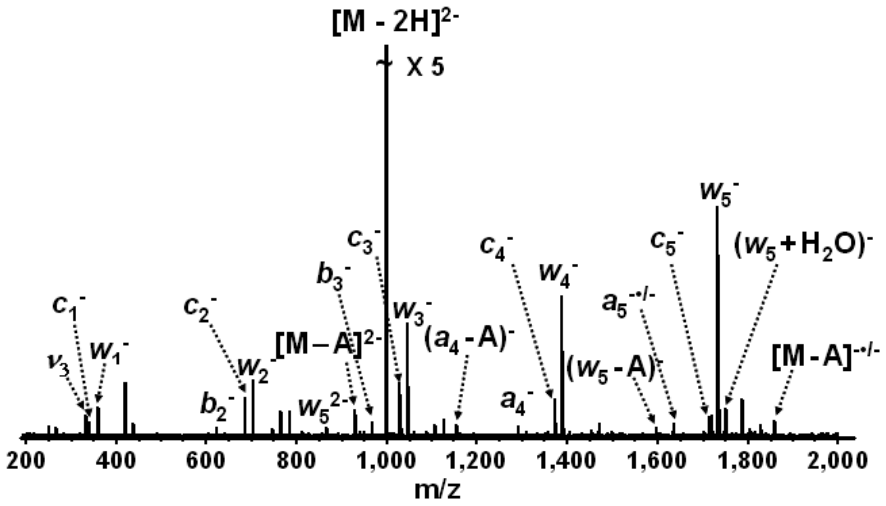

Figure 6-7. EDD (-18.2 V, 2 s, 50 scans) of doubly deprotonated 2'-methoxy A_6. Product ions labeled *w* can also be *d* ions, ions labeled *a* can also be *z* ions, ions labeled *b* can also be *y* ions, and ions labeled *c* can also be *x* ions. Full series of *c*/*x* and *d*/*w* ions are present, allowing full sequencing of the oligonucleotide.

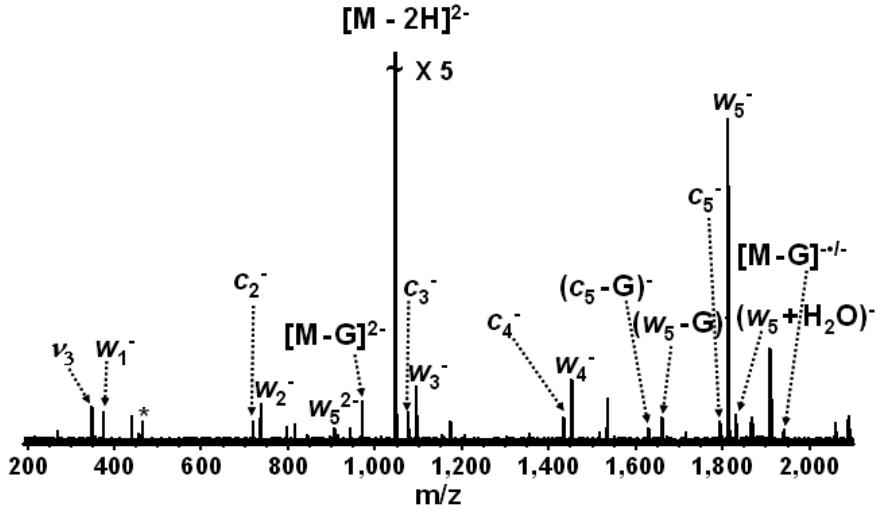

Figure 6-8. EDD (-18.2 V, 2 s, 50 scans) of doubly deprotonated 2'-methoxy G_6. Product ions labeled *w* can also be *d* ions, and ions labeled *c* can also be *x* ions. Full series of *d*/*w* ions are observed, allowing full sequencing of the oligonucleotide. Electronic noise spike is labeled with an asterisk.

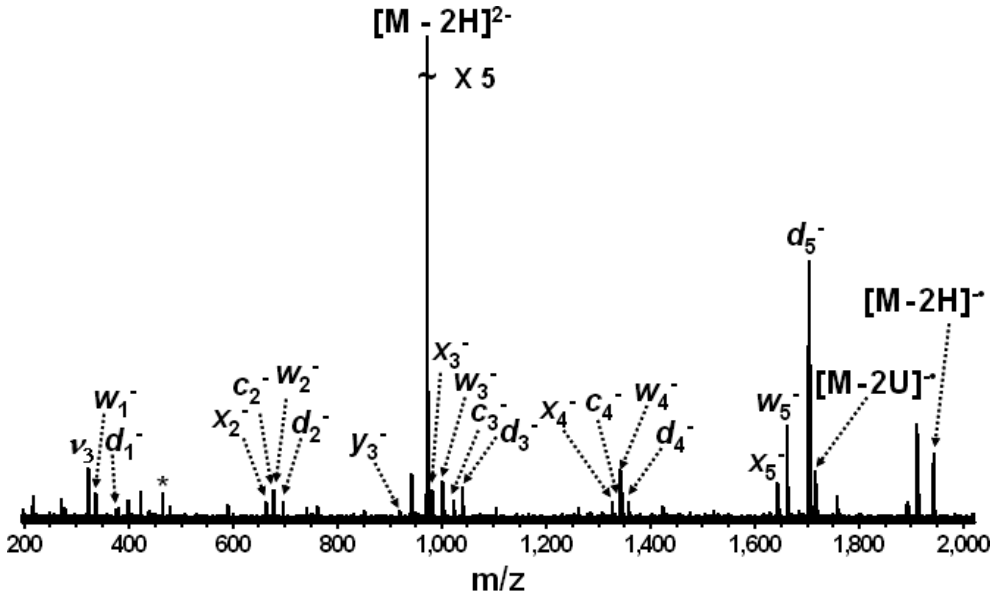

Figure 6-9. EDD (-18.2 V, 2 s, 50 scans) of doubly deprotonated 2'-methoxy GCAUAC. *d*/*w* ion series are mixtures of *d* and *w* ions, and that *c*/*x* ion series are also mixtures. Electronic noise spike is labeled with an asterisk.

6.3.2. Methylphosphonate-containing Oligonucleotides

In the methylphosphonate-containing oligonucleotides characterized here, all backbone phosphate hydroxyl groups were replaced by methyl groups, an approach that has been utilized for development of antisense compounds with a new chiral center, altering their hybridization properties [30]. Figure 6-10 shows an ECD spectrum from doubly protonated methylphosphonate-containing dA_6. Sequence specific w_2/d_2, w_3/d_3, w_4/d_4 and w_5/d_5 ions are observed, together with three ions involving base loss from either a *w*/*d* ion, or from the precursor ions. Abundant charge reduced precursor ions are also present. Complete sequence information could not be obtained due to the lack of the w_1/d_1 ion. Figure 6-11 displays an ECD spectrum from methylphosphonate-containing dC_6. This spectrum is different from that of methylphosphonate-containing dA_6:

although the same incomplete *w*/*d* ion series is observed as in ECD of methylphosphonate-containing dA_6, complementary *a*/*z* ions and extensive base loss from *w*/*d* and *a*/*z* ions are also seen. For *a*/*z* ions, observed masses are one Da lighter than the calculated values (see inset for a_5/z_5), possibly corresponding to hydrogen loss from *a*/*z* even-electron ions (error less than 1 ppm for a_5/z_5), or two hydrogen losses from *a*/*z* radical ions. Double hydrogen losses from radical ions have recently been reported in ECD of peptides, involving H_2 formation with high exothermicity [31]. In ECD of methylphosphonate-containing dG_6 (see Figure 6-12) a similar fragmentation pattern was observed as for methylphosphonate-containing dA_6 with only w_2/d_2-w_5/d_5 ions present as well as base loss from precursor ions. These results demonstrate that ECD fragmentation of methylphosphonate DNA shows a nucleobase dependence. Adenine and guanine are both purines and, due to their larger size compared to cytosine, may have higher propensity for gas-phase intramolecular hydrogen bonding [32], which reduces detection of product ions (as discussed above), thereby possibly explaining the lower amount of product ions detected for these two nucleobases. Figure 6-13 shows an ECD spectrum from triply protonated methylphosphonate-containing d(GCATAC). For this oligonucleotide, full sequence coverage was obtained from the combination of *w* and *d* ion series.

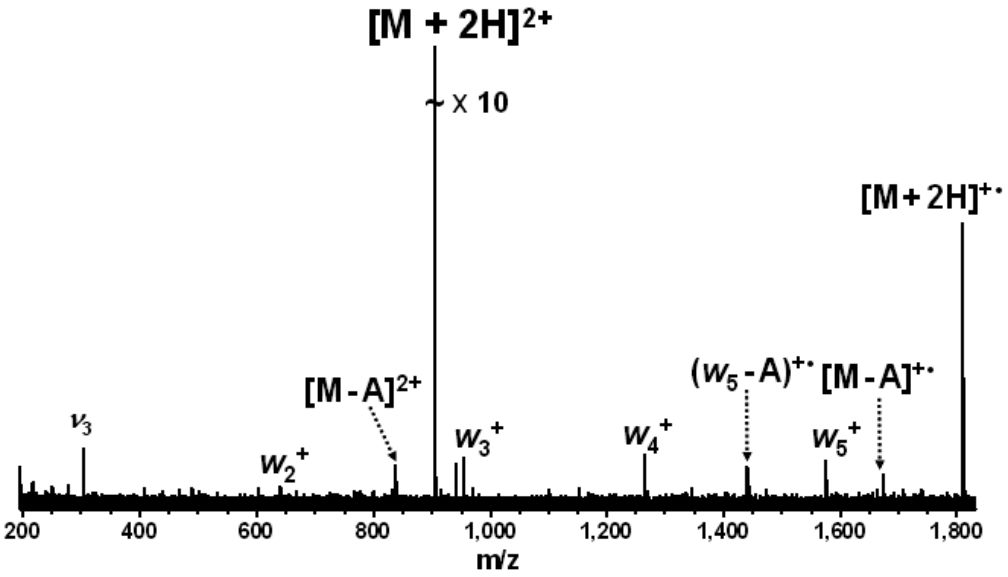

Figure 6-10. ECD (- 1 V bias voltage, 20 ms, 32 scans) of doubly protonated methylphosphonate-containing dA_6. *d*/*w* ions are labeled as *w* ions.

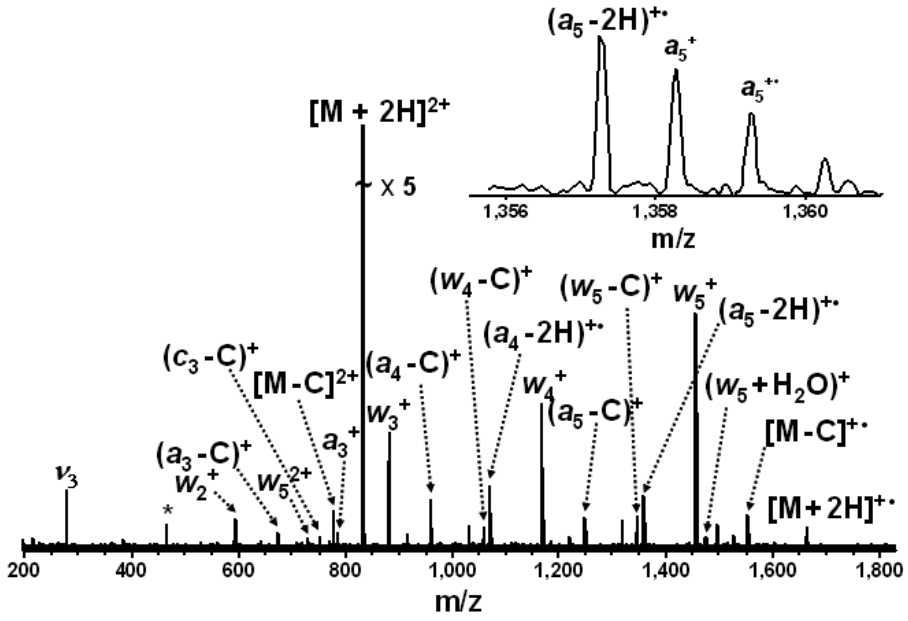

Figure 6-11. ECD (- 1 V bias voltage, 30 ms, 32 scans) of doubly protonated methylphosphonate-containing dC_6. *a*/*z* and *d*/*w* ions are labeled as *a* and *w* ions. The inset shows an expansion of the m/z region of the ion labeled $(a_5 - 2H)^{+\bullet}$.

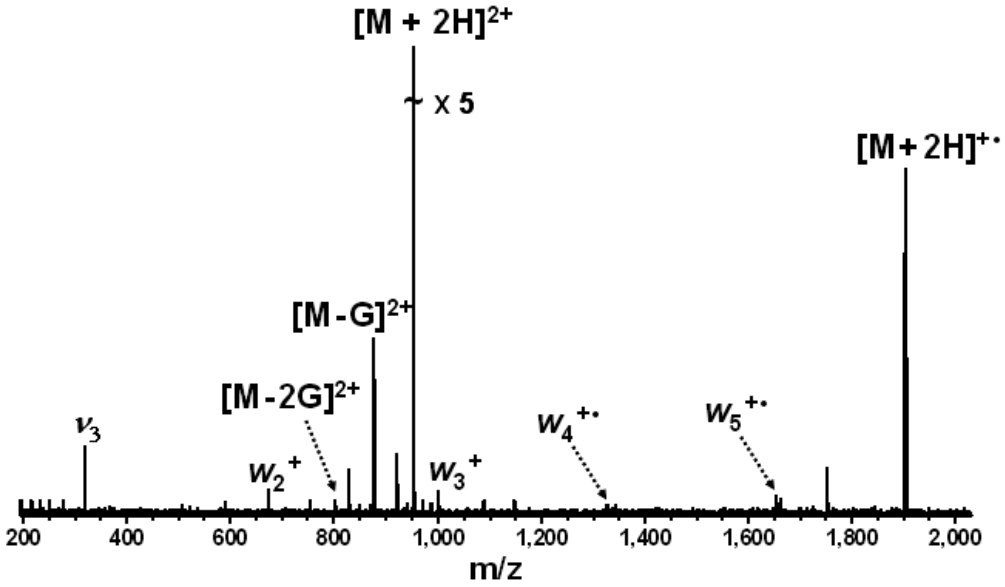

Figure 6-12. ECD (- 1 V bias voltage, 30 ms, 32 scans) of doubly protonated methylphosphonate-containing dG_6. *d*/*w* ions are labeled as *w* ions.

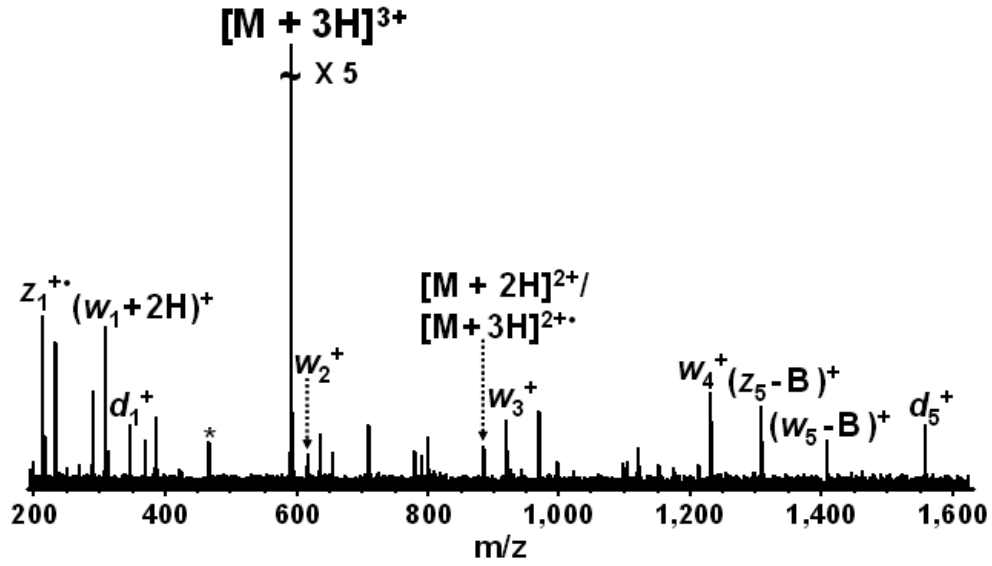

Figure 6-13. ECD (- 1 V bias voltage, 30 ms, 32 scans) of triply protonated methylphosphonate-containing d(GCATAC). Full sequence coverage is obtained from the combination of *w* and *d* ion series.

Figure 6-14 shows an EDD spectrum of doubly deprotonated methylphosphonate-containing dC_6 dissociated at an electron energy of ~17.5 eV (cathode bias voltage of - 18.2 V [28]) with 2 s irradiation time. A complete *d*/*w* ion series, four *c*/*x*-type ions, and two *a*/*z*-type ions are present. We also observed three relatively abundant ions that could not be unambiguously identified due to high mass error. These ions (indicated by question marks after the assignments) have similar mass as the calculated mass of (*a* - C) ions with loss of two hydrogens (the mass error is larger than 20 ppm). The structure and mechanism for formation of these ions are currently under further investigation. Compared with ECD of the same oligonucleotide, the EDD spectrum is easier to interpret and full sequence coverage is provided. For methylphosphonate-containing dA_6, the signal in negative ion mode was too weak to perform EDD, presumably due to the absence of easily deprotonated sites (a consequence of the backbone methylation). Figure 6-15 shows EDD of methylphosphonate-containing dG_6, which resulted in very similar fragmentation as methylphosphonate-containing dC_6 (Figure 6-14). For the former, four possible (*a* - G) ions with two hydrogen losses (mass error is larger than 20 ppm) are seen. Similar behavior was also observed for methylphosphonate-containing dT_6 (see Figure 6-16). An EDD spectrum of methylphosphonate-containing d(GCATAC) is shown in Figure 6-17. Here, complete *d* and *w* ion series, together with two complementary *a* ions, and charge reduced precursor ions are observed but no base loss or unidentified peaks.

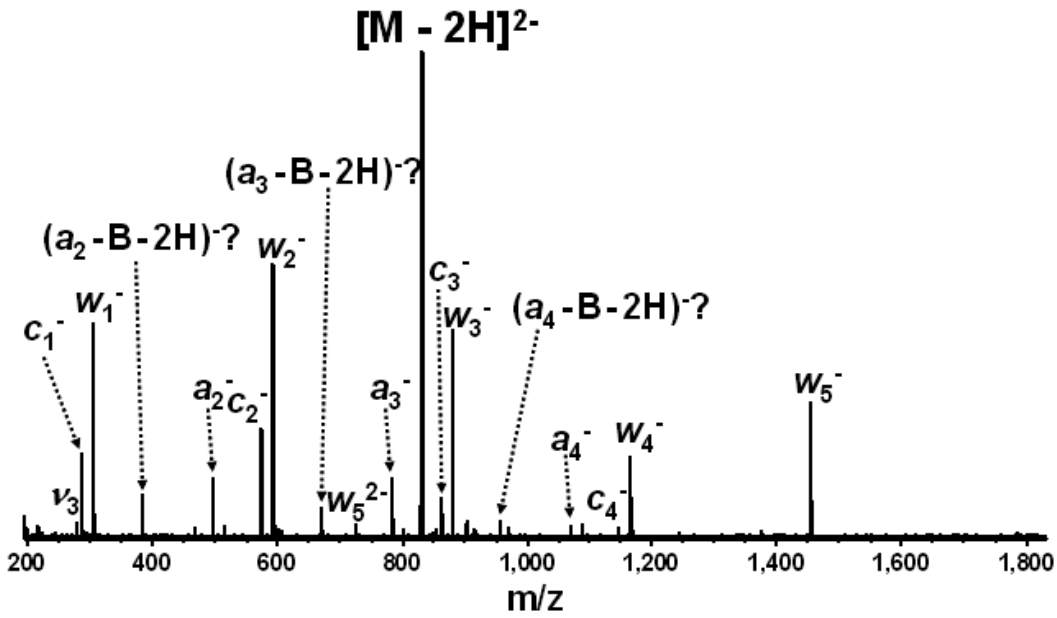

Figure 6-14. EDD of doubly deprotonated methylphosphonate-containing dC_6. Product ions labeled *w* can also be *d* ions, ions labeled *a* can also be *z* ions, and ions labeled *c* can also be *x* ions. A complete series of *d*/*w* ions is observed, allowing full sequencing of the oligonucleotide. Question marks denote assignments with high (>20 ppm) mass error.

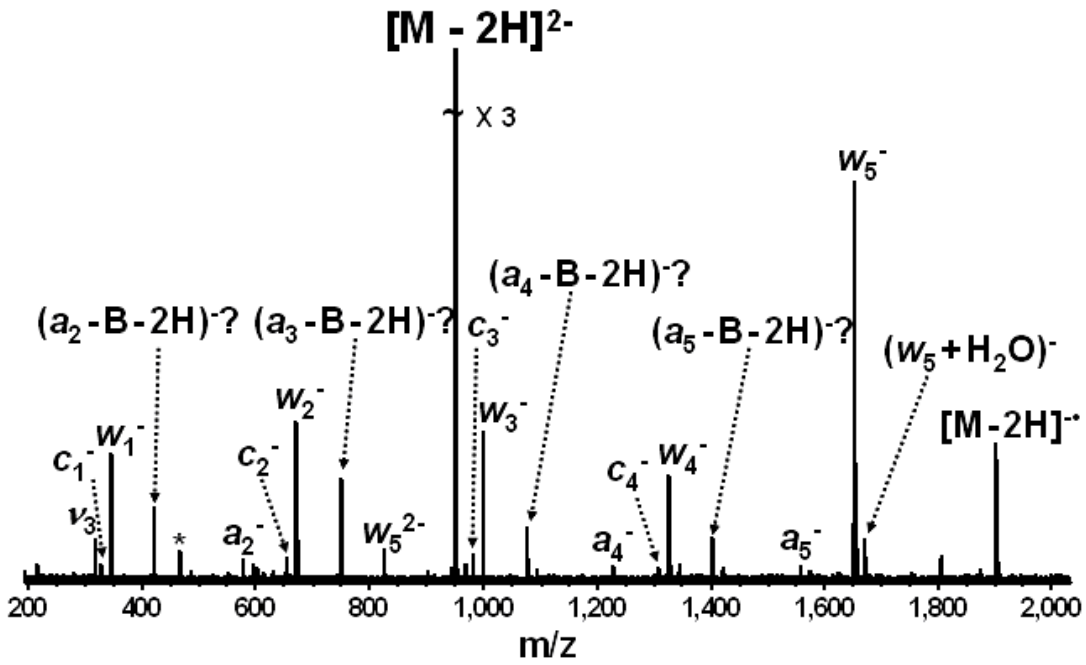

Figure 6-15. EDD of doubly deprotonated methylphosphonate-containing dG_6. Product ions labeled *w* can also be *d* ions, ions labeled *a* can also be *z* ions, and ions labeled *c* can also be *x* ions. A complete series of *d*/*w* ions is observed, allowing full sequencing of the oligonucleotide. Question marks denote assignments with high (>20 ppm) mass error. Electronic noise spike is labeled with an asterisk.

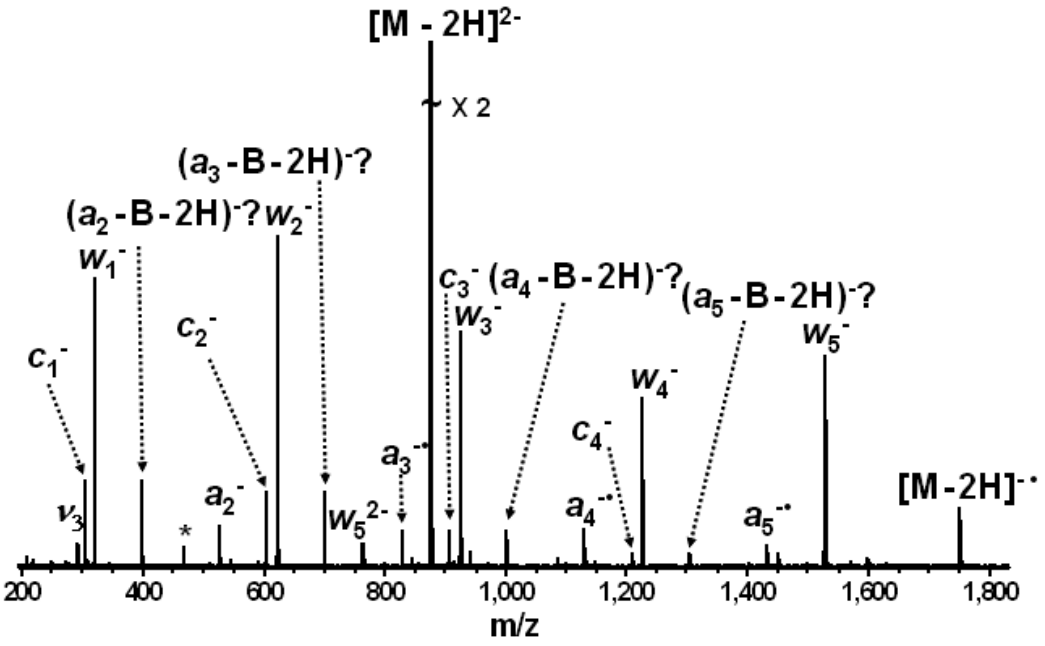

Figure 6-16. EDD of doubly deprotonated methylphosphonate-containing dT_6. Product ions labeled *w* can also be *d* ions, ions labeled *a* can also be *z* ions, and ions labeled *c* can also be *x* ions. A complete series of *d*/*w* ions is observed, allowing full sequencing of the oligonucleotide. Question marks denote assignments with high (>20 ppm) mass error. Electronic noise spike is labeled with an asterisk.

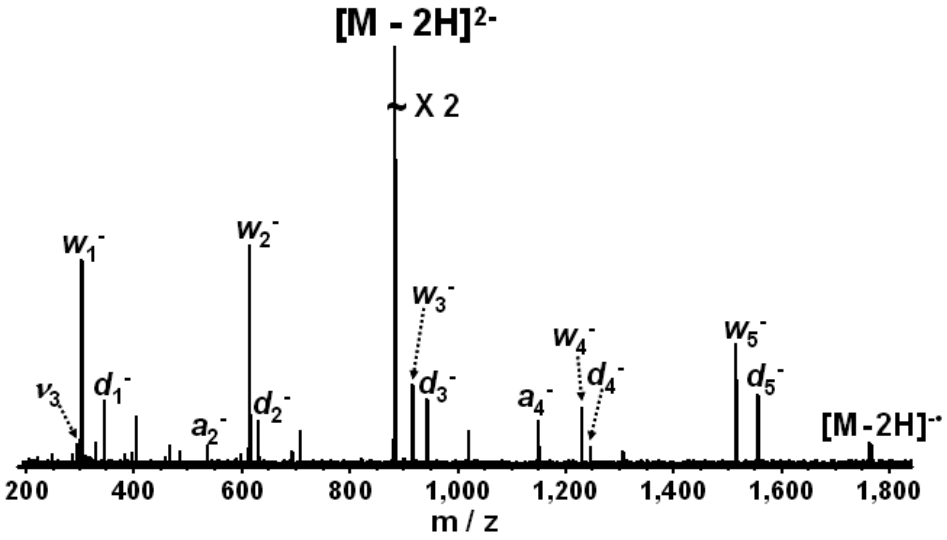

Figure 6-17. EDD (-18.2 V, 2 s, 30 scans) of doubly deprotonated methylphosphonate-containing d(GCATAC). Complete *d* and *w* ion series, together with two complementary *a* ions are observed, allowing full sequencing of the oligonucleotide.

Figure 6-18 shows an IRMPD spectrum of the doubly deprotonated form of d(GCATAC). Here, a complete *w* ion series, four *d* ions, and two *a* ions are observed without the signature base loss that is typically seen from vibrational excitation of unmodified oligodeoxynucleotides [7-9]. The latter result correlates with the CAD oligodeoxynucleotide dissociation mechanism proposed by Gross and co-workers in which fragmentation is initiated by proton transfer from the phosphate backbone to a nucleobase [8]. Such proton transfer is suppressed due to the presence of methyl groups on the backbone. In summary, for the methylphosphonate-containing modified oligonucleotides we have characterized, ECD provided only limited structural information and full sequence coverage was only obtained for methylphosphonate-containing d(GCATAC). However, the combination of two ion series had to be used to

sequence that oligonucleotide with ECD. Compared to IRMPD, EDD appears to yield a similar analytical outcome for methylphosphonate-containing oligodeoxynucleotides.

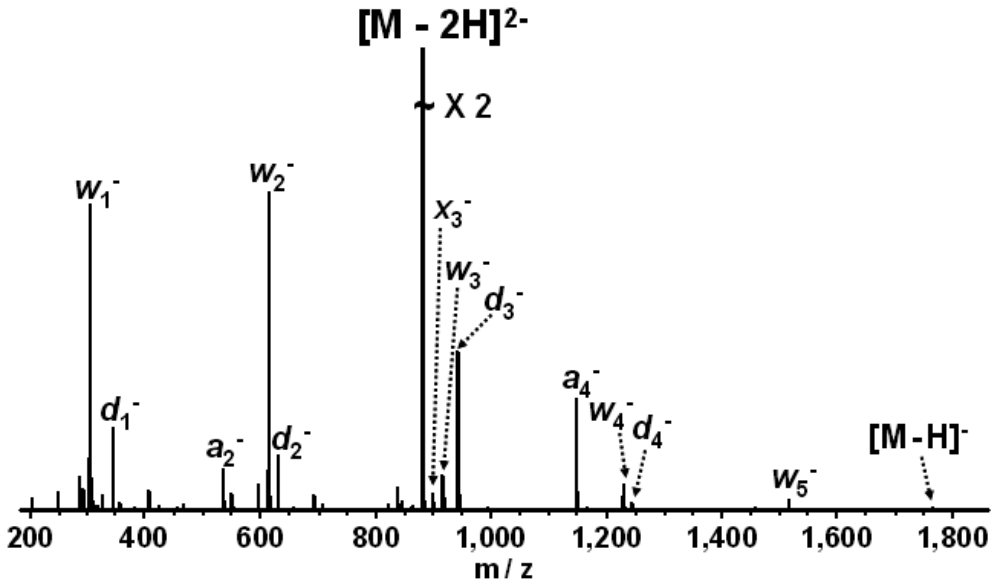

Figure 6-18. IRMPD (10.6 μm, 18 ms irradiation at 7.5 W laser power, 30 scans) of doubly deprotonated methylphosphonate-containing d(GCATAC). A complete *w* ion series provides full sequence coverage.

6.3.3. Oligonucleotides Containing Abasic Sites

Figure 6-19 shows an ECD spectrum of triply protonated d(GCACXTAC). Sequence specific *d*, *w*, *a*, and *z* ions, which provide complete sequence coverage (as summarized in the inset), are observed. The inset also shows a summary of product ions observed in ECD of d(GCACGTAC), d(GCXCGTAC), and d(GCAXGTAC). These data indicate that the position of the abasic site does not influence the fragmentation pattern, thereby suggesting that ECD may constitute a robust strategy for characterizing such oligonucleotides. By contrast, in IRMPD of d(GCACXTAC) (shown in Figure 6-

20), backbone cleavages on the 3' side of the abasic site, and on the 3' side of thymidine are absent, consistent with the CAD cleavage mechanism initiated by proton transfer to a nucleobase (thymine has much lower proton affinity than other nucleobases) [8]. We have recently performed double resonance experiments to characterize the oligodeoxynucleotide IRMPD fragmentation mechanism and found that a similar mechanism involving neutral base loss as the first step is at play in IRMPD [33].

EDD of the three abasic site-containing oligonucleotides discussed above resulted in full sequence coverage from complete *w* ion series. An EDD spectrum of d(GCACXTAC), dissociated at an electron energy of ~17.8 eV (cathode bias voltage of -18.5 V) [28] with 2 s irradiation time is shown in Figure 6-21. In addition to the *w* ions, five *d* ions, four (*a* - B) ions, and one *z* ion are observed. Similar results were also obtained for the other abasic oligonucleotides as shown in the inset of Figure 6-21. As seen in ECD, there is no influence of the abasic site, or the nucleobase thymine, in EDD fragmentation. However, EDD data are easier to interpret and full sequence coverage was obtained in all cases. Full sequencing was also obtained with ECD. However, the latter technique requires positively charged precursor ions, which are more difficult to generate for nucleic acids than negatively charged ions, thus, ECD sensitivity may be lower than that of EDD.

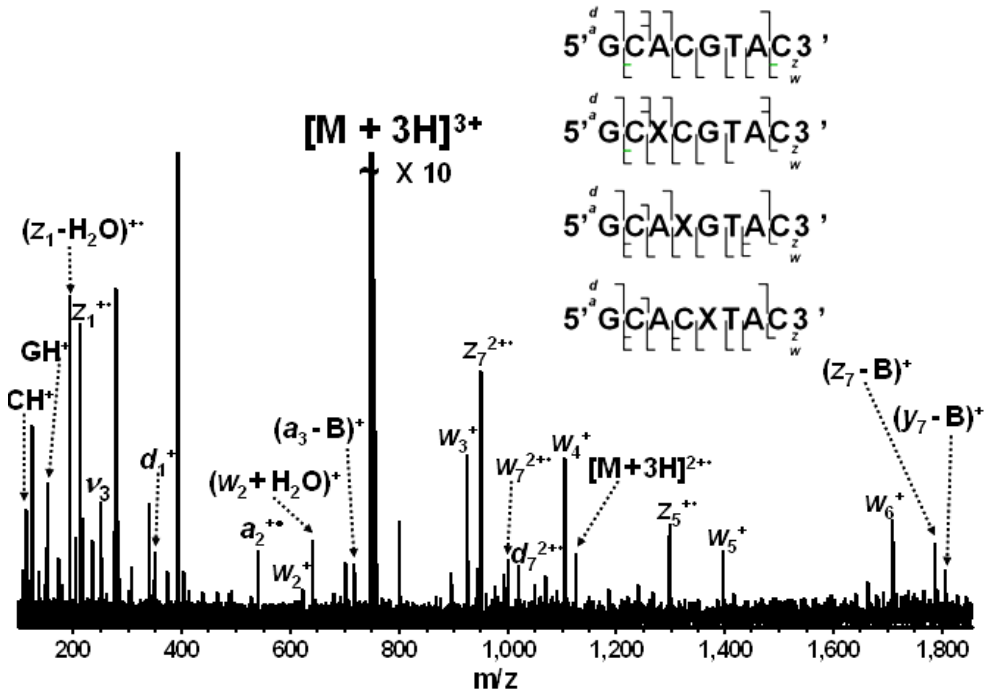

Figure 6-19. ECD (- 1 V bias voltage, 15 ms, 88 scans) of triply protonated d(GCACXTAC) (X denotes an abasic site at which a nucleobase has been replaced by hydrogen). The inset summarizes observed backbone ECD bond cleavages for this oligonucleotide and three related ones for which X is at a different position.

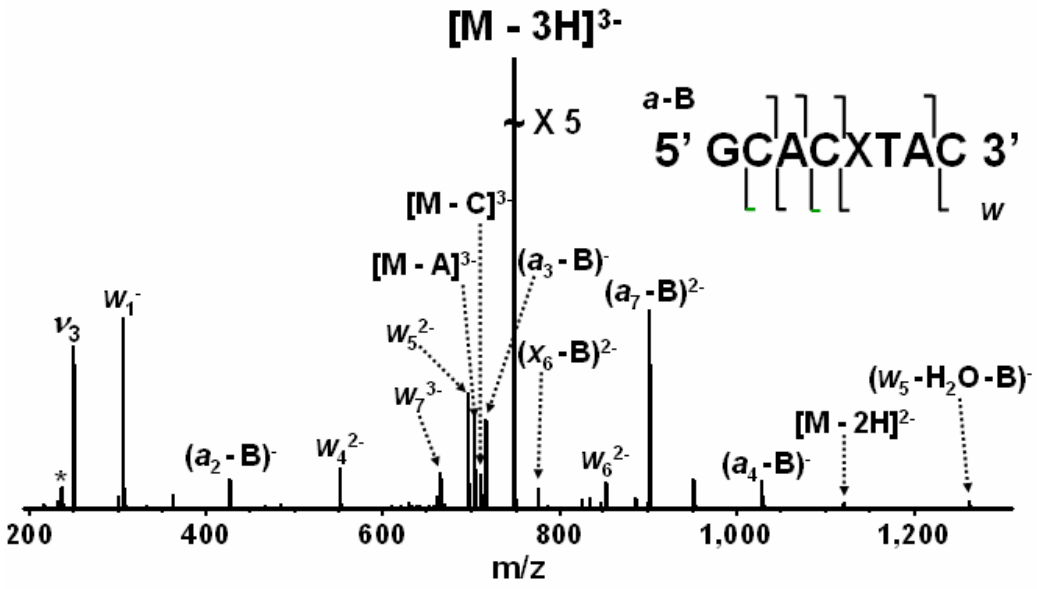

Figure 6-20. IRMPD (10.6 μm, 25 ms irradiation at 7.5 W laser power, 50 scans) of triply deprotonated d(GCACXTAC) (X denotes an abasic site at which a nucleobase has been replaced by hydrogen). Observed backbone bond cleavages are summarized in the inset.

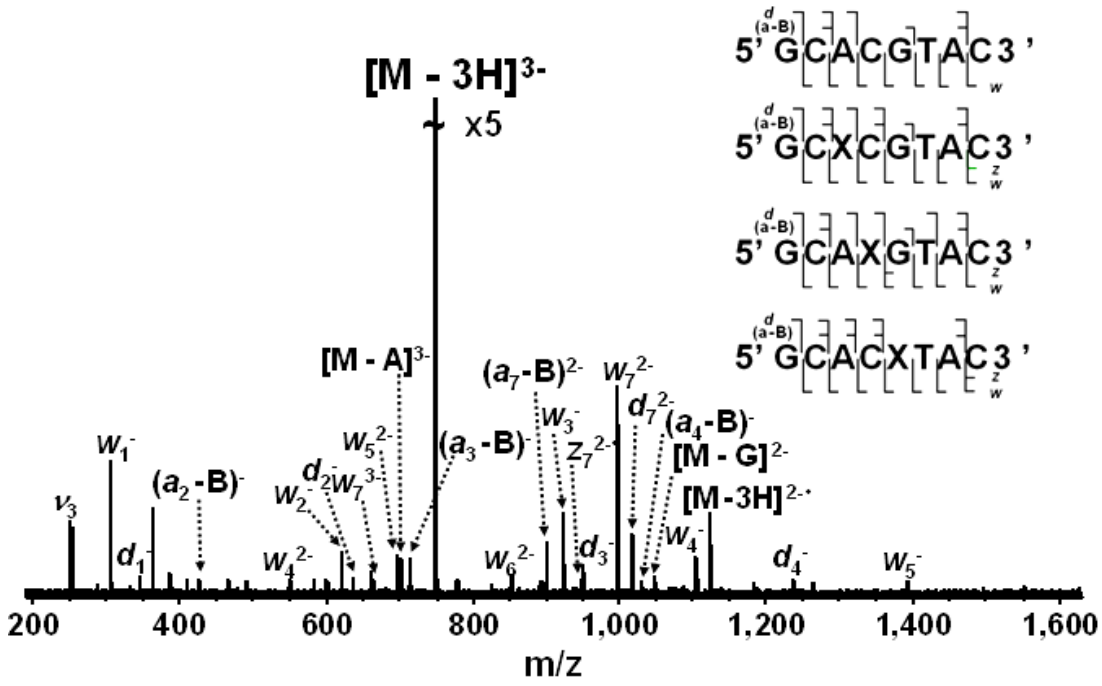

Figure 6-21. EDD (- 18.5 V, 2 s, 50 scans) of triply deprotonated d(GCACXTAC) (X denotes an abasic site at which a nucleobase has been replaced by hydrogen). The inset summarizes observed backbone EDD bond cleavages for this oligonucleotide and three related ones for which X is at a different position.

6.4. CONCLUSION

This article demonstrates application of ECD and EDD to the characterization of three different types of chemically modified oligonucleotides: 2'-methoxy oligomer RNAs, methylphosphonate-containing oligomer DNAs, and oligomer DNAs with abasic sites. Limited backbone cleavage was observed in ECD of 2'-methoxy oligomer RNAs and oligomer DNAs with methylphosphonate backbones. By contrast, for oligomer DNAs containing abasic sites, ECD provided extensive fragmentation, resulting in complete sequence coverage. However, for all three types of modified oligonucleotides,

EDD spectra were easier to interpret and yielded complete sequence coverage in all cases. IRMPD provided valuable data for the characterization of methylphosphonate modified oligonucleotides, presumably due to suppression of base loss as a consequence of the presence of methyl groups that prevent proton transfer to a nucleobase upon activation. However, limited information for oligonucleotides with abasic sites was obtained due to the absence of backbone cleavage on the 3' side of such sites.

6.5. BIBLIOGRAPHY

1. Dias, N.; Stein, C. A. Antisense Oligonucleotides: Basic Concepts and Mechanisms. *Mol. Cancer Ther.* **2002,** *1*, 347-355.
2. Tamm, I. Antisense Therapy in Malignant Diseases: Status Quo and Quo Vadis? *Clin. Sci.* **2006,** *110*, 427-442.
3. Aboul-Fadl, T. Antisense Oligonucleotides: The State of the Art. *Curr. Med. Chem.* **2006,** *12*, 2193-2214.
4. Cook, P. D., *Antisense Drug Technology: Principles, Strategies and Applications*. Crooke S. T., Ed. ed.; Marcel Dekker, Inc.: New York, 2001.
5. Banoub, J. H.; Newton, R. P.; Esmans, E.; Ewing, D. F.; Mackenzie, G. Recent Developments in Mass Spectrometry for the Characterization of Nucleosides, Nucleotides, Oligonucleotides, and Nucleic Acids. *Chem. Rev.* **2005,** *105*, 1869-1916.
6. Muddiman, D. C.; Smith, R. D. Sequencing and Characterization of Larger Oligonucleotides by Electrospray Ionization Fourier Transform Ion Cyclotron Resonance Mass Spectrometry. *Rev. Anal. Chem.* **1998,** *17*, 1-68.

7. Wu, J.; McLuckey, S. A. Gas-phase Fragmentation of Oligonucleotide Ions. *Int. J. Mass Spectrom.* **2004,** *237*, 197-241.

8. Wan, K. X.; Gross, M. L. Fragmentation Mechanisms of Oligodeoxynucleotides: Effects of Replacing Phosphates with Methylphosphonates and Thymines with Other Bases in T-rich Sequences. *J. Am. Soc. Mass Spectrom.* **2001,** *12*, 580-589.

9. Sannes-Lowery, K. A.; Hofstadler, S. A. Sequence Confirmation of Modified Oligonucleotides using IRMPD in the External Reservoir of an Electrospray Ionization Fourier Transform Ion Cyclotron Mass Spectrometer. *J. Am. Soc. Mass Spectrom.* **2003,** *14*, 825-833.

10. Tromp, J. M.; Schürch, S. Gas-Phase Dissociation of Oligoribonucleotides and their Analogs Studied by Electrospray Ionization Tandem Mass Spectrometry. *J. Am. Soc. Mass Spectrom.* **2005,** *16*, 1262-1268.

11. Monn, S. T. M.; Schürch, S. New Aspects of the Fragmentation Mechanisms of Unmodified and Methylphosphonate-Modified Oligonucleotides. *J. Am. Soc. Mass Spectrom.* **2007,** *18*, 984-990.

12. McLuckey, S. A.; Van Berkel, G. J.; Glish, G. L. Tandem Mass Spectrometry of Small, Multiply-charged Oligonucleotides. *J. Am. Soc. Mass Spectrom.* **1992,** *3*, 60-70.

13. Green-Church, K. B.; Limbach, P. A. Mononucleotide Gas-Phase Proton Affinities as Determined by the Kinetic Method. *J. Am. Soc. Mass Spectrom.* **2000,** *11*, 24-32.

14. Podolyan, Y.; Gorb, L.; Leszczynski, J. Protonation of Nucleic Acid Bases. A Comprehensive Post-Hartree-Fock Study of the Energetics and Proton Affinities. *J. Phys. Chem. A* **2000,** *104*, 7346-7352.

15. Zubarev, R. A.; Kelleher, N. L.; McLafferty, F. W. Electron Capture Dissociation of Multiply Charged Protein Cations. A Nonergodic Process. *J. Am. Chem. Soc.* **1998,** *120*, 3265-3266.

16. Zubarev, R. A.; Horn, D. M.; Fridriksson, E. K.; Kelleher, N. L.; Kruger, N. A.; Lewis, M. A.; Carpenter, B. K.; McLafferty, F. W. Electron Capture Dissociation for Structural Characterization of Multiply Charged Protein Cations. *Anal. Chem.* **2000,** *72*, 563-573.

17. Cerda, B. A.; Horn, D. M.; Breuker, K.; McLafferty, F. W. Sequencing of Specific Copolymer Oligomers by Electron-Capture-Dissociation Mass Spectrometry. *J. Am. Chem. Soc.* **2002,** *124*, 9287-9291.

18. Kleinnijenhuis, A. J.; Duursma, M. C.; Breukink, E.; Heeren, R. M. A.; Heck, A. J. R. Localization of Intramolecular Monosulfide Bridges in Lantibiotics Determined with Electron Capture Dissociation. *Anal. Chem.* **2003,** *75*, 3219-3225.

19. Liu, H.; Lee, J. Y.; Sherman, D. H.; Håkansson, K. Collision Activated Dissociation, Infrared Multiphoton Dissociation, and Electron Capture Dissociation of the Bacillus anthracis Siderophore Petrobactin and its Metal Ion Complexes. *J. Am. Soc. Mass Spectrom.* **2007,** *18*, 842-849

20. Håkansson, K.; Hudgins, R. R.; Marshall, A. G.; O'Hair, R. A. J. Electron Capture Dissociation and Infrared Multiphoton Dissociation of Oligodeoxynucleotide Dications. *J. Am. Soc. Mass Spectrom.* **2003,** *14*, 23-41.

21. Schultz, K. N.; Håkansson, K. Rapid Electron Capture Dissociation of Mass-Selectively Accumulated Oligodeoxynucleotide Dications. *Int. J. Mass Spectrom.* **2004,** *234*, 123-130.

22. Budnik, B. A.; Haselmann, K. F.; Zubarev, R. A. Electron Detachment Dissociation of Peptide Di-anions: an Electron-hole Recombination Phenomenon. *Chem. Phys. Lett.* **2001,** *342*, 299-302.

23. Yang, J.; Mo, J.; Adamson, J. T.; Håkansson, K. Characterization of Oligodeoxynucleotides by Electron Detachment Dissociation Fourier Transform Ion Cyclotron Resonance Mass Spectrometry. *Anal. Chem.* **2005,** *77*, 1876-1882.

24. Yang, J.; Håkansson, K. Fragmentation of Oligoribonucleotides from Gas-phase Ion-electron Reactions. *J. Am. Soc. Mass Spectrom.* **2006,** *17*, 1369-1375.

25. Kellersberger, K. A.; Fabris, D., Electron Capture Dissociation (ECD) of Structured Nucleic Acids. In *Proceedings of the 53rd ASMS Conference on Mass Spectrometry and Applied Topics* San Antonio, TX, 2005.

26. de Koning, L. J.; Nibbering, N. M. M.; van Orden, S. L.; Laukien, F. H. Mass Selection of Ions in a Fourier Transform Ion Cyclotron Resonance Trap Using Correlated Harmonic Excitation Fields (CHEF). *Int. J. Mass Spectrom. Ion Processes* **1997,** *165*, 209-219.

27. Olsen, J. V.; Haselmann, K. F.; Nielsen, M. L.; Budnik, B. A.; Nielsen, P. E.; Zubarev, R. A. Comparison of Electron Capture Dissociation and Collisionally Activated Dissociation of Polycations of Peptide Nucleic Acids. *Rapid Commun. Mass Spectrom.* **2001,** *15*, 969-974.

28. Yang, J.; Håkansson, K. Characterization and Optimization of Electron Detachment Dissociation Fourier Transform Ion Cyclotron Resonance Mass Spectrometry. (*in preparation*).

29. Budnik, B. A.; Haselmann, K. F.; Elkin, Y. N.; Gorbach, V. I.; Zubarev, R. A. Applications of Electron-Ion Dissociation Reactions for Analysis of Polycationic Chitooligosaccharides in Fourier Transform Mass Spectrometry. *Anal. Chem.* **2003,** *75*, 5994-6001.

30. Thiviyanathan, V.; Vyazovkina, K. V.; Gozansky, E. K.; Bichenchova, E.; Abramova, T. V.; Luxon, B. A.; Lebedev, A. V.; Gorenstein, D. G. Structure of Hybrid Backbone Methylphosphonate DNA Heteroduplexes: Effect of R and S Stereochemistry. *Biochemistry* **2002,** *41*, 827-838.

31. Savitski, M. M.; Kjeldsen, F.; L., N. M.; Zubarev, R. A. Hydrogen Rearrangement to and from Radical z Fragments in Electron Capture Dissociation of Peptides. *J. Am. Soc. Mass Spectrom.* **2007,** *18*, 113-120.

32. Robinson, J. M.; Greig, M. J.; Griffey, R. H.; Mohan, V.; Laude, D. A. Hydrogen-deuterium Exchange of Nucleotides in the Gas Phase. *Anal. Chem.* **1998,** *70*, 3566-3571.

33. Yang, J.; Håkansson, K. Characterization of Oligodeoxynucleotide Fragmentation Pathways in Infrared Multiphoton Dissociation and Electron Detachment Dissociation by Fourier Transform Ion Cyclotron Double Resonance. (*in preparation*).

CHAPTER 7

CONCLUSION AND FUTURE OUTLOOK

7.1. SUMMARY OF RESULTS

This dissertation focuses on the implementation of EDD on a 7 T commercial FT ICR mass spectrometer and its application for nucleic acid characterization, including both DNA, RNA, and chemically modified oligonucleotides. In order to optimize this reaction and gain further insight into the EDD process, a detailed characterization of instrumental parameters was also undertaken, including the influence of electron current, electron energy distribution, cathode bias voltage, and electron extraction lens voltage. Furthermore, FT-IC double resonance was applied to characterize oligodeoxynucleotide fragmentation pathways in both IRMPD and EDD.

To our knowledge, we demonstrated for the first time EDD experiments performed with a standard heated filament electron source. The achieved oligonucleotide data showed more extensive fragmentation than previous ECD experiments under similar conditions. Implementation of a hollow dispenser cathode electron source increased EDD fragmentation efficiency and sensitivity. In particular, we showed that EDD provides information-rich

fragmentation patterns complementary to vibrational excitation for hexamer oligonucleotides. Complete oligonucleotide sequencing is easily achieved. Compared to ECD, enhanced sensitivity is achieved through negative ion mode operation (on average a 10-fold improvement so far in terms of concentration sensitivity). The detection of doubly charged product ions from doubly charged precursors indicates that EDD conditions promote direct dissociative electronic and/or vibrational excitation although other explanations for the formation of those ions are also discussed.

Electron current and voltage measurements demonstrated that the potential difference, ΔU, between the cathode and an extraction lens is a crucial parameter for successful EDD. The extraction lens voltage serves to regulate the number of electrons passing through the ICR cell. Energy distributions of generated electrons are narrow (< 0.5 V) over a range (- 8 to - 18 V) of cathode bias voltages and measured maxima of the energy distributions are around 0.7 eV lower than the applied cathode bias voltage. Optimum EDD efficiency at fixed electron current (around 4 μA) was obtained at electron energies of 16-22 eV for the oligodeoxynucleotide dT_6 and for the peptide substance P. The electron current decreases dramatically with decreased cathode heating current. However, similar quality EDD could be achieved at lower heating current (1.2 A instead of 1.8 A) by decreasing ΔU. For oligodeoxynucleotides, the EDD efficiency and sequence coverage seems to increase with increasing precursor ion charge state.

We compared ECD and EDD of hexamer oligoribonucleic acids. Here, ECD showed a strong nucleobase dependence: the RNA A_6 generated mostly *c*/*x* and b/*y*-type

ions, similar to the fragmentation patterns observed in CAD and IRMPD, whereas C_6 only yielded *d*/*w*-type ions (similar to ECD of DNA). Other RNAs showed a mixture of those ion types. This behavior supports an ECD cleavage mechanism involving electron capture at the nucleobases, consistent with recent theoretical work for neutral DNA [1]. However, only limited backbone cleavage was observed in ECD, precluding complete sequencing. EDD appears more promising for RNA structural characterization because more extensive backbone cleavage was observed at higher sensitivity. Here, *w* and *d* ion series constituted the most abundant fragmentation channels, similar to EDD of DNA. The only exception was U_6 for which *w*/*d*-type cleavage competed with *c*/x and *b*/*y*-type cleavage. We propose that the EDD cleavage process is initiated via direct electron detachment from the deprotonated phosphate backbone. EDD provided full sequence coverage for all RNAs characterized.

In IRMPD, the most abundant oligodeoxynucleotide product ions are sequence-specific (*a* - B) and *w*-type ions, similar to CAD. We demonstrated for the first time the application of double resonance experiments to establish that neutral base loss from precursor ions precedes oligodeoxynucleotide backbone cleavage in IRMPD. For thymidine-rich oligodeoxynucleotides, fragmentation proceeds through alternative pathways. We also extended the DR approach to study intermediates in the EDD fragmentation process. These results showed that charge reduced radical precursor ions constitute a major intermediate in EDD of dT_6, d(GCATAC), and d(GCATGC).

Furthermore, DR-EDD suggests that (*a*/*z* - T) ions originate from secondary fragmentation of *a*/*z* radical ions for dT_6.

Finally, we extended the application of ECD and EDD to the characterization of three different types of chemically modified oligonucleotides, including 2'- methoxy oligomer RNAs, oligomer DNAs with methylphosphonate backbones, and oligomer DNAs containing abasic sites. Such chemically modified oligonucleotides play important roles in biomedical/pharmaceutical research, particularly for antisense applications. Limited backbone cleavage was observed in ECD of 2'-methoxy oligomer RNAs and methylphosphonate modified oligomer DNAs. However, for oligomer DNAs with abasic sites, ECD was a more effective approach. For all three types of modified oligonucleotides, EDD spectra were more straightforward to interpret and provided full sequence coverage in all cases. IRMPD provided valuable data for the characterization of methylphosphonate modified oligonucleotides, presumably due to suppression of base loss as a consequence of the presence of methyl groups that prevent proton transfer to a nucleobase upon protonation. However, limited information for oligonucleotides with abasic sites was obtained due the absence of backbone cleavage on the 3' side of such sites

7.2. PROSPECTS FOR FUTURE WORK

7.2.1. EDD of Peptide Nucleic Acids

Peptide nucleic acids (PNA) [2] are used for antisense applications, antigene therapeutics, and genetic diagnostics [3-5]. These molecules are analogues of DNA, but

with a backbone composed of repeating N-(2-aminoethyl)glycine units linked by peptide bonds. Standard purine and pyrimidine nucleobases are attached to the PNA backbone by methylene carbonyl bonds. PNA has been shown to bind to complementary DNA strands by Watson-Crick base pairing [3], which provides sequence specific recognition. Due to the unnatural structure of PNA, traditional techniques may be ineffective for their characterization and tandem mass spectrometry has been shown to be a valuable alternative approach [6, 7]. CAD produces *b* and *y* ions (peptide backbone fragmentation nomenclature [8]) from amide bond cleavage as well as facile water loss. By contrast, ECD mainly results in *c* and $z^{\bullet}$ product ions from backbone amine bond cleavage. ECD provides more extensive PNA sequence coverage than CAD [7]. EDD may be an alternative approach to characterize PNAs based on its demonstrated utility for sequencing DNA and RNA oligomers, and chemically modified DNA/RNA.

7.2.2. Fragmentation Pathways in ECD of DNA

In the first DNA ECD publication [9], Håkansson et al. proposed a mechanism proceeding via electron capture at backbone P=O bonds of neutral phosphates, followed by cleavage of C-O bonds to form $a^{\bullet}$ and *w*, or *d* and $z^{\bullet}$ ions. This mechanism involves a zwitterionic intermediate, analogous to suggestions by Syrstad and Turecek [10] as well as Simons and co-workers [11] for ECD of peptides. Since the first DNA ECD experiments, Sanche and co-workers have published density functional theory studies on the interaction between near zero eV electrons and a neutral DNA backbone, supporting a similar cleavage

mechanism in DNA damage [12]. However, their model compound did not include nucleobases. Simons and co-workers have performed more extensive theoretical studies and found that electron attachment to P=O bonds is highly unlikely for near zero eV electrons, but that DNA bases can attach such electrons, thereby inducing backbone C-O bond cleavage [1]. The same authors also showed that electrons in the 2-3 eV range can attach to P=O π^* orbitals but that such attachment induces C-O cleavages at a much lower rate. To further investigate the correlation between these theoretical results and ECD, one should perform ECD of abasic constructs in which one nucleobase has been replaced by a hydrogen, similar to the recent approach by Tromp and Schürch for CAD studies [13]. A reasonable starting point would be polydC because C and T have the lowest energy π^* orbitals [1] and the ionization efficiency of C-containing oligonucleotides in positive mode is high. To be able to distinguish between the two possible backbone C-O cleavages, 5' phosphorylated oligonucleotides should be used. Based on Simons' work, reduced cleavage at the abasic position would be expected. A second set of experiments could involve electron irradiation at higher energies to investigate whether the cleavage frequency at the abasic site increases.

ECD of abasic constructs may also address the role of protons. It should be noted that the theoretical work involved neutral DNA whereas ECD involves interactions between protonated DNA and electrons. Håkansson and co-workers suggested that at least two protons are needed to observe a *w* ion of the type shown in Scheme 7-1 [9]. However they did not elaborate on the sources of those protons. For doubly protonated

polydC, the protons are likely residing at the two end nucleotides as a result of Coulomb repulsion. Thus, if the abasic site is located in the middle, it is likely to be at a position that is not protonated in the unmodified analog. To address the possibility of proton transfer to this position, as has been suggested to occur in CAD [14, 15], one could also investigate ECD of oligonucleotides with thymine, for which the proton affinity is low, at the same position.

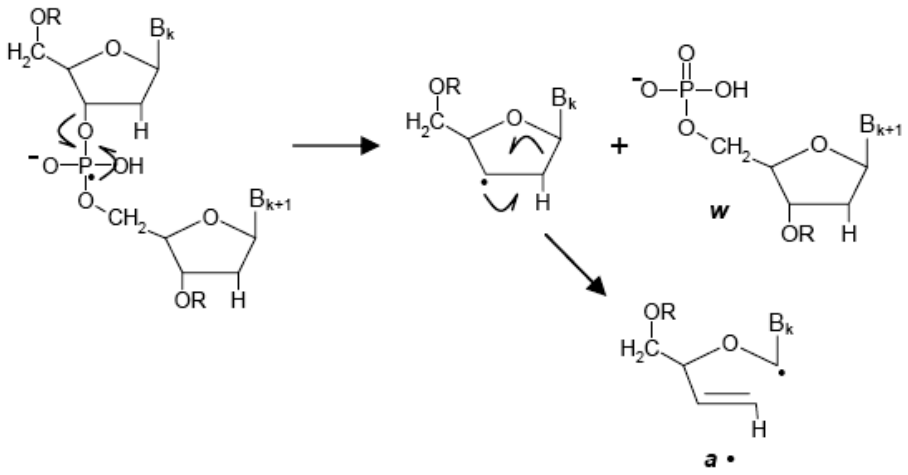

Scheme 7-1. Proposed fragmentation pathway in ECD of DNA. The scheme is adopted from reference [9].

Another pathway to be investigated is the formation of the (*a*/*z* - B) ions observed in ECD, corresponding to cleavage of two covalent bonds. The CAD oligodeoxynucleotide fragmentation mechanism proposed by Gross et al. [14], Smith et al. [15] and others involve protonation and loss of a nucleobase followed by backbone

cleavage. Because we observe *a*/*z* ions, a reverse process is more likely in ECD, as discussed in Chapter 5 for EDD. Double resonance experiments should also be applicable to elucidate the origin of (*a*/*z* - B) ions in ECD as long as potential *a*/*z* ion intermediates have lifetimes of microseconds or longer.

7.2.3. Fragmentation Pathways in ECD of RNA

For RNA, ECD of asymmetric oligonucleotides should be performed to establish whether our observed products [16] are *b* or *y* ions, *c* or *x* ions, or a mixture of both. For these experiments, one could use 5' phosphorylated A_6, C_6, and G_6. The different dissociation patterns observed as compared to DNA suggests that the 2' substituent plays a crucial role in the fragmentation process, consistent with a process initiated at the nucleobases. RNA carries a higher resistance to oxidative and other radical-induced degradation, which has been attributed to its 2' hydroxyl group [17]. Interestingly, charge-reduced $[M + 2H]^{+\bullet}$ radical ions are unusually abundant in ECD of A_6, correlating with a resistance to further cleavage processes. However, backbone cleavage was observed, although through different routes as compared to ECD of DNA. To further address the role of the 2' group, oligonucleotides containing 2'-methoxyethyl groups could be characterized for which previous CAD and IRMPD experiments have shown altered cleavage patterns [13, 18].

7.2.4. Biological Applications of EDD

In chapters 2, 4 and 6 we demonstrated that EDD spectra are straightforward to interpret and yield complete sequence coverage for small unmodified and modified oligomer DNAs and RNAs. These results imply that EDD has potential for characterizing unknown nucleic acids. Such a sequencing strategy would involve: 1) determination of the accurate molecular weight of the DNA/RNA to obtain an approximate residue number; 2) applying EDD to fragment the DNA/RNA; 3) grouping of product ions into *w* and *d* ion series (the fixed mass difference between, e.g., *w* and *y* ions is 79.9663); 4) utilization of *w* and *d* ion series to determine the sequence, including possible modifications.

Our group has shown that EDD can cleave covalent bonds without disrupting labile noncovalent interactions for an oligonucleotide duplex, thereby rendering EDD amenable to probe the gas-phase structure of acidic biomolecules. Of particular interest is the application of this technology to characterize RNA structure and folding.

Metal ions are important for the structure and function of DNA and RNA. For example, Mg^{2+} stabilizes tRNA tertiary structure [19] and mediates interactions between DNA and drug molecules [20]. Another application of EDD would be to characterize nucleic acid complexes containing metal ions, ligands, or drug molecules. Here, it should be possible to infer interaction sites due to the 'soft' character of EDD.

7.3. BIBLIOGRAPHY

1. Berdys, J.; Anusiewicz, I.; Skurski, P.; Simons, J. Damage to Model DNA Fragments from Very Low-Energy (<1 eV) Electrons. *J. Am. Chem. Soc.* **2004,** *126*, 6441-6447.
2. Nielsen, P. E.; Egholm, M.; Berg, R. H.; Buchardt, O. Sequence-selective Recognition of DNA by Strand Displacement with a Thymine-substituted Polyamide. *Science* **1991,** *254*, 1497-1500.
3. Nielsen, P. E. Peptide Nucleic Acid: a Versatile Tool in Genetic Diagnostics and Molecular Biology. *Curr. Opin. Biotechnol.* **2001,** *12*, 16-20.
4. Koppelhus, U.; Nielsen, P. E. Cellular Delivery of Peptide Nucleic Acid (PNA) *Adv. Drug Delivery Rev.* **2003,** *55*, 267-280.
5. Zielinski, J.; Kilk, K.; Peritz, T.; Kannanayakal, T.; Miyashiro, K. Y.; Eiriksottir, E.; Jochems, J.; Langel, U.; Eberwine, J. In Vivo Identification of Ribonucleoprotein-RNA Interactions. *Proc. Natl. Acad. Sci. U. S. A.* **2006,** *103*, 1557-1562.
6. Flora, J. W.; Shillady, D. D.; Muddiman, D. C. An Experimental and Theoretical Study of the Gas-phase Decomposition of Monoprotonated Peptide Nucleic Acids. *J. Am. Soc. Mass Spectrom.* **2000,** *11*, 615-625.
7. Olsen, J. V.; Haselmann, K. F.; Nielsen, M. L.; Budnik, B. A.; Nielsen, P. E.; Zubarev, R. A. Comparison of Electron Capture Dissociation and Collisionally Activated Dissociation of Polycations of Peptide Nucleic Acids. *Rapid Commun. Mass Spectrom.* **2001,** *15*, 969-974.

8. Roepstorff, P.; Fohlman, J. Proposal for a Common Nomenclature for Sequence Ions in Mass Spectra of Peptides. *Biomed. Mass Spectrom.* **1984,** *11*, 601-601.

9. Håkansson, K.; Hudgins, R. R.; Marshall, A. G.; O'Hair, R. A. J. Electron Capture Dissociation and Infrared Multiphoton Dissociation of Oligodeoxynucleotide Dications. *J. Am. Soc. Mass Spectrom.* **2003,** *14*, 23-41.

10. Syrstad, E. A.; Turecek, F. Toward a General Mechanism of Electron Capture Dissociation. *J. Am. Soc. Mass Spectrom.* **2005,** *16*, 208-224.

11. Sobczyk, M.; Anusiewicz, W.; Berdys-Kochanska, J.; Sawicka, A.; Skurski, P.; Simons, J. Coulomb-Assisted Dissociative Electron Attachment: Application to a Model Peptide. *J. Phys. Chem. A* **2005,** *109*, 250-258.

12. Li, X.; Sevilla, M. D.; Sanche, L. Density Functional Theory Studies of Electron Interaction with DNA: Can Zero eV Electrons Induce Strand Breaks? *J. Am. Chem. Soc.* **2003,** *125*, 13668-13669.

13. Tromp, J. M.; Schürch, S. Gas-Phase Dissociation of Oligoribonucleotides and their Analogs Studied by Electrospray Ionization Tandem Mass Spectrometry. *J. Am. Soc. Mass Spectrom.* **2005,** *16*, 1262-1268.

14. Wan, K. X.; Gross, J.; Hillenkamp, F.; Gross, M. L. Fragmentation Mechanisms of Oligodeoxynucleotides Studied by H/D Exchange and Electrospray Ionization Tandem Mass Spectrometry. *J. Am. Soc. Mass Spectrom.* **2001,** *12*, 193-205.

15. Krause, J.; Scalf, M.; Smith, L. M. High Resolution Characterization of DNA Fragment Ions Produced by Ultraviolet Matrix-Assisted Laser Desorption/Ionization

using Linear and Reflecting Time-of-Flight Mass Spectrometry. *J. Am. Soc. Mass Spectrom.* **1999,** *10*, 423-429.

16. Yang, J.; Håkansson, K. Fragmentation of Oligoribonucleotides from Gas-phase Ion-electron Reactions. *J. Am. Soc. Mass Spectrom.* **2006,** *17*, 1369-1375.

17. Thorp, H. H. The importance of being r: greater oxidative stability of RNA compared with DNA. *Chem. Biol.* **2000,** *7*, 33-36.

18. Sannes-Lowery, K. A.; Hofstadler, S. A. Sequence Confirmation of Modified Oligonucleotides using IRMPD in the External Reservoir of an Electrospray Ionization Fourier Transform Ion Cyclotron Mass Spectrometer. *J. Am. Soc. Mass Spectrom.* **2003,** *14*, 825-833.

19. Stein, A.; Crothers, D. M. Conformational Changes of Transfer RNA. The role of Magnesium(II). *Biochemistry* **1976,** *15*, 160-168.

20. Fan, J. Y.; Sun, D.; Yu, H.; Kerwin, S. M.; Hurley, L. H. Self-Assembly of a Quinobenzoxazine-Mg^{2+} Complex on DNA: A New Paradigm for the Structure of a Drug-DNA Complex and Implications for the Structure of the Quinolone Bacterial Gyrase-DNA Complex. *J. Med. Chem.* **1995,** *38*, 408-424.

APPENDIX A

ELECTRON CAPTURE AND ELECTRON DETACHMENT DISSOCIATION OF METAL-OLIGONUCLEOTIDE COMPLEXES

A.1. INTRODUCTION

Our group has shown that divalent metal adduction can greatly improve the ionization efficiency of acidic sulfated peptides in positive mode [1]. In addition, ECD of substance P complexed with divalent metals provided drastically different fragmentation pattern as a function of metal charge carrier and allowed directed bond cleavage [1]. Our group has also demonstrated dominant cross-ring cleavage in ECD of metal-adducted oligosaccharides [2]. For oligonucleotides, we have found that the sequence coverage from ECD is not as high as from EDD (Chapter 2, 4, and 6). We were interested in exploring whether more informative ECD tandem mass spectra could be obtained from oligonucleotide-metal complexes, such as sodium, potassium, and magnesium-adducted cationic species. Such cations exist in biological environments and bind strongly to nucleic acids. For example, magnesium is an important metal cofactor that mediates a large range of enzymatic reactions in nucleic acid biochemistry [3]. For folded RNA

molecules, the interactions with metal ions play a crucial role in the pathway for adopting proper tertiary structure, and the stabilization of that structure [4]. In positive ion mode, oligonucleotides can be difficult to observe as protonated ions and even for HPLC purified samples, sodium-adducted oligonucleotide ions can be more abundant than the corresponding protonated species in the mass spectra. Thus, utilization of metal-adducted species may also increase the sensitivity of oligonucleotide ECD, thereby improving its analytical utility. Here, we present ECD of the oligonucleotide d(GCATAC) complexed with severa; different mono and divalent metal ions. Furthermore, we explore EDD fragmentation patterns of metal-oligonucleotide complexes. We previously found that the charge state of oligonucleotide anions influenced the fragmentation outcome in EDD (see Chapter 3), with increased sequence coverage for higher charge states, presumably due to unfolding of the gas-phase species. The altered behavior of metal-adducted peptides and oligosaccharides has been proposed to be due to altered gas-phase structures [1, 2, 5]. Thus, the presence of metals may play a role in EDD as well, allowing further insight in to this process.

A. 2. EXPERIMENTAL SECTION

A.2.1. Sample Preparation

The reversed-phase HPLC purified oligodeoxynucleotide dGCATAC was purchased from TriLink BioTechnologies (San Diego, CA) as crude sodium salt. Positive mode electrospray solvent consisted of 1:1 (v/v) acetonitrile:water (Fisher) with 0.5% formic acid (ACROS Organics, Fair Lawn, NJ). Negative ion mode electrospray solvent consisted

of 1:1 (v/v) isopropanol:water (Fisher, Fair Lawn, New Jersey) with 10 mM ammonium acetate (Fisher). The final concentration of the oligonucleotide was 10 μM and the metal concentration was varied from 5-20 μM.

A.2.2. Fourier Transform Ion Cyclotron Resonance Mass Spectrometry

All experiments were performed with a 7 Tesla Q-FT-ICR mass spectrometer (Bruker Daltonics, Billerica, MA), shown in Figure 2-1. Oligonucleotide solutions were infused via an external Apollo electrospray ion source at a flow rate of 70 μL/h with the assistance of N_2 nebulizing gas. Both ECD and EDD were performed with an indirectly heated hollow dispenser cathode electron source (Heat Wave, Watsonville, CA). The heater was set to approximately 8.5 V, generating a heating current of 1.8 A. For ECD, the cathode voltage was pulsed to - 1 V for 25-30 ms. A lens located in front of the cathode was kept at + 1 V throughout the experiment. During the EDD event, the cathode voltage was pulsed to - 18.2 V for 2 s. A lens located in front of the cathode was kept at - 19 V throughout the experiment. All mass spectra were acquired with XMASS (version 6.1 Bruker Daltonics) in broadband mode with 256 data points and summed over 15-50 scans. Data processing was performed as described in section 2.2.2.

A.3. RESULTS AND DISCUSSION

A.3.1. ECD of Metal-oligonucleotide Complexes

Figure A-1 shows an ECD spectrum of doubly protonated d(GCATAC). The spectrum mainly contains sequence specific *d*, *w*, *z*, (*w* - B) and (*z* - B) ions. However, in spite of the diversity of fragmentation pathways, full sequence coverage could not be obtained from ECD. ECD of doubly charged d(GCATAC) containing one monovalent metal cation and one proton, or one divalent metal (shown in Figures A-2-A-6) yielded even less product ions and the products observed were of the same nature as for the doubly protonated species. Furthermore, we did not observe any positive mode ionization efficiency increase in ESI of these metal-oligonucleotide complexes. The identical fragmentation processes observed in ECD of metal-adducted d(GCATAC) may suggest that metal ions do not take part in the dissociation process, i.e., electrons are captured at other sites in the molecules.

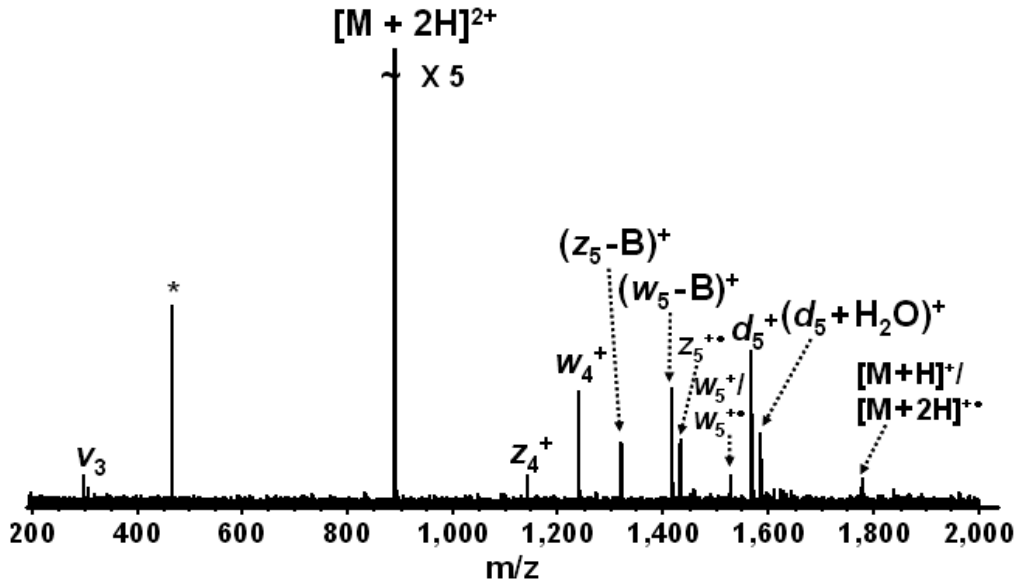

Figure A-1. ECD (1 eV electrons, 30 ms, 50 scans) of doubly protonated d(GCATAC). Electronic noise spike is labeled with an asterisk, ν_3 = harmonic artifact.

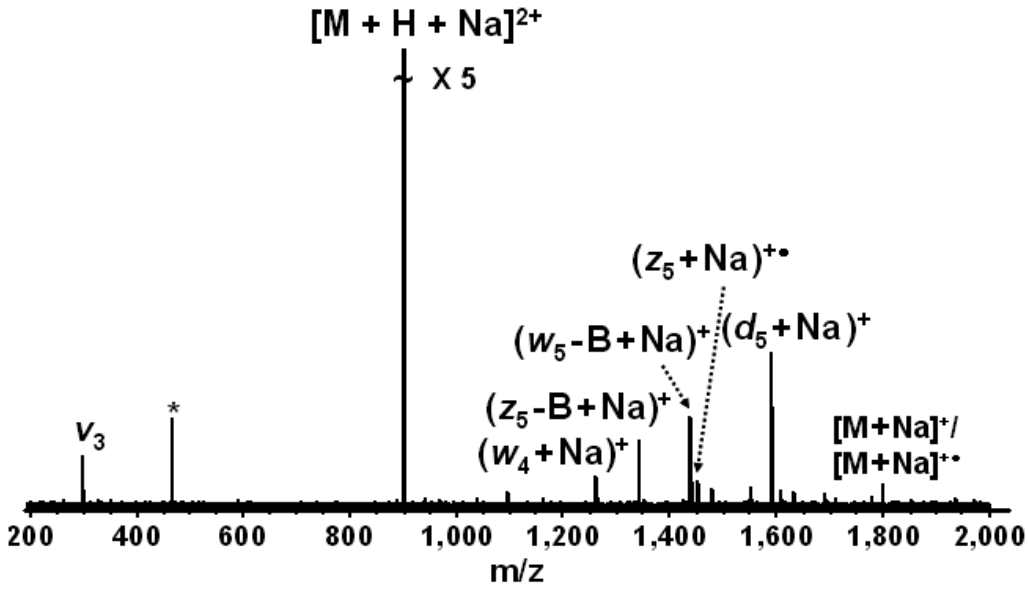

Figure A-2. ECD (1 eV electrons, 25 ms, 50 scans) of $[d(GCATAC) + H + Na]^{2+}$. Electronic noise spike is labeled with an asterisk, ν_3 = harmonic artifact.

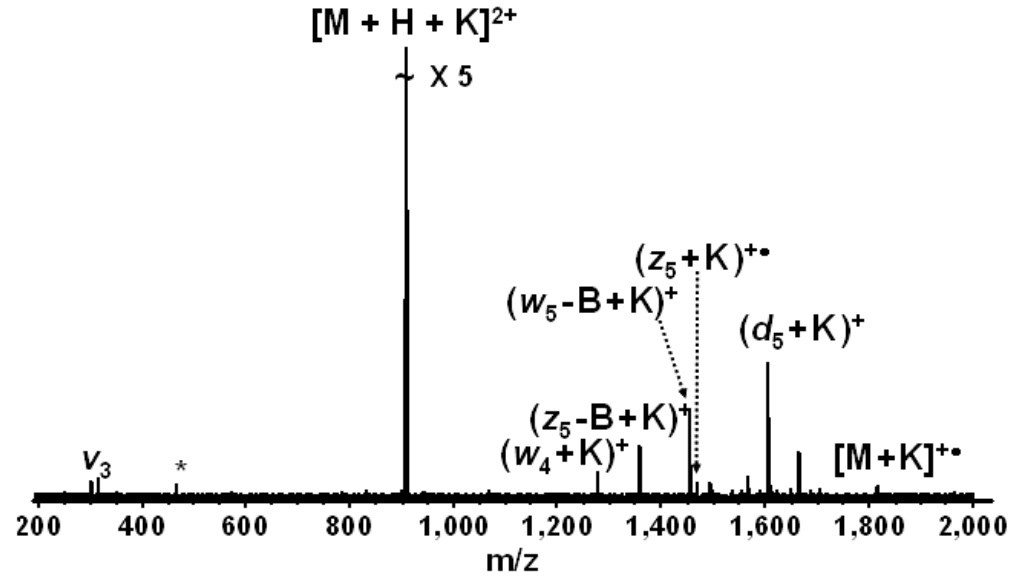

Figure A-3. ECD (1 eV electrons, 25 ms, 50 scans) of $[d(GCATAC) + H + K]^{2+}$. Electronic noise spike is labeled with an asterisk, ν_3 = harmonic artifact.

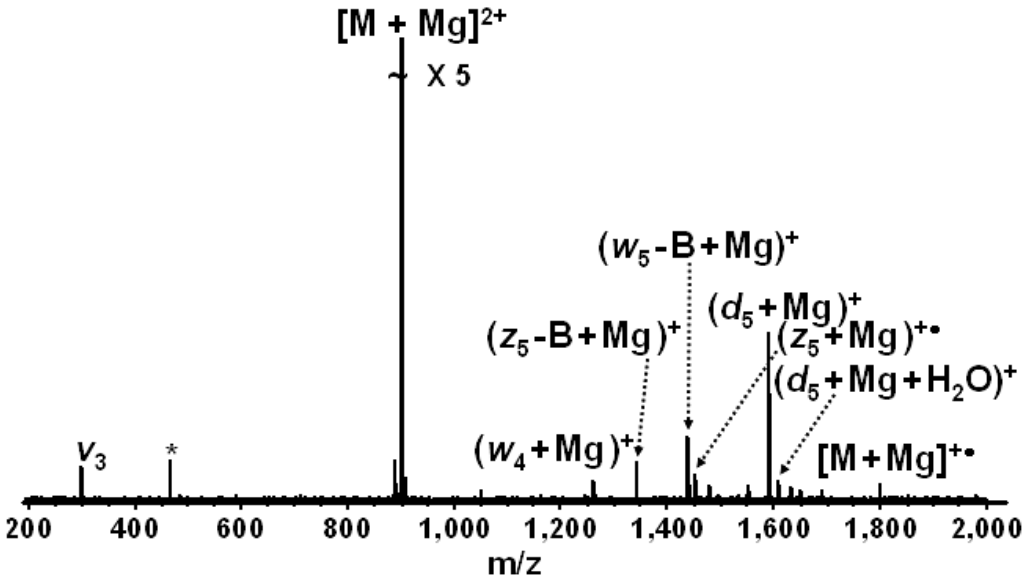

Figure A-4. ECD (1 eV electrons, 25 ms, 50 scans) of $[d(GCATAC) + Mg]^{2+}$. Electronic noise spike is labeled with an asterisk, ν_3 = harmonic artifact.

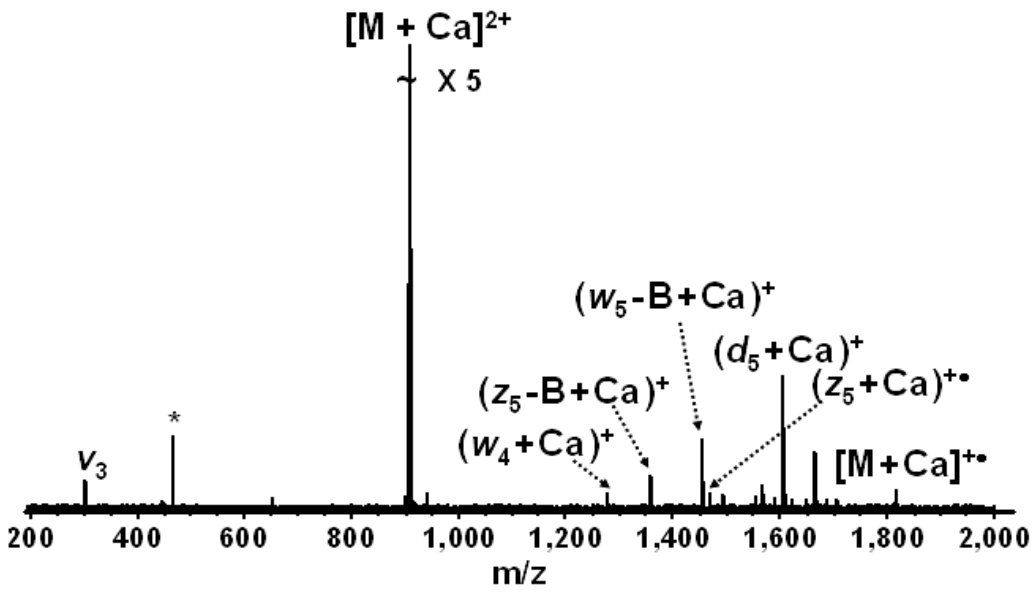

Figure A-5. ECD (1 eV electrons, 30 ms, 50 scans) of $[d(GCATAC) + Ca]^{2+}$. Electronic noise spike is labeled with an asterisk, ν_3 = harmonic artifact.

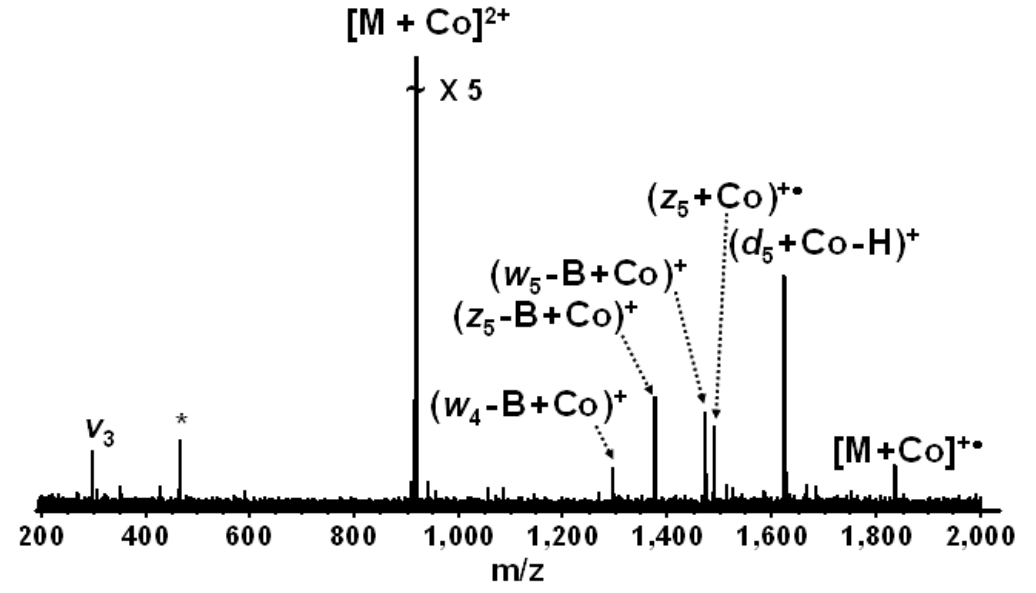

Figure A-6. ECD (1 eV electrons, 25 ms, 50 scans) of $[d(GCATAC) + Co]^{2+}$. Electronic noise spike is labeled with an asterisk, ν_3 = harmonic artifact.

A.3.2. EDD of Metal-oligonucleotide Complexes

Figure A-7 shows an EDD spectrum of doubly deprotonated d(GCATAC), mainly containing a complete *w* ion series, and three *d* ions. In addition, three (*a* - B) ions and one (*x* - B) ion are seen. Base (A and C) loss from precursor ions is also observed, but it is a minor fragmentation pathway. Figure A-8 to A-13 show EDD spectra of d(GCATAC) complexed with sodium, potassium, magnesium, calcium, barium and cobalt, i.e., precursor ions contain either two or three deprotonated sites to yield an overall charge of - 2. Because the negative ion mode ionization efficiency of metal-d(GCATAC) complexes was lower than that of d(GCATAC) alone, longer ion accumulation time was necessary to obtain the same precursor ion abundance. We also observed a much lower EDD fragmentation efficiency for metal-d(GCATAC) complexes than for doubly deprotonated d(GCATAC), resulting in product ions with low signal-to-noise ratio in the former experiments. The latter finding suggests that metal-oligonucleotide anions are more tightly folded in the gas-phase, consistent with Coulomb stabilization by the metals. Furthermore, as in ECD of metal-d(GCATAC) complexes, the nature of product ions did not change compared to free d(GCATAC), suggesting that the metal ions do not take part in the dissociation process. However, EDD of metal-oligonucleotide complexes did not provide novel insights into the EDD fragmentation mechanism.

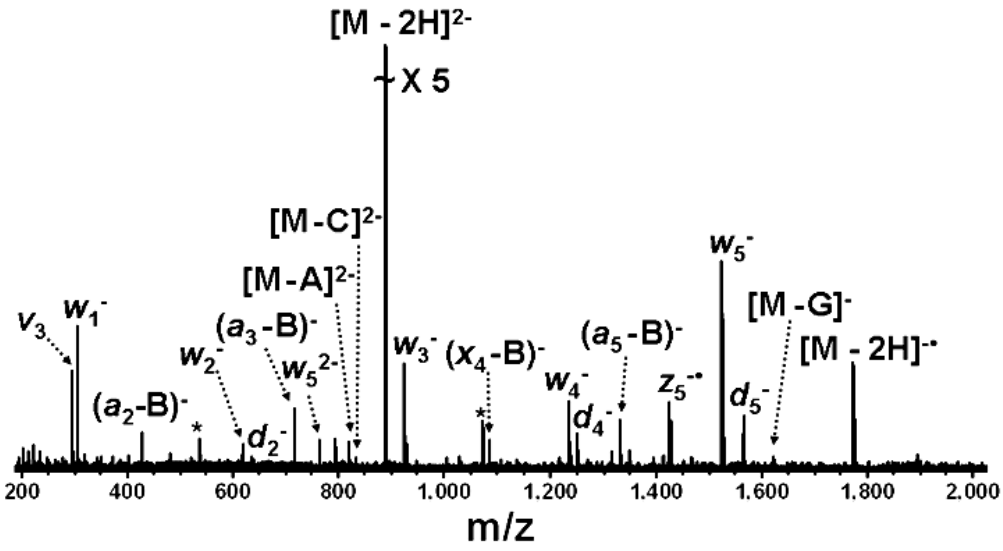

Figure A-7. EDD of doubly deprotoanted d(GCATAC) (18.1 eV electrons, 2 s, 32 scans) resulted in a complete *w* ion series, and three *d* ions. Electronic noise spikes are labeled with asterisks, ν_3 = harmonic artifact.

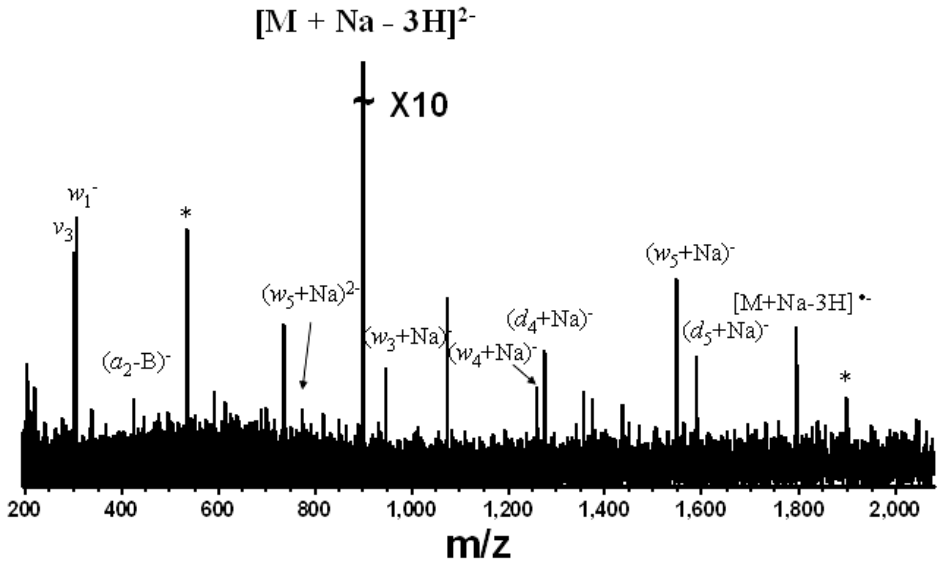

Figure A-8. EDD (18.2 eV electrons, 2 s, 32 scans) of $[d(GCATAC) + Na - 3H]^{2-}$. Electronic noise spikes are labeled with asterisks, ν_3 = harmonic artifact.

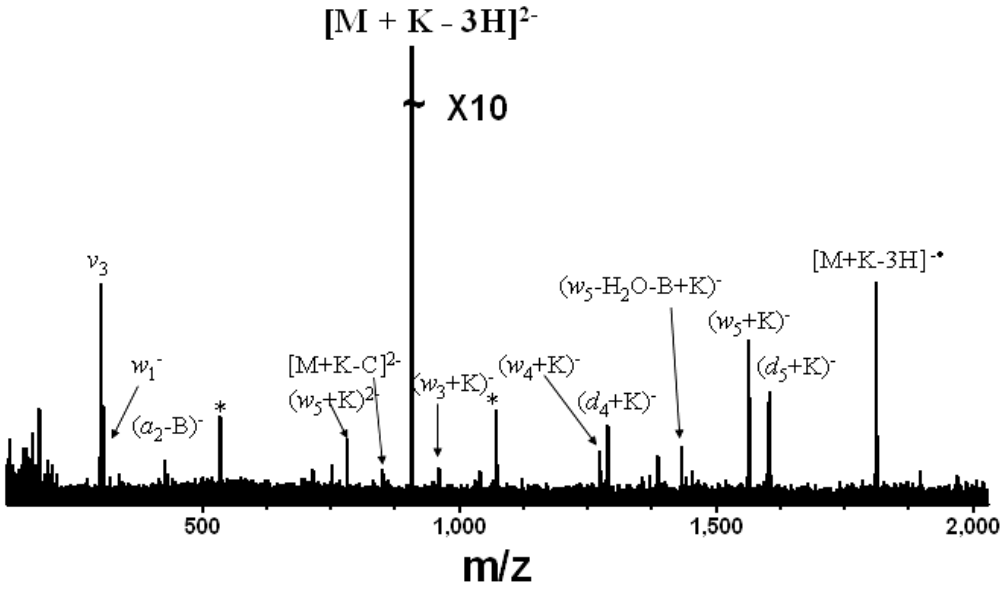

Figure A-9. EDD (18.2 eV electrons, 2 s, 32 scans) of $[d(GCATAC) + K - 3H]^{2-}$. Electronic noise spikes are labeled with asterisks, ν_3 = harmonic artifact.

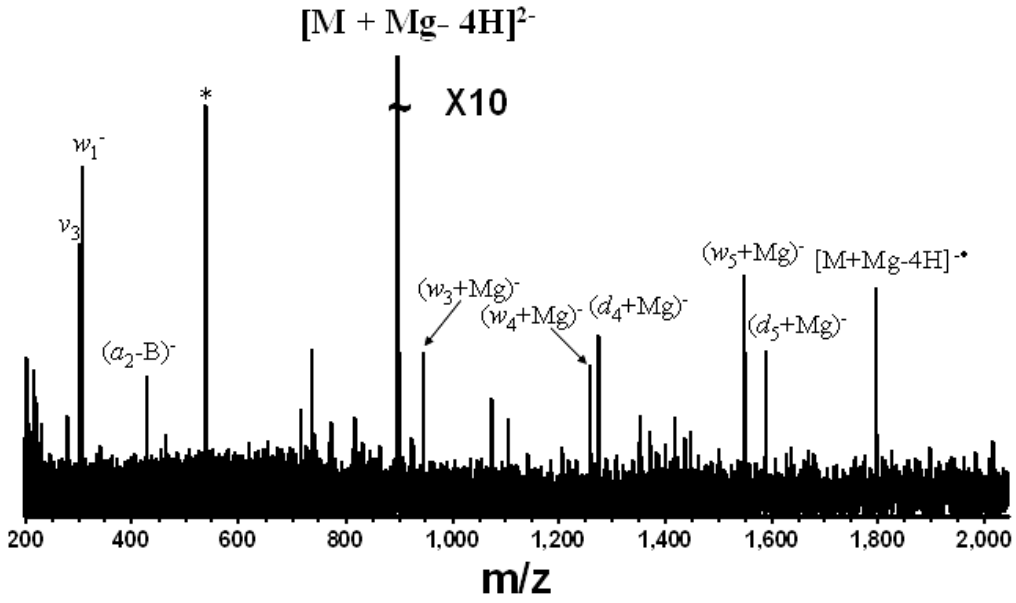

Figure A-10. EDD (18.2 eV electrons, 2 s, 32 scans) of $[d(GCATAC) + Mg - 4H]^{2-}$. Electronic noise spike is labeled with an asterisk, ν_3 = harmonic artifact.

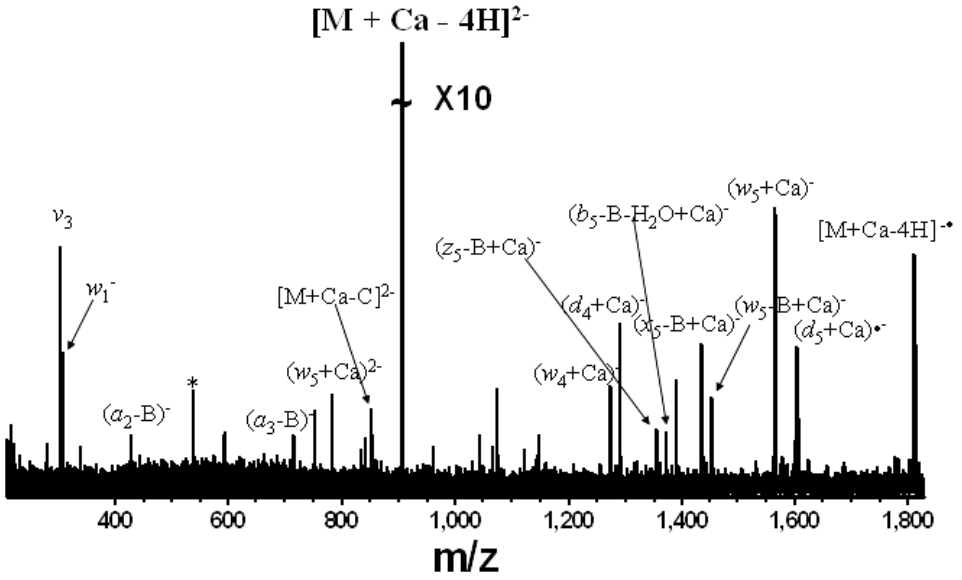

Figure A-11. EDD (18.2 eV electrons, 2 s, 32 scans) of $[d(GCATAC) + Ca - 4H]^{2-}$. Electronic noise spike is labeled with an asterisk, ν_3 = harmonic artifact.

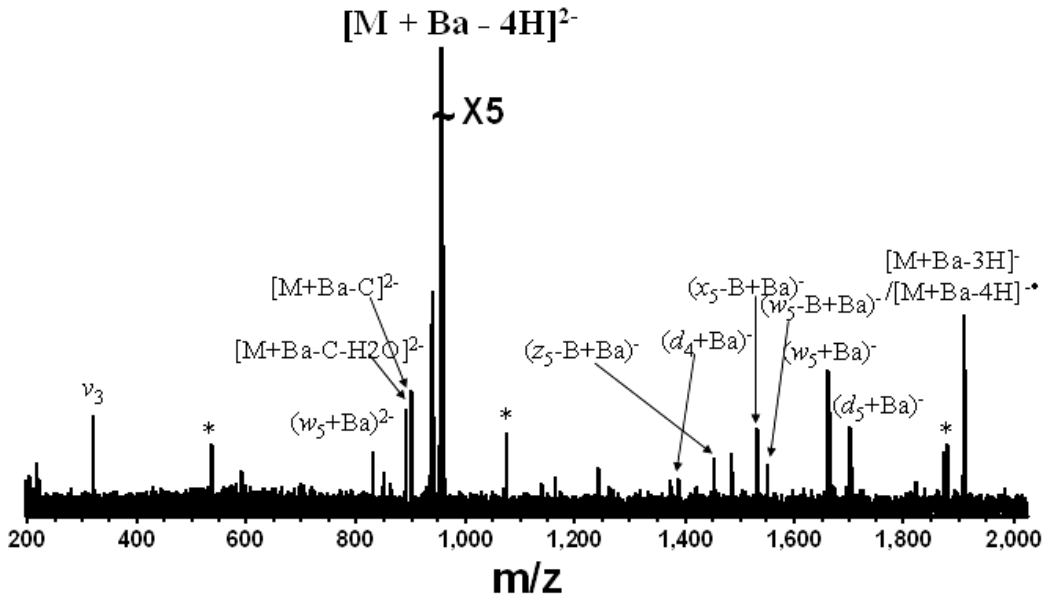

Figure A-12. EDD (18.2 eV electrons, 2 s, 32 scans) of $[d(GCATAC) + Ba - 4H]^{2-}$. Electronic noise spikes are labeled with asterisks, ν_3 = harmonic artifact.

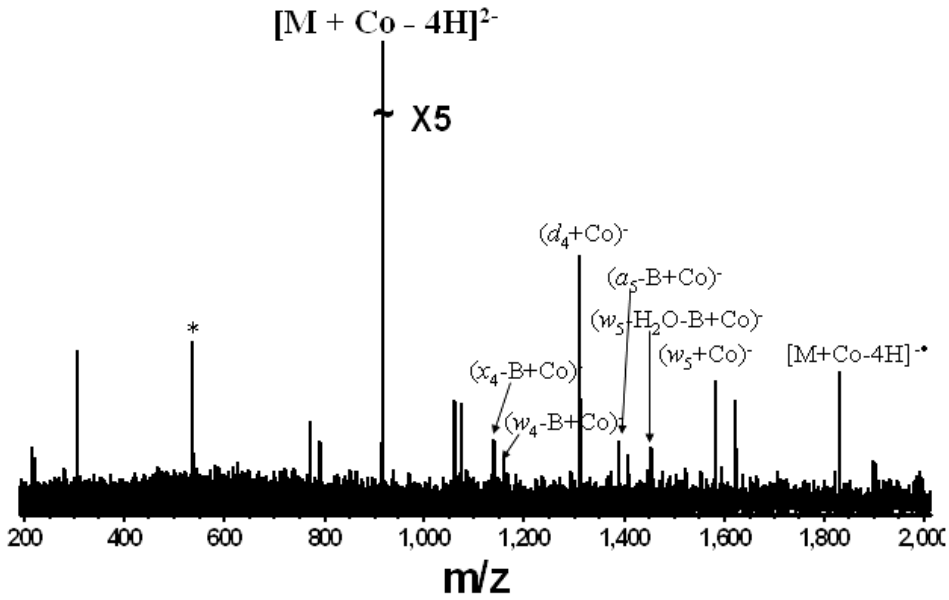

Figure A-13. EDD (18.2 eV electrons, 2 s, 15 scans) of $[d(GCATAC) + Co - 4H]^{2-}$. Electronic noise spike is labeled with an asterisk, ν_3 = harmonic artifact.

A.4. BIBLIOGRAPHY

1. Liu, H. C.; Håkansson, K. Divalent Metal Ion-peptide Interactions Probed by Electron Capture Dissociation of Trications. *J. Am. Soc. Mass Spectrom.* **2007,** *17*, 1731-1741.
2. Adamson, J. T.; Håkansson, K. Electron Capture Dissociation of Oligosaccharides Ionized with Alkali, Alkaline earth, and Transition metals. *Anal. Chem.* **2007,** *79*, 2901-2910.
3. Cowan, J. A. Metal Activation of Enzymes in Nucleic Acid Biochemistry. *Chem. Rev.* **1998,** *98*, 1067-1087.
4. Pyle, A. M. Metal Ions in the Structure and Function of RNA . *J. Biol. Inorg. Chem.* **2002,** *7*, 679-690.

5. Kleinnijenhuis, A. J.; Mihalca, R.; Heeren, R. M. A.; Heck, A. J. R. Atypical Behavior in the Electron Capture Induced Dissociation of Biologically Relevant Transition Metal Ion Complexes of the Peptide Hormone Oxytocin. *Int. J. Mass Spectrom.* **2006,** *253*, 181-192.

APPENDIX B

ELECTRON INDUCED DISSOCIATION OF SINGLY DEPROTONATED OLIGODEOXYNUCLEOTIDES

B.1. INTRODUCTION

MALDI generally produces singly-charged ions in contrast to ESI, which yields multiply charged ions for larger molecules. For ECD and EDD, multiply charged precursor ions are required due to the charge neutralization occurring upon electron capture or detachment, respectively. Thus, these two MS/MS technique are not compatible with MALDI. In this work, we investigate the possibility of applying high energy (~18 eV) electron irradiation (electron induced dissociation, EID) to singly negatively charged oligomeric DNA and compare the resulting product ion spectra to those obtained with IRMPD of the same species. The instrument setup is the same as for EDD experiments (see Chapters 2-6). EID was first shown by Cody and Fresier in 1979 for radical cations [1] and later extended by Wang and McLafferty to even-electron peptide cations [2]. The former experiments utilized a range of electron energies whereas the latter involved 70 eV electrons. More recently, Zubarev and co-workers have demonstrated EID experiments involving 10-13 eV electron irradiation of singly charged even-electron cations [3]. Very recently, our group has demonstrated the utility of EID for characterization of singly deprotonated metabolites [4].

B. 2. EXPERIMENTAL SECTION

B.2.1. Sample Preparation

Reversed-phase HPLC purified oligodeoxynucleotides (dA_6, dC_6 and dT_6) were purchased from TriLink BioTechnologies (San Diego, CA) as their crude sodium salts. Negative ion mode electrospray solvent consisted of 1:1 (v/v) isopropanol:water (Fisher, Fair Lawn, New Jersey) with 10 mM ammonium acetate (Fisher). The final concentration of samples was 10-20 μM.

B.2.2. Fourier Transform Ion Cyclotron Resonance Mass Spectrometry

All experiments were performed with a 7 Tesla Q-FT-ICR mass spectrometer (Bruker Daltonics, Billerica, MA), shown in Figure 2-1. Oligonucleotide solutions were infused via an external Apollo electrospray ion source operating in negative ion mode at a flow rate of 70 μL/h with the assistance of N_2 nebulizing gas. Singly deprotonated precursor ions were mass-selectively externally accumulated and EID was performed in the ICR cell with an indirectly heated hollow dispenser cathode electron source (Heat Wave, Watsonville, CA). The cathode voltage was pulsed to ~ - 18 V for 2 s. The heater was set to approximately 8.5 V, generating a heating current of 1.8 A. IRMPD was performed with a vertically mounted 25 W, 10.6 μm, CO_2 laser (Synrad, Mukilteo, WA). Photon irradiation was performed for 20 ms at 10 W laser power. All mass spectra were acquired with XMASS (version 6.1 Bruker Daltonics) in broadband mode with 256 data points and summed over 32 scans. Data processing was performed as described in section 2.2.2.

B.3. RESULTS AND DISCUSSION

Figure B-1 shows an EID spectrum of singly deprotonated dA_6. EID mainly resulted in sequence specific *d*/*w*, (*a*/*z* - B), (*w*/*d* - B), and (*c*/*x* - B) ion (these ions cannot be distinguished based on mass alone due to the symmetry of dA_6). Neutral base loss from precursor ions is also observed. High m/z product ions dominate over low m/z ones. The fragmentation pattern is different from EDD of the same oligonucleotide (see Chapter 2): In EID, base loss was the major fragmentation pathway and full sequence coverage was not obtained whereas a complete *d*/*w* ions series was observed in EDD. Figure B-2 shows IRMPD of the same singly deprotonated oligomer DNA, which resulted in extensive *c*/*x*, *w*, (*a* - B), (*w*/*d* - B), and (*c*/*x* - B) product ions. Water loss and secondary base loss are observed as well. There are also some unidentified ions, which cannot be predicted based on known fragmentation pathways. Full sequence coverage is obtained from the complete *w* ion series. Compared with IRMPD, the EID spectrum is easier to interpret but the product ion signal-to-noise ratio is not as high as in IRMPD. EID and IRMPD results for singly deprotonated dC_6 (Figures B-3 and B-4, respectively) were similar as those for dA_6. By contrast, EID of singly deprotonated dT_6 (Figure B-5) showed a fragmentation pattern different from those of dA_6 and dC_6. Here, no base loss was seen and the major fragments correspond to *d*/*w* and *a*/*z* type ions. We also detected one a_5/z_5 radical ion (error less than 7 ppm and with an isotopic distribution), which may be formed from direct homolytic bond cleavage. IRMPD of singly deprotonated dT_6 resulted in extensive *a*, *b*/*y*, *c*/*x*, *w*, (*a* - B), (*w* - B), and (*c*/*x* - B) ions. Two water losses from *c* ions were observed as well.

Because the EID experimental conditions are the same as those previously applied for EDD, we believe EID-type fragmentation may also occur during EDD experiments.

Such direct vibrational and/or electronic excitation may explain the observation of doubly charged *w* and *d* ions in EDD of oligomer DNA and RNA as well as the lack of influence on product ion abundances seen in some DR-EDD experiments (Chapter 5). Overall, EID spectra of singly charged oligomer DNA are less complex than IRMPD spectra, however, full sequence coverage could not be obtained from EID, presumably due to low fragmentation efficiency. Nevertheless, EID may have potential for characterizing other molecules for which only singly negatively charged ions can be obtained.

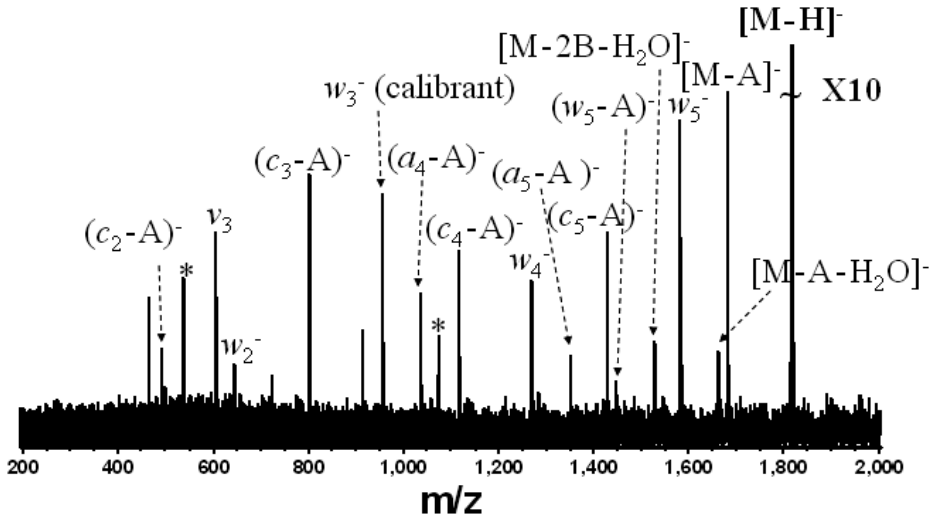

Figure B-1. EID (18.1 eV electrons, 2 s, 32 scans) of singly deprotonated dA_6. *d*/*w*, (*a*/*z* - B), (*d*/*w* - B) and (*c*/*x* - B) ions are observed (only one of the labels is given). Electronic noise spikes are labeled with asterisks.

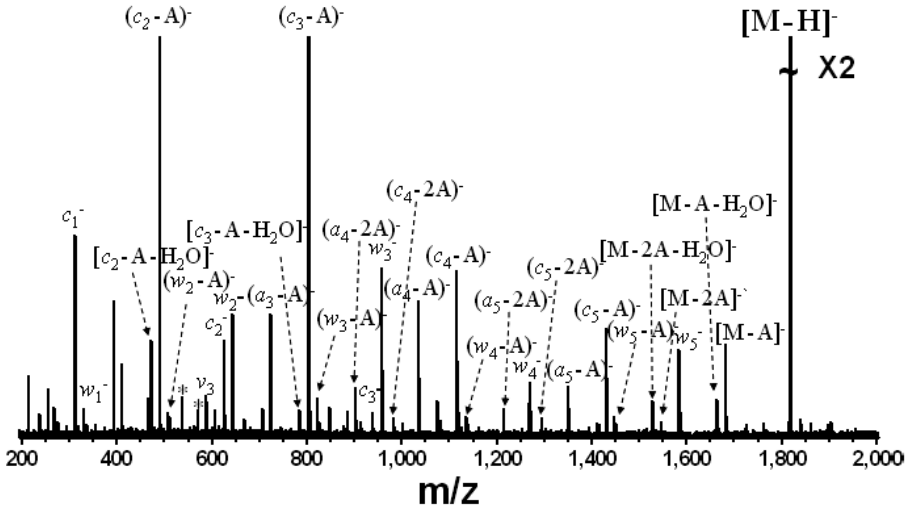

Figure B-2. IRMPD (10 W, 20 ms, 32 scans) of singly deprotonated dA_6. Mainly *c*/*x*, *d*/*w*, (*a*/*z* - B), (*d*/*w* - B) and (*c*/*x* - B) ions are observed. Electronic noise spikes are labeled with asterisks.

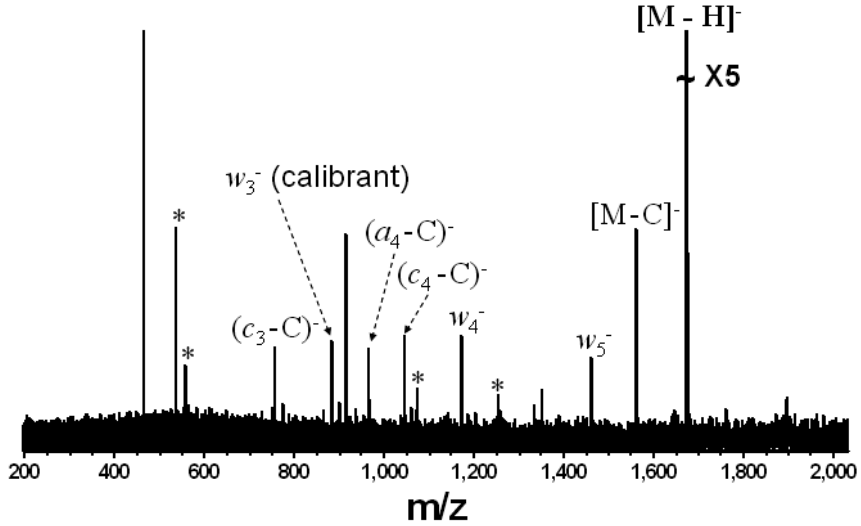

Figure B-3. EID (18.1 eV electrons, 2 s, 32 scans) of singly deprotonated dC_6. *d*/*w*, (*a*/*z* - B), (*d*/*w* - B), and (*c*/*x* - B) ions are observed. Electronic noise spikes are labeled with asterisks.

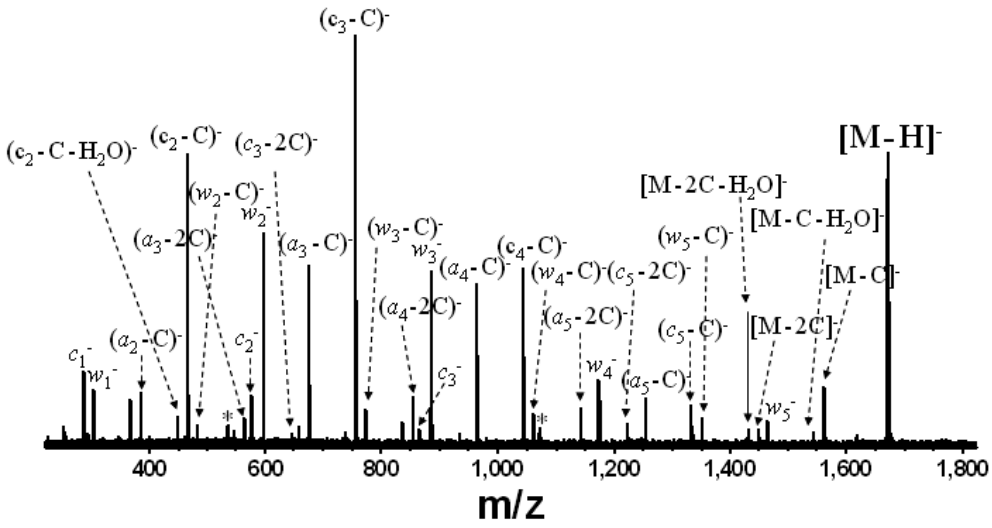

Figure B-4. IRMPD (10 W, 20 ms, 32 scans) of singly deprotonated dC_6. Mainly *c*/*x*, *d*/*w*, (*a*/*z* - B), (*d*/*w* - B), and (*c*/*x* - B) ions are observed. Electronic noise spikes are labeled with asterisks.

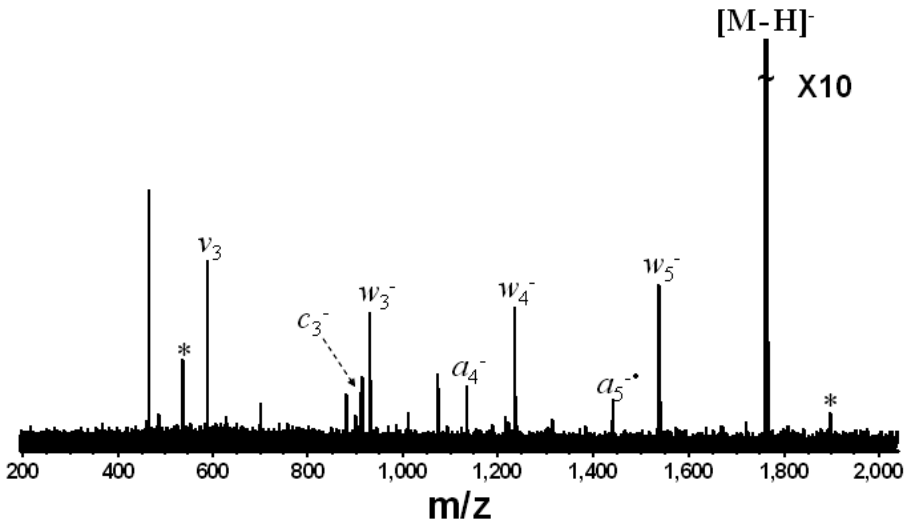

Figure B-5. EID (18.1 eV electrons, 2 s, 32 scans) of singly deprotonated dT_6. Mainly *d*/*w*, *c*/*x*, and *b*/*y* ions are observed. Electronic noise spikes are labeled with asterisks.

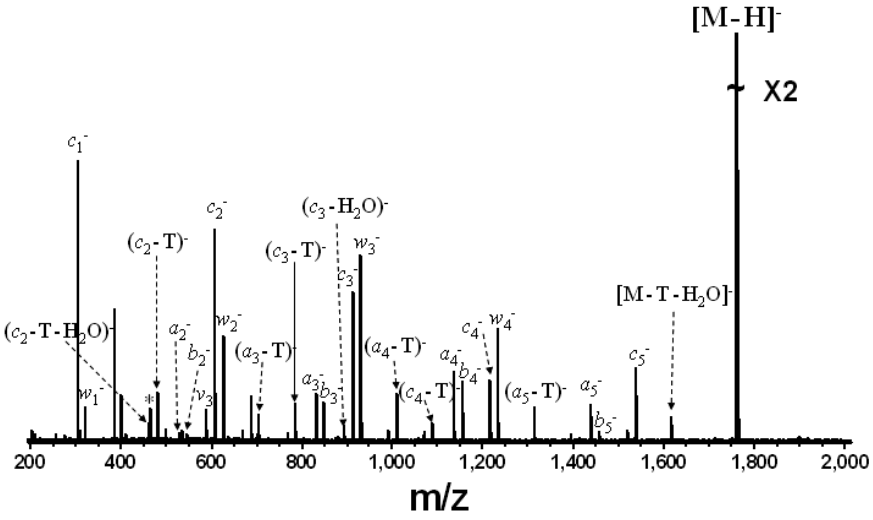

Figure B-6. IRMPD (10 W, 20 ms, 32 scans) of singly deprotonated dT_6. Mainly *a*/*z*, *b*/*y*, *c*/*x*, *d*/*w*, (*a*/*z* - B), and (*c*/*x* - B) ions are observed. Electronic noise spikes are labeled with asterisks.

B.4. BIBLIOGRAPHY

1. Cody, R. B.; Freiser, B. S. Electron Impact Excitation of Ions from Organics: an Alternative to Collision Induced Dissociation. *Anal. Chem.* **1979,** *51*, 547 - 551.
2. Wang, B. H.; Mclafferty, F. W. Electron-impact Excitation of Ions From Larger Organic-molecules. *Org. Mass Spectrom.* **1990,** *25*, 554-556
3. Budnik, B. A.; Haselmann, K. F.; Elkin, Y. N.; Gorbach, V. I.; Zubarev, R. A. Applications of electron-ion dissociation reactions for analysis of polycationic chitooligosaccharides in Fourier transform mass spectrometry. *Anal Chem* **2003,** *75*, 5994-6001.
4. Yoo, H. J.; Liu, H. C.; Håkansson, K. Infrared Multiphoton Dissociation and Electron-Induced Dissociation as Alternative MS/MS Strategies for Metabolite Identification. *Anal. Chem.* **2007**, Accepted.